

OCRWM	ERRATA 002		3. QA: QA 4. Page 1 of 3
1. Condition Report No. CR-1100		2. DC Tracking Number 38363	
5. Product DI <u>MDL-NBS-HS-000004</u>	6. Title <u>Seepage Calibration Model and Seepage Testing Data</u>	7. Revision <u>02</u>	
8. Description of Error		9. Clarification/Restriction	
<p>A search of DIRS indicates you are currently using DIRS Reference 161530 <i>Drift-Scale Coupled Processes (DST and TH Seepage) Models</i>, MDL-NBS-HS-000015 REV 00, which has been assigned URN 1087. This document has never been approved and the URN is invalid. The DIRS reference has been marked as bad and cannot be used.</p>		<p>The model report, <i>Seepage Calibration Model and Seepage Testing Data</i> (DI: MDL-NBS-HS-000004 REV02) and associated DIRS have been corrected to reference DIRS 166512 [BSC (Bechtel SAIC Company) 2003. <i>Drift-Scale Coupled Processes (DST and TH Seepage) Models</i>. MDL-NBS-HS-000015 REV 00C. Las Vegas, Nevada: Bechtel SAIC Company. ACC: MOL.20030910.0160. TBV-5666.] (See attached, corrected report page 140 and corrected DIRS page 5.)</p>	
10. Responsible Manager (Print Name) <u>Paul E. Dixon</u>		Initials <u>PED</u>	Date <u>2/17/04</u>

- 160780 BSC (Bechtel SAIC Company) 2002. *Risk Information to Support Prioritization of Performance Assessment Models*. TDR-WIS-PA-000009 REV 01 ICN 01. Las Vegas, Nevada: Bechtel SAIC Company. ACC: MOL.20021017.0045.
- 160313 BSC (Bechtel SAIC Company) 2002. *Scientific Processes Guidelines Manual*. MIS-WIS-MD-000001 REV 01. Las Vegas, Nevada: Bechtel SAIC Company. ACC: MOL.20020923.0176.
- 160819 BSC (Bechtel SAIC Company) 2002. *Technical Work Plan for: Performance Assessment Unsaturated Zone*. TWP-NBS-HS-000003 REV 02. Las Vegas, Nevada: Bechtel SAIC Company. ACC: MOL.20030102.0108.
- 160146 BSC (Bechtel SAIC Company) 2002. *Total System Performance Assessment-License Application Methods and Approach*. TDR-WIS-PA-000006 REV 00. Las Vegas, Nevada: Bechtel SAIC Company. ACC: MOL.20020923.0175.
- 161066 BSC (Bechtel SAIC Company) 2002. *User's Manual (UM) for iTOUGH2 V5.0*. DI: 10003-UM-5.0-00. Las Vegas, Nevada: Bechtel SAIC Company. ACC: MOL.20020923.0147.
- 166512 BSC (Bechtel SAIC Company) 2003. *Drift-Scale Coupled Processes (DST and TH Seepage) Models*. MDL-NBS-HS-000015 REV 00C. Las Vegas, Nevada: Bechtel SAIC Company. ACC: MOL.20030910.0160. TBV-5666.
- 150929 Campbell, G.S. and Norman, J.M. 1998. *An Introduction to Environmental Biophysics*. 2nd Edition. New York, New York: Springer-Verlag. TIC: 243951.
- 104368 Carrera, J. and Neuman, S.P. 1986. "Estimation of Aquifer Parameters Under Transient and Steady State Conditions: 1. Maximum Likelihood Method Incorporating Prior Information." *Water Resources Research*, 22, (2), 199-210. Washington, D.C.: American Geophysical Union. TIC: 245915.
- 141187 CRWMS M&O (Civilian Radioactive Waste Management System Management and Operating Contractor) 2000. *Conceptual and Numerical Models for UZ Flow and Transport*. MDL-NBS-HS-000005 REV 00. Las Vegas, Nevada: CRWMS M&O. ACC: MOL.19990721.0526.
- 153314 CRWMS M&O 2000. *Seepage Model for PA Including Drift Collapse*. MDL-NBS-HS-000002 REV 01. Las Vegas, Nevada: CRWMS M&O. ACC: MOL.20010221.0147.
- 154291 CRWMS M&O 2001. *Abstraction of Drift Seepage*. ANL-NBS-MD-000005 REV 01. Las Vegas, Nevada: CRWMS M&O. ACC: MOL.20010309.0019.
- 153045 CRWMS M&O 2001. *Seepage Calibration Model and Seepage Testing Data*. MDL-NBS-HS-000004 REV 01. Las Vegas, Nevada: CRWMS M&O. ACC: MOL.20010122.0093.

16	User's Manual (UM) for iTOUGH2 V5.0. DI: 10003-UM-5.0-00. Las Vegas, Nevada: Bechtel SAIC Company. ACC: <u>MOL.20020923.0147</u> . 161066		Only		Genuchten model in iTOUGH2 V5.0	
17	BSC (Bechtel SAIC Company) 2003. <i>Drift-Scale Coupled Processes (DST and TH Seepage) Models</i> . MDL-NBS-HS-000015 REV 00C. Las Vegas, Nevada: Bechtel SAIC Company. ACC: <u>MOL.20030910.0160</u> . TBV-5666 166512	Entire	Reference Only	1, 6.3.1, 6.3.3.2, 6.3.4, 8.2	TH Seepage Model	N/A
18	Campbell, G.S. and Norman, J.M. 1998. <i>An Introduction to Environmental Biophysics</i> . 2nd Edition. New York, New York: Springer-Verlag. TIC: <u>243951</u> . 150929	Eqs. 3.11, 3.17	N/A - Corroborative Information	6.6.1.3	Kelvin's equation	N/A
19	Carrera, J. and Neuman, S.P. 1986. "Estimation of Aquifer Parameters Under Transient and Steady State Conditions: 1. Maximum Likelihood Method Incorporating Prior Information." <i>Water Resources Research</i> , 22, (2), 199-210. Washington, D.C.: American Geophysical Union. TIC: <u>245915</u> . 104368	Entire	Reference Only	6.6.3.3	Inverse modeling theory	N/A
20	CRWMS M&O 1999. <i>Software Routine: ECRB-XYZ</i> . V.03. PC. 30093-V.03. 147402	Entire	Qualified Software	3, 6.6.2.3; Table 1	General software use	N/A
21	CRWMS M&O 2000. <i>Conceptual and Numerical Models for UZ Flow and Transport</i> . MDL-NBS-HS-000005 REV 00. Las Vegas, Nevada: CRWMS M&O. ACC: <u>MOL.19990721.0526</u> . 141187	5, 6.4.2, 6.4.4	Reference Only	6.3.2	UZ Model description	N/A
	CRWMS M&O 2000. <i>Seepage Model for PA Including Drift Collapse</i> . MDL-NBS-HS-000002 REV 01. Las Vegas,	Entire	Reference Only	1, 6.3.3.3, 8.2	Seepage Model for Performance Assessment	N/A

OCRWM	ERRATA 001		3. QA: QA 4. Page 1 of 2
1. Condition Report No. 1079		2. DC Tracking Number 38240	
5. Product DI <u>MDL-NBS-HS-000004</u>	6. Title <u>Seepage Calibration Model and Seepage Testing Data</u>		7. Revision <u>02</u>
8. Description of Error		9. Clarification/Restriction	
<p>1. Numbers on Table 14, p. 106 of the Seepage Calibration Model (SCM) MDL-NBS-HS-000004, Rev02 do not reflect those contained in the raw data of DTN: LB0302SCMREV02.001[1]tar.</p> <p>2. A reference error was uncovered in Table 14. Runs 83 and 80 are actually 86 and 89.</p>		<p>Replace Table 14, p. 106 of MDL-NBS-HS-000004 , Rev02 with the new version shown on the attached Table 14 as follows:</p> <ul style="list-style-type: none"> - Lower Lithophysal Zone (Tptpll), Column 1 (Test Event), "80" was changed to "89" for Niche 1620, BH #4, "83" was changed to "86" for Niche 1620, BH #5. - Lower Lithophysal Zone (Tptpll), Column 9 (Max.), "1840.8" was changed to "1840.7" 	
10. Responsible Manager (Print Name) Paul Dixon		Initials PRD	Date 1-23-04

Table 14. Summary Statistics of Estimated Capillary-Strength Parameter for Lower Lithophysal Zone and Middle Nonlithophysal Zone (DTN: LB0302SCMREV02.002)

Lower Lithophysal Zone (Ttptll)								
Test Event ⁽¹⁾	Location	Interval	Number of Inversions ⁽²⁾	Estimate 1/a [Pa]				
				Mean	Std. Dev. ⁽³⁾	Std. Error ⁽⁴⁾	Min.	Max.
65–69	SYBT-ECRB-LA#1	zone 2	17	534.3	56.8	13.8	447.7	674.1
61, 62	SYBT-ECRB-LA#2	zone 2	21	557.1	56.4	12.3	457.1	676.1
63, 64	SYBT-ECRB-LA#2	zone 3	19	534.8	57.8	13.3	443.1	645.7
70, 71	SYBT-ECRB-LA#3	zone 1	23	452.0	54.7	11.4	382.8	616.6
89	Niche 1620	BH #4	30	671.2	223.2	40.8	356.0	1197.0
86	Niche 1620	BH #5	24	740.5	339.0	69.2	231.1	1840.7
Mean ⁽⁵⁾ =				581.6				
Std. Dev. ⁽⁶⁾ =				105.0				
Middle Nonlithophysal Zone (Ttptmn)								
4, 6, 8	Niche 3107	UM	1	741	—	—	—	—
41, 43	Niche 4788	UL	1	646	—	—	—	—
45, 48	Niche 4788	UM	1	603	—	—	—	—
50, 51	Niche 4788	UR	1	427	—	—	—	—
Mean ⁽⁵⁾ =				604.3				
Std. Dev. ⁽⁶⁾ =				131.5				
<p>(1) See Table 11 on Page 62. Data from all indicated test events were jointly inverted.</p> <p>(2) Each inversion is based on a different realization of the heterogeneous permeability field.</p> <p>(3) Represents estimation uncertainty on account of small-scale heterogeneity (not available for estimates for the middle nonlithophysal zone).</p> <p>(4) Standard error of mean.</p> <p>(5) Represents average for given hydrogeologic unit.</p> <p>(6) Represents spatial variability.</p>								

OCRWM

MODEL COVER SHEET

1. QA: QA
Page 1 of 100

2. Type of Mathematical Model

- Process Model Abstraction Model System Model

Describe Intended Use of Model

The purpose of the Seepage Calibration Model (SCM) is (1) to establish the conceptual basis for the Seepage Model for Performance Assessment (SMPA), and (2) to derive seepage-relevant, model-relevant parameters and their distributions for use in the SMPA and seepage abstraction in support of the Total System Performance Assessment for License Application (TSPA-LA). The SCM is intended to be used only within this Model Report for the estimation of seepage-relevant parameters through calibration of the model against seepage-rate data from liquid-retention tests performed in several niches and in the Cross Drift.

3. Title

Seepage Calibration Model and Seepage Testing Data "

4. ID (including Rev. No. and Change No., if applicable):

MDL-NBS-FS-000004 REV02

6. Total Attachments

7

6. Attachment Number - No. of Pages in Each

I-18, II-4, III-10, IV-2, V-24, VI-4, VII-3

	Printed Name	Signature	Date
7. Originator	S. Finstade	SIGNATURE ON FILE	4/7/03
8. CSO	M. Zhu	SIGNATURE ON FILE	4/07/03
9. Checker	F. Parvoff	SIGNATURE ON FILE	4/07/03
10. QER	K. McFall	SIGNATURE ON FILE	4/7/03
11. Responsible Manager/Lead	S. Finstade	SIGNATURE ON FILE	4/7/03
12. Responsible Manager	J.S.Y. Wang Paul Dixon	SIGNATURE ON FILE	4/7/03

13. Remarks

Block 7. Additional contributors are R.C. Trantz: Seepage testing in niches; P.J. Cook: Seepage testing in ECRS Cross Drift; T.A. Chazotte: Analysis of seepage-rate data from Niches 1620; and G.F. Ahlert: Analysis of seepage-rate data from Niches 3107, 3650, and 4788.

OFFICE OF CIVILIAN RADIOACTIVE WASTE MANAGEMENT
MODEL REVISION RECORD

1. Page: 2 of 150

2. Model Title:
Seepage Calibration Model and Seepage Testing Data

3. DI (including Rev. No. and Change No., if applicable):

MDL-NBS-HS-000004 REV02

4. Revision/Change No.	5. Description of Revision/Change
REV00	Initial Issue.
REV01	The Seepage Calibration Model is recalibrated against new long-term liquid-release test data. The entire model documentation was revised according to AP-3.10Q, Rev. 2, ICN 3, Step 5.9d)2); the changes were too extensive to use revision tracking of individual modifications.
REV02	Entire model documentation was revised. Side bars are not used because the changes were too extensive to use Step 5.9d)1) per AP-SIII.10Q/Rev.1/ICN 0.

CONTENTS

	Page
ACRONYMS	17
1. PURPOSE	19
2. QUALITY ASSURANCE	21
3. USE OF SOFTWARE.....	23
4. INPUTS.....	27
4.1 DATA AND PARAMETERS.....	27
4.2 CRITERIA	30
4.3 CODES AND STANDARDS	31
5. ASSUMPTIONS	33
5.1 FRACTURE POROSITY	33
5.2 INFORMATION ABOUT BOREHOLE SYBT-ECRB-LA#1	33
6. DISCUSSION OF SEEPAGE CALIBRATION MODEL	35
6.1 MODELING OBJECTIVES AND DEFINITIONS	35
6.1.1 Objectives.....	35
6.1.2 Definitions.....	35
6.1.3 Scientific Notebooks	36
6.2 FEATURES, EVENTS, AND PROCESSES.....	36
6.3 BASE-CASE CONCEPTUAL MODEL	38
6.3.1 Seepage Phenomena and Processes.....	38
6.3.2 Continuum Approach.....	39
6.3.3 Factors and Properties Affecting Seepage During Liquid-Release Tests	42
6.3.3.1 Percolation Flux	43
6.3.3.2 Formation Properties.....	44
6.3.3.3 Drift Geometry.....	46
6.3.3.4 Evaporation Conditions.....	47
6.3.3.5 Lithophysal Cavities.....	49
6.3.4 General Modeling and Data-Analysis Approach	49
6.4 ALTERNATIVE CONCEPTUAL MODELS	52
6.4.1 Discrete Fracture Network Model.....	52
6.4.2 Seepage Governed by Ponding Probability.....	54
6.4.3 Inferring Seepage from Geochemical Data.....	55
6.4.4 Inferring Seepage Threshold Directly From Liquid-Release Tests	55
6.5 DESCRIPTION OF SEEPAGE EXPERIMENTS.....	56
6.5.1 Test Location and Borehole Configuration.....	56
6.5.2 Air-Injection Tests.....	59
6.5.3 Liquid-Release Tests.....	60
6.5.4 Relative Humidity and Evaporation Rate Measurements	65

CONTENTS (continued)

	Page
6.6 MODEL FORMULATION.....	66
6.6.1 Mathematical Model	66
6.6.1.1 Unsaturated Flow	66
6.6.1.2 Onset of Seepage.....	67
6.6.1.3 Incorporation of Evaporation Effects.....	69
6.6.1.4 Estimation of Evaporative Boundary-Layer Thickness	70
6.6.1.5 Summary Description of Inverse Modeling Methodology	72
6.6.2 Development of Forward Model.....	74
6.6.2.1 Generation of Permeability Field	74
6.6.2.2 Mesh Generation	79
6.6.2.3 Boundary Conditions.....	82
6.6.2.4 Initial Conditions.....	83
6.6.3 Inversion.....	83
6.6.3.1 Parameter Selection.....	84
6.6.3.2 Data Selection	87
6.6.3.3 Calibration Results	90
6.6.4 Summary and Compilation of Results	104
6.7 IMPACT OF RELATIVE HUMIDITY ON SEEPAGE.....	107
6.8 DESCRIPTION OF BARRIER CAPABILITY.....	108
7. VALIDATION	113
7.1 LEVEL OF RELATIVE MODEL IMPORTANCE	113
7.2 VALIDATION ACTIVITIES AND CONFIDENCE EVALUATION CRITERIA....	113
7.2.1 Confidence Building during Model Development.....	114
7.2.2 Post-Development Activities.....	115
7.2.2.1 Corroboration with Data from Field Experiments	115
7.2.2.2 Corroboration through Comparison of Data with Pre-Test Model Predictions.....	116
7.2.2.3 Corroboration Through Technical Review by Publication in Refereed Journals.....	117
7.3 RESULTS OF MODEL VALIDATION ACTIVITIES	117
7.4 SUMMARY OF MODEL VALIDATION	129
8. CONCLUSIONS.....	131
8.1 SUMMARY AND CONCLUSIONS	131
8.2 MODEL OUTPUT, UNCERTAINTIES, AND LIMITATIONS.....	133
8.3 ADEQUACY OF INPUT DATA AND MODELING APPROACH	135
8.4 RECOMMENDATIONS	136
8.5 OUTPUT DTNS.....	137
9. INPUTS AND REFERENCES	139
9.1 DOCUMENTS CITED	139
9.2 CODES, STANDARDS, REGULATIONS, AND PROCEDURES	145

CONTENTS (continued)

	Page
9.3 SOURCE DATA, LISTED BY DATA TRACKING NUMBER.....	145
9.4 OUTPUT DATA, LISTED BY DATA TRACKING NUMBER.....	148
10. ATTACHMENTS	149
ATTACHMENT I LIST OF COMPUTER FILES SUBMITTED WITH THIS MODEL REPORT UNDER DTN: LB0302SCMREV02.001.....	I-1
ATTACHMENT II VARIOGRAM FITTING.....	II-1
ATTACHMENT III MESH GENERATION FOR SIMULATION OF SEEPAGE TESTS IN ECRB.....	III-1
ATTACHMENT IV MESH GENERATION FOR SIMULATION OF SEEPAGE TESTS IN NICHE 3107, 3650, AND 4788	IV-1
ATTACHMENT V MESH GENERATION FOR SEEPAGE TEST SIMULATIONS IN NICHE 1620	V-1
ATTACHMENT VI PREPARATION OF SEEPAGE RATE AND RELATIVE- HUMIDITY DATA FOR THE SIMULATION OF LIQUID-RELEASE TESTS IN THE ECRB CROSS DRIFT	VI-1
ATTACHMENT VII EXECUTION OF MULTIPLE INVERSIONS OF DATA FROM ECRB	VII-1

INTENTIONALLY LEFT BLANK

FIGURES

		Page
1.	Schematic showing two fractures intersecting a drift: (a) a two-dimensional fracture network model assumes that all fractures are parallel to the drift axis, preventing flow diversion within the fracture plane; (b) a 2D (and 3D) fracture continuum model considers flow diversion occurring within multiple fracture planes that are approximately perpendicular to the drift axis.	40
2.	Two-dimensional discrete feature model (after Finsterle 2000 [151875], Plate 1): (a) high-resolution permeability field; (b) discrete flow path and discrete seepage behavior	53
3.	Two-dimensional discrete fracture network model (after Liu et al. 2002 [160230], Figures 1 and 2): (a) fracture network; (b) flow paths	53
4.	Schematic geologic map showing approximate location of niches and systematic testing boreholes SYBT-ECRB-LA#1–3. The shape of the openings is approximate.....	57
5.	(a) Capillary-pressure curves and (b) relative-permeability curves for different illustrative van Genuchten parameters.	67
6.	Schematic description of seepage condition. A change in $1/\alpha$ has a greater impact on the seepage threshold saturation than a change in m	69
7.	Relative humidity, temperature, and measured and fitted evaporation rates from experiments conducted outside Niche 1620 (DTN: LB0207NICH5LIQ.001 [160408]). Relative humidity is higher during nights and weekends, and evaporation is decreased accordingly.	71
8.	Relative humidity, temperature, and measured and fitted evaporation rates from experiments conducted inside Niche 1620 (DTN: LB0207NICH5LIQ.001 [160408])	71
9.	Cumulative frequency distribution of the log-transformed permeability values and corresponding cumulative normal probability density function for Niche 1620. Permeability data from DTN: LB0110AKN5POST.001 [156904]; histogram and cumulative probability distribution in DTN: LB0302SCMREV02.001.	75
10.	Empirical post-excavation air-permeability semivariograms and spherical semivariogram model for Niche 1620. See Table 14 for geostatistical parameters of the spherical semivariogram model. Permeability data from DTN: LB0110AKN5POST.001 [156904]; semivariogram in DTN: LB0302SCMREV02.001.	76

FIGURES (continued)

	Page
11. Post-excavation permeability data of Niche 1620, borehole #3 and the corresponding generated permeability values from one representative realization, which honors the measured data. Permeability data from DTN: LB0110AKN5POST.001 [156904]; generated permeabilities in DTN: LB0302SCMREV02.001.....	76
12. Empirical post-excavation air-permeability semivariograms and fitted spherical semivariogram models for Niches 3107, 3650, and 4788. See Table 14 for geostatistical parameters of the spherical semivariogram models. Permeability data from DTN: LB990601233124.001 [105888] and DTN: LB0011AIRKTEST.001 [153155]; semivariograms in DTN: LB0010SCMREV01.001 [154292].....	77
13. Cumulative distribution functions of air permeabilities for Niches 3107, 3650, and 4788. Permeability data from DTN: LB990601233124.001 [105888] and DTN: LB0011AIRKTEST.001 [153155]; cumulative distribution function in DTN: LB0010SCMREV01.001 [154292].....	78
14. Numerical grid with one realization of the permeability field used for the simulation of liquid-release tests conducted in zone 2 of borehole SYBT-ECRB-LA#2. Only half of the drift is simulated because of symmetry. The vertical position of the injection interval (indicated in light gray) is appropriately adjusted for the simulation of seepage experiments conducted in other test zones. Multiple realizations of the permeability field are generated. All mesh files in DTN: LB0302SCMREV02.001.....	80
15. Numerical grid with one realization of the permeability field used for the simulation of liquid-release tests conducted in Niche 1620, (a) borehole #4, (b) borehole #5. In this visualization, the meshes are split into two parts to expose the boreholes (indicated by thick black lines) and the injection interval (thick white lines). Multiple realizations of the permeability field are generated. Note the rough ceilings as well as the left and right slots of Mesh (b). All mesh files in DTN: LB0302SCMREV02.001.....	81
16. Computational meshes and permeability field for 3D seepage calibration model used for the analysis of seepage data from (a) Niche 3650, centered 4.42 m from the collar of borehole UM, (b) Niche 3650, centered 5.64 m from the collar of borehole UM, (c) Niche 3107, and (d) Niche 4788. Note that the meshes are shown from an angle below horizontal to display the ceiling roughness incorporated into Meshes (c) and (d). All mesh files in DTN: LB0010SCMREV01.001 [154292].....	82

FIGURES (continued)

	Page
17. Interference between concurrent liquid-release tests in borehole #3 (21–22 ft) and borehole #5 (28–29 ft). Note that 7/15/2002 is Day 195. Data from DTN: LB0209NICH5LIQ.001 [160796].....	89
18. (a) Flux and (b) saturation distribution at the end of liquid-release testing in zone 2 of borehole SYBT-ECRB-LA#1. Based on output DTN: LB0302SCMREV02.001.....	91
19. Calibration of seepage-rate data from liquid-release tests in zone 2 of borehole SYBT-ECRB-LA#1. Blue symbols represent measured data; the red line is the calculated seepage rate. The measured release rates are shown in dark gray; the black solid line shows the injection rate used in the model. Relative-humidity data are shown as a green dashed line. All curves representing measured data derived from DTN: LB0110ECRBLIQR.002 [156879]; calculated seepage in DTN: LB0302SCMREV02.001.....	92
20. Calibration of seepage-rate data from liquid-release tests in zone 2 of borehole SYBT-ECRB-LA#1. Blue symbols represent measured seepage-rate data; the red lines are the results obtained with 17 calibrated models, each using a different realization of the underlying heterogeneous permeability field. Seepage-rate data derived from DTN: LB0110ECRBLIQR.002 [156879]; calculated seepage in DTN: LB0302SCMREV02.001.....	93
21. Saturation distribution simulated with model calibrated against seepage-rate data from liquid-release tests conducted in zone 2 of borehole SYBT-ECRB-LA#2; (a) initial distribution, (b) after 10 days, (c) 20 days, and (d) 30 days. Triangles indicate seep locations and seepage amount. Based on output DTN: LB0302SCMREV02.001.....	94
22. Calibration of seepage-rate data from liquid-release tests conducted in zone 2 of borehole SYBT-ECRB-LA#2. Blue symbols represent measured data; the red line is the calculated seepage rate. The measured release rates are shown in dark gray; the black solid line shows the injection rate used in the model. Relative-humidity data are shown as a green dashed line. All curves representing measured data are derived from DTN: LB0110SYST0015.001 [160409]; calculated seepage in DTN: LB0302SCMREV02.001.....	96
23. Calibration of seepage-rate data from liquid-release tests conducted in zone 3 of borehole SYBT-ECRB-LA#2. Blue symbols represent measured data; the red line is the calculated seepage rate. The measured release rates are shown in dark gray; the black solid line shows the injection rate used in the model. Relative-humidity data are shown as a green dashed line. All curves	

FIGURES (continued)

	Page
representing measured data are derived from DTN: LB0110SYST0015.001 [160409]; calculated seepage in DTN: LB0302SCMREV02.001.....	96
24. Calibration of seepage-rate data from liquid-release tests conducted in zone 1 of borehole SYBT-ECRB-LA#3. Blue symbols represent measured data; the red line is the calculated seepage rate. The measured release rates are shown in dark gray; the black solid line shows the injection rate used in the model. Relative-humidity data are shown as a green dashed line. All curves representing measured data are derived from DTN: LB0203ECRB LIQR.001 [158462]; calculated seepage in DTN: LB0302SCMREV02.001.....	97
25. Calibration of seepage-rate data from liquid-release tests conducted in interval 10–11 ft of borehole #4 in Niche 1620. Blue symbols represent measured data; the red line is the calculated seepage rate. The measured release rates are shown in dark gray; the black solid line shows the injection rate used in the model. All curves representing measured data are derived from DTN: LB0211NICH5LIQ.001 [160792]; calculated seepage in DTN: LB0302SCMREV02.001.....	98
26. Simulated (a) saturation and (b) flux distribution at the end of liquid-release testing (after 13 days) in interval 10–11 ft of borehole #4 in Niche 1620. Based on output DTN: LB0302SCMREV02.001.....	99
27. Calibration of seepage-rate data from liquid-release tests conducted in interval 28–29 ft of borehole #5 in Niche 1620. Blue symbols represent measured data; the red line is the calculated seepage rate. The measured release rates are shown in dark gray; the black solid line shows the injection rate used in the model. All curves representing measured data are derived from DTN: LB0209NICH5LIQ.001 [160796]; calculated seepage in DTN: LB0302SCMREV02.001.....	100
28. Simulated (a) saturation and (b) flux distribution at the end of liquid-release testing (after 13 days) in interval 28–29 ft of borehole #5 in Niche 1620. Based on output DTN: LB0302SCMREV02.001.....	101
29. Comparison between simulated and measured seepage rates from three liquid-release tests conducted in interval UM 4.88–5.18 of Niche 3107. Measured data derived from DTN: LB0010NICH3LIQ.001 [153144]; calculated seepage in DTN: LB0010SCMREV01.001 [154292].....	102
30. Simulated late-time saturation distribution for liquid-release tests in Niche 4788, intervals (a) UL 6.72–7.93 (11/03/1999), (b) UM 6.10–6.40 (11/16/1999), and (c) UR 5.18–5.48 (12/07/1999). The step in the displayed	

FIGURES (continued)

	Page
grid contains the injection interval. Figure based on DTN: LB0010SCMREV01.001 [154292].....	103
31. Comparison between simulated and measured seepage rates from six liquid-release tests conducted in three different borehole intervals of Niche 4788. Data from a given interval are inverted simultaneously. Measured data derived from DTN: LB0010NICH4LIQ.001 [153145]; calculated seepage in DTN: LB0010SCMREV01.001 [154292].....	104
32. Histograms and related Normal distributions of van Genuchten capillary-strength parameter $1/\alpha$ for (a) the middle nonlithophysal zone, and (b) the lower lithophysal zone. These distributions represent spatial variability. The squares indicate the values obtained at individual locations. For the lower lithophysal zone, the squares represent means from multiple inversions, which are plotted along with the standard error of the mean. (The vertical position of the symbols is of no significance.) Parameters in output DTN: LB0302SCMREV02.002.	105
33. Effect of relative humidity on seepage and evaporation percentages, based on the simulation of a liquid-release test in interval 10–11 ft of borehole #4 in Niche 1620. Flow percentages are plotted 13 days after the start of liquid release. See Figure 34 for the seepage and evaporation rates as a function of time with relative humidity of 85%. Note that flow percentage is calculated relative to liquid-release rate. Simulation results in output DTN: LB0302SCMREV02.001.	108
34. Rates of water released, evaporated, diverted around the niche, stored in the formation above the niche, and captured in the seepage collection system as a function of time. A detailed rate balance on Day 10 (denoted by Example Time) is given in Table 16. Seepage-rate data from DTN: LB0211NICH5LIQ.001 [160792]; simulation results in output DTN: LB0302SCMREV02.001.	109
35. Water collected in the slot on the side of Niche 1620 proving flow diversion around the opening. Liquid was released in interval 28–29 ft of borehole #5. All curves representing measured data are derived from DTN: LB0209NICH5LIQ.001 [160796]; simulation results in output DTN: LB0302SCMREV02.001.	111
36. Liquid-release rates, measured seepage rates, and range of predicted seepage rates containing 90% of the 100 Monte Carlo simulations of the experiment conducted in zone 1 of borehole SYBT-ECRB-LA#2; (a) Event 52, (b) Event 53, and (c) Event 54. All curves representing measured data are derived from	

FIGURES (continued)

	Page
DTN: LB00090012213U.002 [153154]; simulation results in output DTN: LB0302SCMREV02.001.	118
37. Liquid-release rates, measured seepage rates, and range of predicted seepage rates containing 90% of the 100 Monte Carlo simulations of the experiment conducted in zone 2 of borehole SYBT-ECRB-LA#2. All curves representing measured data are derived from DTN: LB00090012213U.002 [153154]; simulation results in output DTN: LB0302SCMREV02.001.	119
38. Liquid-release rates, measured seepage rates, and range of predicted seepage rates containing 90% of the 100 Monte Carlo simulations of the experiment conducted in zone 3 of borehole SYBT-ECRB-LA#2. All curves representing measured data are derived from DTN: LB00090012213U.002 [153154]; simulation results in output DTN: LB0302SCMREV02.001.	120
39. Liquid-release rates, measured seepage rates, and range of predicted seepage rates containing 90% of the 100 Monte Carlo simulations of the experiment conducted in zone 2 of borehole SYBT-ECRB-LA#3. All curves representing measured data are derived from DTN: LB0203ECRBLIQR.001 [158462]; simulation results in output DTN: LB0302SCMREV02.001.	120
40. Liquid-release rates, measured seepage rates, and range of predicted seepage rates containing 90% of the 100 Monte Carlo simulations of the experiment conducted in interval 28–29 ft of borehole #5 in Niche 1620, starting on 05/06/2002. All curves representing measured data are derived from DTN: LB0207NICH5LIQ.001 [160408]; simulation results in output DTN: LB0302SCMREV02.001.	121
41. Liquid-release rates, measured seepage rates, and range of predicted seepage rates containing 90% of the 100 Monte Carlo simulations of the experiment conducted in interval 28–29 ft of borehole #5 in Niche 1620, starting 07/15/2002. Effective validation period is between Day 25 and Day 35. All curves representing measured data are derived from DTN: LB0209NICH5LIQ.001 [160796]; simulation results in output DTN: LB0302SCMREV02.001.	122
42. Liquid-release rates, measured seepage rates, and range of predicted seepage rates containing 90% of the 100 Monte Carlo simulations of the experiment conducted in interval 10–11 ft of borehole #4 Niche 1620. Data for Days 1 through 13 were used for calibration; validation period is between Day 14 and Day 31. All curves representing measured data are derived from DTN: LB0211NICH5LIQ.001 [160792]; simulation results in output DTN: LB0302SCMREV02.001.	123

FIGURES (continued)

	Page
43. Validation of Seepage Calibration Model and Tptpmn seepage-relevant parameters using data from Niche 3107 (Events 1, 2, 3, 4, 7, 9, 10, 11, 12 of Table 12). Linear uncertainty propagation analysis was used to calculate the uncertainty band of the model predictions. All curves representing measured data derived from DTN: LB0010NICH3LIQ.001 [153144]; simulation results in DTN: LB0010SCMREV01.001 [154292].	124
44. Validation of Seepage Calibration Model and Tptpmn seepage-relevant parameters using data from Niche 4788 (Events 40, 42, 44, 47, and 49 of Table 12). Linear uncertainty propagation analysis was used to calculate the uncertainty band of the model predictions. All curves representing measured data derived from DTN: LB0010NICH4LIQ.001 [153145]; simulation results in DTN: LB0010SCMREV01.001 [154292].	126
45. Validation of Seepage Calibration Model and Tptpmn seepage-relevant parameters using data from Niche 3650. Monte Carlo simulations were performed to estimate the prediction range. Measured data are derived from DTN: LB980001233124.004 [136583]; simulation results in DTN: LB0010SCMREV01.001 [154292].	128
46. Comparison between pre-test seepage-rate prediction with preliminary Seepage Calibration Model and observed seepage-rate data. The range of predicted seepage covers the uncertainty band approximately on the 95% confidence level. The pre-test prediction results from DTN: LB0207PRESCMN5.002 [161192]; the seepage data from DTN: LB0209NICH5LIQ.001 [160796].	129

INTENTIONALLY LEFT BLANK

TABLES

		Page
1.	Qualified Software Used in this Report	23
2.	Software Products Exempt from Qualification under AP-SI.1Q	25
3.	Input Data	28
4.	Hydrogeologic Input Parameters.....	29
5.	Mesh Coordinates and Flow Field Used to Calculate Local Percolation Flux	29
6.	Project Requirements and YMRP Acceptance Criteria Applicable to this Model Report.....	30
7.	Scientific Notebooks	36
8.	FEPs Addressed in this Model Report	36
9.	Borehole Designations in Niches	58
10.	Mean and Standard Deviation of Post-Excavation Log-Air-Permeability Values.....	60
11.	Liquid-Release Test Events, Approximate Release Rate, Occurrence of Seepage, and Their Use for Calibration or Validation Purposes.....	62
12.	Boundary-Layer Thickness Estimated Using Equation (11) and Relative Humidity, Temperature, and the Evaporation Data from a Free Water Surface Shown in Figure 7 and Figure 8. Boundary-layer thickness in DTN: LB0302SCMREV02.002 and reflected in meshes of DTN: LB0302SCMREV02.001	72
13.	Geostatistical Parameters of Spherical Semivariogram Models (DTN: LB0302SCMREV02.002).....	78
14.	Summary Statistics of Estimated Capillary-Strength Parameter for Lower Lithophysal Zone and Middle Nonlithophysal Zone (DTN: LB0302SCMREV02.002).....	106
15.	Mass Balance for Typical Seepage Test in Borehole #4 of Niche 1620, on 9/27/2002 at 16:20 (Day 10). Note that the model release includes an ambient infiltration rate of 2.20 mm/year (0.067 ml/min). Measured data derived from DTN: LB0211NICH5LIQ.001 [160792]; simulation results in output DTN: LB0302SCMREV02.001	110

TABLES (continued)

	Page
16. Mean and Standard Deviation of Capillary-Strength Parameter $1/\alpha$ for Lower Lithophysal Zone and Middle Nonlithophysal Zone (DTN: LB0302SCMREV02.002)	134
17. Output DTNs	137

ACRONYMS

2D	two-dimensional
3D	three-dimensional
ACC	Accession Number
AFM	Active Fracture Model
AMR	Analysis/Model Report
BH	borehole
BSC	Bechtel SAIC Company
CS	construction station
DFNM	Discrete Fracture Network Model
DIRS	Document Input Reference System
DTN	Data Tracking Number
EBS	Engineered Barrier System
ECRB	enhanced characterization of repository block
ESF	Exploratory Studies Facility
FEP	features, events, and processes
FOSM	first-order-second-moment
FY	Fiscal Year
LA	License Application
LBNL	Lawrence Berkeley National Laboratory
M&O	Management and Operating Contractor
NRC	U.S. Nuclear Regulatory Commission
PA	Performance Assessment
Q	Qualified
QA	Quality Assurance
SCM	Seepage Calibration Model
SMPA	Seepage Model for Performance Assessment
SN	Scientific Notebook
Std. Dev.	standard deviation
STN	Software Tracking Number
TBV	To Be Verified
TDMS	Technical Data Management System
TH	thermal hydrologic

ACRONYMS (Continued)

THC	thermal hydrologic chemical
TPO	Technical Product Output
Tptpll	lower lithophysal zone of Topopah Spring Tuff
Tptpmn	middle nonlithophysal zone of Topopah Spring Tuff
TSPA	Total System Performance Assessment
TSPA-LA	Total System Performance Assessment for License Application
TSw	Topopah Spring welded unit
TWP	Technical Work Plan
UL	upper left
UM	upper middle
UR	upper right
U.S.	United States
UZ	Unsaturated Zone
UZ Model	Unsaturated Zone Flow and Transport Model
WP	Work Package
YMRP	Yucca Mountain Review Plan

1. PURPOSE

The purpose of this Model Report is to document the Seepage Calibration Model (SCM). The SCM is developed (1) to establish the conceptual basis for the Seepage Model for Performance Assessment (SMPA), and (2) to derive seepage-relevant, model-related parameters and their distributions for use in the SMPA and seepage abstraction in support of the Total System Performance Assessment for License Application (TSPA-LA).

The SCM is intended to be used only within this Model Report for the estimation of seepage-relevant parameters through calibration of the model against seepage-rate data from liquid-release tests performed in several niches along the Exploratory Studies Facility (ESF) Main Drift and in the Cross Drift. The SCM does not predict seepage into waste emplacement drifts under thermal or ambient conditions. Seepage predictions for waste emplacement drifts under ambient conditions will be performed with the SMPA (see upcoming REV 02 of CRWMS M&O 2000 [153314]), which inherits the conceptual basis and model-related parameters from the SCM. Seepage during the thermal period is examined separately in the Thermal Hydrologic (TH) Seepage Model (see BSC 2003 [161530]).

The scope of this work is (1) to evaluate seepage rates measured during liquid-release experiments performed in several niches in the Exploratory Studies Facility (ESF) and in the Cross Drift, which was excavated for enhanced characterization of the repository block (ECRB); (2) to evaluate air-permeability data measured in boreholes above the niches and the Cross Drift to obtain the permeability structure for the seepage model; (3) to use inverse modeling to calibrate the SCM and to estimate seepage-relevant, model-related parameters on the drift scale; (4) to estimate the epistemic uncertainty of the derived parameters, based on the goodness-of-fit to the observed data and the sensitivity of calculated seepage with respect to the parameters of interest; (5) to characterize the aleatory uncertainty of the parameters as a result of spatial variability; (6) to evaluate prediction uncertainty based on linear uncertainty-propagation analyses and Monte Carlo simulations; (7) to validate the SCM during model development, and validate using the post-development activities outlined in the Technical Work Plan (TWP, see below); (8) to provide the technical basis for the resolution of unconfirmed issues previously labeled “to be verified” (TBV); and (9) to provide the basis for a screening argument for certain seepage-related features, events, and processes (FEPs).

The primary caveats and limitations in the scope of this Model Report and the results from the SCM are as follows:

- The seepage models are intended to provide estimates of the seepage flux averaged over a 5 m drift segment (the approximate length of a waste package). The seepage models are not expected to quantitatively predict individual seepage events or the precise spatial seepage distribution along the drift.
- By definition, the derived parameters are related to the specific model structure used, i.e., these parameters are only applicable to a conceptual and numerical model similar to the SCM. (Note that the SCM and the SMPA are compatible in this sense.) The parameters are also process specific and scale dependent, i.e., while they can be

considered optimal for seepage calculations on the drift scale, they are not necessarily applicable to other processes on different scales.

- The effective parameters derived in this Model Report capture many processes and features leading to dripping of formation water into a large underground opening. However, this does not include water dripping as a result of condensate accumulation on the drift surface or other in-drift moisture redistribution processes.

More detailed discussion of the appropriateness of the modeling approach, the sufficiency of the data, and the inherent limitations and caveats can be found throughout this Model Report.

The technical scope, content, and management of this Model Report are described in the planning document *Technical Work Plan for: Performance Assessment Unsaturated Zone* (BSC 2002 [160819], Section 1.13). The software programs GSLIB Module GAMV3 V1.201 (LBNL 2000 [153099]) and EarthVision V4.0 (Dynamic Graphics 2003 [162369]) were used (see Table 1) but not planned in the TWP. There were no other deviations from the TWP. In Section 4.2, criteria for acceptance of this Model Report are identified; no additional criteria were identified in the TWP.

This Model Report revises the Analysis/Model Report (AMR) MDL-NBS-HS-000004 REV 01, *Seepage Calibration Model and Seepage Testing Data* (CRWMS M&O 2001 [153045]) to include new seepage data from liquid-release tests performed in the lower lithophysal zone of the Topopah Spring welded unit (Ttptll). These new data were collected in Niche 1620 and in additional boreholes drilled as part of the systematic testing in the ECRB. Moreover, evaporation at the drift surface has now been incorporated into the model to reduce a potential bias on the estimated parameters. This model enhancement obliterates the need for making the nonconservative evaporation assumption discussed in CRWMS M&O (2001 [153045], Sections 5.6, 7.3, 7.4, and 7.5).

No new testing in the middle nonlithophysal zone of the Topopah Spring welded unit (Ttptmn) was conducted, and thus no new analyses were performed. The previously obtained results are included in this Model Report for completeness.

This Model Report supports the reports that document the SMPA (see upcoming REV 02 of CRWMS M&O 2000 [153314]), seepage abstraction (see upcoming Model Report MDL-NBS-HS-000019 REV 00, which will supersede CRWMS M&O (2001 [154291])), and TSPA-LA. This report also addresses the following issues: The development of a collection system in Niche 1620 for mass balance considerations (see Sections 6.5.3 and 6.8); monitoring and estimation of evaporation effects (see Sections 6.3.3.4, 6.5.4, 6.6.1.3, 6.6.1.4, 6.6.2.3, and 6.6.3.3); inclusion of film flow effects (see Sections 6.1.2, 6.3.3, 6.3.3.2, 6.3.4, and 6.6.3.1); inclusion of effects from small-scale irregularities at the drift surface (see Sections 6.3.3, 6.3.3.2, 6.3.3.3, 6.3.3.5, 6.3.4, 6.6.2.2, 6.6.3, 6.6.3.3, 8.2, and Attachments III–V); justification of the continuum approach (see Sections 6.3.2, 6.3.3.2, 6.3.4, and 6.4.1); discussion of differences between continuum models and discrete fracture network models (see Sections 6.3.2 and 6.4.1); and the use of Niche 1620 data to improve parameter estimates (see Sections 1, 4.1, 6.5, 6.6.2, 6.6.3, 7.3, 7.4, 8.1, and 8.2).

2. QUALITY ASSURANCE

Development of this model report and the supporting modeling activities have been determined to be subject to the Yucca Mountain Project's quality assurance (QA) program as indicated in *Technical Work Plan for: Performance Assessment Unsaturated Zone*, TWP-NBS-HS-000003 REV 02 (BSC 2002 [160819], Section 8.2, Work Package (WP) AUZM09). Approved QA procedures identified in the TWP (BSC 2002 [160819], Section 4) have been used to conduct and document the activities described in this model report. The TWP also identifies the methods used to control the electronic management of data (BSC 2002 [160819], Section 8.4, WP AUZM09) during the modeling and documentation activities.

This model report examines the properties of natural barriers identified in AP-2.22Q, *Classification Criteria and Maintenance of the Monitored Geologic Repository Q-List* as "Quality Level – 1" items important to waste isolation. The report contributes to the analysis and modeling data used to support performance assessment (PA). The conclusions of this model report do not affect the proposed repository design or engineered features important to safety, as defined in AP-2.22Q.

INTENTIONALLY LEFT BLANK

3. USE OF SOFTWARE

The software programs used in this study are listed in Table 1. These are appropriate for the intended application and were used only within the range of validation. They were obtained from Software Configuration Management and qualified under AP-SI.1Q, *Software Management*. The qualification and baseline status of the software programs listed in Table 1 is given in the Document Input Reference System (DIRS).

Table 1. Qualified Software Used in this Report

Software Name	Version	Software Tracking Number	Reference
iTOUGH2	4.0	10003-4.0-00	LBNL 1999 [139918]
iTOUGH2	5.0	10003-5.0-00	LBNL 2002 [160106]
GSLIB Module SISIM	1.203	10001-1.0MSISIMV1.203-00	LBNL 1999 [134136]
GSLIB Module SISIM	1.204	10397-1.0SISIMV1.204-00	LBNL 2000 [153100]
GSLIB Module GAMV2	1.201	10087-1.0MGAMV2V1.201-00	LBNL 1999 [134139]
GSLIB Module GAMV3	1.201	10398-1.0GAMV3V1.201-00	LBNL 2000 [153099]
EarthVision	4.0	10174-4.0-00	Dynamic Graphics 2003 [162369]
AddCoord	1.0	10355-1.0-00	LBNL 2000 [152814]
MoveMesh	1.0	10358-1.0-00	LBNL 2000 [152824]
AddBound	1.0	10357-1.0-00	LBNL 2000 [152823]
Perm2Mesh	1.0	10359-1.0-00	LBNL 2000 [152826]
CutNiche	1.2	10356-1.2-00	LBNL 2000 [152815]
CutNiche	1.3	10402-1.3-00	LBNL 2000 [152828]
CutDrift	1.0	10375-1.0-00	LBNL 2000 [152816]
AddBorehole	1.0	10373-1.0-00	LBNL 2000 [152822]
ECRB-XYZ	.03	30093-V.03	CRWMS M&O 1999 [147402]
EXT	1.0	10047-1.0-00	LBNL 1999 [134141]

The use of the software programs identified in Table 1 is documented in Section 6 and in the supporting scientific notebooks (SNs). A summary description of the programs and their use is given below.

The software program iTOUGH2 V4.0 (LBNL 1999 [139918]) provides forward and inverse modeling capabilities for unsaturated and multiphase flow in fractured porous media. The iTOUGH2 V5.0 (LBNL 2002 [160106]) program has—among other features—the extended capability of efficiently simulating evaporation effects (BSC 2002 [161067], Section 1.2). Both programs are used in this Model Report for simulating liquid-release experiments and predicting seepage rates. Moreover, they solve the inverse problem by automatically calibrating the model against measured data, and calculate prediction uncertainties for model validation.

The GSLIB modules GAMV2 V1.201 and GAMV3 V1.201 (LBNL 1999 [134139]; LBNL 2000 [153099]) analyze spatial correlation of, respectively, two-dimensional (2D) and three-dimensional (3D), irregularly spaced datasets. These programs are used for the geostatistical analysis of air-permeability data.

The GSLIB module SISIM V1.203 (LBNL 1999 [134136]) generates 3D, spatially correlated random fields by means of sequential indicator simulations. It is used in this Model Report to generate spatially correlated fields of log-permeability modifiers. Module SISIM V1.204 (LBNL 2000 [153100]) is an extended version of SISIM V1.203 (LBNL 1999 [134136]), in which coordinates are directly output along with the log-permeability modifiers, making the use of software program AddCoord V1.0 (see below; LBNL 2000 [152814]) unnecessary.

The following utility programs support the generation of computational meshes. The software program MoveMesh V1.0 (LBNL 2000 [152824]) adds a constant to the coordinates of a mesh file, translating the coordinate system. The software program AddBound V1.0 (LBNL 2000 [152823]) adds boundary elements to a mesh file. The software program AddCoord V1.0 (LBNL 2000 [152814]) adds coordinates to the output file of SISIM V1.203 (LBNL 1999 [134136]) in preparation for its use by the software program Perm2Mesh V1.0 (LBNL 2000 [152826]), which maps a field of log-permeability modifiers onto a mesh file. The visualization software EarthVision V4.0 (Dynamic Graphics 2003 [162369]) is used to extract coordinates of the rough ceilings of Niches 3107 and 4788 in preparation for the use of the software program CutNiche V1.2 (LBNL 2000 [152815]), which cuts a niche with a rough ceiling from a mesh file. The software program CutNiche V1.3 (LBNL 2000 [152828]) cuts a smooth niche from a mesh file. The software program CutDrift V1.0 (LBNL 2000 [152816]) cuts a cylindrical drift from a mesh file. The software program AddBorehole V1.0 (LBNL 2000 [152822]) inserts a borehole into a mesh file. The software program ECRB-XYZ V.03 (CRWMS M&O 1999 [147402]) calculates the coordinates of a given ECRB station number, so the location of ECRB test beds can be related to the coordinates of the computational mesh.

The software program EXT V1.0 (LBNL 1999 [134141]) takes the forward output file from iTOUGH2 (V4.0 or V5.0) and converts it into a Tecplot (all versions, see Table 2) input file; this software is used for visualization purposes only.

Table 2 summarizes the commercial off-the-shelf software used in support of this Model Report. This software is exempt from qualification under AP-SI.1Q. Computations performed using the standard functions of the software products listed in Table 2 are described in the model documentation (Section 6) and the cited attachments. For visualization purposes, certain units have been converted using the equation utility of Tecplot. A factor of 1/86,400 was used to convert time from seconds to days; a factor of 1/60,000 was used to convert water flow rates from milliliter per minute (ml/min) to kilograms per second (kg/s), which implies a water density of 1 gram per milliliter (g/ml). All information needed to reproduce the work, including the input, formulae or algorithm, and output, is included in this Model Report and the cited references.

Table 2. Software Products Exempt from Qualification under AP-SI.1Q

Software Name	Version	Platform Information	Used for...
MS EXCEL	97 (SR-2)	PC, Windows 98	Data reduction, computation, graphical representation of output
	2000 (9.0.3821 SR-1)	PC, Windows 98	
	2000 (9.0.3821 SR-1)	PC, Windows 2000 Professional	
MS WORD	2000 (9.0.3821 SR-1)	PC, Windows 98	Word processing
	2000 (9.0.3821 SR-1)	PC, Windows 2000 Professional	
vim	6.0.12	PC, Linux	Text editing
Adobe Illustrator	V8.0.1	Mac, MacOS 9.0.4	Schematic figures
MS PowerPoint	2000 (9.0.3821 SR-1)	PC, Windows 98	
Tecplot	8.0-1-0	Sun, SunOS 5.5.1	Technical figures
	8.0-0-6	PC, Windows 98	
	7.5	PC, Windows 98	
	9.0-3-0	PC, Windows 2000 Professional	
Exceed	V6.1/V5.3	PC, Windows 98	Communication and file transfer between PC and Unix workstation
F-Secure	V5.1 (Build 21)	PC, Windows 2000 Professional	

INTENTIONALLY LEFT BLANK

4. INPUTS

4.1 DATA AND PARAMETERS

All input data and parameters needed for the development of the Seepage Calibration Model (SCM) are obtained from the Technical Data Management System (TDMS). As stated in Section 1, the SCM is used to estimate seepage-relevant parameters through model calibration. In general, calibration is a process of fixing certain parameters considered known, relatively certain, or insensitive, and adjusting others that are unknown, uncertain, or highly sensitive to minimize the misfit between measured data and model output. Input data are measured in or refer to the middle nonlithophysal and the lower lithophysal zones of the Topopah Spring welded unit (the repository units). Appropriate data for the middle nonlithophysal zone have been measured in Niches 3107, 3650, and 4788, and appropriate data for the lower lithophysal zone have been measured in Niche 1620 and in boreholes SYBT-ECRB-LA#1–#3 drilled into the ceiling of the ECRB Cross Drift. Specific input data sets and the associated Data Tracking Numbers (DTNs) are listed in Table 3; specific input parameters are listed in Table 4; Technical Product Output (TPO) used as input to calculate local percolation fluxes is summarized in Table 5. These data and parameters are considered appropriate as input for the development of the SCM for the following reasons:

- *Profile alignments and borehole (BH) survey information* (Table 3). These survey data are considered appropriate as a basis for defining niche geometry and identifying injection elements in the numerical mesh.
- *Air-permeability data* (Table 3). These data are used as a basis for the geostatistical analysis and generation of spatially correlated permeability fields near the niches and the ECRB Cross Drift. The data are location-specific and on the appropriate scale, and thus suitable for representing the local rock properties and the structure of sub-drift-scale heterogeneities.
- *Liquid-release test data* (Table 3). These data are used for calibration and validation of the SCM. Liquid-release test data are appropriate for the calibration of the SCM and the estimation of seepage-relevant parameters, because they reflect the salient processes and features affecting seepage. Moreover, they are taken on a representative scale comparable to that of a waste emplacement drift.
- *Calibrated drift-scale fracture properties for the middle nonlithophysal and lower lithophysal zone of the Topopah Spring welded unit*. Because they are directly measured or derived from data collected at Yucca Mountain, these fracture parameters are considered appropriate to be used as reference input parameters. Only the parameters that are fixed during an inversion, and for which no location-specific data are available, are needed as input; this subset is summarized in Table 4. Because of their small sensitivity on predicted seepage rates (see Section 6.6.3.1), a minor change in any of these input parameters has a negligible impact on the estimated model parameters or the conclusions of this Model Report.

- *Coordinates of the Unsaturated Zone Flow and Transport Model (UZ Model) grid and calculated flow rates for extraction of background percolation flux (Table 5). No direct observation of percolation flux is available. The percolation fluxes calculated by the UZ Model are based on the current understanding of unsaturated flow at Yucca Mountain and are thus considered appropriate.*

Table 3. Input Data

DTN	DIRS #	Data Description
Niche Geometry		
MO0003GSC00096.000	[152167]	ESF Niche 3650 (Niche 2) profile alignment
MO0002GSC00076.000	[152623]	ESF Niche 3650 (Niche 2) borehole as-built information
MO0003GSC00103.000	[152176]	ESF Niche 3107 (Niche 3) profile alignment
MO0002GSC00064.000	[152625]	ESF Niche 3107 (Niche 3) borehole as-built information
MO0008GSC00273.000	[152626]	ESF Niche 4788 (Niche 4) profile alignment
MO0107GSC01069.000 ^{&}	[156941]	ESF Niche 4788 (Niche 4) borehole as-built information
MO0009GSC00332.000	[155370]	ECRB Niche 1620 (Niche 5) profile survey data
MO0107GSC01061.000	[155369]	ECRB Niche 1620 (Niche 5) slot survey data
MO0209GSC02116.000	[160407]	ECRB Niche 1620 (Niche 5) survey data for collars, bottoms, and intervals
LB0301N5CEILNG.001	[161733]	ECRB Niche 1620 (Niche 5) detailed niche ceiling roughness data
Air-Permeability Data		
LB0011AIRKTEST.001	[153155]	Air permeability data from ESF Niche 3650 (Niche 2)
LB990601233124.001	[105888]	Air permeability data from ESF Niches 3107 (Niche 3) and 4788 (Niche 4)
LB0110AKN5POST.001	[156904]	Air permeability data from ECRB Niche 1620 (Niche 5)
LB00090012213U.001	[153141]	Air permeability data from ECRB borehole SYBT-ECRB-LA#2
Liquid-Release Test Data		
LB0010NICH3LIQ.001	[153144]	Liquid-release test data from ESF Niche 3107 (Niche 3), March 1999
LB0010NICH4LIQ.001	[153145]	Liquid-release test data from ESF Niche 4788 (Niche 4), Nov. 1999
LB0207NICH5LIQ.001	[160408]	Liquid-release test data from ECRB Niche 1620 (Niche 5), June 2000
LB0209NICH5LIQ.001	[160796]	Liquid-release test data from ECRB Niche 1620 (Niche 5), June 2002
LB0211NICH5LIQ.001	[160792]	Liquid-release test data from ECRB Niche 1620 (Niche 5), August 2002
LB0110ECRBLIQR.002	[156879]	Liquid-release test data from ECRB borehole SYBT-ECRB-LA#1, Feb. 2001
LB00090012213U.002	[153154]	Liquid-release test data from ECRB borehole SYBT-ECRB-LA#2, May 2000
LB0110SYST0015.001	[160409]	Liquid-release test data from ECRB borehole SYBT-ECRB-LA#2, Oct. 2000
LB0203ECRBLIQR.001	[158462]	Liquid-release test data from ECRB borehole SYBT-ECRB-LA#3, May 2001
^{&} This DTN superseded MO0008GSC00310.000 [152627], which was the source for borehole coordinates available at the time of model development for Niche 4788. Borehole coordinates in both DTNs are identical, i.e., there is no impact on the models, analyses, and conclusions presented in this Model Report.		

Table 4. Hydrogeologic Input Parameters

DTN	DIRS #	Parameter	Value	Units
Middle Nonlithophysal Zone of Topopah Spring Welded Unit (Fracture Parameter for tsw34)				
LB997141233129.001	[104055]	van Genuchten parameter, m	0.608	[dimensionless]
LB997141233129.001	[104055]	Residual liquid saturation, S_{lr}	0.01	[dimensionless]
LB997141233129.001	[104055]	Satiated saturation, S_{ls}	1.00	[dimensionless]
Lower Lithophysal Zone of Topopah Spring Welded Unit (Fracture Parameters for tsw35)				
LB997141233129.001	[104055]	van Genuchten parameter, m	0.611	[dimensionless]
LB997141233129.001	[104055]	Residual liquid saturation, S_{lr}	0.01	[dimensionless]
LB997141233129.001	[104055]	Satiated saturation, S_{ls}	1.00	[dimensionless]

Table 5. Mesh Coordinates and Flow Field Used to Calculate Local Percolation Flux

DTN	DIRS #	TPO Description
LB990701233129.001	[106785]	3D UZ model grid, including coordinates
LB990801233129.003	[122757]	Calculated percolation flux, flow field #3

The collection of the input data used for the development and calibration of the SCM is described in detail in BSC (2001 [158463], Sections 6.2 and 6.11) and is summarized in Section 6.5. The analysis of the seepage-rate data is described in Section 6.6.3. Uncertainties in the input data and parameters are addressed throughout Section 6 and are summarized in Section 8.2.

4.2 CRITERIA

The licensing criteria for postclosure performance assessment are stated in 10 CFR 63 [156605]. The requirements to be satisfied by TSPA are identified in the *Yucca Mountain Project Requirements Document* (Curry and Loros 2002 [157916]). The acceptance criteria that will be used by the Nuclear Regulatory Commission (NRC) to determine whether the technical requirements have been met are identified in *Yucca Mountain Review Plan, Information Only* (YMRP; NRC 2003 [162418]). The pertinent requirements and criteria for this model report are summarized in Table 6.

Table 6. Project Requirements and YMRP Acceptance Criteria Applicable to this Model Report

Requirement Number ^a	Requirement Title ^a	10 CFR 63 Link	YMRP Acceptance Criteria ^b
PRD-002/T-015	Requirements for Performance Assessment	10 CFR 63.114 [156605]	Criteria 1 to 4 for <i>Quantity and Chemistry of Water Contacting Waste Packages and Waste Forms apply to 10 CFR 63.114 (a–c)</i> .
PRD-002/T-016	Requirements for Multiple Barriers	10 CFR 63.115 [156605]	Criteria 1 to 3 for <i>System Description and Demonstration of Multiple Barriers apply to 10 CFR 63.115 (a, b)</i>
^a from Curry and Loros (2002 [157916]) ^b from NRC (2003 [162418], Sections 2.2.1.3.3.3 and 2.2.1.1.3)			

The acceptance criteria identified in Section 2.2.1.3.3.3 of the YMRP (NRC 2003 [162418]) are given below, followed by a short description of their applicability to this Model Report:

- Acceptance Criterion 1, *System Description and Model Integration are Adequate*:
The physics of the seepage phenomenon is adequately incorporated into an appropriate seepage process model based on a sufficient technical basis, supported by field data and sensitivity analyses. The approach and model is documented in a transparent and traceable manner.
- Acceptance Criterion 2, *Data are Sufficient for Model Justification*:
Hydrological values used are adequately justified and described. Liquid-release tests were designed and conducted with the explicit objective of providing sufficient seepage-relevant data for the formulation of the conceptual model and for the calibration and validation of the seepage process model. Sufficient seepage-rate data were collected to characterize the seepage-related properties of the natural system.
- Acceptance Criterion 3, *Data Uncertainty is Characterized and Propagated Through the Model Abstraction*
The parameters used in and derived by the seepage process model are technically defensible; they are based on and consistent with available data from Yucca Mountain; uncertainties and variabilities are evaluated and reasonably accounted for and adequately represented.

- Acceptance Criterion 4, *Model Uncertainty is Characterized and Propagated Through the Model Abstraction*:

The selected modeling approach is consistent with available data and current scientific understanding; alternative modeling approaches to the seepage process model are discussed.

The acceptance criteria identified in Section 2.2.1.1.3 of the YMRP (NRC 2003 [162418]) are given below, followed by a short description of their applicability to this Model Report:

- Acceptance Criterion 1, *Identification of Barriers is Adequate*:

Barriers are adequately identified and linked to their capability.

- Acceptance Criterion 2, *Description of Barrier Capability to Isolate Waste Is Acceptable*:

The capability of the barrier to prevent or substantially reduce the rate of movement of water is consistent with the definition of a barrier at 10 CFR 63.2, and is adequately identified and described, including the uncertainty associated with the barrier's capability.

- Acceptance Criterion 3, *Technical Basis for Barrier Capability is Adequately Presented*:

The technical basis for assertions of barrier capability is commensurate with the importance of the barrier's capability and the associated uncertainties.

4.3 CODES AND STANDARDS

No specific, formally established standards have been identified as applying to this modeling activity.

INTENTIONALLY LEFT BLANK

5. ASSUMPTIONS

This section contains a list of assumptions used for the development of the Seepage Calibration Model (SCM). Each statement of an assumption is immediately followed by the rationale for why the assumption is considered valid or reasonable. Assumptions in immediately preceding upstream documentations have no significant impact on the results of the present model or they are discussed in the following subsections.

5.1 FRACTURE POROSITY

Assumption: Fracture porosity is assumed to be approximately 1%.

Rationale: A fracture-porosity estimate for the lower lithophysal zone of 0.96% is provided in DTN: LB0205REVUZPRP.001 [159525]. As demonstrated in Section 6.6.3.1, fracture porosity has a negligible impact on late-time, near-steady seepage rates and has thus a negligible impact on the estimated parameters. Therefore, no further confirmation is required for this assumption. The assumption is used for the seepage models of the lower lithophysal zone, discussed throughout Sections 6 and 7.

5.2 INFORMATION ABOUT BOREHOLE SYBT-ECRB-LA#1

Assumption: Borehole SYBT-ECRB-LA#1 is upward-inclined at nominal angle of 15° from the drift axis. Packers are set to isolate an injection zone between 3.0 m and 4.9 m (zone 2) from the collar (BSC 2001 [158463], p. 241).

Rationale: The borehole inclination and interval location information is taken from a reliable and controlled source. A potential deviation between the nominal and as-built drilling inclination or packer location is expected to be minor and would have no significant impact on the estimated parameters or conclusions presented in this Model Report. This assumption, used in Section 6.6.2.2 and Table III-1, does not require further confirmation.

INTENTIONALLY LEFT BLANK

6. DISCUSSION OF SEEPAGE CALIBRATION MODEL

6.1 MODELING OBJECTIVES AND DEFINITIONS

6.1.1 Objectives

The following sections describe the development, calibration, and validation of the Seepage Calibration Model (SCM). The purpose of the SCM is to provide a methodological and conceptual basis for the subsequent development of the Seepage Model for Performance Assessment (SMPA). Furthermore, seepage-relevant parameters are derived as input to the abstraction for drift seepage.

The seepage models are not expected to accurately predict individual seepage events or the precise spatial distribution along the drift. Instead, the seepage models are intended to provide estimates of the seepage flux averaged over a 5 m drift segment (the approximate length of a waste package) as a function of the percolation flux on the drift scale. The seepage experiments and modeling approach are designed to address seepage on this specific scale.

6.1.2 Definitions

Seepage is defined as flow of liquid water into an underground opening such as a niche, the ECRB Cross Drift, or a waste emplacement drift; the water originates from the rock mass and forms drops that subsequently detach from the opening surface. According to this definition, seepage does not include advective or diffusive vapor flow into the opening or condensation of water vapor on surfaces, which may lead to drop formation and drop detachment. Some of the water entering an underground opening may also evaporate or flow along the wall, thus not contributing to seepage in the narrow sense defined here. Note, however, that evaporation, condensation, and film flow along the surface of the opening affect the moisture conditions in the waste emplacement drift and may thus impact repository performance.

Seepage rate is the amount of water seeping into the opening per unit of time.

Seepage flux is defined as the seepage rate per unit of projected drift wall area.

Seepage percentage is defined as the ratio of seepage flux divided by percolation flux. As outlined in Section 6.1.1, a five-meter long drift section (the approximate length of a waste package) is used as the reference scale for calculating percolation and seepage fluxes. In the context of liquid-release tests, seepage percentage is the ratio of the rate or amount of water that seeped into the niche divided by the rate or amount of water released.

Seepage threshold is defined here as the critical percolation flux below which no seepage occurs, i.e., all percolating water is diverted around the opening, evaporates, or flows along the drift surface as a thin water film. Note that Philip et al. (1989 [105743]) did not consider evaporation and film-flow effects when defining the critical seepage conditions.

Seepage fraction is defined as the fraction of waste packages affected by seepage. This is equivalent to the fraction of 5 m drift sections that exhibit a nonzero seepage percentage.

6.1.3 Scientific Notebooks

The scientific notebooks (SN) listed in Table 7 provide details potentially needed to reproduce the modeling work discussed in this Model Report.

Table 7. Scientific Notebooks

LBNL Scientific Notebook ID	M&O Scientific Notebook ID	Relevant Pages	Citation
YMP-LBNL-SAF-1	SN-LBNL-SCI-087-V1	1–4, 100–102, 139	Finsterle 1999 [153448]
YMP-LBNL-SAF-2	SN-LBNL-SCI-171-V1	1–2, 34–42, 47–95	Finsterle 2002 [161043]
YMP-LBNL-SAF-3	SN-LBNL-SCI-228-V1	1–26, 31–37	Wang 2003 [161456]
YMP-LBNL-SAF-TG-1	SN-LBNL-SCI-223-V1	9–44	Wang 2003 [161456]
YMP-LBNL-RCT-DSM-1	SN-LBNL-SCI-157-V1	1–37	Trautz 2001 [161044]
YMP-LBNL-RCT-2	SN-LBNL-SCI-156-V1	35–45	Trautz 2001 [156903]
YMP-LBNL-JSW-6C	SN-LBNL-SCI-122-V1	108–123	Wang 1999 [153449]
YMP-LBNL-DSM-CFA-1	SN-LBNL-SCI-180-V1	4–6, 8–10, 13, 15–58	Ahlers 2002 [161045]
YMP-LBNL-YSW-JH-2	SN-LBNL-SCI-143-V1	124	Hinds 2001 [155955]
YMP-LBNL-RCT-RH-1	SN-LBNL-SCI-175-V1	27–29	Hedegaard 2002 [161046]

6.2 FEATURES, EVENTS, AND PROCESSES

Table 8 contains a list of Features, Events, and Processes (FEPs) taken from the LA FEP List (DTN: MO0301SEPFEPS1.000 [161496]). The LA FEP List is a revision to the previous project FEP list (Freeze et al. 2001 [154365]) used to develop the list of included FEPs in the *Technical Work Plan for: Performance Assessment Unsaturated Zone* (BSC 2002 [160819], Table 2-6). The selected FEPs are those taken from the LA FEP List that are associated with the subject matter of this report, regardless of the anticipated status for exclusion or inclusion in TSPA-LA as represented in BSC (2002 [160819], Table 2-6). The results of this model are part of the basis for the treatment of FEPs as discussed in the *Total System Performance Assessment-License Application Methods and Approach* (BSC 2002 [160146], Section 3.2.2). The cross-reference for each FEP to the relevant sections of this report is also given in Table 8.

Table 8. FEPs Addressed in this Model Report

FEP No.	FEP Name	Section Where FEP is Addressed	Summary Description
1.1.02.00.0B	Mechanical effects of excavation/ construction in EBS	6.3.3.2, 6.3.4, 6.5.2, 6.6.3.1, 6.6.3.3	Excavation effects are taken into account through the use of post-excavation air-permeability data and the estimation of a capillary-strength parameter determined from seepage data that reflect seepage from an excavation-disturbed zone around a large opening (niche or drift).

1.2.02.01.0A	Fractures	6.3.2, 6.3.3.2, 6.3.4, 6.5.2, 6.6.3.1, 6.6.3.3	Fracture properties are determined from post-excavation air-permeability data and through estimation of seepage-relevant fracture continuum capillary-strength parameter
2.1.08.02.0A	Enhanced influx at the repository	6.3.1, 6.3.2, 6.3.3, 6.6, 6.8	The impact of an underground opening on the unsaturated flow field (including dry-out from evaporation, capillary-barrier effect, and flow diversion around the drift) is captured in the seepage process model by solving the equations governing unsaturated flow in fractured porous media and by specifying appropriate boundary conditions at the drift wall. It leads to reduced (not enhanced) influx.
2.2.01.01.0A	Mechanical effects of excavation/ construction in the near field	6.3.3.2, 6.3.4, 6.5.2, 6.6.3.1, 6.6.3.3	Excavation effects are taken into account through the use of post-excavation air-permeability data and the estimation of a capillary-strength parameter determined from seepage data that reflect seepage from an excavation-disturbed zone around a large opening (niche or drift).
2.2.03.02.0A	Rock properties of host rock and other units	4.1, 6.5.2, 8.2	Location-specific rock properties are (1) taken from UZ Model, (2) determined from local air-permeability data (including measures of heterogeneity and spatial correlation), and (3) determined through inverse modeling. Variability is accounted for on various scales.
2.2.07.02.0A	Unsaturated groundwater flow in the geosphere	6.3.2, 6.6.1.1	Unsaturated flow processes are accounted for in the conceptual and mathematical model.
2.2.07.04.0A	Focusing of unsaturated flow (fingers, weeps)	6.3.1, 6.3.3.1, 6.6.2.1, 6.6.3.3	Explicitly modeled heterogeneity induces flow focusing. Impact of small-scale flow focusing effects on seepage are included in effective parameter.
2.2.07.08.0A	Fracture flow in the UZ	6.3.2, 6.3.3.2, 6.6.2.1	Liquid flow through unsaturated fractures is simulated using site-specific fracture properties; explicit inclusion of heterogeneity leads to flow channeling.
2.2.07.09.0A	Matrix imbibition in the UZ	6.3.3.2	Matrix imbibition is considered small under near-steady seepage conditions and is therefore neglected.
2.2.07.18.0A	Film flow into the repository	6.1.2, 6.3.2, 6.3.3.2, 6.3.4, 6.6.3.1	If water originating from film flow seeps into the opening during a liquid-release test, it is reflected in the corresponding seepage data point used for model calibration, i.e., film flow is automatically accounted for in the estimated seepage-related parameter and thus in the prediction of seepage into waste emplacement drifts.
2.2.07.20.0A	Flow diversion around repository drifts	6.3.1, 6.3.2, 6.3.3, 6.6, 6.8	The impact of an underground opening on the unsaturated flow field (including dry-out from evaporation, capillary-barrier effect, and flow diversion around the drift) is captured in the seepage process model by solving the equations governing unsaturated flow in fractured porous media and by specifying appropriate boundary conditions at the drift wall. Drift shadow is simulated as a result of seepage exclusion.

6.3 BASE-CASE CONCEPTUAL MODEL

6.3.1 Seepage Phenomena and Processes

To understand the seepage process and to identify the factors affecting seepage, a description is given of the fate of water percolating through the unsaturated zone of Yucca Mountain, eventually encountering the immediate vicinity of a waste emplacement drift. This description is based on and consistent with the related discussion found in the scientific literature (see, for example, Philip et al. (1989 [105743]) and Finsterle (2000 [151875]) and references therein).

Water that penetrates the ground surface and reaches a depth that is unaffected by evapotranspiration starts to percolate downwards, driven by gravity and capillary forces. The detailed flow path is determined by the degree of fracturing, fracture geometry, orientation, and connectivity, as well as the hydrogeologic properties of the fractures and the matrix. Depending on these factors, the water phase in the unsaturated fracture network will either disperse or focus along the flow path. Tilted contacts between hydrogeologic units (especially between welded and nonwelded tuffs) may affect the overall flow pattern or lead to a change in the frequency and spacing of flow channels. However, the channeling process is likely to diminish with depth. As flow concentration continues to occur, the distance between the individual channels carrying focused flow increases, so the likelihood of two channels meeting and merging decreases with depth. Flow focusing and dispersion of flow paths also happens *within* a rough-walled fracture, where asperity contacts and locally larger fracture openings lead to small-scale redistribution of water within the fracture. A general discussion of channeling effects under unsaturated flow conditions can be found in Birkholzer and Tsang (1997 [119397]). Flow focusing is important for seepage, because seepage depends on the local rather than average percolation flux.

As water approaches the potential waste emplacement drift (one to several meters above the drift ceiling), conditions change in several ways, all affecting the amount of water that will eventually seep into the opening. The water may first encounter a dry-out zone caused by drift ventilation. The dry-out zone may also develop as a result of increased temperatures, in which case it is referred to as a boiling zone. Under these thermal conditions, the dry-out zone may be surrounded by a two-phase zone in which heat-pipe effects determine water, vapor, and heat fluxes, and a condensation zone with increased saturation. (Note that ventilation and elevated temperatures are limited in time and thus do not affect long-term seepage.)

In addition, formation properties around the openings are likely to be altered as a result of stress redistribution during drift excavation, which leads to local opening or partial closing of fractures and potentially the creation of new fractures. Thermal expansion of the rock matrix may also induce changes in apertures. Finally, the local chemical environment, which is altered by evaporation and thermal effects, may lead to dissolution and precipitation of minerals, again affecting porosity, permeability, and capillarity of the fracture system as well as fracture-matrix interaction. Again, such thermally and geochemically induced alterations were of no significance during the ambient liquid-release tests analyzed by the SCM. In general, however, all the conditions discussed above lead to a flow pattern in the vicinity of a waste emplacement drift different from that in the undisturbed formation under ambient conditions.

Provided that liquid water penetrates the boiling or dry-out zone (for details, see BSC (2003 [161530])), it reaches the immediate vicinity of the drift wall, where (at least under ambient conditions) a boundary layer of increased saturation is expected to develop as a result of the capillary barrier effect (Philip et al. 1989 [105743]). The water is prevented from seeping into the drift because of capillary suction, which retains the wetting fluid in the pore space. This barrier effect leads to a local saturation build-up and the development of a boundary layer in the formation immediately adjacent to the drift. If permeability and capillarity of the fracture network within this boundary layer are sufficiently high, all or a portion of the water is diverted around the drift under partially saturated conditions. Locally, however, the water potential in the formation may be higher than that in the drift, and water exits the formation. At the drift surface, the water either evaporates, or follows the inclined, rough wall in a thin film, or forms a drop that grows and eventually detaches (Or and Ghezzehei 2000 [144773]). Only this last mechanism is considered drift seepage according to the definition of Section 6.1.2.

To summarize, the rate of water dripping into an opening in an unsaturated geologic formation is expected to be less than the downward percolation rate because (1) the cavity acts as a capillary barrier, (2) water may flow along the drift surface without dripping into the opening, and (3) water may evaporate. Even if the seepage threshold were exceeded and seepage occurred, the seepage flux would be lower than the percolation flux.

Section 6.3.2 describes the rationale and justification for using a heterogeneous continuum model for the simulation of drift seepage. Section 6.3.3 discusses specific factors and properties affecting seepage during liquid-release tests and how they are incorporated into the conceptual model.

6.3.2 Continuum Approach

The Seepage Calibration Model is conceptualized as a heterogeneous continuum model. The continuum approach can be considered appropriate for seepage studies if it is capable of predicting seepage rates for a drift in a fractured formation.

Water flow through the TSw and seepage into openings at Yucca Mountain occurs predominantly through the fracture network, suggesting that a discrete fracture network model is more appropriate than a fracture continuum model for the reproduction and prediction of drift seepage. However, it is important to recognize that flow diversion around the opening occurs primarily *within* the fracture plane (in-plane diversion). The need to engage multiple fractures arises only if the fracture is too short and the flow path within the fracture plane is interrupted. In this case, water is diverted into the next connected fracture. This fracture is again unlikely to be perfectly parallel to the drift axis, allowing the in-plane flow-diversion process to continue. The situation is schematically illustrated in Figure 1, which shows two fractures intersected by a drift. In Figure 1a, the two fractures are aligned with the drift axis (which is an implicit assumption made in all two-dimensional fracture network models used to predict drift seepage). As an artifact of this specific and unrealistic fracture orientation, in-plane flow diversion is prevented, and the resulting impact of discreteness on seepage is exaggerated. Two-dimensional fracture network models (including those shown by Finsterle (2000 [151875], Plate 1) and Liu et al. (2002 [160230], Figures 1–6)) represent extreme cases that may not be representative of and appropriate for site-specific seepage modeling. (The advantages and disadvantages of the discrete fracture network model are further discussed in Section 6.4.1).

In Figure 1b, the fractures are approximately perpendicular to the drift axis. Flow diversion occurs within the fracture plane, a process that is appropriately captured by a heterogeneous fracture continuum model even for a single fracture. In-plane flow occurring in multiple fractures can be readily combined and described by an effective fracture continuum.

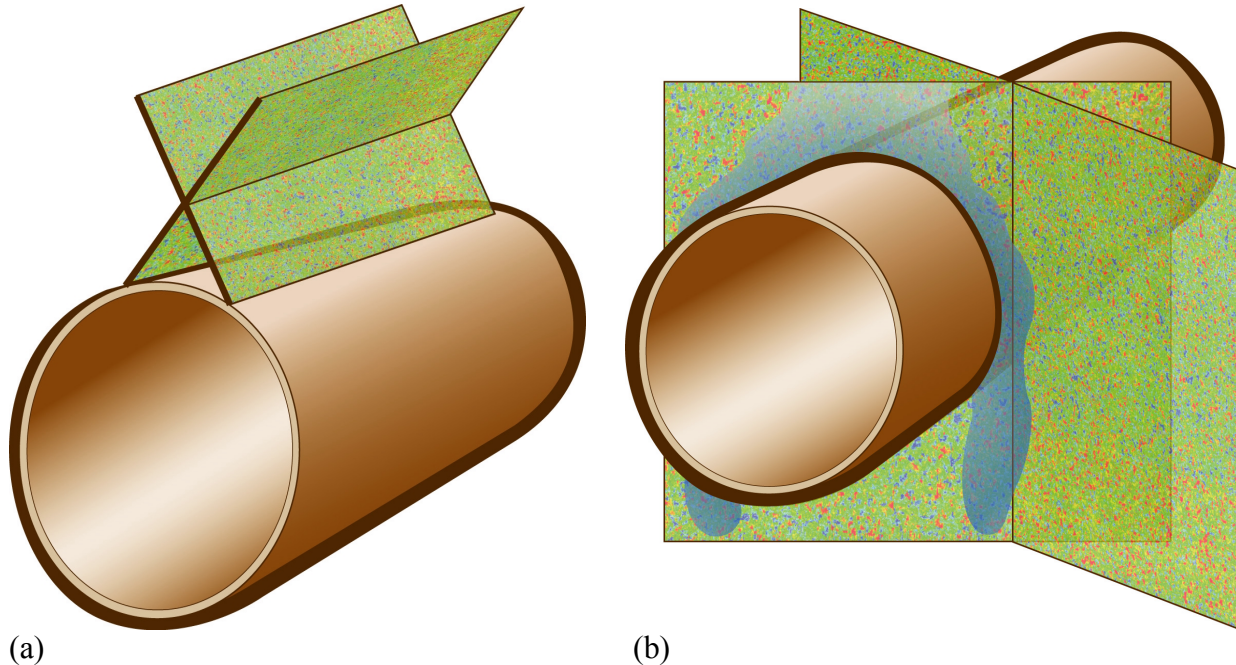


Figure 1. Schematic showing two fractures intersecting a drift: (a) a two-dimensional fracture network model assumes that all fractures are parallel to the drift axis, preventing flow diversion within the fracture plane; (b) a 2D (and 3D) fracture continuum model considers flow diversion occurring within multiple fracture planes that are approximately perpendicular to the drift axis.

Given the significance of in-plane flow diversion around the drift in combination with relatively high fracture density of variable orientation (Mongano et al. 1999 [149850], pp. 65–72, 76–79), a three-dimensional, heterogeneous fracture continuum model is an appropriate conceptualization. It captures the relevant processes more realistically than, for example, a two-dimensional discrete fracture network model.

In addition, the appropriateness of the continuum approach to simulate flow through fractured rock was studied by Jackson et al. (2000 [141523]) using synthetic and actual field data. They concluded that heterogeneous continuum representations of fractured media are self-consistent, i.e., appropriately estimated effective continuum parameters are able to represent the underlying fracture-network characteristics.

Finsterle (2000 [151875]) demonstrated that seepage into underground openings excavated from a fractured formation could be simulated using a model based on the continuum concept, provided that the model is calibrated against seepage-relevant data (such as data from liquid-release tests). Synthetically generated data from a model that exhibits discrete flow and seepage behavior were used to calibrate a simplified fracture continuum model. The calibrated continuum model was used to predict average seepage rates into a sufficiently large section of an under-

ground opening for low percolation fluxes, i.e., conditions significantly different from those encountered during calibration. The extrapolation from high-rate liquid-release tests to low-rate percolation fluxes is equivalent to the extrapolation from the calibration runs performed with the SCM to the predictive simulations that will be performed by the SMPA. As discussed in Finsterle (2000 [151875]), the extrapolated seepage predictions performed with the continuum model were consistent with the synthetically generated data from the discrete-feature model under low percolation conditions. This demonstrates that (1) the calibrated continuum model and discrete-feature model yield consistent estimates of average seepage rates, and (2) that the continuum approach is appropriate for performing seepage predictions even if extrapolated to percolation fluxes that are significantly lower than those induced by liquid-release tests, which were performed at relatively high injection rates to generate seepage data useable for model calibration. Note that the discrete-feature model used in the study makes the extreme assumption that all fractures are oriented parallel to the drift axis, as discussed above and illustrated in Figure 1a. Even under these unfavorable conditions, the continuum approach proved to be appropriate.

Note that the fracture density and hydraulic parameters used by Liu et al. (2002 [160230]; see also Figure 3a below) result in very little flow diversion around the opening. This is a direct result of the unrealistic assumption that all fractures are parallel to the drift axis, which prevents in-plane flow diversion. In such a two-dimensional discrete fracture network model, flow diversion occurs only if the fracture density and/or the capillary-strength parameter are high. This was recognized by Liu et al. (2002 [160230], p. 15-8), who concluded that fracture network models need to be *three-dimensional* for them to be able to realistically evaluate the capillary barrier effects in fractured formations. As discussed above, in-plane flow diversion in a three-dimensional fracture network can be appropriately represented by a heterogeneous continuum model. A calibrated continuum model is appropriate even in the extreme case where all fractures are perfectly parallel to the drift axis, as demonstrated by Finsterle (2000 [151875]) and discussed in the previous paragraph. Note that the synthetic fracture network and hydraulic parameters used in the discrete model of Finsterle (2000 [151875]; see also Figure 2a below) induced some flow diversion. This difference in flow diversion capability between the models of Finsterle (2000 [151875]) and Liu et al. (2002 [160230]) is caused by their respective parameter choices. This difference, however, does not affect the finding that the continuum approach captures the seepage-relevant processes more appropriately than two-dimensional discrete fracture network models. The advantages and disadvantages of the discrete fracture network model are further discussed in Section 6.4.1.

The continuum approach is considered appropriate for seepage studies if applied within the framework described in this Model Report. Inverse modeling should be used for the estimation of process-specific, model-related, and scale-dependent parameters, and the same or similar conceptual model should be used for the subsequent seepage predictions, specifically the SMPA.

Adopting the continuum approach, water flow under unsaturated conditions is governed by Richards' equation (Richards 1931 [104252]), which states that isothermal flow of water in a porous medium or rough-walled fracture occurs under the combined effect of gravitational and capillary forces, that flow resistance is a function of saturation, and that (for the purposes of this representation) movement of the nonwetting air phase can be neglected. This general concept is believed reasonable, because gravitational force is ubiquitous, and rough-walled or partially filled fractures exert varying degrees of capillary pressure at different saturation levels.

Relative permeability and capillary pressure are described as continuous functions of effective liquid saturation, following the expressions given by the van Genuchten-Mualem model (van Genuchten 1980 [100610], pp. 892–893) as implemented in the iTOUGH2 code (BSC 2002 [161066], Section 4.3.2). The applicability of relative permeability and capillary pressure functions is appropriate also for fractures that are rough-walled and/or partially filled with porous material. The constant of proportionality—relative permeability—is saturation-dependent because porous-medium continuum laws also apply to water flow through fractures filled with porous material, and in the absence of fracture fillings, the thickness of the water film and connectivity of liquid islands on the fracture surface are saturation dependent (Tokunaga and Wan 1997 [139195]).

Capillary strength (represented by the $1/\alpha$ parameter) and permeability are considered uncorrelated. The functional relationship describing the potential correlation between permeability and capillary strength is unknown. An increase in the effective (continuum) permeability of a fracture block may be attributed to larger fracture apertures (which would reduce capillary strength) or to an increase in fracture density (which would not affect capillary strength). The capillary-strength parameter $1/\alpha$ is taken to be constant for a given test bed, and will be subjected to estimation by inverse modeling.

The van Genuchten-Mualem model is the basic model used in the suite of UZ models (CRWMS M&O 2000 [141187], Sections 5 and 6.4.4); it is chosen in this work to ensure consistency. The mountain-scale models may use a modified version of the van Genuchten-Mualem functions to account for the fact that unsaturated flow is restricted to a limited number of (active) fractures and that flow within a fracture is likely to be channelized. Both effects lead to different effective saturations determining capillary pressure and relative permeability, and they reduce fracture-matrix interaction. This revised model was developed by Liu et al. (1998 [105729]) and is referred to as the Active Fracture Model (AFM). For drift-scale seepage models under ambient conditions, the standard van Genuchten-Mualem model is employed rather than the AFM, because (1) flow segregation into active and inactive portions of the fracture network is a large-scale effect not engaged during the short-distance liquid-release tests; (2) flow channeling within fractures is partially accounted for through explicit modeling of small-scale heterogeneity; (3) the correction of the fracture-matrix interface area (the main effect captured by the AFM) is insignificant for seepage because of insignificant matrix imbibition during the calibration period (see Section 6.3.3.2); and (4) the potential impact of all AFM effects on seepage are automatically reflected in the observed seepage-rate data, which are used to estimate an effective capillary-strength parameter suitable for simulations with a conceptually consistent seepage-prediction model.

This general model conceptualization is consistent with that of the UZ Model (CRWMS M&O 2000 [141187], Section 5 and 6.4.2). The calibration process and the consistent conceptualization in the downstream models (specifically the SMPA) make this a valid and reasonable approach.

6.3.3 Factors and Properties Affecting Seepage During Liquid-Release Tests

Seepage is a process that occurs at the interface between the natural and engineered systems. Consequently, seepage is not only affected by hydrogeological factors (such as formation properties and flow conditions in the natural environment), but also by the engineered system

itself. This second set of factors affecting the amount and distribution of seepage includes the design of the repository and waste emplacement drifts (location and geometry), the method of construction (excavation effects, drift surface roughness, ground support, backfill), and the conditions within the drifts (heat load and ventilation, which determine the relative humidity, evaporation potential, and the extent of the dry-out zone).

The engineered barriers in the waste emplacement drift will be exposed to seeping water if (1) a flow channel exists that carries water through the (potentially dry) zone around the drift, (2) the local percolation flux in this flow channel is high enough to overcome the local seepage threshold, and (3) the water droplets forming at the drift wall do not evaporate or dissipate in a thin film flowing along the surface.

The following subsections describe in more detail the key factors affecting drift seepage and how they are included in the base-case conceptual model.

The most important factors are the magnitude of the local percolation flux in relation to the formation's permeability, the strength of the capillary forces in the fractures, the connectivity of the fracture network in the boundary layer, the local topography of the rough drift wall, and the thermodynamic conditions in the drift.

6.3.3.1 Percolation Flux

General Description

The magnitude of the percolation flux is a key factor determining seepage. Seepage is initiated if the local percolation fluxes in individual flow channels and their accumulation near the drift ceiling exceeds the diversion capacity of the capillary barrier (which is caused by the presence of the drift), the evaporation potential of the atmosphere in the drift, and the capacity of thin films to carry water along the drift surface. Because it is the local (rather than average) percolation flux that controls the onset of seepage, the distribution of flow channels on all scales becomes a critical aspect for drift seepage. Flow focusing could concentrate water onto a particular drift segment and lead to a flux that exceeds the seepage threshold. On the other hand, if flow is concentrated in one location, flow will be reduced in other areas (potentially below the prevalent seepage threshold) and may lead to overall less seepage. Therefore, the distribution of flow channels, their frequency, width, and hydrologic properties determine the seepage probability and seepage amounts.

The spatial distribution of flow channels may change with the average percolation flux and potentially with time. The flux in a flow channel may be near steady state or episodic with a wide spectrum, ranging from high-frequency fluctuations triggered by flow instabilities, to intermediate variabilities in percolation fluxes in response to changing weather conditions, to long-term variations from climate changes.

In summary, the local (rather than average) percolation flux reaching the drift is the most important factor determining whether seepage occurs, the seepage rate, and the spatial and temporal distribution of seepage events.

Model Conceptualization

The actual percolation flux and its distribution are unknown. Estimates of the average, steady-state percolation fluxes at the locations of the liquid-release tests are taken from the UZ Model (see Section 6.6.2.3) and applied at the top of the corresponding drift seepage models. Note that large-scale redistribution of infiltration and percolation fluxes is captured in the mountain-scale UZ Model; intermediate-scale flow concentrations is accounted for in the TSPA calculations through the use of a probabilistic flow focusing factor. Small-scale flow concentration is included in the SCM by explicitly modeling small-scale heterogeneities (see Section 6.6.2.1).

The transient SCM simulations capture the time-dependent boundary conditions, saturation, and seepage-rate changes induced by the intermittent water release during seepage testing. Potential occurrence of small-scale, high-frequency episodic flow events is reflected in the seepage-rate data used for calibration. The cumulative effect of these episodic events on seepage is therefore appropriately captured in the estimation of an effective capillary-strength parameter. Low-frequency fluctuations in the background percolation flux on account of weather-condition or climate changes are of no significance because of the comparatively short duration of the liquid-release tests. In summary, the high-frequency episodic flow events are captured in the effective, seepage-relevant capillary-strength parameter, whereas the low-frequency transient events are accounted for in the UZ Model, which provides a time-dependent percolation flux as input to the seepage TSPA calculations. Additional issues related to the amount, variability, and uncertainty of percolation flux, lateral flow diversion, as well as large- and intermediate-scale flow concentration are also addressed by the UZ Model, seepage abstraction, and TSPA calculations.

6.3.3.2 Formation Properties

General Description

The key formation properties determining the effectiveness of the capillary barrier are (1) the capillary strength and (2) the tangential conductivity in the boundary layer near the drift wall. Geologic formations with strong capillarity and high tangential conductivity exhibit a high seepage threshold (i.e., low seepage), whereas a weak capillary barrier effect (i.e., high seepage) is expected if water retention is small or if the tangential permeability is insufficient to promote flow diversion.

Porous formations with strong capillarity tend to have low permeability and vice versa, which is a correlation that reduces the probability of encountering parameter combinations conducive to extreme (low or high) seepage behavior, making seepage relatively uniform across different geologic units. However, this negative correlation between conductivity and capillary strength may not apply to a fractured system, specifically if considering the seepage process. A certain hydraulic conductivity may result from a network consisting of a few, large fractures or, alternatively, many small, well-connected fractures. The first network would exhibit weak capillarity, whereas the second network has strong capillarity, i.e., capillarity is not necessarily correlated to permeability. Moreover, if the predominant fracture orientation happens to be aligned with the drift axis (see Figure 1a), little or no tangential conductivity is available, flow diversion is reduced or prevented, and seepage is increased. Even if fractures are normal to the drift axis, they may be too small or poorly connected, i.e., they would not be able to facilitate a continuous

flow path from the apex of the drift to its spring line. For flow diversion to occur, the fracture system must have sufficient connectivity and permeability to provide the necessary effective conductivity in tangential direction around the drift.

Matrix permeability is low, and the potential for imbibition of substantial amounts of water into the matrix is limited because of relatively low porosity and relatively high initial liquid saturation. In a fracture-matrix system, the transient effects from matrix imbibition are restricted to intermediate times, i.e., they are insignificant (1) for a short-term liquid-release test with insufficient time for matrix imbibition, and (2) for a long-term seepage experiment, when near-steady late-time data are no longer affected by matrix imbibition. Most liquid-release tests analyzed in this Model Report are sufficiently long to yield near-steady seepage rates that are insignificantly affected by potential matrix imbibition.

Heterogeneities in formation properties impact seepage as they promote flow concentration and increase the probability of locally breaching the capillary barrier.

Model Conceptualization

Seepage-related fracture properties on all relevant scales are not available and cannot be reliably derived from fracture-trace maps, considering that the mapped geometric characteristics and hydraulic properties are not related in a simple or unique way. However, as discussed in Sections 6.3.2 and 6.4.1 and demonstrated in Finsterle (2000 [151875]), it is not necessary to develop a discrete fracture network model for predicting average seepage on the scale of a waste package.

In this work, the capillarity and the conductivity are conceptualized as *effective* properties that are specifically determined for their intended use in a drift seepage model. The corresponding model parameters must not only represent the average hydraulic characteristics of individual fractures, but also the connectivity, density, geometry, and orientation of the fracture network as it relates to the geometry and orientation of the underground opening. Moreover, they must account for seepage processes that cannot be explicitly implemented in the conceptual model (such as film flow and small-scale roughness in the drift ceiling), and compensate for certain artifacts related to the finite discretization of the numerical model. Model calibration against data that reflect all relevant seepage processes is the approach relied upon to determine these effective parameters.

The SCM is conceptualized as a heterogeneous fracture continuum model (see also Section 6.3.2). The seepage-relevant capillary-strength parameter is determined by calibrating the model against seepage-rate data from liquid-release tests (see Section 6.5.3). These data reflect the seepage process and contain information about seepage-relevant capillary properties of the fractured formation in the vicinity of an open drift. Thus, the inversely determined effective capillary-strength parameter is considered pertinent and appropriate for the intended use of the model.

The simulated seepage can be increased by decreasing capillary strength or permeability. Consequently, the two parameters are negatively correlated if inversely determined from seepage-rate data. Because only seepage data are available for calibration, the parameters are expected to be strongly correlated. That is, it is unlikely that they can be determined independently from one

another and with a reasonably low estimation uncertainty. To reduce correlations and to improve the conditioning of the inverse problem, only the capillary-strength parameter is estimated through inverse modeling, whereas the permeability is fixed during the inversion. The choice of this calibration parameter is further discussed in Section 6.6.3.1.

The permeability field is considered the result of a stochastic process. Its geostatistical properties are determined from air-injection tests (see Section and 6.5.2). Multiple realizations of the permeability field are generated and used in the inversions of data from the lower lithophysal zone.

The permeability field generated for simulations with the SCM are representative of the conditions currently encountered at the test locations of Yucca Mountain. Therefore, thermally and geochemically induced property changes do not need to be considered in this Model Report. They are addressed by the TH Seepage Model (BSC 2003 [161530]) and the Thermal-Hydrologic-Chemical (THC) Seepage Model (BSC 2002 [158375]).

6.3.3.3 Drift Geometry

General Description

The overall drift size and geometry impact the seepage threshold and the seepage amount. Generally, a large drift exhibits a significantly lower seepage threshold because more water accumulates in the boundary layer as it migrates over a longer diversion distance around the wide opening. Because of the nonlinear impact of cavity size on seepage (Philip et al. 1989 [105743]), seepage into large openings cannot be easily inferred from cumulative seepage into small cavities.

The effectiveness of a capillary barrier is highest if the shape of the cavity follows an equipotential surface. In a homogeneous medium, parabolic cavities are more efficient in preventing seepage than circular or flat-roofed openings. Breakouts in the drift ceiling, as a result of rock fall and general drift degradation, may change the overall drift geometry and lead to local topographic lows, which may trap water, reduce or prevent flow diversion, and thus initiate seepage. In addition, small-scale surface roughness tends to increase seepage if the amplitude of the irregularity is on the order of boundary-layer thickness. The latter is determined by the capillary strength of the formation.

In a heterogeneous, fractured formation, the importance of drift shape and drift geometry may be diminished relative to that of flow channeling and local ponding conditions (see Birkholzer et al. (1999 [105170], pp. 372–379) and Section 6.4.2).

Model Conceptualization

The impact of the overall geometry of the underground opening (ECRB Cross Drift or niche) on seepage is accounted for through explicit discretization of the cavity. The ECRB Cross Drift is approximated as being cylindrical, with a diameter of 5.0 m. The overall geometry of the niches is taken from survey data, thus including some medium-scale roughness from rock fall and large lithophysal cavities.

Small-scale roughness is indirectly included through a discretization effect. The length of the last vertical connection from the gridblocks representing the formation and the interface denoting the drift surface is 0.05 m (see Attachment III, Attachment IV, and Attachment V; see also discussion in Section 6.6.1.2). The choice of this nodal distance affects seepage because no horizontal flow diversion can occur closer than 0.05 m from the drift wall. Since water is laterally diverted only if capillary suction is on the order of 0.05 m or higher, the discretization has an effect similar to that of (1) drift-wall roughness of amplitude of 0.05 m, with troughs at the gridblock centers and ridges along the gridblock interfaces, or (2) short fractures cutting into the opening, with a distance to the next fracture intersection of 0.05 m. Consequently, the effective capillary-strength parameter estimated by inverse modeling depends on the chosen discretization; it contains a geometric component related to the length of the nodal distance between the formation and the drift. The estimate is thus model-related, and the discretization between the calibration model and the prediction model must be consistent.

In summary, the geometric factors affecting seepage are accounted for through (1) explicit discretization of the opening (which includes the overall shape as well as medium-scale roughness from break-outs lithophysal cavities), (2) by preventing flow diversion in a 0.05 m thick layer around the drift (mimicking small-scale surface roughness with a 0.05 m amplitude of the irregularities), and (3) the estimation of an effective capillary-strength parameter. The inclusion of small-scale surface roughness (exceeding an amplitude of 0.05 meters) and discrete effects from small fractures into an effective capillary-strength parameter is appropriate because their impact on seepage rates is directly related to capillarity.

Note that the nominal diameter of a repository drift is 5.5 m, which is slightly larger than that of the ECRB Cross Drift (5.0 m). This difference is of no significance, because the seepage-related parameters are determined using a model with the correct diameter (5.0 m) to be used for the analysis of liquid-release tests in the ECRB Cross Drift. These parameters are then applied in the prediction model, which simulates seepage into an opening with a 5.5 m diameter. The impact of drift-shape changes as a result of drift degradation is discussed in the upcoming revision REV 02 of CRWMS M&O (2000 [153314]).

6.3.3.4 Evaporation Conditions

General Description

Reduced relative humidity in the underground opening leads to evaporation of water at the drift surface and the development of a dry-out zone in the vicinity of the cavity. Part or all of the water reaching the ceiling of the opening during a liquid-release test may evaporate, depending on the evaporation potential in the drift and the wet area exposed to evaporation. The evaporation potential depends on the relative humidity in the opening and the thickness of a diffusive boundary layer at the drift surface, which in turn is governed by the air velocity in the ventilated drift.

The size of the wet spot developing at the drift ceiling depends on the formation properties, the spreading mechanism along the drift surface, and evaporation itself. As water injected during a liquid-release test reaches the opening, it spreads along the surface on account of surface adhesion within the rough surface. As a result, water potentially seeping into the opening may not only form droplets or lines of water along fracture traces with a small surface area, but may

spread across the drift surface over a relatively large area. This phenomenon is qualitatively confirmed by the geometry of the wet spot observed at the niche ceiling during seepage experiments (BSC 2001 [158463], Section 6.2.1.3.4, Figure 6.2.1-7; Trautz and Wang 2002 [160335], Figures 7 and 9). The geometry of the wet spot does not have a clear correlation with the visible fracture traces. Even though water first appears along fracture traces (Trautz and Wang 2002 [160335], Figure 10), the wet spot grows in an areal fashion. It is obvious from the short arrival time and the average speed at which the leading edge of the plume moves across the ceiling that the water is not transmitted through the matrix, but spreads along the ceiling as a surface film, possibly supported by flow through microfractures. Evaporation from such wet areas is similar to evaporation from a free water surface, where the evaporation rate is governed by one-dimensional vapor diffusion across a relatively thin boundary layer of linearly decreasing vapor concentration. Temporal shrinkage of the wet spot can be correlated to increased evaporation as a result of changed ventilation regime, highlighting the coupled nature of the process.

In a closed-off and humidified niche, potential evaporation at the wall or in the capture system is expected to be small compared to the amount of water being released. Seepage experiments in the middle nonlithophysal zone of the Topopah Spring welded unit were conducted in niches that were closed off by a bulkhead, which leads to comparatively high relative humidity and low air circulation. Moreover, a humidifier was used in some of the experiments to ensure high relative humidity. For these conditions, Ho (1997 [141521]) and Or and Ghezzehei (2000 [144773]) provide a detailed description of evaporation mechanisms on the scale of individual water droplets within fractures or emerging from fractured formations. The evapo-infiltration threshold calculated by Ho (1997 [141521], p. 2670) is significantly lower than the applied injection rates, suggesting a very minor influence of evaporation on measured seepage rates in experiments conducted in the niches.

Model Conceptualization

Evaporation effects are included in the modeling of liquid-release tests performed in the ventilated ECRB Cross Drift as well as in Niche 1620. Evaporation effects are neglected in the modeling of liquid-release tests conducted in the closed-off niches in the middle nonlithophysal zone, i.e., Niches 3107, 3650, and 4788. As demonstrated in Section 6.7, the impact of slight evaporation in a closed-off and moisturized niche on seepage rates—and thus on the estimation of seepage-relevant parameters—is minor.

Evaporation effects are accounted for in the model by prescribing the measured relative humidity in the opening as a temporally varying water-potential boundary condition. Evaporation is calculated as a function of the water-potential gradient at the drift surface, the vapor diffusion coefficient, and the thickness of the diffusive boundary layer, which is estimated from evaporation pan measurements. A detailed description of the corresponding conceptual and mathematical model and the estimation of the evaporation boundary-layer thickness is given in Sections 6.6.1.3 and 6.6.1.4.

Predictions of long-term seepage using the SMPA are based on the presumption of 100% relative humidity in the waste emplacement drifts, yielding higher seepage estimates than those expected in a ventilated environment.

6.3.3.5 Lithophysal Cavities

General Description

The impact of lithophysal cavities on flow and seepage is twofold: (1) lithophysal cavities are essentially obstacles to water flow because they act as capillary barriers, focusing the water that flows around them; (2) lithophysal cavities intersected by the drift lead to a rough drift wall, potentially creating seepage points at local topographic lows. Both effects tend to promote seepage.

Model Conceptualization

The effect of lithophysal cavities on seepage can be captured through the estimation of an effective capillary-strength parameter, making the explicit inclusion of lithophysal cavities into the process model unnecessary. This approach is considered appropriate for the following reasons: (1) omitting lithophysal cavities in the process model used for inverse modeling yields lower estimates of the capillary-strength parameter; (2) consistency between the calibration model (the SCM) and the prediction model (the SMPA) removes the impact of a potential estimation bias; (3) the approach allows for the development of a single SMPA conceptual model for both the middle nonlithophysal and lower lithophysal zones, yielding a single look-up table for TSPA to sample from; and (4) explicit modeling of lithophysal cavities is not warranted because of insufficient information regarding their location, shape, and frequency. Note that the impact of lithophysal cavities on surface roughness in Niche 1620 is accounted for through explicit discretization of the niche's geometry, based on survey data (see Attachment V).

6.3.4 General Modeling and Data-Analysis Approach

The key element of the approach chosen to simulate seepage and determine seepage-relevant parameters is the reliance on inverse modeling. Given the complexity of the seepage process in a fractured porous medium, it is considered unfeasible to develop a detailed process model with a deterministic calculation of unsaturated water flow, through a fracture network that exhibits multiscale variabilities in hydraulic properties. Such a model would also require an accurate representation of the seepage process, which includes effects from small-scale roughness and small-scale heterogeneities, film flow within fractures and along the drift surface, drop formation and detachment, and other processes. While modeling these processes is theoretically possible, the necessary characterization data needed to warrant such a detailed simulation are not available.

The difficulties mentioned above can be effectively overcome by recognizing that (1) detailed simulation of individual seeps is not necessary to estimate average seepage rates into waste emplacement drifts, (2) certain factors affecting seepage can be lumped into an effective parameter, (3) calibrating a model against data from seepage experiments ensures that the model captures the relevant processes, (4) estimating effective parameters partly compensates for processes and features that are not explicitly considered in the model, and (5) the estimated parameters are optimal and can be directly used in the prediction model.

The main advantage of this approach is that it relies directly on seepage-rate data, which inherently contain information about the relevant processes. Moreover, the calibration data (seepage

rates on the scale of a drift section) are very similar to the measure of interest for the subsequent predictions. The consistency between the calibration model used to derive seepage-relevant parameters and the prediction model used to forecast seepage minimizes potential conceptual differences and large systematic errors. The advantages of the selected method over alternative approaches are further evaluated in Section 6.4.

The SCM is conceptualized as a three-dimensional, heterogeneous continuum model. The continuum mainly represents the dense fracture network that dominates the seepage process. The SCM is conceptually consistent with the unsaturated zone site-scale model and submodels thereof, specifically the SMPA and TH Seepage Model (BSC 2003 [161530]). This makes it straightforward to embed the SCM into the current modeling framework.

As will be discussed in Section 6.6.3.2, the SCM is calibrated against late-time seepage-rate data from liquid-release tests. Early-time seepage data are discarded because they are affected by storage effects and the properties of a few fractures connecting the injection interval with the opening. These fractures are not necessarily representative of the fracture network that is engaged in flow diversion around the entire opening under steady-state conditions. Late-time data are more representative of near-steady conditions and are less influenced by storage effects. Moreover, the relatively large amount of released water at late time has likely encountered a significant portion of the capillary barrier. As a result, the late-time seepage data better reflect average conditions on the scale of interest.

Liquid-release tests directly supporting the SCM were conducted in two different hydrogeologic units, in multiple test beds, boreholes, and intervals. Each test event probes a different portion of the rock and a different section of the underground opening. The question arises how the available data should be combined to yield suitable averages and reasonable measures of variability and uncertainty, which are needed for model validation and the subsequent PA calculations. The goal is to obtain a probability density function of the seepage-relevant parameters that reflects both estimation uncertainty and spatial variability. These two aspects are discussed separately in the following paragraphs.

Parameter estimates determined by inverse modeling are uncertain because they are derived from limited data, which exhibit random and potentially systematic measurement errors, and because the model is a simplification of the real system, which introduces systematic and random modeling errors. As discussed above, estimating model-related parameters mitigates the impact of some of the residual systematic errors. Estimation uncertainty as a result of random noise in the seepage data is relatively minor (see Sections 6.6.3.3 and 8.2). However, there remains irreducible uncertainty because of small-scale heterogeneity that affects individual seepage tests. The details of these small-scale heterogeneities are unknown (i.e., they cannot be described deterministically) and vary from location to location (i.e., they are spatially variable). Consequently, they are considered the result of a stochastic process that must be described by geostatistical parameters and modeled by performing multiple geostatistical simulations. Each seepage data set is obtained from a certain test bed (niche or section of ECRB Cross Drift); it can be considered one realization from a number of statistically similar geologic systems. The lack of knowledge regarding the details of this specific realization makes the inversely determined parameter estimate uncertain. This uncertainty is examined by performing multiple inversions of the same data set using different realizations of the underlying heterogeneous permeability field,

yielding a distribution of estimated capillary-strength parameters rather than a single value. In addition to capturing the random nature of the permeability field and its impact on seepage, each realization will induce some ergodic fluctuations, which reflect the fact that the model statistics are inferred from sparse air-permeability sampling (i.e., they are not deemed exactly representative of the population statistics). The average of all inversions performed with different permeability fields for a given interval yields one estimate representative of that location.

The average parameters obtained from multiple simultaneous inversions of one or more seepage events conducted in a certain test interval are considered independent, each reflecting the seepage-relevant properties at a given location on the drift scale. These estimates are then combined to yield a parameter distribution for the entire hydrogeologic unit. This distribution reflects spatial variability. By sampling from the distribution of the resulting parameter estimates, probabilistic predictions of seepage across the repository horizon can capture the spatial variability of average seepage on the scale of the 5 m long drift segment. Uncertainty in this average seepage rate as a result of small-scale heterogeneity is calculated based on multiple seepage prediction runs by the SMPA, using multiple realizations of the underlying permeability field.

A comparison of seepage predictions with observable data (such as seepage data from transient liquid-release tests involving a finite amount of water) is a necessary step in model development and confidence building. However, models are often developed—and most usefully—to infer behavior that cannot be directly observed (such as long-term near-steady seepage under naturally low percolation fluxes). The appropriateness of such an extrapolation of the model beyond its tested grounds needs to be assessed. While rigorous model testing is fundamentally not possible (Oreskes et al. 1994 [152512]), validation of the model for a limited purpose can be accomplished. The SCM is partially tested against observable data from seepage experiments that were not used for model calibration. The purpose of this validation exercise is to determine whether the model is appropriate and adequate for its intended use. Remaining uncertainty will be quantified during the seepage abstraction process and propagated through the PA models. Additional remarks about model validation can be found in Section 7.1.

The development of the SCM involves the following steps:

1. Geostatistical parameters of the permeability field are determined from the results of air-injection test data.
2. Multiple realizations of the permeability field are generated, each being consistent with the geostatistical properties of the measured air permeabilities.
3. A numerical mesh is generated. This step involves (a) making a primary 3D grid, (b) translating coordinates to center the mesh, (c) mapping the permeability field onto the mesh, (d) cutting out the opening (niche or drift) from the mesh, (e) adding top and bottom boundary elements as well as an evaporation boundary in the opening, and (f) modifying elements representing injection intervals.
4. An input file defining the forward problem is prepared. This step involves (a) assembling parameters representing hydrogeologic properties, (b) assigning appropriate properties to elements representing the excavation and borehole intervals, (c) extracting the back-

- ground percolation flux from the UZ Model, (d) assigning appropriate initial and boundary conditions, and (e) selecting computational parameters and program options.
5. Steady-state runs are performed to obtain initial conditions for the subsequent simulation of transient seepage experiments.
 6. Injection rates are specified as time-dependent source terms.
 7. Test events are selected for calibration. Seepage rates are calculated from the cumulative seepage data.
 8. An input file defining the inverse problem is prepared. This step involves (a) selecting the parameters to be estimated and their initial guesses, (b) selecting points in time at which calibration should occur, (c) specifying the data against which calibration should occur, (d) assigning measurement uncertainties to the data sets as weighting factors, and (e) selecting computational parameters and program options.
 9. Seepage-relevant, model-related parameters are determined by automatic model calibration using iTOUGH2 V4.0 (LBNL 1999 [139918]) and V5.0 (LBNL 2002 [160106]). In each inversion, seepage-rate data from multiple test events are jointly inverted.
 10. The model is tested by comparing predicted seepage rates to observed data from seepage experiments not used during model calibration. Prediction uncertainty is calculated by iTOUGH2 V4.0 (LBNL 1999 [139918]) and V5.0 (LBNL 2002 [160106]) using first-order-second-moment (FOSM) uncertainty propagation analysis and Monte Carlo simulations.

6.4 ALTERNATIVE CONCEPTUAL MODELS

The following subsections contain short descriptions of potential alternative ways to evaluate seepage into waste emplacement drifts at Yucca Mountain. These alternative conceptual models are discussed in a qualitative manner, and references to more detailed analyses are given, if available. No quantitative evaluations of these alternative conceptual models are presented in this Model Report.

Natural analogues for seepage also support the concepts of the base-case model; they are briefly reviewed in Section 7.2.1.

In general, the choice of a conceptual model should be based on a careful consideration of the study objectives, the available database in comparison with the data needs, the uncertainty in the input parameters and the corresponding prediction uncertainties and computational aspects.

6.4.1 Discrete Fracture Network Model

A discrete fracture network model (DFNM) is an alternative conceptual model to the heterogeneous continuum model used in this Model Report (Pruess et al. 1999 [117112], pp. 307–309). A high-resolution DFNM is capable of generating channelized flow and discrete seepage events, as demonstrated by Finsterle (2000 [151875], Plate 1) and Liu et al. (2002 [160230], Figure 5). Note that two-dimensional DFNMs such as those shown in Figure 2 and Figure 3 make the

implicit assumption that the fractures are oriented parallel to the drift axis. This assumption exaggerates the discreteness of the flow and seepage behavior as flow diversion within the fracture plane is not possible (see also Figure 1 and related discussion in Section 6.3.2).

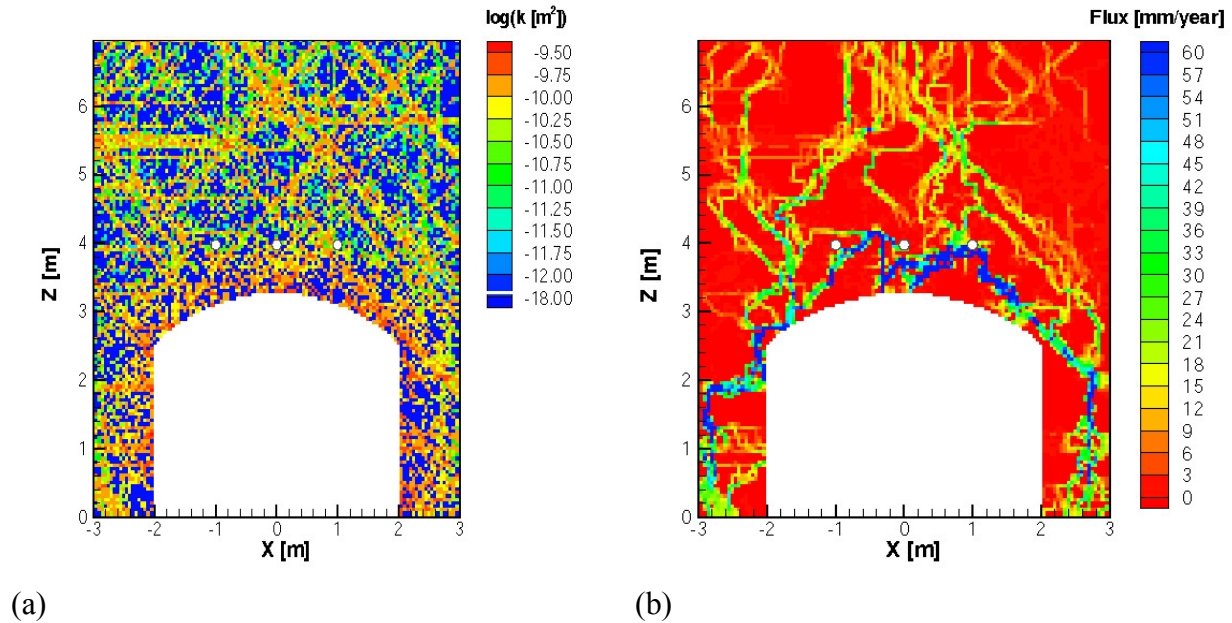


Figure 2. Two-dimensional discrete feature model (after Finsterle 2000 [151875], Plate 1): (a) high-resolution permeability field; (b) discrete flow path and discrete seepage behavior

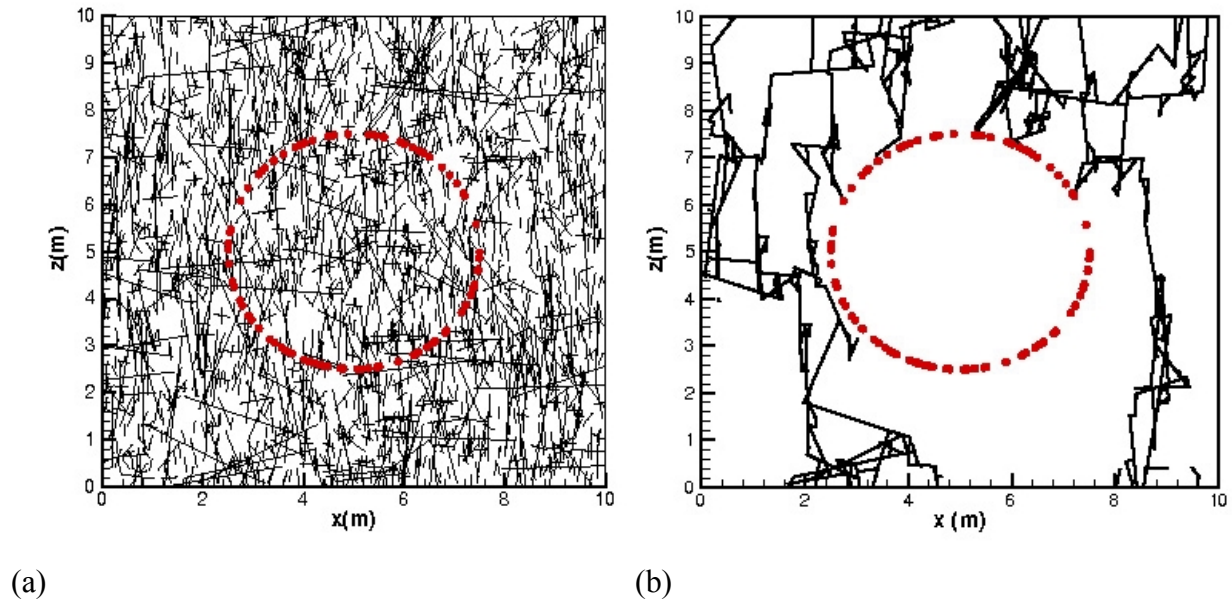


Figure 3. Two-dimensional discrete fracture network model (after Liu et al. 2002 [160230], Figures 1 and 2): (a) fracture network; (b) flow paths

The development of a defensible DFNM requires collecting a very large amount of geometric and hydrologic data. While part of the required geometric information can be obtained from fracture mappings, the description of the network remains incomplete and potentially biased towards fractures of a certain orientation and a certain size. Moreover, unsaturated hydrological parameters on the scale of individual fractures are required, along with conceptual models and simplifying assumptions regarding unsaturated flow within fractures and across fracture intersections. The databases required to develop a defensible DFNM are currently not available and are generally difficult or even impossible to obtain for site-specific simulations. As a result, the cumulative effect of all the input uncertainties is likely to outweigh the apparent advantage of a detailed representation of the fracture network. To reduce prediction uncertainties, the DFNM must be calibrated against hydrogeologic data—that is, an approach very similar to that outlined in Section 6.3.4 must be followed.

The appropriateness of using a continuum model for the prediction of average seepage quantities was demonstrated in Finsterle (2000 [151875]). In this study, seepage predictions with a calibrated fracture continuum model were compared to those of a DFNM, yielding consistent results even when applied outside the range of calibration. Given these results, the parsimony of the continuum model is considered a key advantage over the complexity of the DFNM, which is difficult to support or justify despite its visual appeal. Moreover, a two-dimensional DFNM is not capable of capturing flow diversion within the fracture plane, a mechanism appropriately represented by a 2D (or 3D) continuum model.

For the reasons outlined above, the full development of a DFNM as a potential alternative to the base-case continuum model was considered unwarranted, infeasible, and unnecessary. Seepage calculations with a calibrated DFNM are likely to corroborate the findings of this Model Report.

6.4.2 Seepage Governed by Ponding Probability

As an alternative conceptual model to a seepage process model, Birkholzer et al. (1999 [105170], pp. 372–379) related seepage to the local ponding probability, which was derived from the variability of the permeability field. Their approach assumed that—in strongly heterogeneous formations—seepage is predominantly affected by pressure variations governed by local heterogeneity rather than the presence and geometry of the capillary barrier. This is different from the behavior in a homogeneous system, where the geometry of the capillary barrier has a strong impact on seepage (Philip et al. 1989 [105743]). Strong medium- to small-scale heterogeneities tend to increase seepage because they increase channeling and local ponding. This effect is included in the current seepage process models through the estimation of effective, seepage-specific parameters for a heterogeneous medium with a heterogeneous permeability field. While the approach presented by Birkholzer et al. (1999 [105170], pp. 372–379) may provide guidelines for how to extrapolate seepage predictions to other units or drift geometries, it nonetheless requires a calibration step similar to that described in this Model Report. The approach is therefore not further considered. Nevertheless, the concept that ponding probability affects seepage is consistent with and thus corroborates the base-case model, which produces random seepage locations as a result of local ponding in a stochastic permeability field.

6.4.3 Inferring Seepage from Geochemical Data

Observations of calcite and opal in lithophysal cavities could be used to estimate long-term seepage rates into these small openings (BSC 2002 [160247], Section 6.10.1). Calcite is assumed to precipitate from downward-percolating meteoric water because of (1) evaporation, (2) CO₂ outgassing as a result of the geothermal gradient, and (3) interaction with a gas phase containing less CO₂ than the gas with which the water was last equilibrated. Considering these calcite-precipitation mechanisms and assuming certain water-to-calcite ratios, seepage into lithophysal cavities can be estimated from calcite-deposition data. The analysis of calcite and opal precipitation data shows that (1) not all lithophysal cavities encountered seepage, and (2) seepage flux derived from mineral deposits is a very small fraction of percolation flux. Both conclusions corroborate the general concept of a capillary barrier reducing seepage below the value of the percolation flux.

The advantage of using geochemical information to infer seepage is the fact that calcite and opal were deposited over a long period of time under natural percolation conditions. The disadvantage of this approach is that (1) seepage is inferred in an indirect manner, requiring a number of geochemical models with their associated assumptions—in addition to hydrogeologic model assumptions; (2) the calcite depositions on lithophysal cavity floors may not originate from dripping water (i.e., seepage); in fact, there is a lack of evidence of dripping from cavity ceilings (absence of stalactites or stalagmites), even where fractures containing coatings intersect lithophysae ceilings (Whelan et al. 2002 [160442], p. 744); (3) the data reflect seepage into (small) cavities instead of seepage into a (large) waste emplacement drift; since the size of the underground opening impacts seepage in a nonlinear fashion, a hydrological, physically based process model is required to estimate seepage on the scale of interest; (4) seepage into lithophysal cavities does not include potential impacts from the excavation-disturbed zone around a mechanically constructed drift; and (5) the historic record and the approach does not allow making predictions into the future under changed conditions.

As shown by Marshall et al. (2000 [151018], Figure 1), the seepage rates estimated from the calcite-deposition data are significantly lower than those predicted by TSPA using data derived from the SMPA, which is based on the methodology outlined in this Model Report.

6.4.4 Inferring Seepage Threshold Directly From Liquid-Release Tests

Trautz and Wang (2002 [160335], Section 5) estimated the seepage threshold directly from the liquid-release test data, based on a number of simplifying assumptions (with regard to the cross-sectional area of the flow path between the borehole and the ceiling, evaporation, and the steady-state flow field). Once the seepage threshold was determined, a capillary-strength parameter was derived assuming seepage into a cylindrical cavity excavated from a homogeneous porous medium (Trautz and Wang 2002 [160335], Section 6). The base-case model outlined in this Model Report relies on fewer assumptions than the simplified alternative conceptual model and predicts a lower seepage threshold; the base-case model described in this Model Report is therefore the preferred conceptualization.

6.5 DESCRIPTION OF SEEPAGE EXPERIMENTS

6.5.1 Test Location and Borehole Configuration

The data used for the development, calibration, and validation of the SCM were collected as part of the ESF Drift Seepage Test and Niche Moisture Study, an ongoing field-testing program. Drift-scale seepage tests were initiated in 1997 to investigate potential seepage into an underground opening representing a waste emplacement drift. Short drifts ranging from 6.3 m to 15.0 m in length were constructed at various locations along the ESF and the ECRB Cross Drift. Boreholes were installed prior to and after the drifts were excavated to facilitate characterization of the rock using air-injection tests and investigation of seepage processes using liquid-release tests. The short excavations are called “niches,” and the drift-scale seepage tests are collectively referred to as the Niche Study. In Niche 1620, a horizontal slot on the side of the niche (also referred to as “batwing”) was excavated to obtain direct evidence of the flow-diversion capability of the capillary barrier (see Section 6.8).

A second study referred to as the Systematic Borehole Testing Program was initiated in 2000 to complement the niche seepage experiments. The purpose of the program is to provide broad, systematic coverage and characterization of the lower lithophysal zone (Tptpll) of the Topopah Spring welded unit (TSw). Systematic characterization of the Tptpll is accomplished by performing air-injection and liquid-release tests in approximately 20 m long boreholes drilled into the ceiling approximately every 30 m along the ECRB Cross Drift.

The data used in this Model Report are a subset of seepage tests from the Niche Studies and the Systematic Borehole Testing Program. A few tests failed and are not used in this Model Report (see discussion of Table 11 below). Data include air permeabilities and seepage-rate values from tests conducted at three niche sites located along the Main Drift of the ESF, one niche in the ECRB Cross Drift, and in three systematic testing boreholes drilled into the ceiling of the Cross Drift (see Figure 4). The first three niche sites are located along the west side of the ESF in the Ttpmn and were selected for study based on fracture and hydrologic data collected in the ESF. The first niche site at construction station (CS) 31+07 (hereafter referred to as Niche 3107) consists of a 6.3 m long drift located in an area of relatively low fracture density. Niche 3107 is located in close proximity to CS 30+62, where the Cross Drift crosses over the Main Drift of the ESF. The second niche site, at CS 36+50 (Niche 3650), consists of a 9 m long drift located in a competent rock mass exhibiting relatively moderate fracture density. The third niche site, at CS 47+88, (Niche 4788) consists of an 8.2 m long drift located in an area exhibiting relatively high fracture density. Niche 4788 is located in a 950 m long exposure of an intensely fractured zone. Fractures in this zone are not uniformly spaced, but instead occur in clusters of closely spaced fractures. The 15.0 m long Niche 1620 is located on the south side of the ECRB Cross Drift in the Tptpll.

Table 9. Borehole Designations in Niches

Niche	Borehole	Designation in DTN	DTN of Borehole Survey	DIRS#
3107 (Niche 3)	UL	ESF-MD-NICHE 3107 #5	MO0002GSC00064.000	[152625]
	UM	ESF-MD-NICHE 3107 #6		
	UR	ESF-MD-NICHE 3107 #7		
3650 (Niche 2)	UL	ESF-MD-NICHE 3650 #1	MO0002GSC00076.000	[152623]
	UM	ESF-MD-NICHE 3650 #2		
	UR	ESF-MD-NICHE 3650 #3		
4788 (Niche 4)	UL	ESF-MD-NICHE 4788 #5	MO0107GSC01069.000	[156941]
	UM	ESF-MD-NICHE 4788 #6		
	UR	ESF-MD-NICHE 4788 #7		
1620 (Niche 5)	#1	ECRB-NICHE 1620 #1	MO0209GSC02116.000	[160407]
	#2	ECRB-NICHE 1620 #2		
	#3	ECRB-NICHE 1620 #3		
	#4	ECRB-NICHE 1620 #4		
	#5	ECRB-NICHE 1620 #5		
	#6	ECRB-NICHE 1620 #6		
	#7	ECRB-NICHE 1620 #7		

All boreholes listed in Table 9 are approximately parallel to the niche axis. Air-injection tests were conducted in several, 1 ft (0.3 m) long borehole packed-off intervals both prior to and after niche excavation to determine the permeability distribution of the formation, as well as to study potential permeability changes as a result of stress relief during niche excavation. After niche construction, water was injected at a specified rate into intervals of the same boreholes to observe, document, and quantify any water migrating to and seeping into the niche.

The systematic testing boreholes SYBT-ECRB-LA#1, 2, and 3 are drilled from the ECRB and located in the moderately to densely welded, devitrified, and vapor-phase altered lower lithophysal zone (Tptpll).

Borehole SYBT-ECRB-LA#1 is collared from the drift crown at ECRB construction station CD 17+49. It is upward-inclined at nominal 15° from the drift axis. Packers are set to isolate an injection zone between 3.0 m and 4.9 m (zone 2) from the collar (BSC 2001 [158463], p. 241). Borehole SYBT-ECRB-LA#2 is collared from the drift crown at ECRB construction station CD 17+26. It is upward-inclined at nominal 15° from the drift axis. Packers are set to isolate three 6 ft (1.8 m) long injection zones between 17 ft (5.2 m) and 23 ft (7.0 m) (zone 1), 33 ft (10.1 m) and 39 ft (11.9 m) (zone 2), and 49 ft (15.0 m) and 55 ft (16.8 m) (zone 3) from the collar (DTN: LB00090012213U.002 [153154]). Borehole SYBT-ECRB-LA#3 is collared from the drift crown at ECRB construction station CD 16+95. It is upward-inclined at nominal 15° from the drift axis. Packers are set to isolate three 6 ft (1.8 m) long injection zones between 18 ft (5.5 m) and 24 ft (7.3 m) (zone 1), 34 ft (10.4 m) and 40 ft (12.2 m) (zone 2), and 50 ft (15.2 m) and 56 ft (17.1 m) (zone 3) from the collar (DTN: LB0203ECRB LIQR.001 [158462]).

6.5.2 Air-Injection Tests

The purpose of the air-injection tests was to estimate permeabilities as a basis for the stochastic generation of heterogeneous permeability fields. The tests were performed by isolating a short section of the boreholes (1 ft [0.3 m] in niches, 6 ft [1.8 m] in systematic testing borehole SYBT-ECRB-LA#2), using an inflatable packer system, and then injecting compressed air at a constant rate into the isolated injection interval. The pressure buildup in the injection interval and in nearby observation intervals was monitored with time until steady-state conditions were reached, which typically occurred within a few minutes. Air injection was terminated after reaching steady-state pressures, and the decline in air pressure was then monitored as it recovered to its initial pre-test condition. Air-permeability values were derived from the steady-state pressure data based on a commonly used analytical solution (BSC 2001 [158463], Section 6.1.2.1; LeCain 1995 [101700], p. 10, Eq. (15)).

Permeabilities determined from air-injection tests are considered representative of the absolute permeability of the excavation-disturbed zone around the opening. This is reasonable, because post-excavation air-injection tests were conducted in a network of essentially dry fractures, i.e., no empirical relative permeability function is needed to translate air conductivity into absolute permeability. Since air-injection tests are a standard method to obtain permeability values, the use of these values during both calibration and prediction of seepage ensures consistency. The distributions representing variability and uncertainty in permeability (see upcoming Model Report MDL-NBS-HS-000019 REV 00 (CRWMS M&O 2001 [154291])) are developed also based on air-permeability data. This consistency reduces the impact of a potential bias.

The air permeabilities around the niches and the ECRB Cross Drift are affected by excavation (BSC 2001 [158463], Section 6.1.2.2; Wang and Elsworth 1999 [104366], pp. 752–756). Since seepage is determined by the formation properties in the immediate vicinity of the opening, it is reasonable to use post-excavation air-permeability data for seepage calculations. Data that are located outside the footprint of the niches were removed from the data set (Ahlers 2002 [161045], p. 20; Trautz 2001 [161044], p. 20) because they represent a separate population of air permeabilities performed in an area of relatively undisturbed, lower-permeability rock. Mean and standard deviations for each of the four locations are summarized in Table 10. Here, standard deviations reflect spatial variability within the test bed. The number of log-permeability values available is indicated in the last column. Mean permeabilities and their spatial variability as calculated for the three niches located in the middle nonlithophysal zone are consistent with one another. Permeability in the lower lithophysal zone is approximately one order of magnitude larger. The variability as measured in Niche 1620 is significantly larger than that obtained in borehole SYBT-ECRB-LA#2. This is partly a result of the injection intervals of borehole SYBT-ECRB-LA#2 being six times longer than those in Niche 1620. Note no air-permeability data are available from boreholes SYBT-ECRB-LA#1 and SYBT-ECRB-LA#3 because of equipment problems during air-injection testing.

Table 10. Mean and Standard Deviation of Post-Excavation Log-Air-Permeability Values

Location	Input DTN	Scientific Notebook Reference	Mean Log(k [m ²])	Std. Dev.	n
Niche 3107	LB990601233124.001 [105888]	Ahlers 2002 [161045], pp. 39–40	-12.14	0.80	78
Niche 3650	LB0011AIRKTEST.001 [153155]	Trautz 2001 [161044], pp. 19–25	-11.66	0.72	84
Niche 4788	LB990601233124.001 [105888]	Ahlers 2002 [161045], pp. 15–21	-11.79	0.84	63
Niche 1620	LB0110AKN5POST.001 [156904]	Wang 2003 [161456], SN-LBNL-SCI-223-V1, pp. 19–20	-10.95	1.31	61
SYBT-ECRB-LA#2	LB00090012213U.001 [153141]	Finsterle 2002 [161043], pp. 54–55	-10.73	0.21	6

6.5.3 Liquid-Release Tests

Multiple liquid-release tests were performed in the niches and the ECRB Cross Drift to characterize seepage into a large underground opening (BSC 2001 [158463], Sections 6.2 and 6.11). The tests were performed by sealing a short section of the borehole above the opening using an inflatable packer system and then releasing water at a specified rate into the isolated test interval. Any water that migrated from the borehole to the ceiling and dripped into the opening was captured and weighed. Only a small amount of water (approximately one liter per test event) was released during testing at Niche 3650, and only the total amount of water that seeped into the capture system was recorded. Seepage experiments at Niches 3107, 4788, 1620, and in the systematic testing boreholes SYBT-ECRB-LA#1–3 involved significantly more water, which was injected over longer periods, and cumulative seepage was recorded as a function of time.

In many intervals, multiple liquid-release tests were conducted using different injection rates with different lengths of inactivity between individual test events. The reason for using different injection rates and different injection schedules was to collect data that are sensitive to percolation rate and water storage effects. While the inverse modeling approach pursued in this Model Report does not require data above and below the seepage threshold, increasing the sensitivity of the data to seepage-related effects improves the identifiability of seepage-relevant parameters.

Table 11 summarizes the test events used for the calibration and validation of the SCM. The approximate release rate (defined as the injection rate minus the return flow) is indicated in Column 4. As shown in Column 5, 52 out of 90 test events led to seepage into the capture system. Potential seepage was not recorded in two cases (Events 5 and 46) because of an equipment failure. While no data are available to be used for calibration or validation from these three test events, the injections that occurred were nevertheless modeled because the released water has a potential impact on subsequent test events. Column 6 indicates whether a specific test event was used for calibration (C) or validation (V). A few additional seepage tests were conducted in Niche 3650 that were not used, because only a very small amount of water was released and generally no seepage was observed. Injection attempts at zone 3 of borehole SYBT-ECRB-LA#3 (Event 77) failed because the zone was too tight. A few test events in Niche 1620 were not analyzed because of various difficulties (Event 78: data logger problem; Events 79 and 80: packer problem; Event 82: seepage partially bypassed capture system; Event 83: pump problem). Partial test interference with Events 83 and 84 was observed during Events 87 and 88 (see also discussion of Figure 17 below).

The events without any seepage cannot be used for calibration (unless jointly inverted with other tests that exhibit seepage), because the corresponding inverse problem would be ill posed. These tests (along with tests showing seepage) are therefore used for validation of the SCM. The small amount of water released during the short-term tests performed in Niche 3560 makes it difficult to reliably estimate seepage parameters on the drift scale. If used for calibration, these tests yield small-scale parameter values that are likely biased towards the properties of the few fractures connecting the release point with the niche ceiling. These fractures may not be representative of the fracture network taking part in the diversion of water around the entire niche, which is the behavior to be modeled under steady-state flow conditions. Moreover, storage effects are significant in short-term tests but are also poorly identifiable. For these reasons, the Niche 3650 liquid-release tests are used for validation purposes only.

Table 11. Liquid-Release Test Events, Approximate Release Rate, Occurrence of Seepage, and Their Use for Calibration or Validation Purposes

Event	Starting Date of Test	Borehole, Interval	Approximate Release Rate [ml/min]	Seepage?	Calibration, Validation
Niche 3107, DTN: LB0010NICH3LIQ.001 [153144]					
1	03/10/99	UL, 5.49–5.80 m	1.5	No	V
2	03/30/99	UL, 5.49–5.80 m	2.0	No	V
3	09/17/99	UL, 5.49–5.80 m	1.5	No	V
4	03/04/99	UM, 4.88–5.18 m	0.9	No	C
5	04/07/99	UM, 4.88–5.18 m	5.8	?	–
6	04/27/99	UM, 4.88–5.18 m	2.4	Yes	C
7	04/30/99	UM, 4.88–5.18 m	0.8	No	V
8	05/06/99	UM, 4.88–5.18 m	5.4	Yes	C
9	09/21/99	UM, 4.88–5.18 m	5.0	Yes	V
10	09/23/99	UM, 4.88–5.18 m	5.3	Yes	V
11	09/27/99	UM, 4.88–5.18 m	5.4	Yes	V
12	10/11/99	UM, 4.88–5.18 m	5.4	Yes	V
Niche 3650, DTN: LB980001233124.004 [136583]					
13	12/11/97	UL, 5.18–5.49 m	4.7	No	V
14	02/12/98	UL, 5.18–5.49 m	0.4	No	V
15	12/11/97	UL, 5.79–6.10 m	12.1	No	V
16	12/11/97	UL, 6.40–6.71 m	12.7	No	V
17	12/10/97	UL, 7.01–7.32 m	116.9	Yes	V
18	01/06/98	UL, 7.01–7.32 m	11.4	No	V
19	11/13/97	UM, 4.27–4.57 m	121.1	Yes	V
20	12/03/97	UM, 4.27–4.57 m	30.2	Yes	V
21	12/03/97	UM, 4.27–4.57 m	30.4	Yes	V
22	01/07/98	UM, 4.27–4.57 m	2.8	Yes	V
23	02/10/98	UM, 4.27–4.57 m	1.0	No	V
24	11/12/97	UM, 4.88–5.18 m	173.5	Yes	V
25	12/04/97	UM, 4.88–5.18 m	30.4	Yes	V
26	12/05/97	UM, 4.88–5.18 m	8.6	Yes	V
27	01/08/98	UM, 4.88–5.18 m	2.8	No	V
28	03/06/98	UM, 4.88–5.18 m	0.8	No	V
29	11/13/97	UM, 5.49–5.79 m	124.1	Yes	V
30	12/04/97	UM, 5.49–5.79 m	30.2	Yes	V
31	01/09/98	UM, 5.49–5.79 m	3.5	Yes	V
32	02/11/98	UM, 5.49–5.79 m	0.8	No	V

Table 11 (cont.). Liquid-Release Test Events, Approximate Release Rate, Occurrence of Seepage, and Their Use for Calibration or Validation Purposes

Event	Starting Date of Test	Borehole, Interval	Approximate Release Rate [ml/min]	Seepage?	Calibration, Validation
33	11/13/1997	UM, 6.10–6.40 m	30.8	No	V
34	12/04/1997	UM, 6.10–6.40 m	11.5	No	V
35	01/12/1998	UM, 6.10–6.40 m	47.5	No	V
36	01/14/1998	UR, 4.27–4.57 m	11.9	Yes	V
37	02/05/1998	UR, 4.27–4.57 m	3.3	No	V
38	01/15/1998	UR, 4.88–5.18 m	11.4	Yes	V
39	02/06/1998	UR, 4.88–5.18 m	3.2	No	V
Niche 4788, DTN: LB0010NICH4LIQ.001 [153145]					
40	11/03/1999	UL, 7.62–7.93 m	5.5	Yes	V
41	11/30/1999	UL, 7.62–7.93 m	3.1	Yes	C
42	01/24/2000	UL, 7.62–7.93 m	0.5	No	V
43	06/26/2000	UL, 7.62–7.93 m	1.2	Yes	C
44	11/16/1999	UM, 6.10–6.40 m	5.5	Yes	V
45	12/10/1999	UM, 6.10–6.40 m	2.3	Yes	C
46	02/09/2000	UM, 6.10–6.40 m	0.5	?	–
47	03/14/2000	UM, 6.10–6.40 m	0.5	No	V
48	06/08/2000	UM, 6.10–6.40 m	1.2	Yes	C
49	12/07/1999	UR, 5.18–5.48 m	5.5	Yes	V
50	01/05/2000	UR, 5.18–5.48 m	2.4	Yes	C
51	02/14/2000	UR, 5.18–5.48 m	0.5	Yes	C
SYBT-ECRB-LA#2, DTN: LB00090012213U.002 [153154]					
52	05/11/2000	LA#2, zone 1	>450	Yes	V
53	05/17/2000	LA#2, zone 1	34.9	Yes	V
54	05/23/2000	LA#2, zone 1	26.3	Yes	V
55	05/23/2000	LA#2, zone 2	29.5	Yes	V
56	06/01/2000	LA#2, zone 2	31.6	Yes	V
57	05/17/2000	LA#2, zone 3	16.8	No	V
58	05/23/2000	LA#2, zone 3	26.1	No	V
59	06/01/2000	LA#2, zone 3	35.6	No	V
60	06/14/2000	LA#2, zone 3	37.8	Yes	V

Table 11 (cont.). Liquid-Release Test Events, Approximate Release Rate, Occurrence of Seepage, and Their Use for Calibration or Validation Purposes

Event	Starting Date of Test	Borehole, Interval	Approximate Release Rate [ml/min]	Seepage?	Calibration, Validation
SYBT-ECRB-LA#2, DTN: LB0110SYST0015.001 [160409]					
61	10/23/2000	LA#2, zone 2	33.0	Yes	C
62	11/27/2000	LA#2, zone 2	35.3	Yes	C
63	10/23/2000	LA#2, zone 3	38.0	Yes	C
64	11/27/2000	LA#2, zone 3	40.8	Yes	C
SYBT-ECRB-LA#1, DTN: LB0110ECRBLIQR.002 [156879]					
65	02/28/2001	LA#1, zone 2	17.0	No	C
66	04/03/2001	LA#1, zone 2	41.2	Yes	C
67	04/09/2001	LA#1, zone 2	43.9	Yes	C
68	04/17/2001	LA#1, zone 2	44.5	Yes	C
69	04/25/2001	LA#1, zone 2	43.1	Yes	C
SYBT-ECRB-LA#3, DTN: LB0203ECRBLIQR.001 [158462]					
70	05/17/2001	LA#3, zone 1	36.4	No	C
71	05/23/2001	LA#3, zone 1	24.7	Yes	C
72	05/17/2001	LA#3, zone 2	71.2	No	V
73	06/20/2001	LA#3, zone 2	31.2	No	V
74	07/05/2001	LA#3, zone 2	65.7	No	V
75	07/13/2001	LA#3, zone 2	47.9	No	V
76	07/16/2002	LA#3, zone 2	32.4	No	V
77	05/17/2001	LA#3, zone 3	0.0	No	–
Niche 1620, DTN: LB0207NICH5LIQ.001 [160408]					
78	05/06/2002	#5, 28–29 ft	72.0	Yes	V
79	05/06/2002	#2, 21–22 ft	120.0	No	–
80	05/17/2002	#2, 21–22 ft	120.0	No	–
81	05/16/2002	#5, 28–29 ft	60.0	Yes	V
82	05/21/2002	#5, 28–29 ft	72.0	Yes	–
Niche 1620, DTN: LB0209NICH5LIQ.001 [160796]					
83	07/17/2002	#3, 21–22 ft	55.0	Yes	–
84	07/29/2002	#3, 21–22 ft	33.0	Yes	–
85	08/14/2002	#3, 21–22 ft	9.0	Yes	–
86	07/15/2002	#5, 28–29 ft	25.8	Yes	C
87	07/31/2002	#5, 28–29 ft	25.8	Yes	V
88	08/05/2002	#5, 28–29 ft	11.3	Yes	V

Table 11 (cont.). Liquid-Release Test Events, Approximate Release Rate, Occurrence of Seepage, and Their Use for Calibration or Validation Purposes

Event	Starting Date of Test	Borehole, Interval	Approximate Release Rate [ml/min]	Seepage?	Calibration, Validation
Niche 1620, DTN: LB0211NICH5LIQ.001 [160792]					
89	09/17/2002	#4, 10–11ft	9.9	Yes	C
90	10/01/2002	#4, 10–11ft	4.8	No	V

6.5.4 Relative Humidity and Evaporation Rate Measurements

Reduced relative humidity in the ESF Main Drift, the ECRB Cross Drift, and the niches lead to partial evaporation of the water that reaches the opening, effectively reducing seepage. Neglecting evaporation effects in a seepage prediction model leads to higher seepage rates and is thus conservative. However, an overestimation of seepage in a model used for parameter determination would be compensated by a nonconservative increase in the estimated capillary-strength parameter. Following the recommendations made to address the evaporation issue (CRWMS M&O 2001 [153045], Section 7.5), humidity in the closed-off Niches 3107 and 4788 was artificially increased to reduce the evaporation potential, and relative humidity was monitored (BSC 2001 [158463], Figures 6.2.1-4 and 6.2.1-5). In the systematic testing area, additional curtains were installed on the two ends of the V-shaped seepage capture PVC curtains (BSC 2001 [158463], Figure 6.11.1-2) to reduce air circulation in the ventilated ECRB Cross Drift (after June 2000). In addition, relative humidity and evaporation rates from an open pan were measured (see, for example, BSC 2001 [158463], Figures 6.11.2-8 through 6.11.2-11). Relative humidity and evaporation rate were also measured in Niche 1620 (DTN: LB0207NICH5LIQ.001 [160408] and DTN: LB0211NICH5LIQ.001 [160792]).

The evaporation-rate data will be used to estimate the thickness of the diffusive boundary layer (see Section 6.6.1.4). The relative-humidity data will be applied as a time-dependent boundary condition determining the water potential in the opening.

6.6 MODEL FORMULATION

6.6.1 Mathematical Model

The mathematical model for unsaturated flow is based on the conceptual model outlined in the previous sections. The basic theoretical foundation for unsaturated flow in a continuum is outlined first, with a short discussion of the capillary pressure curve and its relevance for seepage (Sections 6.6.1.1 and 6.6.1.2). The incorporation of evaporation from a wetted porous surface is described in Sections 6.6.1.3 and 6.6.1.4. Section 6.6.1.5 contains a summary description of the inverse modeling methodology.

6.6.1.1 Unsaturated Flow

Flow in unsaturated porous or fractured media is described by the rate of change in liquid saturation and the flow rate at any given point. The continuum concept (see Section 6.3.2) stipulates the following equation of continuity, which describes the rate at which liquid saturation changes at a given point (Bear 1972 [156269], pp. 496, Equation 9.4.39):

$$\phi \rho \frac{\partial S}{\partial t} = \frac{\partial}{\partial x} q_x + \frac{\partial}{\partial y} q_y + \frac{\partial}{\partial z} q_z \quad (1)$$

Here, t [s] is time, ϕ [dimensionless] is porosity, S [dimensionless] is liquid saturation, ρ [kg m⁻³] is liquid density, and q [kg m⁻² s⁻¹] is the flow rate along the principal axes (x , y , and z). Considering that liquid flow is driven by gravity and pressure gradients (see Section 6.3.2), the liquid-flow rate is described by the Buckingham-Darcy law as follows (after Bear 1972 [156269], pp. 487–488, Equations 9.4.20 and 9.4.21):

$$q_x = \frac{k_r \rho}{\mu} k_x \frac{\partial P_c}{\partial x}, \quad q_y = \frac{k_r \rho}{\mu} k_y \frac{\partial P_c}{\partial y}, \quad \text{and} \quad q_z = \frac{k_r \rho}{\mu} k_z \frac{\partial}{\partial z} (P_c + \rho g z) \quad (2)$$

Here, k [m²] is absolute permeability, k_r [dimensionless] is relative permeability, μ [Pa·s] is liquid viscosity, g [m s⁻²] is gravitational acceleration, z [m] is the vertical coordinate (positive upward), and P_c [Pa] is the (negatively defined) capillary pressure. Substituting Equation (2) into Equation (1) leads to the governing equation of flow in unsaturated porous media (after Bear 1972 [156269], p. 496, Equation 9.4.41):

$$\phi \rho \frac{\partial S}{\partial t} = \text{div} \left[k \frac{k_r \rho}{\mu} \nabla (P_c + \rho g z) \right] \quad (3)$$

In Richards' equation, the relative permeability (k_r) and capillary pressure (P_c) are functions of liquid saturation as given, for example, by van Genuchten's model (after van Genuchten 1980 [100610], after Equations [8] and [3]):

$$k_r = S_e^{1/2} \left[1 - \left(1 - S_e^{1/m} \right)^m \right]^2 \quad (4)$$

$$P_c = -\frac{1}{\alpha} [S_e^{-1/m} - 1]^{1-m} \quad (5)$$

In van Genuchten's equations, the effective saturation, S_e , is defined as

$$S_e = \frac{S - S_{lr}}{1 - S_{lr}} \quad (6)$$

where S_{lr} is residual liquid saturation, and $1/\alpha > 0$ [Pa] and $0 < m < 1$ [dimensionless] are fitting parameters. The roles of the parameters in the capillary pressure and relative permeability functions are illustrated in Figure 5. The parameter $1/\alpha$ describes the point of inflection in the capillary-pressure function (Equation (5)) shown in Figure 5a. The factor $1/\alpha$ scales the capillary pressure curve and is therefore referred to as the capillary-strength parameter.

The parameter m determines the slopes of the capillary pressure and relative permeability functions. It is a measure of the spread of the effective pore size distribution; a large m value implies a narrow pore size distribution. The use of continuous relative-permeability and capillary-pressure functions, which apply to porous media, is considered appropriate also for small fracture segments that are rough-walled and/or partially filled with porous material.

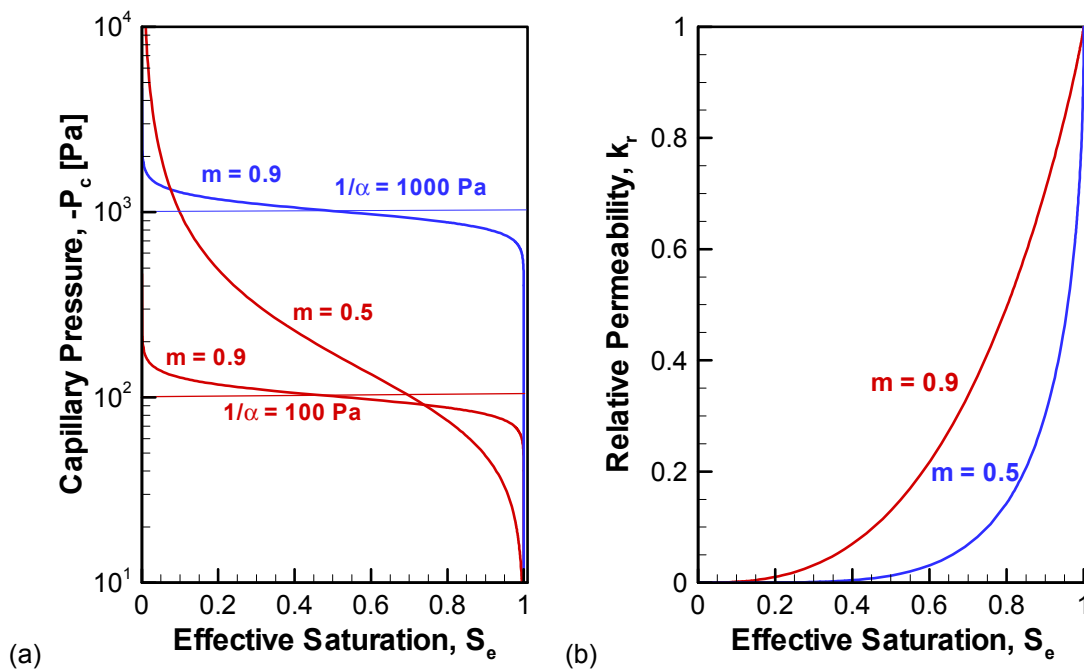


Figure 5. (a) Capillary-pressure curves and (b) relative-permeability curves for different illustrative van Genuchten parameters.

6.6.1.2 Onset of Seepage

For a circular opening in a homogeneous medium, the threshold for liquid entry into the cavity is full saturation at the apex (Philip et al. 1989 [105743]). For the liquid that enters the opening to

form a drop at the opening wall and detach (see definition of seepage in Section 6.1.2), a positive pressure that offsets the drop pressure is required (Or and Ghezzehei 2000 [144773], pp. 390-392).

For a numerical model in which the continuum is discretized into discrete gridblocks, the condition for seepage is determined by the total water-potential gradient at the connection between the fractured medium and the opening as depicted in Figure 6. From Equation (2) it follows that downward seepage in a discrete numerical mesh, $q_z > 0$, occurs only when the following condition is satisfied:

$$P_c + \rho g \Delta z > 0 \quad (7)$$

where P_c is the capillary pressure at the last node adjacent to the opening. Given that the capillary pressure in the opening is zero, the numerical threshold capillary pressure is defined as $P_c^* = -\rho g \Delta z$, where Δz is the distance between the last node and the opening. The numerical threshold capillary pressure P_c^* therefore depends on the nodal distance between the last node and the opening. The opening surface does not need to be fully saturated for seepage to commence as given by the analytical solutions of Philip et al. (1989 [105743]). As indicated in Figure 6, given a numerical grid, the seepage-threshold liquid saturation is lower for larger Δz and for lower capillary strength ($1/\alpha$). Consequently, whether liquid that reaches the surface seeps or is diverted around the opening (effectiveness of the capillary barrier) is primarily determined by the $1/\alpha$ parameter. Note that the relative permeability function (Equation (4)) does not depend on $1/\alpha$. Hence, the capillary-strength parameter is the main subject of the SCM presented in this report (see also discussion in Section 6.6.3.1). The fact that the seepage threshold depends on the length of the nodal distance to the opening makes the values of the estimated capillary-strength parameter ($1/\alpha$) applicable only to numerical models of comparable discretization (Section 6.6.2.2).

Figure 6 shows that a reasonable variation in the m parameter has only a limited effect on the seepage threshold saturation; a stronger effect is seen for a change in $1/\alpha$, which tends to vary more than m . Therefore, fixing the parameter m appears reasonable as confirmed by the formal sensitivity analysis (see Section 6.6.3.1 below). Moreover, any potential variability of m is accounted for in the calibrated $1/\alpha$ parameter. The relative sensitivity and potential identifiability of seepage-relevant parameters are further discussed in Section 6.6.3.1.

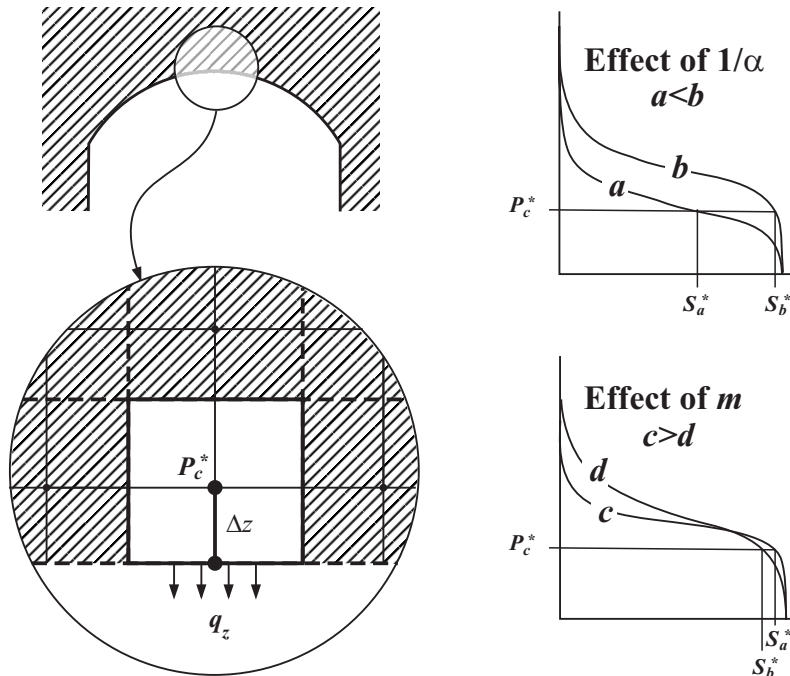


Figure 6. Schematic description of seepage condition. A change in $1/\alpha$ has a greater impact on the seepage threshold saturation than a change in m .

6.6.1.3 Incorporation of Evaporation Effects

Part of the liquid that reaches the surface of the underground opening evaporates by virtue of the vapor concentration gradient at the surface. Considering that the evaporation is an isothermal diffusive process, the evaporative flux (q_e [$\text{kg m}^{-2} \text{s}^{-1}$]) applied at the wall of the opening is given by:

$$q_e = D \frac{dC}{dx} \quad (8)$$

where D [$\text{m}^2 \text{sec}^{-1}$] is the vapor diffusion coefficient and C [kg m^{-3}] is the vapor concentration. The vapor concentration at the surface of the opening (C^o) is related to the capillary pressure by Kelvin's equation (after Campbell and Norman 1998 [150929], Eqs. 3.11 and 3.17):

$$C^o = \frac{M_w P_{sat}}{RT} \exp\left[\frac{P_c M_w}{\rho R T}\right] \quad (9)$$

where M_w [$0.01802 \text{ kg mol}^{-1}$] is the molecular mass of water, R [$8.314 \text{ J K}^{-1} \text{ mol}^{-1}$] is the universal gas constant, P_{sat} [Pa] is the saturated vapor pressure, T [K] is the temperature, and the expression $\exp[P_c M_w / (\rho R T)]$ denotes the relative humidity (Ho 1997 [141521], Eq. 10). The vapor concentration of bulk air of the opening (C^∞) is related to the relative humidity h by

$$C^\infty = \frac{P_{sat} \cdot M_w \cdot h}{R \cdot T}. \quad (10)$$

The vapor concentration undergoes a gradual transition from C^o to C^∞ within a finite distance away from the opening surface, here referred to as the evaporative boundary layer, whose thickness (δ) is inversely related to the airflow velocity (e.g., Rohsenow and Choi 1961 [158324], pp. 36–40). The vapor concentration gradient is presumed linear within the boundary layer. Then, Equation (8) can be rewritten as:

$$q_e = D \frac{C^o - C^\infty}{\delta} \quad (11)$$

The vapor diffusion coefficient depends on temperature and pressure as given by (Pruess 1987 [100684], pp. 5–6):

$$D = D^o \left(\frac{10^5}{P} \right) \cdot \left(\frac{T}{273.15} \right)^{1.8} \quad (12)$$

where $D^o = 2.13 \times 10^{-5} \text{ m}^2 \text{ s}^{-1}$ is the vapor diffusion coefficient at standard conditions of $T = 273.15 \text{ K}$ and $P = 10^5 \text{ Pa}$.

The implementation of evaporation effects into iTOUGH2 V5.0 (LBNL 2002 [160106]) is described in detail in BSC (2002 [161067], Section 1.2).

6.6.1.4 Estimation of Evaporative Boundary-Layer Thickness

The thickness of the evaporative boundary layer (δ , see Equation (11)) can be estimated by calibration using evaporation data measured under known vapor concentration and temperature conditions. The δ values employed in this Model Report were obtained by calibration using free-water evaporation data collected inside and outside of Niche 1620 (DTN: LB0207NICH5LIQ.001 [160408]) (Section 6.5.4). The vapor concentration at the surface of free water is given by Equation (9) with $P_c = 0 \text{ Pa}$.

The available evaporation data are grouped into three classes based on airflow velocity; (1) inside Niche 1620 without ventilation, (2) outside of Niche 1620 with active ventilation, and (3) outside of Niche 1620 without active ventilation, the regime usually encountered during nights and weekends. In Figure 7 and Figure 8, the relative humidity, temperature and measured and fitted evaporation rates are plotted for inside and outside of Niche 1620, respectively (Wang 2003 [161456], SN-LBNL-SCI-223-V1, pp. 22–25).

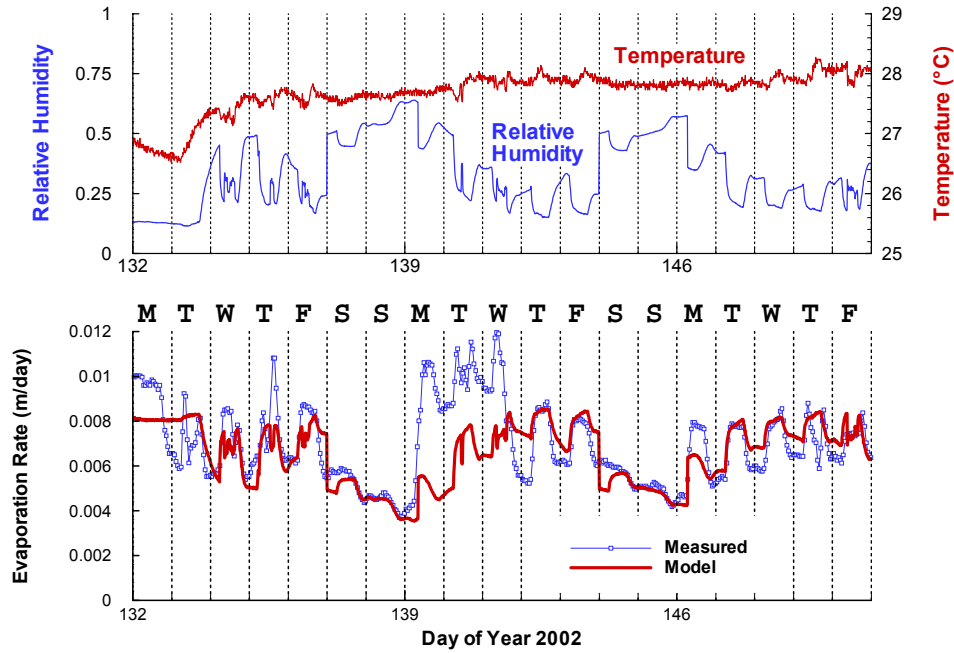


Figure 7. Relative humidity, temperature, and measured and fitted evaporation rates from experiments conducted outside Niche 1620 (DTN: LB0207NICH5LIQ.001 [160408]). Relative humidity is higher during nights and weekends, and evaporation is decreased accordingly.

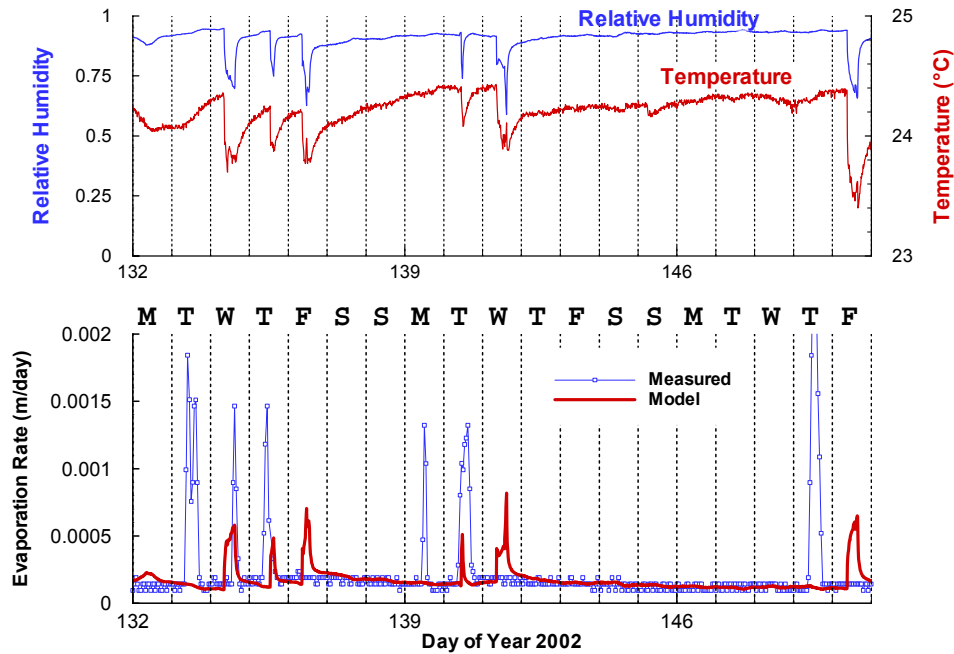


Figure 8. Relative humidity, temperature, and measured and fitted evaporation rates from experiments conducted inside Niche 1620 (DTN: LB0207NICH5LIQ.001 [160408]).

The boundary-layer thickness was estimated by fitting Equation (11) to the evaporation data (Wang 2003 [161456], SN-LBNL-SCI-223-V1, pp. 22–25); the estimated values are listed in Table 12.

Table 12. Boundary-Layer Thickness Estimated Using Equation (11) and Relative Humidity, Temperature, and the Evaporation Data from a Free Water Surface Shown in Figure 7 and Figure 8. Boundary-layer thickness in DTN: LB0302SCMREV02.002 and reflected in meshes of DTN: LB0302SCMREV02.001.

Location of Evaporation Experiment	Boundary-layer thickness (mm)	Used For Simulation of Liquid-Release Tests in...
Inside Niche 1620	20.0	Niche 1620 (Niche 5)
Outside Niche 1620, Weekdays (ventilation on)	5.0	ECRB (no end curtains)
Outside Niche 1620 Weekends (ventilation off)	7.5	ECRB (with end curtains)

An evaporative boundary-layer thickness $\delta = 0.02$ m was used for the simulation of liquid-release tests in Niche 1620. Some of the liquid-release tests performed in the open drift of the ECRB were exposed to ventilation; a boundary-layer thickness $\delta = 0.005$ m was used for these simulations. In more recent tests, additional curtains were installed at the two ends of the V-shaped seepage capture curtains to reduce air circulation and thus partly protect the seepage section of the drift from ventilation effects; a boundary-layer thickness $\delta = 0.0075$ m was used for these simulations.

6.6.1.5 Summary Description of Inverse Modeling Methodology

The inverse modeling approach followed here is based on the classical weighted least-squares method, which consists of minimizing the objective function

$$S = \mathbf{r}^T \mathbf{C}_{zz}^{-1} \mathbf{r} \quad (13)$$

The residual vector \mathbf{r} contains the differences between the measured seepage rate, z^* , and the corresponding model prediction, $z(\mathbf{p})$, which is a function of the unknown, n -dimensional parameter vector \mathbf{p} , i.e., $r_i = (z_i^* - z(\mathbf{p})_i)$, $i = 1 \dots m$, where m is the number of calibration points. The inverse of the covariance matrix \mathbf{C}_{zz} , which holds the expected variances of the final residuals on its diagonal, is used as a weighting matrix. The objective function is a measure of the misfit between the model output and the measured data. The objective function is automatically minimized using the Levenberg-Marquardt algorithm implemented in iTOUGH2 V5.0 (Finsterle 1999 [104367], Section 2.7.4).

The covariance matrix of the estimated parameters is asymptotically given by:

$$\mathbf{C}_{pp} = s_0^2 (\mathbf{J}^T \mathbf{C}_{zz}^{-1} \mathbf{J})^{-1} \quad (14)$$

where \mathbf{J} is an $m \times n$ Jacobian matrix holding the partial derivatives of the predicted seepage with respect to the unknown parameters, $J_{ij} = \partial z_i / \partial p_j$, and s_0^2 is the estimated error variance, which represents the variance of the mean weighted residual; it is an aggregate measure of goodness-of-fit:

$$s_0^2 = \frac{\mathbf{r}^T \mathbf{C}_{zz}^{-1} \mathbf{r}}{m - n} \quad (15)$$

The impact of parameter uncertainty (expressed through matrix \mathbf{C}_{pp}) on model predictions can be evaluated by means of first-order-second-moment uncertainty propagation analysis. The covariance matrix of the model prediction, $\mathbf{C}_{\hat{z}\hat{z}}$, is calculated based on a linearity and normality assumption using

$$\mathbf{C}_{\hat{z}\hat{z}} = \mathbf{J} \mathbf{C}_{pp} \mathbf{J}^T \quad (16)$$

The inverse modeling methodology and its numerical implementation are described in detail in the iTOUGH2 software documentation, specifically Finsterle (1999 [104367], Section 2).

6.6.2 Development of Forward Model

The numerical model constructed to simulate liquid-release tests and seepage into the underground openings is referred to as the forward model. Different forward models were created for the different test locations and liquid-release events. During the inversion, the seepage rates calculated by the forward model are compared to the measured seepage rates at discrete points in time. (If the calibration time does not coincide with a data collection time, the comparison occurs against a value linearly interpolated between the measurements). The discrepancies between the two rates are then used to automatically update the input parameters of the forward model. The solution to both the forward and inverse problem is calculated by iTOUGH2 V4.0 (LBNL 1999 [139918]) and V5.0 (LBNL 2002 [160106]).

6.6.2.1 Generation of Permeability Field

Air-injection tests performed in borehole intervals at the experimental sites were used to estimate effective permeabilities (see Section 6.5.2, Table 10). The spatial structure of the permeability data was analyzed, and the resulting geostatistical parameters were used to generate spatially correlated permeability fields (for details, see Attachment III, Attachment IV, and Attachment V). Multiple realizations of the permeability field were simulated by changing the seed number of the random-number generator of the software SISIM V1.203 (LBNL 1999 [134136]) and V1.204 (LBNL 2000 [153100]) (see Figure III-5). The permeability fields were eventually mapped onto the numerical grid (see Section 6.6.2.2).

The GSLIB modules GAMV2 V1.201 (LBNL 1999 [134139]) and GAMV3 V1.201 (LBNL 2000 [153099]) were used to analyze spatial correlation of, respectively, two-dimensional and three-dimensional, irregularly spaced, log-transformed air-permeability data. Sequential indicator simulation (Deutsch and Journel 1992 [100567], p. 151) as implemented in the GSLIB modules SISIM V1.203 (LBNL 1999 [134136]) and V1.204 (LBNL 2000 [153100]) was used to generate spatially correlated, random fields of log-transformed permeability modifiers (see Figure III-2).

Borehole SYBT-ECRB-LA#2, Lower Lithophysal Zone

Six air-injection tests were performed in 6 ft (approximately 1.8 m) long intervals of borehole SYBT-ECRB-LA#2 (DTN: LB00090012213U.001 [153141]), providing an estimate of mean log-permeability at the experimental site of -10.73 (corresponding to a permeability of $1.86 \times 10^{-11} \text{ m}^2$) with a standard deviation of 0.21 (see Table 10). Variability in permeability on the scale of a gridblock (which is 1 ft long) is expected to be higher than the standard deviation reported in Table 10. For the purpose of generating a heterogeneous field, permeability is taken to be log-normally distributed with a standard deviation of one order of magnitude. The number of data points was insufficient to reveal the spatial correlation structure of the permeability field. A weak spatial correlation was prescribed (consistent with the geostatistical results from air-permeability data in the middle nonlithophysal zone, see below). A correlation length of 0.2 m was specified. Multiple realizations of the permeability field were generated.

Niche 1620, Lower Lithophysal Zone

A total of 61 air-injection tests were conducted in three boreholes (boreholes #2, #3, and #5) above Niche 1620 (DTN: LB0110AKN5POST.001 [156904]). The length of the injection interval was 1 ft. The mean and standard deviation of the log-transformed permeability values are provided in Table 10. The permeability values are approximately log-normally distributed as shown in Figure 9.

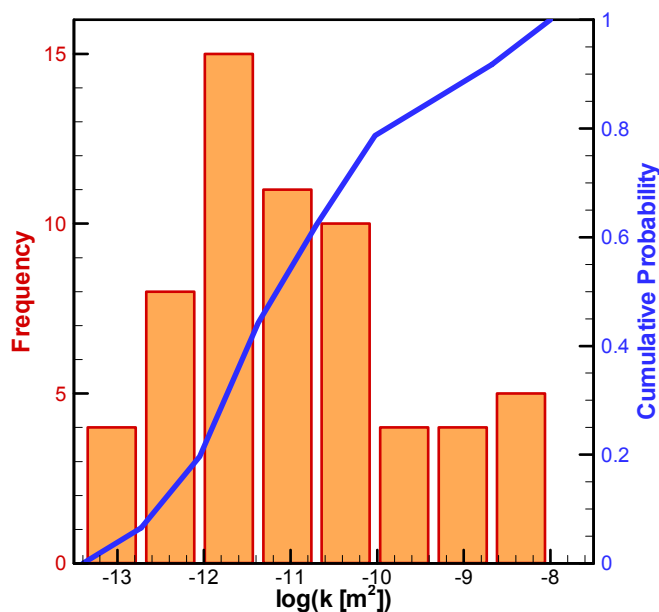


Figure 9. Cumulative frequency distribution of the log-transformed permeability values and corresponding cumulative normal probability density function for Niche 1620. Permeability data from DTN: LB0110AKN5POST.001 [156904]; histogram and cumulative probability distribution in DTN: LB0302SCMREV02.001.

The post-excavation air-permeability data were geostatistically analyzed using the software GAMV3 V1.201 (LBNL 2000 [153099]) to calculate the empirical semivariogram specific to Niche 1620. The nugget effect, correlation length, and sill values were determined by fitting a spherical semivariogram (Deutsch and Journel 1992 [100567], p. 23) to the empirical semivariogram (Wang 2003 [161456], SN-LBNL-SCI-223-V1, p. 16). Figure 10 shows the empirical semivariogram and corresponding theoretical spherical semivariogram of Niche 1620. The geostatistical parameters are provided in Table 13 below. The generated spatially correlated permeability field is conditioned on the measured post-excavation air-permeability data as shown in Figure 11. The stochastic simulation approach may generate permeability values that are considerably different from those at the neighboring conditioning points, i.e., the field is more heterogeneous than one created by means of an interpolation technique. Multiple realizations were generated.

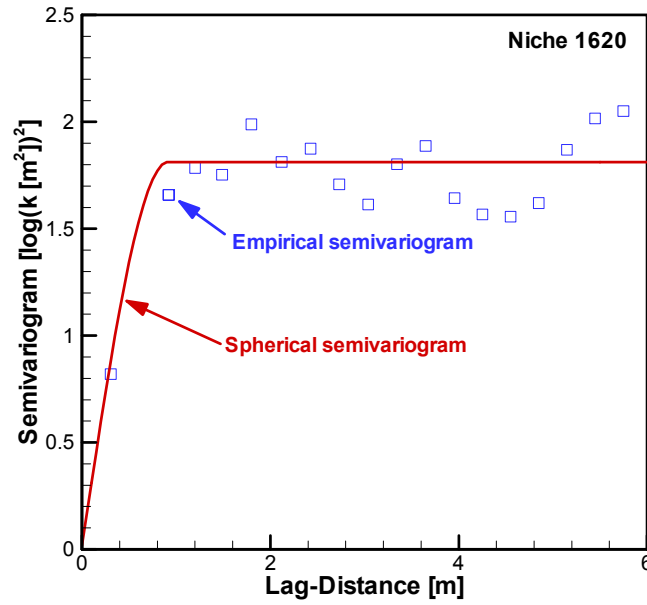


Figure 10. Empirical post-excitation air-permeability semivariograms and spherical semivariogram model for Niche 1620. See Table 13 for geostatistical parameters of the spherical semivariogram model. Permeability data from DTN: LB0110AKN5POST.001 [156904]; semivariogram in DTN: LB0302SCMREV02.001.

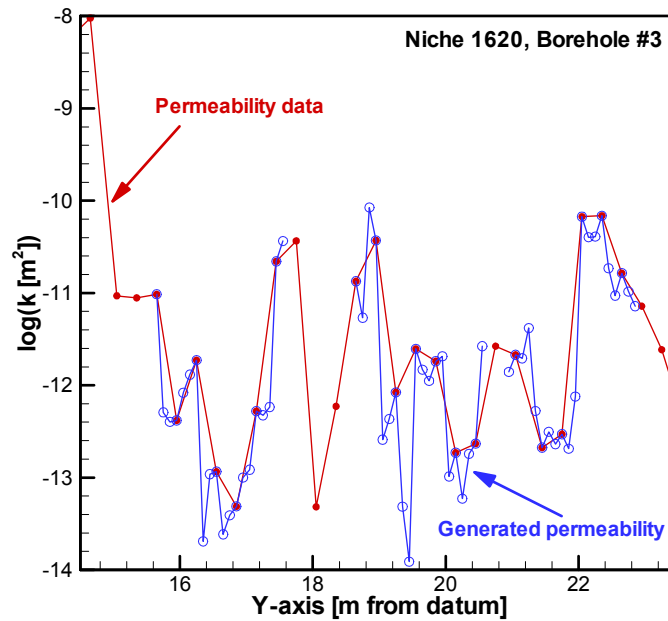


Figure 11. Post-excitation permeability data of Niche 1620, borehole #3 and the corresponding generated permeability values from one representative realization, which honors the measured data. Permeability data from DTN: LB0110AKN5POST.001 [156904]; generated permeabilities in DTN: LB0302SCMREV02.001.

Niches 3107, 3650, and 4788, Middle Nonlithophysal Zone

A total of 225 air-injection tests were performed in 10 boreholes above Niche 3107 (DTN: LB990601233124.001 [105888]), Niche 3650 (DTN: LB0011AIRKTEST.001 [153155]), and Niche 4788 (DTN: LB990601233124.001 [105888]). The mean, standard deviation, and number of air-permeability data for each niche are shown in Table 10.

For Niche 3650, the software GAMV2 V1.201 (LBNL 1999 [134139]) was used to calculate the empirical semivariogram, given that all intervals in boreholes UL, UM, and UR lie within a two-dimensional plane. The appropriateness of this presumption was confirmed by surveyed borehole alignments for Niche 3650 (DTN: MO0002GSC00076.000 [152623]). For Niches 3107 and 4788, the software GAMV3 V1.201 (LBNL 2000 [153099]) was used to calculate the empirical semivariogram. The three-dimensional coordinates of the permeability data were taken from the detailed borehole alignment surveys (DTN: MO0002GSC00064.000 [152625] and DTN: MO0107GSC01069.000 [156941]).

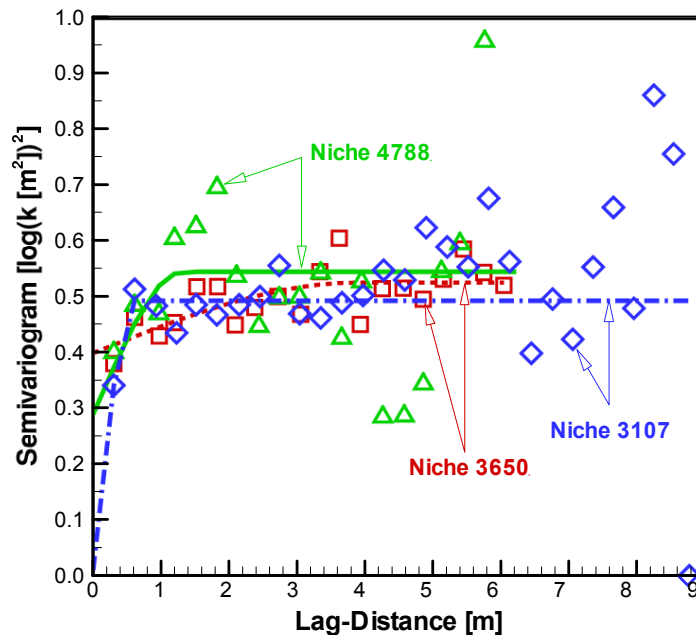


Figure 12. Empirical post-excitation air-permeability semivariograms and fitted spherical semivariogram models for Niches 3107, 3650, and 4788. See Table 13 for geostatistical parameters of the spherical semivariogram models. Permeability data from DTN: LB990601233124.001 [105888] and DTN: LB0011AIRKTEST.001 [153155]; semivariograms in DTN: LB0010SCMREV01.001 [154292].

Spherical semivariogram models (Deutsch and Journel 1992 [100567], p. 23) with the geostatistical parameters shown in Table 13 are used to represent the empirical log-permeability semivariograms. The empirical semivariograms (symbols) and the corresponding spherical semivariogram models (lines) are shown in Figure 12. Note that the relatively large correlation length obtained for Niche 3650 should not be misinterpreted as suggesting that the permeability field is strongly correlated. All three semivariograms shown in Figure 12 exhibit either a short correlation length (i.e., on the order of 1 meter or less) or a nugget effect that is close to the sill

value. It can therefore be concluded that the permeability is random without a noticeable or significant spatial correlation. No nugget effect is evident for the Niche 3107 data, resulting in a permeability field that is slightly spatially correlated (see Figure 16c below).

Table 13. Geostatistical Parameters of Spherical Semivariogram Models (DTN: LB0302SCMREV02.002)

Niche	Nugget effect [log(k) ²]	Correlation length [m]	Sill value [log(k) ²]
Niche 1620	0.02	0.91	1.81
Niche 3107	0.01	0.61	0.49
Niche 3650	0.40	3.87	0.53
Niche 4788	0.29	1.31	0.55

The spherical semivariogram models, along with the cumulative distribution functions shown in Figure 13, are used as input to the software SISIM V1.203 (LBNL 1999 [134136]) for Niches 3107 and 4788; the software SISIM V1.204 (LBNL 2000 [153100]) is used for Niche 3650. The random permeability field is conditioned on the measured post-excavation air-permeability data. For Niches 3107 and 4788, coordinates are added to the permeability field using software AddCoord V1.0 (LBNL 2000 [152814]). The resulting permeability fields are mapped onto the numerical grid of the SCM for each of the niches, as described below in Section 6.6.2.2. Only one permeability field is produced for each niche. The generation of permeability fields is documented in Scientific Notebooks Finsterle (1999 [153448], p. 139) and Ahlers (2002 [161045], pp. 13, 15–19, 21, 39–40, 58).

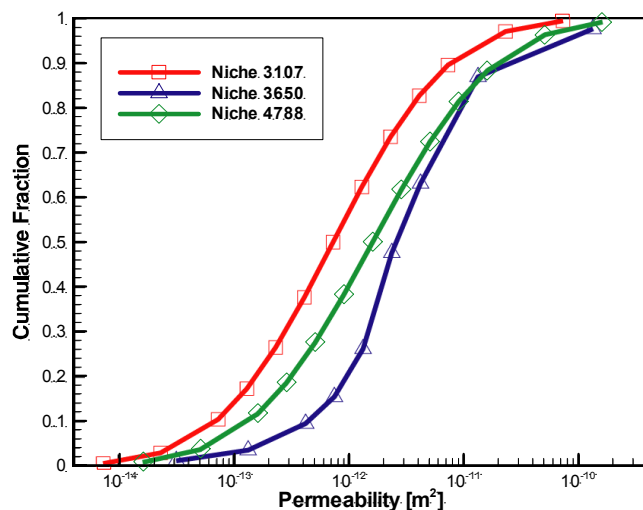


Figure 13. Cumulative distribution functions of air permeabilities for Niches 3107, 3650, and 4788. Permeability data from DTN: LB990601233124.001 [105888] and DTN: LB0011AIRKTEST.001 [153155]; cumulative distribution function in DTN: LB0010SCMREV01.001 [154292].

6.6.2.2 Mesh Generation

Three-dimensional meshes of a section of the ECRB Cross Drift and Niches 1620, 3107, 3650, and 4788 were created in several steps. The following general steps were followed for all the meshes. Detailed and specific descriptions pertaining to the Cross Drift and different niches are provided in Attachment III, Attachment IV, and Attachment V.

1. A primary 3D mesh is generated, consisting of regular gridblocks. The Y-axis is aligned with the drift or niche axis.
2. Constants are added to the coordinates of the primary mesh using software MoveMesh V1.0 (LBNL 2000 [152824]) to shift the origin of the mesh to an appropriate datum.
3. A random, spatially correlated field of log-permeability modifiers is generated using software SISIM V1.203 and SISIM V1.204 (LBNL 1999 [134136]; LBNL 2000 [153100]) as described in Section 6.6.2.1. Multiple realizations are created for locations in the lower lithophysal zone.
4. The heterogeneous field of log-permeability modifiers is mapped onto the mesh using software Perm2Mesh V1.0 (LBNL 2000 [152826]).
5. For the tests in the ECRB Cross Drift, a cylindrical drift is cut from the primary mesh using the software CutDrift V1.0 (LBNL 2000 [152816]); for Niche 3650, a smooth niche is cut using software CutNiche V1.3 (LBNL 2000 [152828]); for Niches 1620, 3107, and 4788, an irregularly shaped niche is cut using software CutNiche V1.2 (LBNL 2000 [152815]).
6. Software AddBound V1.0 (LBNL 2000 [152823]) is used to attach boundary elements at the top and bottom of the model domain. The bottom boundary gridblock is assigned to a special material domain to allow specifying a free-drainage boundary condition.
7. Gridblocks along the boreholes are modified to represent the injection intervals. For the inclined boreholes in the ECRB Cross Drift, software AddBorehole V1.0 (LBNL 2000 [152822]) was used for this task.
8. The drift or niche gridblocks are assigned a large volume so that Dirichlet boundary conditions can be specified. Flux into these gridblocks represents seepage.
9. For the tests in the ECRB Cross Drift and Niche 1620, new evaporation gridblocks are added and connected to the same formation elements as do the drift and niche gridblocks, respectively. The nodal distance from the formation gridblocks to the evaporation gridblocks is set to the diffusive boundary-layer thickness (see Table 12). Flux into these elements represents evaporation.
10. A single time step is performed using a generic TOUGH2 input *onestep* file (as input to iTOUGH2 V4.0 or V5.0; see Figure III-4) to test the mesh and to obtain cross-referencing information.

Typical meshes created for the simulation of liquid-release tests in the ECRB Cross Drift, Niche 1620, and Niches 3107, 3650, and 4788 are shown in Figure 14, Figure 15, and Figure 16, respectively.

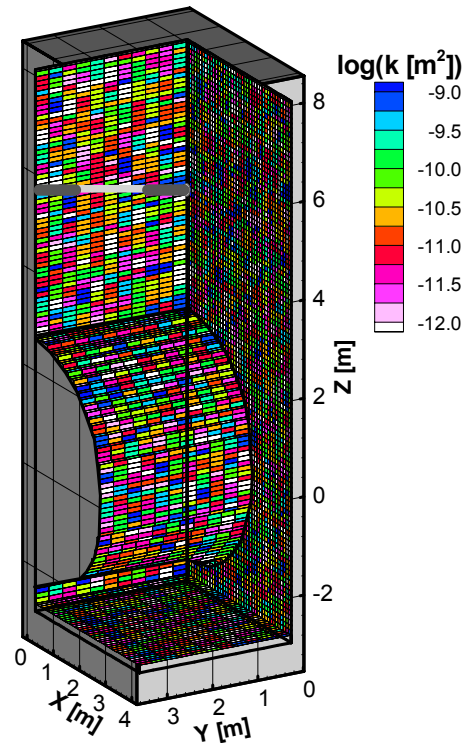


Figure 14. Numerical grid with one realization of the permeability field used for the simulation of liquid-release tests conducted in zone 2 of borehole SYBT-ECRB-LA#2. Only half of the drift is simulated because of symmetry. The vertical position of the injection interval (indicated in light gray) is appropriately adjusted for the simulation of seepage experiments conducted in other test zones. Multiple realizations of the permeability field are generated. All mesh files in DTN: LB0302SCMREV02.001.

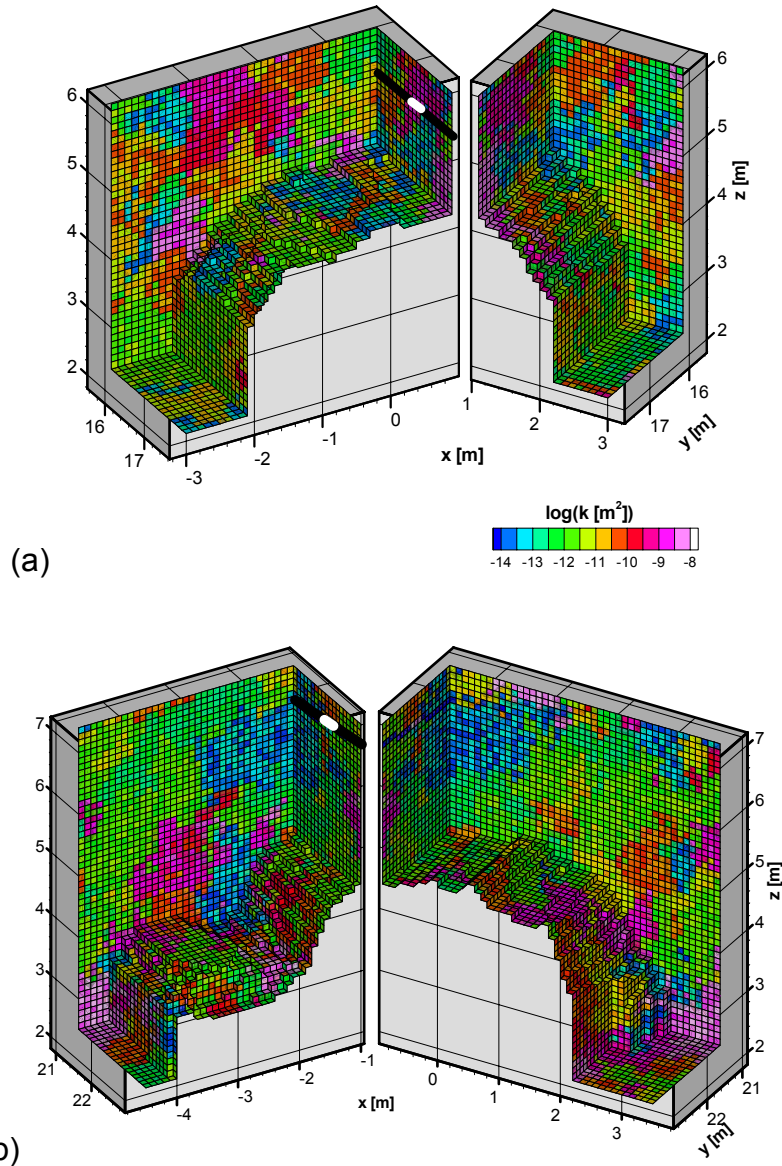


Figure 15. Numerical grid with one realization of the permeability field used for the simulation of liquid-release tests conducted in Niche 1620, (a) borehole #4, (b) borehole #5. In this visualization, the meshes are split into two parts to expose the boreholes (indicated by thick black lines) and the injection interval (thick white lines). Multiple realizations of the permeability field are generated. Note the rough ceilings as well as the left and right slots of Mesh (b). All mesh files in DTN: LB0302SCMREV02.001.

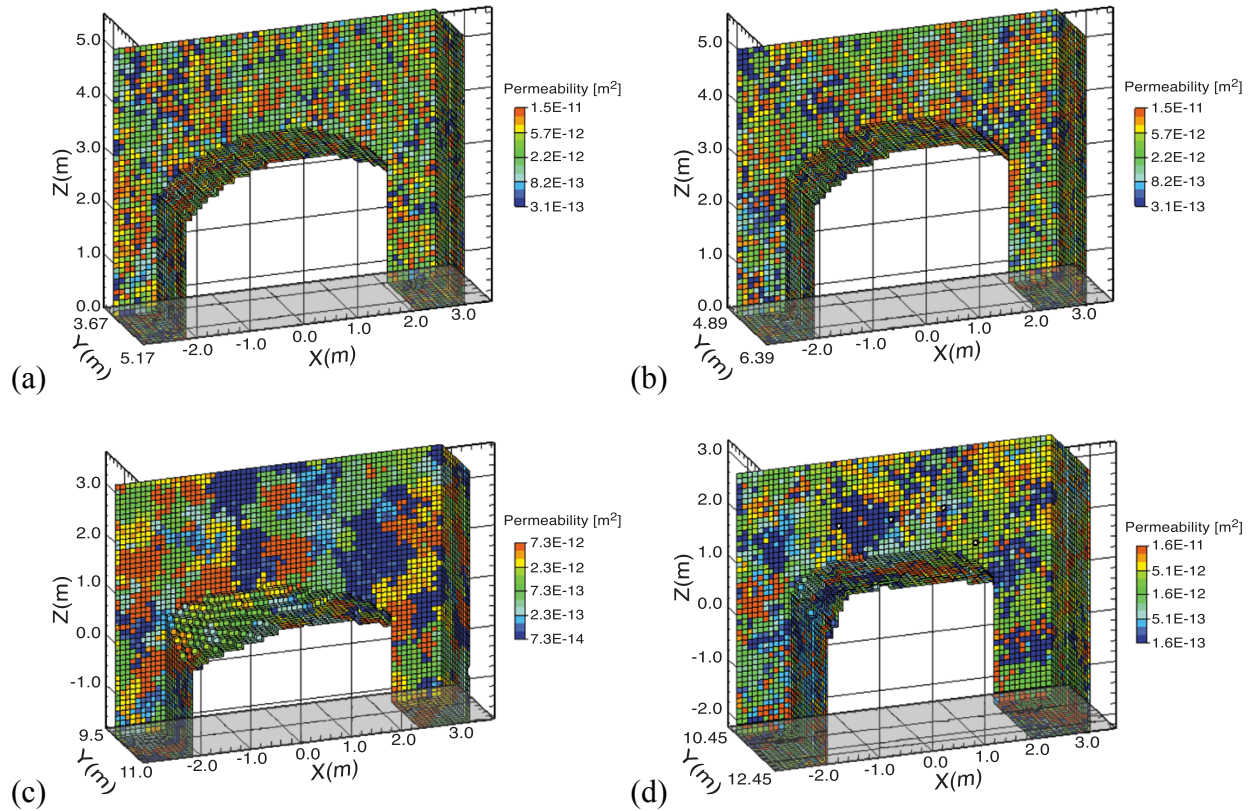


Figure 16. Computational meshes and permeability field for 3D seepage calibration model used for the analysis of seepage data from (a) Niche 3650, centered 4.42 m from the collar of borehole UM, (b) Niche 3650, centered 5.64 m from the collar of borehole UM, (c) Niche 3107, and (d) Niche 4788. Note that the meshes are shown from an angle below horizontal to display the ceiling roughness incorporated into Meshes (c) and (d). All mesh files in DTN: LB0010SCMREV01.001 [154292].

6.6.2.3 Boundary Conditions

No-flow boundary conditions are specified at the left, right, front, and back sides of the model. A free-drainage boundary condition (Finsterle 1998 [103783], pp. 14–15) is applied at the bottom to prevent an unphysical capillary boundary effect. All elements representing large openings (i.e., borehole intervals, drift sections, or niches) are assigned a zero capillary pressure independent of saturation. The evaporation elements are set at a capillary pressure equivalent to the prevailing relative humidity h according to Kelvin's equation,

$$p_c = -\frac{RT}{M_w} \rho_w \ln(h) \quad (17)$$

as discussed in Section 6.6.1.3. Water is allowed to enter, but prevented from exiting the drift or niche.

A constant flux boundary condition is applied at the top of the model to represent background percolation. The percolation flux at the experimental site is taken from the UZ Model (DTN: LB990801233129.003 [122757]). (Note that slight changes in the calculated percolation flux as a

result of future revisions of the UZ Model will not impact the estimates and conclusions presented in this Model Report). Software ECRB-XYZ V.03 (CRWMS M&O 1999 [147402]) is used to calculate the coordinates of Cross Drift construction station CS 1726 (Hinds 2001 [155955], p. 124). The gridblock closest to these coordinates and those of Niches 3107, 3650, and 4788 are identified from the UZ Model mesh file (DTN: LB990701233129.001 [106785]), and the corresponding percolation flux for the present-day, mean infiltration scenario is extracted from the UZ Model output file (DTN: LB990801233129.003 [122757]) (Ahlers 2002 [161045], pp. 29–31, 45, 55).

The resulting percolation flux of approximately 13.6 mm/yr is injected into a single boundary element connected to all gridblocks across the top of the ECRB Cross Drift and Niche 1620 model domains. Percolation fluxes of approximately 2.54 mm/yr for Niche 3107, 2.80 mm/yr for Niche 3650, and 2.02 mm/yr for Niche 4788 are injected at the top of the respective model domains. Note that the inflow into the model is non-uniform as a result of the heterogeneity in the permeability field.

As evident from Figure 18, the average background percolation flux is significantly less than the local flux induced by releasing water from the injection intervals. The impact of the background percolation flux on simulated seepage rates is thus very limited.

For the simulation of liquid-release tests, release rates and test durations are determined for each event (see Table 11) and applied to the gridblocks representing the injection interval (Ahlers 2002 [161045], pp. 8–10, 34–35, 47; Finsterle 2002 [161043], p. 57; Wang 2003 [161456], SN-LBNL-SCI-228-V1, pp. 16–17, 19–20).

6.6.2.4 Initial Conditions

The initial saturation distribution is calculated from the steady-state flow field obtained for background percolation, followed by a simulation of reduced relative humidity, which creates a dry-out zone around the ventilated opening (Niche 1620 and ECRB Cross Drift only).

The initial saturation distribution in the fracture continuum is generally low but nonuniform. It is not expected to have a significant impact on simulation results. The variability in the initial saturation distribution is a result of formation heterogeneities and the presence of the underground opening and a dry-out zone (if evaporation is simulated). Since the steady-state flow field changes if the input parameters are updated during the inversion, a steady-state run precedes each transient liquid-release test simulation performed as part of the inversion process.

Details about the steady-state simulations performed to create initial conditions for the subsequent simulation of liquid-release tests can be found in Attachment VII.

6.6.3 Inversion

The software iTOUGH2 V4.0 (LBNL 1999 [139918]) and V5.0 (LBNL 2002 [160106]) is used to automatically calibrate the forward models against seepage-rate data. The iTOUGH2 V5.0 (LBNL 2002 [160106]) program is used for calibrating liquid-release tests performed in the lower lithophysal zone (Tptpl; Niche 1620 and systematic seepage testing in the ECRB Cross Drift); these models include evaporation effects (see Sections 6.3.3.4, and 6.6.1.3). The

iTOUGH2 V4.0 (LBNL 1999 [139918]) program was used for the analysis of tests conducted in closed-off Niches 3107 and 4788 located in the middle nonlithophysal zone (Ttpmn), where evaporation is significantly reduced and thus not considered (see Sections 6.3.3.4 and 6.7). The parameters and data selected for model calibration are described below in Sections 6.6.3.1 and 6.6.3.2, respectively. The results of the inversions are discussed in Section 6.6.3.3.

6.6.3.1 Parameter Selection

Inverse modeling requires selecting one or more parameters that are considered unknown or uncertain and that are to be adjusted to match the model calculations to the observed data. All the other input parameters to the numerical model, including model-domain geometry as well as initial and boundary conditions, are fixed during the inversion and are thus by definition part of the model structure. The estimated parameters are optimal for and depend on this model structure.

The selection of the parameter to be estimated can be based on (1) the physical understanding of the system behavior as it relates to the observed data, (2) a sensitivity analysis, or (3) a synthetic inversion using a derivative-based algorithm, which reveals both the sensitivity coefficients and parameter correlations. In a first step, the parameters most likely to affect seepage rates are selected, based on the understanding of the physical system behavior. Subsequently, these parameters are subjected to a synthetic inversion to identify the most sensitive parameters and their correlation structure. Finally, a selection of the parameters to be estimated is made based on their overall sensitivity, relative independence, and the availability and reliability of prior knowledge.

The seepage process and impact of parameterized hydrogeologic properties on seepage rates has been discussed in Section 6.3.3. To summarize, the seepage rates observed during liquid-release tests are most strongly affected by the following parameters:

1. Parameters of the capillary pressure function are expected to affect seepage rates because they determine the effectiveness of the capillary barrier. The two parameters of interest are the van Genuchten capillary-strength parameter $1/\alpha$ and m , which is related to the pore size distribution index. Both parameters have been discussed in Section 6.6.1.1.
2. Effective permeability impacts the flow-diversion capability of the fractured formation and thus seepage rates.
3. Porosity can be interpreted as an effective parameter capturing storage effects. Storage effects may be significant at early times, for short-duration experiments, and if only a small amount of water is injected (as in the liquid-release tests conducted in Niche 3650).

A synthetic inversion (using the layout and test conditions of the liquid-release test conducted in zone 2 of borehole SYBT-ECRB-LA#2) was conducted to determine the sensitivities and correlation structure of the four parameters (1) $\log(1/\alpha)$, where $1/\alpha$ [Pa] is the van Genuchten capillary-strength parameter, (2) n [dimensionless], which is related to the van Genuchten parameter m by $n = 1/(1-m)$, (3) $\log(k)$, where k [m^2] is the reference permeability of the heterogeneous permeability field, and (4) $\log(\phi)$, where ϕ [dimensionless] is the effective

porosity. The residual liquid saturation (another parameter of the relative-permeability and capillary-pressure functions) is expected to be much less important as seepage is initiated near full saturation. A separate sensitivity study was performed to examine the impact of the evaporation boundary-layer thickness δ (see Section 6.6.1.4) on the estimated parameters. The key parameter $\log(1/\alpha)$ was estimated using boundary-layer thicknesses of 0.50 cm, 0.75 cm, and 2.00 cm (see Table 12).

The sensitivity measure reported below is the sum of the absolute values of the sensitivity coefficients, which is defined as the partial derivative of the calculated seepage rate with respect to the parameter of interest. The correlation coefficients are obtained from the parameter covariance matrix given by Equation (15). Because the inverse problem is highly nonlinear, the results of this synthetic analysis depends on the *a priori* parameter values. The values used are sufficiently close to the best estimates obtained by the actual inversion, i.e., there is no need to repeat the sensitivity analysis after calibration. The analysis should be considered qualitative in nature.

The results from the synthetic inversion (Wang 2003 [161456], SN-LBNL-SCI-228-V1, pp. 33, 35–36) and from the sensitivity analysis regarding the evaporation boundary-layer thickness (Wang 2003 [161456], SN-LBNL-SCI-228-V1, pp. 24–25) can be summarized as follows:

1. The capillary-strength parameter $\log(1/\alpha)$ has the largest impact on calculated seepage rates. Provided that $\log(1/\alpha)$ varies less than $\log(k)$ (approximately proportional to the square-root of the permeability variation), both parameters are about equally important for seepage predictions.
2. The two parameters $\log(1/\alpha)$ and $\log(k)$ are strongly negatively correlated, i.e., an increase in seepage rates by a reduction of $\log(1/\alpha)$ can almost be completely compensated by an appropriate increase in $\log(k)$.
3. Overall, $\log(k)$ is the parameter most strongly correlated to all other parameters, i.e., permeability is difficult to estimate from seepage-rate data alone. Permeability should be derived from independent information; this independent information is available from the air-injection tests (see Section 6.5.2).
4. The van Genuchten parameter n is relatively insensitive and at the same time strongly correlated to all the other parameters.
5. Porosity is the least-sensitive parameter. However, since its impact is restricted to only a portion of the data (i.e., the onset of seepage and early-time seepage rates), it is the least-correlated parameter. If the available data are potentially influenced by storage effects (e.g., data from short-term liquid-release tests with small injection volumes), porosity could be included in the estimation process.
6. Changes in the evaporation boundary-layer thickness δ within the range considered have a limited impact on the estimated parameter $\log(1/\alpha)$. Choosing a thin boundary layer of 0.75 cm (an estimate based on evaporation and relative-humidity data in an open drift section, see Section 6.6.1.4) leads to a relatively low $\log(1/\alpha)$ value.

The sensitivity analysis and correlation structure inferred from the synthetic inversion provides guidance for the final selection of parameters to be subjected to estimation by automatic model calibration.

The following decisions regarding parameter selection have been made:

1. As few parameters as possible should be selected to avoid overparameterization. If the observed seepage rates can be successfully reproduced by the calibrated model and the estimated model parameters can be considered reasonable, the relative parsimony of the model and the small number of adjustable parameters provides confidence that the physical processes governing seepage are appropriately represented by the model.
2. The capillary-strength parameter $\log(1/\alpha)$ is selected as the primary target parameter to be estimated by calibrating the SCM against seepage-rate data from the liquid-release tests. Capillarity is the main process behind the seepage exclusion phenomenon, as confirmed by the large sensitivity of the calculated seepage rate to changes in the key parameter of the capillary pressure-saturation relationship. The seepage-relevant capillary-strength parameter on the drift scale cannot be derived from standard laboratory or field measurements, or inferred from secondary information (such as fracture trace maps and aperture measurements). The parameter is suitable for the inclusion of a number of small-scale features and effects (such as surface roughness, film flow, drop detachment), and even numerical artifacts, such as increased seepage induced by discretization effects. It is important to realize that all the effects lumped into the $\log(1/\alpha)$ parameter are related or analogous to a capillarity effect, justifying the approach.
3. Permeability as the second important parameter affecting drift seepage is not estimated from seepage-rate data, but is taken from and conditioned on the air-permeability data. Fixing permeability at values that are determined independently from seepage-rate data is a reasonable means to resolve the non-uniqueness issue that arises from the strong correlation of permeability to all the other parameters. The support scale of the air-permeability data is consistent with that of the numerical grid. It allows determination and inclusion of heterogeneity into the model, which is an important feature affecting seepage. The stochastic nature and uncertainty in the heterogeneous permeability field is accounted for by performing multiple inversions using different realizations of the simulated permeability field.
4. Porosity is used as an effective parameter to capture storage effects. Porosity is only estimated in those liquid-release tests that involved little water, and where evaporation effects (which have an impact similar to increased storage) are not explicitly accounted for, affecting the early-time seepage-rate data. The analysis of liquid-release tests performed in the middle nonlithophysal zone (Niches 3107 and 4788) include the estimation of porosity; the tests conducted in the lower lithophysal zone (Niche 1620 and systematic seepage testing area in the ECRB Cross Drift) use a fixed value for porosity of approximately 1% (DTN: LB0205REVUZPRP.001 [159525]) and include only the estimation of $\log(1/\alpha)$. Note that the estimated porosity value is of no interest for the subsequent prediction of steady-state seepage into waste emplacement drifts. It is only determined here to avoid an unwanted bias in the concurrently estimated $\log(1/\alpha)$ parameter, to which it is negatively correlated.

5. All other parameters are fixed at the values given in Table 4. They become part of the model structure along with initial and boundary conditions (see Sections 6.6.2.4 and 6.6.2.3, respectively), and spatial discretization (specifically the length of the nodal distance to the drift element, see Sections 6.3.3.3, 6.6.1.2, and 8.2). Since the estimated parameters are likely to be correlated to these fixed parameters and would change if the model structure were modified, the estimated values are to be considered model-related.

In summary, the logarithm of the capillary-strength parameter $1/\alpha$, which enters the van Genuchten capillary-pressure function (see Equation (5)) is estimated as an effective, seepage-relevant, model-related parameter through automatic calibration of the SCM against seepage-rate data from liquid-release tests. For tests conducted in the middle nonlithophysal zone, porosity is also determined to be an effective parameter, accounting for storage effects.

6.6.3.2 Data Selection

As described in BSC (2001 [158463], Sections 6.2 and 6.11) and summarized in Section 6.5.3, an automatic data acquisition system was set up to monitor the cumulative amount of water seeping into the capture system installed within the niches and the ECRB Cross Drift. Taking the derivative of these cumulative seepage data (see Attachment VI) yields the seepage rates to be used for calibration. Note that measurement noise in the cumulative seepage data induces fluctuations in the calculated seepage rates. If no or little seepage occurs, these fluctuations may lead to negative seepage-rate values. These nonphysical data points are of no concern, because the numerical model (which always produces physical, non-negative seepage rates) does not attempt to track the high-frequency fluctuations from measurement noise (the random component of the data are described by the stochastic model of the inversion); instead, the model follows the smooth, deterministic component of the seepage-rate data, which is non-negative.

Seepage rates are used instead of cumulative seepage data because an error in the prediction of the early-time seepage behavior leads to a shift in the cumulative seepage curve. Such a shift induces a bias in the estimated parameters, even if only late-time data were used in the inversion. In general, early-time seepage data are relatively strongly affected by storage effects. Moreover, they reflect the properties of only a few fractures that connect the injection interval with the point at the drift surface where seepage is initiated. These fractures may not be representative of the drift-scale properties of the fracture network engaged in the seepage process under near-steady-state conditions. These few fractures are likely to be conceptually different from the larger-scale network providing connectivity for flow diversion around the drift. Consequently, matching early-time data potentially leads to an unwanted bias in the estimated parameters. Late-time, near-steady data are less affected by storage effects, allowing for a more representative estimation of $\log(1/\alpha)$.

The following paragraphs discuss the data sets used for calibration (see also Table 11).

Borehole SYBT-ECRB-LA#1, Lower Lithophysal Zone
DTN: LB0110ECRB LIQR.002 [156879]

Only one borehole interval (zone 2) was available for liquid-release testing in borehole SYBT-ECRB-LA#1 (BSC 2001 [158463], p. 241). Starting on 2/28/2001, water was released for a

period of almost a month at an average rate of approximately 17 ml/min. No seepage was induced. In the following month, four tests with approximate release rates between 41 ml/min and 45 ml/min were performed, interrupted by phases of inactivity that lasted from a few hours to approximately 6 days. These higher-rate tests led to seepage. Seepage-rate data from all five tests (Events 65–69 of Table 11) are used for calibration. During the two-month testing period, the relative humidity in the drift varied between about 10% and 60% (BSC 2001 [158463], Figure 6.11.2-11c). Data preparation is described in Attachment VI and Wang 2003 [161456], SN-LBNL-SCI-228-V1, pp. 15–17).

Borehole SYBT-ECRB-LA#2, Lower Lithophysal Zone

DTN: LB00090012213U.002 [153154], DTN: LB0110SYST0015.001 [160409]

Borehole SYBT-ECRB-LA#2 was tested twice, in May/June 2000 and October/November 2000. Humidity in the drift was not controlled or monitored during the earlier tests; these tests will therefore not be used for calibration, but for validation with an assumed relative humidity. During the second test period starting 10/23/2000, long-term liquid-release tests were conducted in zones 2 and 3 (Events 61–64 of Table 11) with approximate release rates ranging between 33 ml/min and 41 ml/min. The relative humidity in the testing area (partly protected from air circulation by curtains installed at the two ends of the V-shaped seepage capture curtains) varied between approximately 30% and 90% (BSC 2001 [158463], Figure 6.11.2-8). Data preparation is described in Finsterle (2002 [161043], p. 133) and Wang (2003 [161456], SN-LBNL-SCI-228-V1, pp. 18–21).

Borehole SYBT-ECRB-LA#3, Lower Lithophysal Zone

DTN: LB0203ECRB LIQR.001 [158462]

Test events 70 and 71 (see Table 11) were conducted in zone 1 of borehole SYBT-ECRB-LA#3, starting on 5/17/2001. Despite the higher release rate of approximately 36 ml/min during the first test, which lasted for about 4 days, no seepage was observed. A long-term test (26 days) at an average rate of approximately 25 ml/min produced somewhat erratic seepage, with seepage rates reaching approximately 10 ml/min, but decreasing during the last 10 days of the test. Relative humidity varied between 10% and 50%. Data preparation is described in Wang (2003 [161456], SN-LBNL-SCI-228-V1, pp. 15–17).

Niche 1620, Lower Lithophysal Zone

DTN: LB0209NICH5LIQ.001 [160796] and DTN: LB0211NICH5LIQ.001 [160792]

During test events 86 and 87 (see Table 11), water was released at an approximate rate of 26 ml/min from interval 28–29 ft of borehole #5; the tests started 7/15/2002 (Day 195 since 01/01/2002) and continued until 8/5/2002 (Day 216). In concurrently conducted tests, water was released from interval 21–22 ft of borehole #3 between 7/17/2002 (Day 197) and 7/19/2002 (Day 199; Event 83), and again between 7/29/2002 (Day 208) and 8/9/2002 (Day 221; Event 84; shaded zones in Figure 17). It is apparent from Figure 17 that part of the water released in borehole #3 was captured in the trays intended to collect seepage from the liquid-release tests conducted in borehole #5. Because of this test interference, only the late-time data of Event 86 up to 7/30/2002 (Day 209) are considered for calibration. During Event 89 (Table 11), water was released at an almost constant rate of approximately 9.9 ml/min from interval 10–11 ft of

borehole #4; the test started 9/17/2002 and continued until 10/1/2002. Seepage started on 9/19/2002 and increased gradually until it reached almost steady state on 9/24/2002. Data preparation is described in Wang (2003 [161456], SN-LBNL-SCI-223-V1, pp. 30–34).

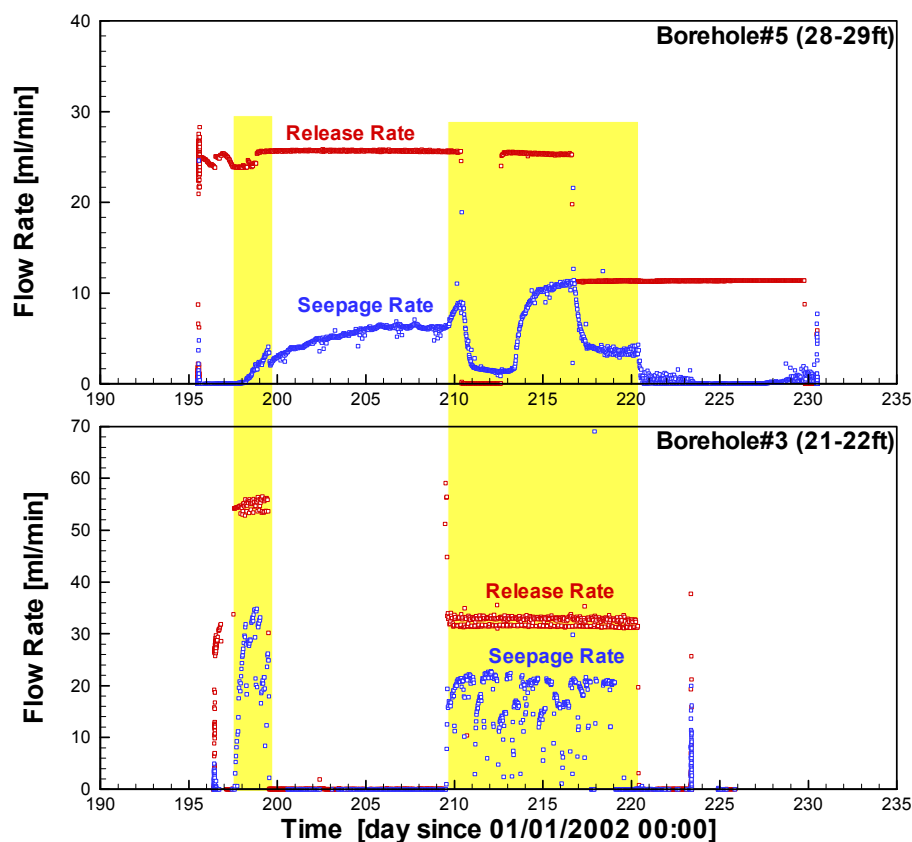


Figure 17. Interference between concurrent liquid-release tests in borehole #3 (21–22 ft) and borehole #5 (28–29 ft). Note that 7/15/2002 is Day 195. Data from DTN: LB0209NICH5LIQ.001 [160796].

Niche 3107, Middle Nonlithophysal Zone
DTN: LB0010NICH3LIQ.001 [153144]

Two intervals were tested in Niche 3107. However, only test events in one interval (UM 4.88–5.18) resulted in seepage (see Events 6, 8–12 in Table 11). The tests in the other interval (UL 5.49–5.80) are not useable for calibration, as no seepage was observed (see Events 1–3), which would lead to an ill-posed inverse problem. Nevertheless, these data will be used for validation purposes. Of the nine tests performed in interval UM 4.88–5.18, three are selected for model calibration because of their variety in injection and seepage rates. The tests starting on 3/4/1999, 4/27/1999, and 5/6/1999 are characteristic of all the tests performed in this interval. The 3/4/1999 test (Event 4) was conducted at a low injection rate of approximately 0.9 ml/min, resulting in no seepage. The 4/27/1999 test (Event 6) used a medium rate of about 2.4 ml/min and resulted in a small amount of seepage. Finally, the 5/6/1999 test (Event 8) was performed with a higher rate of approximately 5.4 ml/min, which resulted in substantial seepage. The remaining tests (Events 7, 9–12) in this interval are reserved for validation. Data preparation is described in Ahlers (2002 [161045], pp. 41, 47–48).

Niche 4788, Middle Nonlithophysal Zone
DTN: LB0010NICH4LIQ.001 [153145]

Three intervals were tested in Niche 4788, all leading to seepage. Each test performed in a given interval was conducted with a different release rate (except in interval UM 6.10–6.40, where three low-rate tests were performed; only the test on 3/14/2000 was a long-term test). In each interval, the low- and medium-rate tests that resulted in seepage were selected for model calibration (Events 41, 43, 45, 48, 50, and 51 in Table 11). The highest-rate and lowest-rate seepage tests are reserved for validation (Events 40, 42, 44, 47, 49) to determine whether seepage model predictions can be successfully extrapolated to conditions beyond the calibration range. Data preparation is described in Ahlers (2002 [161045], pp. 26–27, 34–36).

6.6.3.3 Calibration Results

The software iTOUGH2 V4.0 (LBNL 1999 [139918]) for tests without significant evaporation effects, or iTOUGH2 V5.0 (LBNL 2002 [160106]) for tests with evaporation effects, is used to match the transient seepage-rate data (see Section 6.6.3.2) by automatically updating the parameters of interest (see Section 6.6.3.1). The inverse modeling approach follows the concept described by Carrera and Neuman (1986 [104368]) and Finsterle (1999 [104367]). The misfit between calculated and measured seepage is evaluated using the least-squares objective function (Equation (13)). The objective function is minimized using the Levenberg-Marquardt algorithm (Finsterle 1999 [104367], pp. 44–45).

The inversion results are presented as follows. First, the simulated system behavior obtained with the calibrated model is qualitatively described for selected tests and points in time. Second, the match between the simulated and observed seepage-rate data is shown. Third, the estimated parameters are discussed. Finally, the results from the individual inversions are combined and summarized (see Section 6.6.4) to obtain a parameter distribution for subsequent model validation. Input and output files from a representative inversion are discussed in Attachment VII.

Borehole SYBT-ECRB-LA#1, Lower Lithophysal Zone

The overall simulated system behavior during liquid-release tests from inclined boreholes drilled from the ECRB is qualitatively visualized in Figure 18 (and for other boreholes in Figure 21, Figure 26, Figure 28, and Figure 30). Figure 18a shows the flux distribution at the end of the testing period. The flow field above the injection point represents the natural background percolation flux, with flow channeling occurring as a result of explicitly modeled small-scale heterogeneity. It is apparent that flow channels are established within a short distance below the top boundary. The injection interval (zone 2 of borehole SYBT-ECRB-LA#1) is relatively close to the crown of the drift. Local flux below the water release point is very high. Water is partly diverted around the opening. The low relative humidity (less than 50%) leads to substantial evaporation, extracting most of the injected water from the formation before it reaches the spring line of the drift. Flow diversion around the drift and the removal of water that seeped into the capture system leads to reduced fluxes below the drift, an effect referred to as the shadow zone.

The saturation distribution at the end of seepage testing (Event 69 of Table 11) shows that the fracture continuum is essentially dry (less than 10%) under natural percolation conditions (Figure

18b). Injecting at rates on the order of 40 ml/min increases saturation without completely saturating the pore space, i.e., the flow regime remains unsaturated. As a result of the capillary-barrier effect, saturations are highest in the immediate vicinity of the drift, which induces a capillary-pressure gradient promoting flow diversion. Seepage and evaporation removes water from the formation as it flows around the drift, explaining why no significant saturation increase can be observed at the spring line. In contrast, during the liquid-release tests performed in the closed-off niches, where evaporation is significantly reduced, water reaches the spring line and drains to depth as shown, for example, in Figure 26a and Figure 28a, and evidenced by seepage into the horizontal slot excavated from the side of Niche 1620 (see also Section 6.7). Additional discussions of the flow and seepage behavior will be given below for tests in borehole SYBT-ECRB-LA#2.

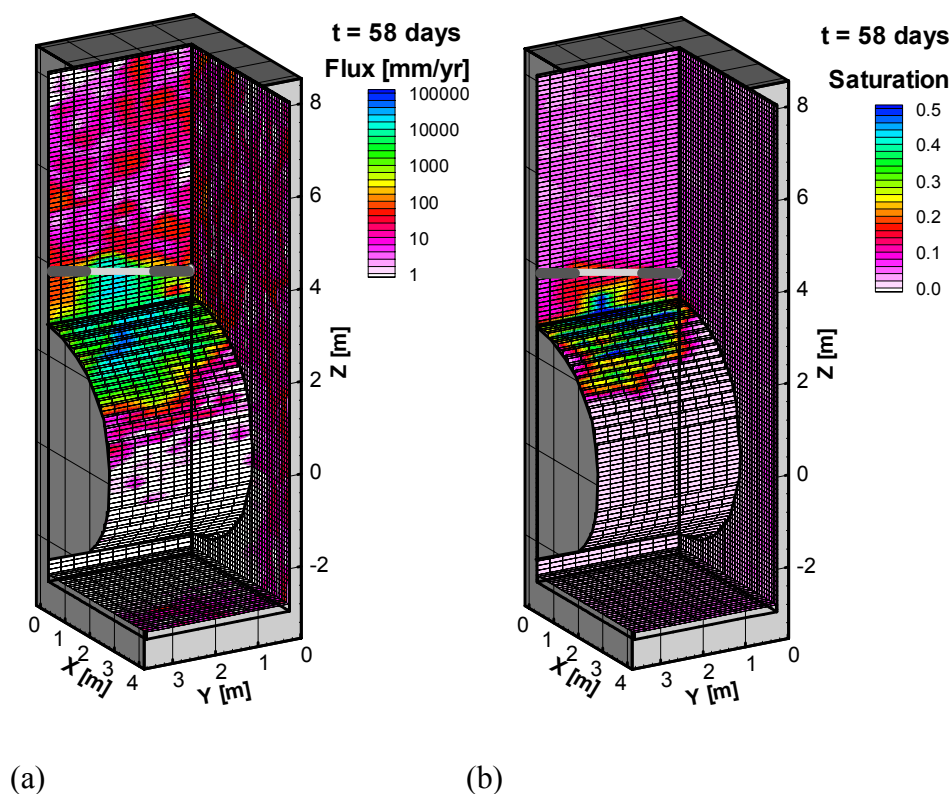


Figure 18. (a) Flux and (b) saturation distribution at the end of liquid-release testing in zone 2 of borehole SYBT-ECRB-LA#1. Based on output DTN: LB0302SCMREV02.001.

The match of the calculated seepage rates (red line) to the observed data (blue symbols) for this test is shown in Figure 19, along with the measured and modeled release rates (gray and black lines) and the relative-humidity data (green line). The model correctly replicates the initial, 34-day long no-seepage period. The increase in release rates induces seepage, the magnitude of which is well reproduced by the calibrated model. After each test interruption, seepage rates are reestablished more quickly in the model than observed in the field. The discrepancy between model and data is more pronounced after longer periods of inactivity (i.e., for the test events starting at 34 and 40 days, which followed interruptions of approximately $5\frac{1}{4}$ and $3\frac{3}{4}$ days, respectively) suggesting that a storage mechanism (e.g., storage in the injection lines and borehole intervals, imbibition into the dried-out matrix, filling of lithophysal cavities, and/or storage

within the capture system, i.e., between the trays or capture curtain and the balance measuring cumulative seepage) is not appropriately accounted for. The discrepancies in these early-time data, however, are minor and are not expected to significantly bias the parameter estimate. Because transient system responses introduced by test interruptions and rate changes are reproduced by specifying time-varying boundary conditions, their potential impact on seepage is appropriately captured.

A total of 17 inversions were performed, each with a different realization of the underlying, heterogeneous permeability field. The quality of the matches obtained with each inversion is consistent, as shown in Figure 20.

The $1/\alpha$ estimate has a mean, standard deviation, and standard error of 534 Pa, 57 Pa, and 14 Pa, respectively (see Table 14 below). (Note that the statistics are performed for $1/\alpha$ instead of $\log(1/\alpha)$. Using the backtransformed values is justified by the small standard deviation of the estimates.) The estimation uncertainty of an individual inversion (given by Equation (14)) is on the order of a few pascals. This estimation uncertainty accounts for the residual misfit of the calibrated model to the data and the sensitivity of the calculated seepage rates with respect to $1/\alpha$. This uncertainty measure is not propagated through the suite of seepage models, because it is significantly less than the uncertainty stemming from small-scale heterogeneities (which is examined by performing multiple inversions with multiple realizations of the permeability field, amounting to 57 Pascals (Pa) in this case) and spatial variability (which is examined by inverting data from tests conducted at different locations, amounting to approximately 100 Pa—see Section 6.6.4).

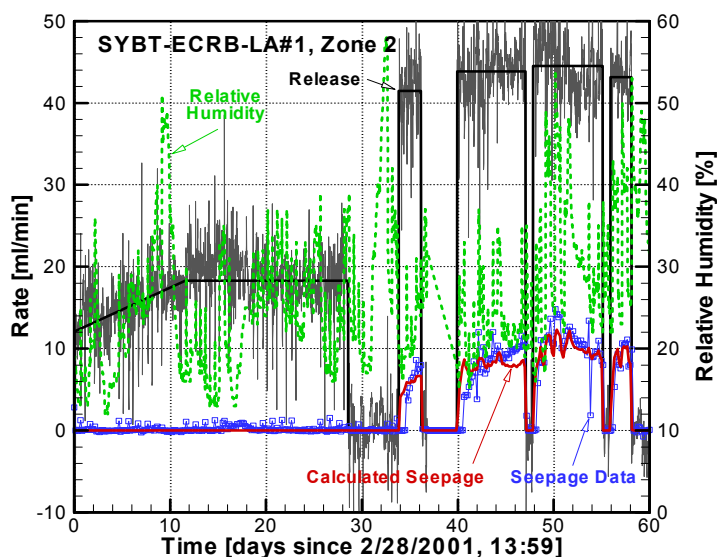


Figure 19. Calibration of seepage-rate data from liquid-release tests in zone 2 of borehole SYBT-ECRB-LA#1. Blue symbols represent measured data; the red line is the calculated seepage rate. The measured release rates are shown in dark gray; the black solid line shows the injection rate used in the model. Relative-humidity data are shown as a green dashed line. All curves representing measured data derived from DTN: LB0110ECRBLIQR.002 [156879]; calculated seepage in DTN: LB0302SCMREV02.001.

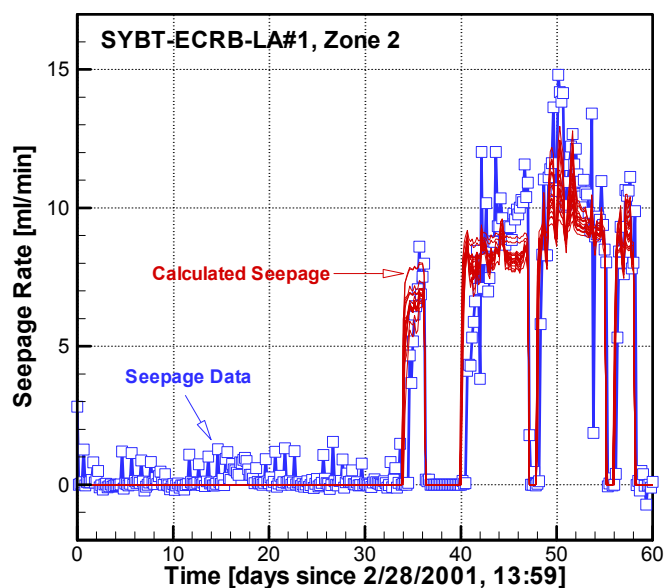


Figure 20. Calibration of seepage-rate data from liquid-release tests in zone 2 of borehole SYBT-ECRB-LA#1. Blue symbols represent measured seepage-rate data; the red lines are the results obtained with 17 calibrated models, each using a different realization of the underlying heterogeneous permeability field. Seepage-rate data derived from DTN: LB0110ECRBLIQR.002 [156879]; calculated seepage in DTN: LB0302SCMREV02.001.

Borehole SYBT-ECRB-LA#2, Lower Lithophysal Zone

Multiple liquid-release tests were performed in zones 2 and 3 of borehole SYBT-ECRB-LA#2. The propagation of the liquid plume from the tests in zone 2 is visualized in Figure 21. After 10 days of injection (Figure 21b), water is diverted around the drift approximately to the elevation of the spring line. After 20 days (Figure 21c), however, the plume has shrunk significantly as a result of increased evaporation (see discussion of Figure 22 below). Increased relative humidity prior to the 30-day time mark reduces evaporation and thus enables water to flow around the drift. Figure 21d also highlights the shadow zone created by flow diversion around the drift.

Figure 21 suggests that horizontal spreading of the liquid plume is partly restricted by the limited extension of the model domain in the Y-direction. This boundary effect increases seepage. The impact of the increased seepage on the estimated $1/\alpha$ value is minor compared to the parameter's uncertainty (Wang 2003 [161456], SN-LBNL-SCI-228-V1, p. 32).

Despite the SCM being a continuum model, seepage occurs at only a few discrete locations (indicated by triangles), consistent with qualitative observations of drip locations. Seepage locations are affected by heterogeneity. In the current realization, some seepage occurs near the crown of the drift; however, most water enters the drift from a location approximately halfway between the crown and the spring line (see Figure 21d).

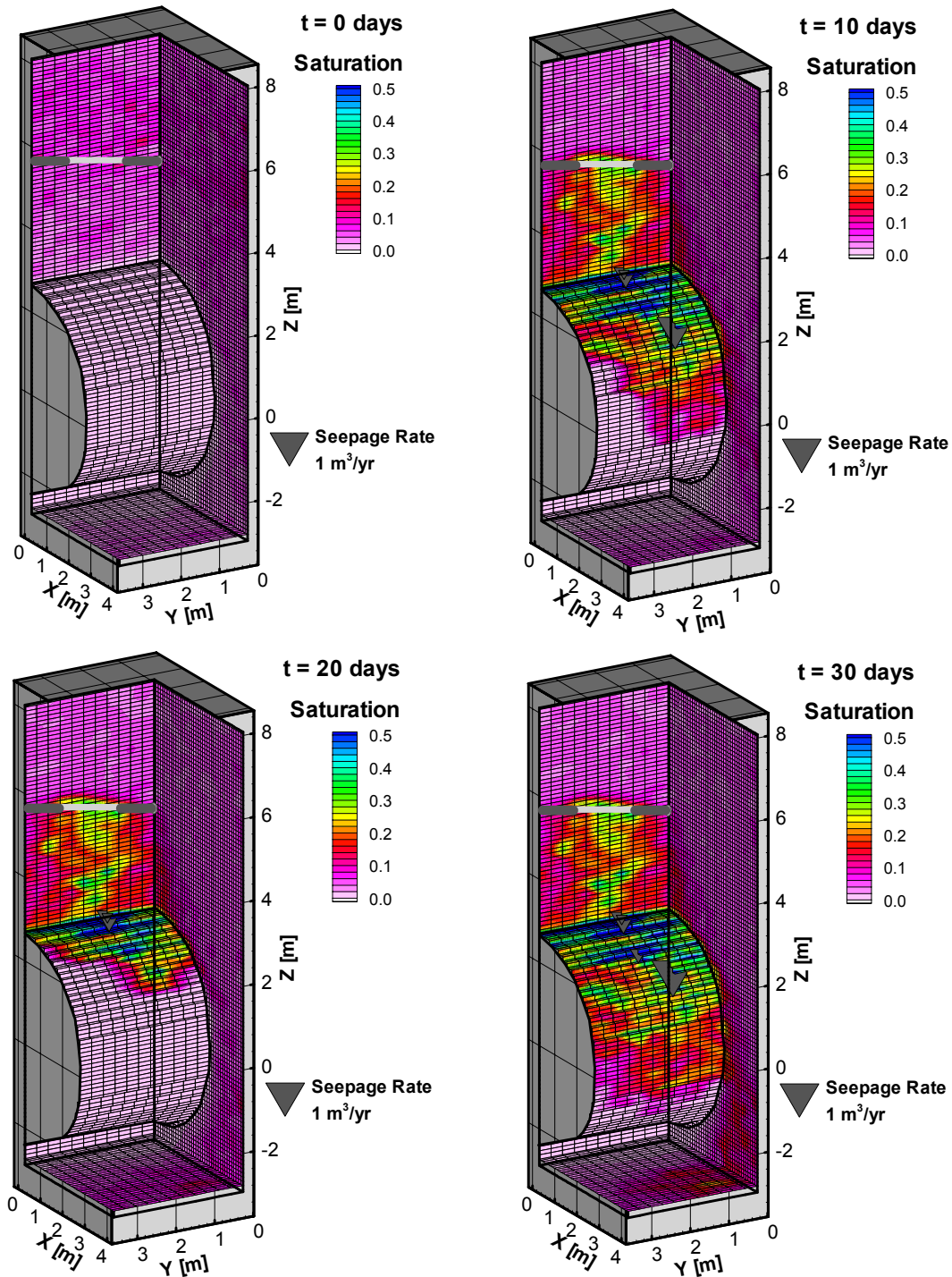


Figure 21. Saturation distribution simulated with model calibrated against seepage-rate data from liquid-release tests conducted in zone 2 of borehole SYBT-ECRB-LA#2; (a) initial distribution, (b) after 10 days, (c) 20 days, and (d) 30 days. Triangles indicate seep locations and seepage amount. Based on output DTN: LB0302SCMREV02.001.

Comparisons between measured and calculated seepage rates for the tests in zones 2 and 3 are shown in Figure 22 and Figure 23, respectively. Fluctuations in both data sets can be correlated to the drastic changes in relative humidity, which drives evaporation. The model captures this evaporation effect reasonably well, tracking increases in measured seepage rates as relative humidity increases and vice versa. These results provide confidence that the conceptual model represents the key processes and their interactions appropriately, including:

1. Unsaturated flow using a continuum representation of fracture flow based on Richards' equation (see Section 6.6.1.1);
2. Seepage into the opening, accounting for the capillary-barrier effect (see Section 6.6.1.2);
3. Vaporization of water from the drift surface, using a simplified evaporation model (see Section 6.6.1.3).

The rather complex system behavior, which includes expansion and shrinkage of the liquid plume along the drift surface, signifies the importance of handling unsaturated flow, seepage, and evaporation in a fully coupled manner.

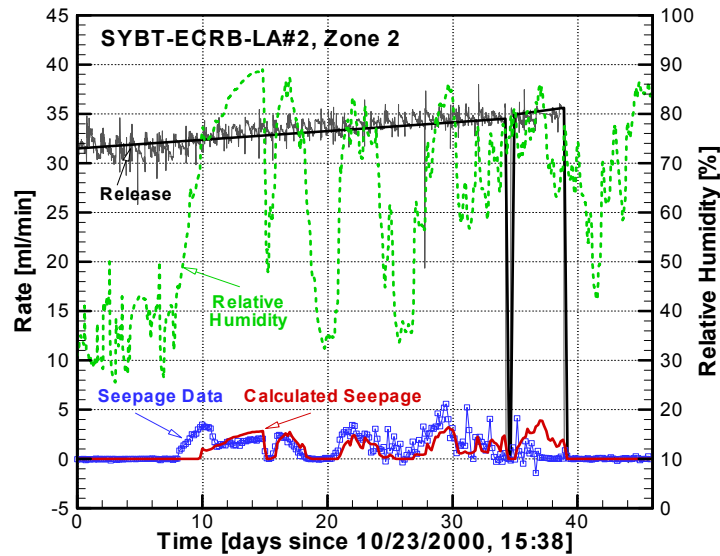


Figure 22. Calibration of seepage-rate data from liquid-release tests conducted in zone 2 of borehole SYBT-ECRB-LA#2. Blue symbols represent measured data; the red line is the calculated seepage rate. The measured release rates are shown in dark gray; the black solid line shows the injection rate used in the model. Relative-humidity data are shown as a green dashed line. All curves representing measured data are derived from DTN: LB0110SYST0015.001 [160409]; calculated seepage in DTN: LB0302SCMREV02.001.

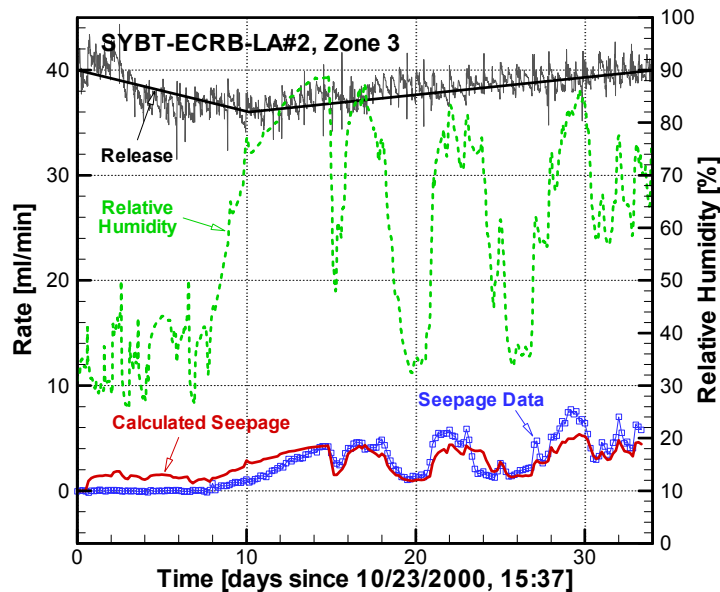


Figure 23. Calibration of seepage-rate data from liquid-release tests conducted in zone 3 of borehole SYBT-ECRB-LA#2. Blue symbols represent measured data; the red line is the calculated seepage rate. The measured release rates are shown in dark gray; the black solid line shows the injection rate used in the model. Relative-humidity data are shown as a green dashed line. All curves representing measured data are derived from DTN: LB0110SYST0015.001 [160409]; calculated seepage in DTN: LB0302SCMREV02.001.

The capillary-strength parameter $1/\alpha$ was determined based on 21 inversions of seepage-rate data from zone 2, and 19 inversions of data from zone 3. The means and standard deviations (557 ± 56 Pa for zone 2 and 535 ± 58 Pa for zone 3; see Table 14 below) are consistent with those obtained in borehole SYBT-ECRB-LA#1.

Borehole SYBT-ECRB-LA#3, Lower Lithophysal Zone

The calibration of liquid-release tests from zone 1 of borehole SYBT-ECRB-LA#3 revealed some systematic inconsistencies between the data and the model. As shown in Figure 24, the model produces considerable seepage during the simulation of the first test event, while no seepage was observed in the field despite the high release rate. Furthermore, the model predicts a more or less uniform seepage rate for the second test event, whereas the data show a continuous increase in seepage for approximately 10 days, followed by a decrease. Nevertheless, the inversion yields a reasonable reproduction of the average seepage rate. The mean $1/\alpha$ value of 452 ± 55 Pa (based on 23 inversions; see Table 14 below) is lower than the previous estimates.

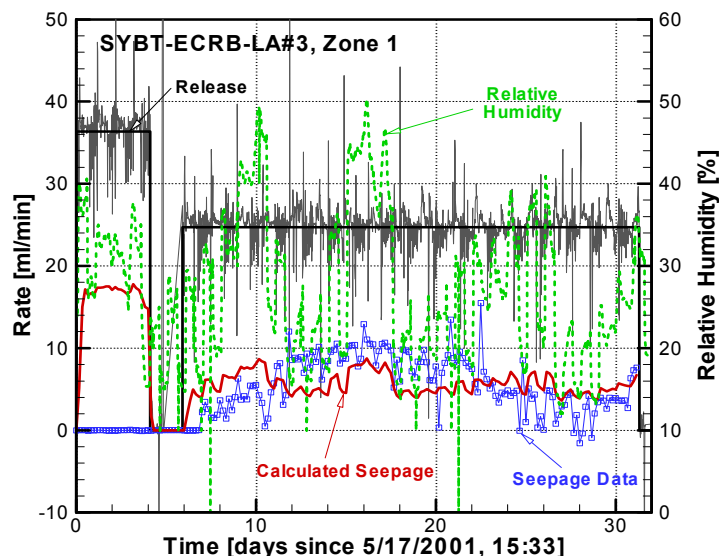


Figure 24. Calibration of seepage-rate data from liquid-release tests conducted in zone 1 of borehole SYBT-ECRB-LA#3. Blue symbols represent measured data; the red line is the calculated seepage rate. The measured release rates are shown in dark gray; the black solid line shows the injection rate used in the model. Relative-humidity data are shown as a green dashed line. All curves representing measured data are derived from DTN: LB0203ECRBLIQR.001 [158462]; calculated seepage in DTN: LB0302SCMREV02.001.

Niche 1620, Borehole #4, Interval 10–11 ft, Lower Lithophysal Zone

During Test Event 89, liquid was released at a fairly constant rate. Seepage was observed after two days and continued to increase for four days, reaching almost steady state on the sixth day.

The test was simulated with a constant release rate of 9.9 ml/min and a constant relative humidity of 85%. The model produced seepage 12 hours after liquid release started, and reached a constant seepage rate after 36 hours (see Figure 25). The saturation and flux at the end of the test (see Figure 26) show that there is significant diversion of injected liquid around the niche. Thirty inversions with 30 different realizations of the underlying heterogeneous permeability field were performed, resulting in a calibrated capillary-strength parameter $1/\alpha$ of 671 ± 223 Pa. The standard error of the mean is 41 Pa.

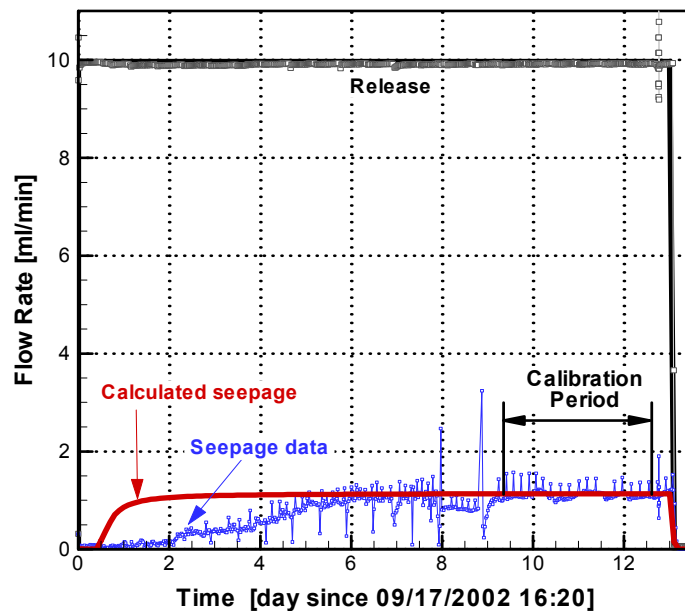


Figure 25. Calibration of seepage-rate data from liquid-release tests conducted in interval 10–11 ft of borehole #4 in Niche 1620. Blue symbols represent measured data; the red line is the calculated seepage rate. The measured release rates are shown in dark gray; the black solid line shows the injection rate used in the model. All curves representing measured data are derived from DTN: LB0211NICH5LIQ.001 [160792]; calculated seepage in DTN: LB0302SCMREV02.001.

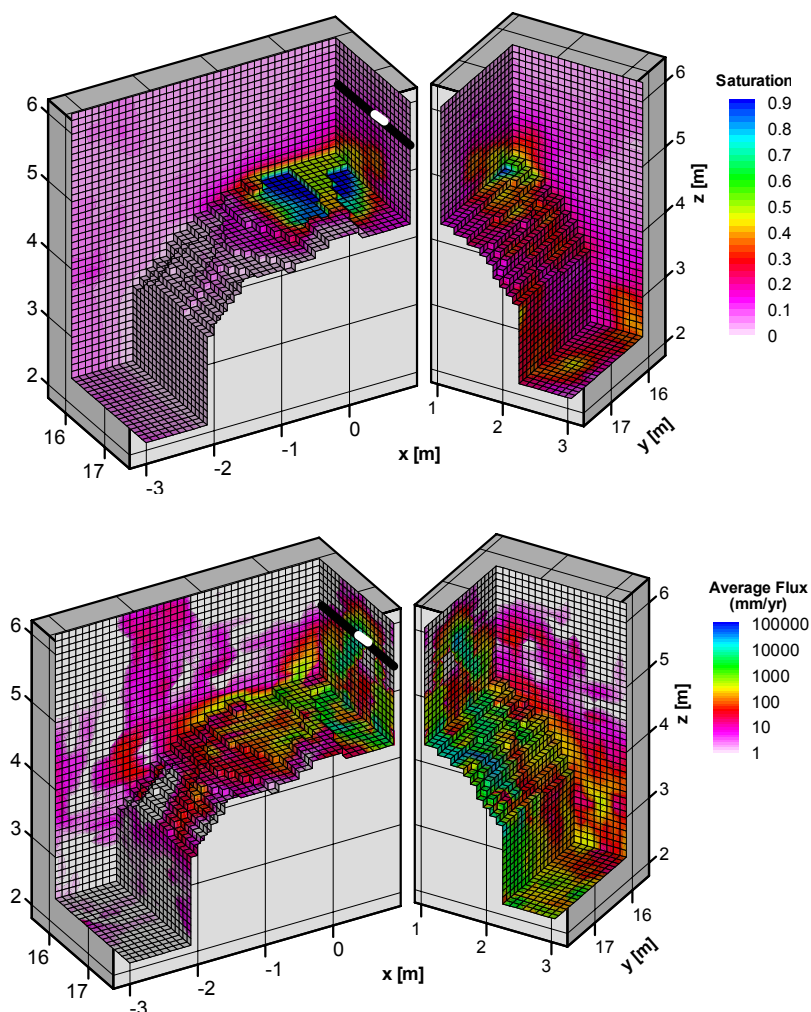


Figure 26. Simulated (a) saturation and (b) flux distribution at the end of liquid-release testing (after 13 days) in interval 10–11 ft of borehole #4 in Niche 1620. Based on output DTN: LB0302SCMREV02.001

Niche 1620, Borehole #5, Interval 28–29 ft, Lower Lithophysal Zone

In Test Event 86, water was released at a rate of approximately 25.8 ml/min. The slight fluctuations in the release data that occurred during the first four days were reproduced in the seepage model. Seepage started on the second day and continued at an increasing rate, until it reached a constant rate on the tenth day (see Figure 27). The slight interference from Event 83 that occurred during the third day of Event 86 affected only the transient stage of the seepage data and was considered insignificant in the calibration process (see also discussion of Figure 17). The simulated relative humidity was kept constant at 85%, consistent with the averaged observed relative humidity during the test. The saturation and flux at the end of the test (see Figure 28) show that there is significant flow diversion of injected liquid around the niche towards the left slot. (See Section 6.7 for a detailed discussion on the significance of seepage into the slot in confirming the capillary-barrier concept.) Twenty-four inversions with different realizations of the underlying heterogeneous permeability field were performed, resulting in a calibrated

capillary-strength parameter $1/\alpha$ of 740 ± 339 Pa. The standard error of the mean is 69 Pa (see Table 14 below).

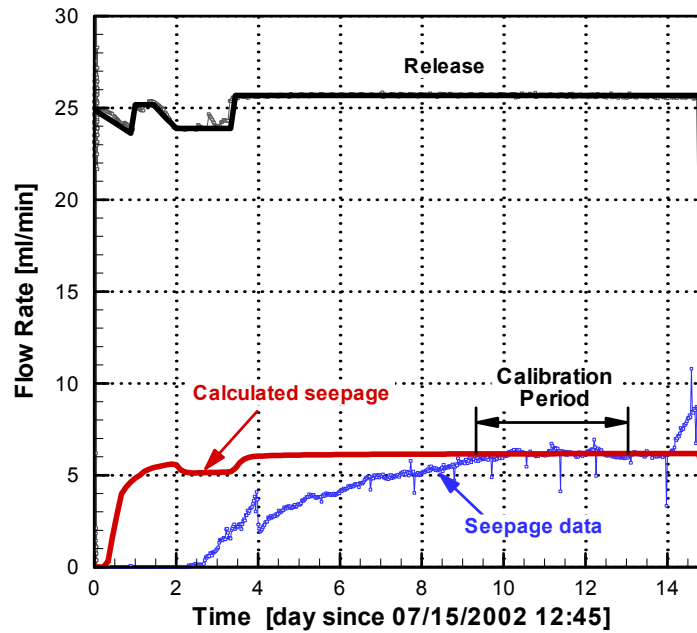


Figure 27. Calibration of seepage-rate data from liquid-release tests conducted in interval 28–29 ft of borehole #5 in Niche 1620. Blue symbols represent measured data; the red line is the calculated seepage rate. The measured release rates are shown in dark gray; the black solid line shows the injection rate used in the model. All curves representing measured data are derived from DTN: LB0209NICH5LIQ.001 [160796]; calculated seepage in DTN: LB0302SCMREV02.001.

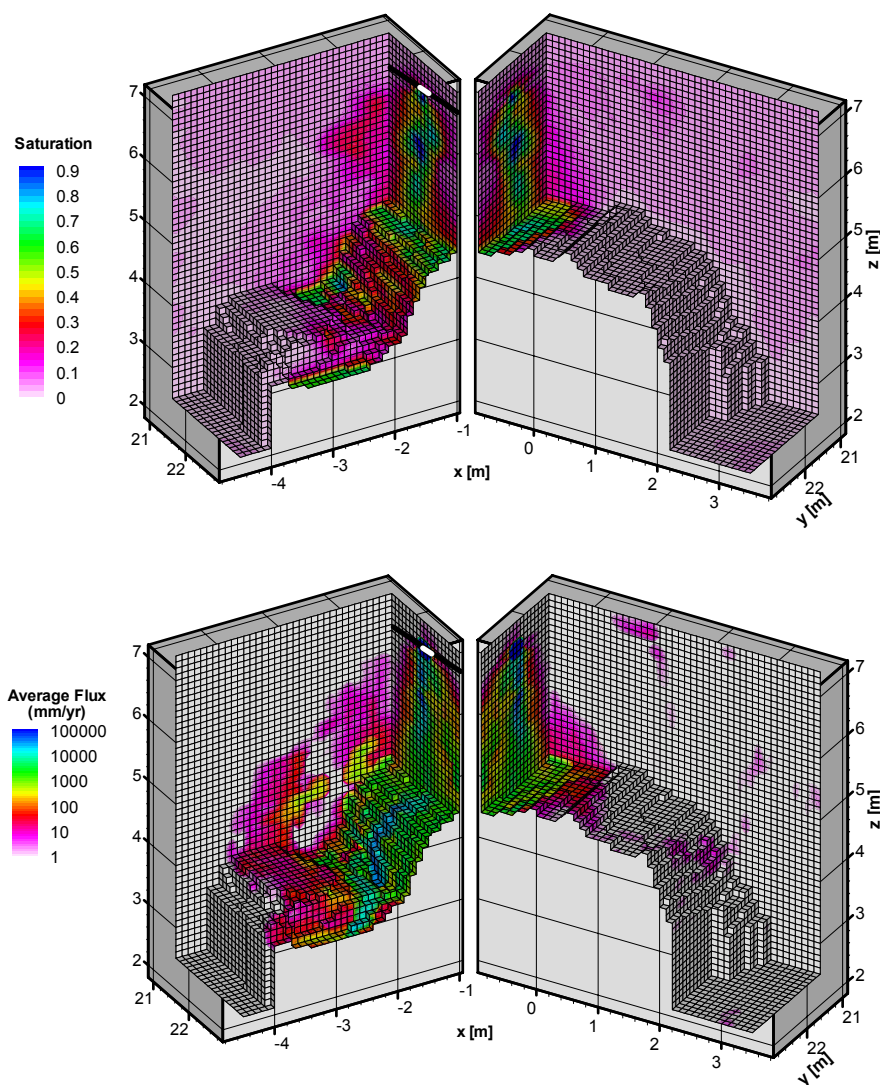


Figure 28. Simulated (a) saturation and (b) flux distribution at the end of liquid-release testing (after 13 days) in interval 28–29 ft of borehole #5 in Niche 1620. Based on output DTN: LB0302SCMREV02.001.

Niche 3107, Middle Nonlithophysal Zone

Data from three liquid-release tests performed in the center borehole UM (see inset in Figure 4) were inverted simultaneously. The inversions are based on one realization of the underlying heterogeneous permeability field. The match between the measured and calculated seepage rates is shown in Figure 29. The first low-rate test did not yield seepage. The seepage-rate data of the test conducted with the intermediate rate were considered less reliable, and a smaller weight was assigned to these data for the inversion. As a result, the model slightly overpredicts these data, whereas the other two jointly inverted test events were well matched. A relatively high $1/\alpha$ estimate of 741 Pa was obtained. The estimate will be combined with those obtained from Niche 4788 to yield a single value for the middle nonlithophysal zone (see Section 6.6.4).

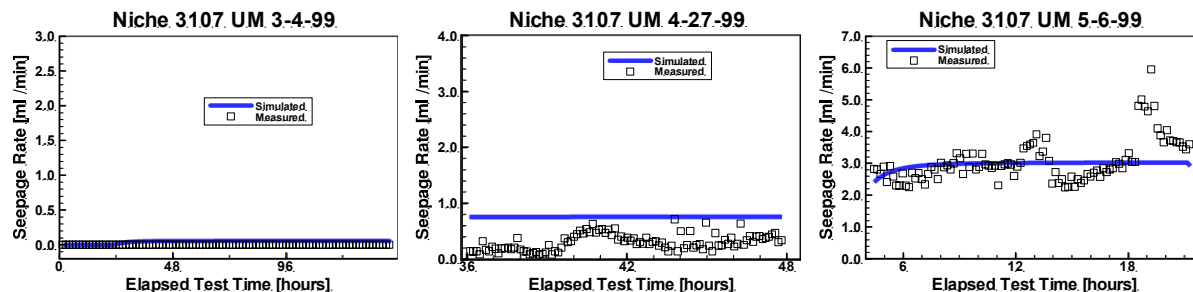


Figure 29. Comparison between simulated and measured seepage rates from three liquid-release tests conducted in interval UM 4.88–5.18 of Niche 3107. Measured data derived from DTN: LB0010NICH3LIQ.001 [153144]; calculated seepage in DTN: LB0010SCMREV01.001 [154292].

Niche 4788, Middle Nonlithophysal Zone

Calibrated parameters are produced separately for each interval tested in Niche 4788. The horizontal separation distance between adjacent borehole intervals is greater than the vertical distance between the injection intervals and the ceiling of the niche. Since water flow is predominantly gravity driven, test interference is unlikely. Additionally, flow is diverted around the niche on different (albeit overlapping) paths. The water injected into the intervals on the side boreholes (UL and UR, see insert in Figure 4) is expected to be diverted to the respective sides of the niche, testing the flow system and capillary barrier on either side of the niche. The water injected into the center borehole (UM) encounters the flow system near the crown of the niche as well as on the sides. Figure 30 shows the simulated late-time saturations from liquid-release tests in each of the three boreholes above Niche 4788. The relative independence of the flow systems in Niche 4788 leads to a strategy of estimating a separate $1/\alpha$ parameter for each interval (intervals UL 7.62–7.93, UM 6.10–6.40, and UR 5.18–5.48).

The calibrated model matches the data reasonably well (see Figure 31) given that multiple test events performed with different injection rates were inverted simultaneously (note the different scales on the Y-axes). The model overpredicts the seepage rates from the test performed in borehole UM on 12-10-99. In this case, the minimization algorithm was likely trapped in a local minimum. The $1/\alpha$ estimates (based on one realization of the underlying heterogeneous permeability field) for the three boreholes UL, UM, and UR are 646 Pa, 603 Pa, and 427 Pa, respectively. These three estimates will be combined with that from Niche 3107 to yield an average value for the middle nonlithophysal zone (see Section 6.6.4). Additional information on calibrations of the tests conducted in the middle nonlithophysal zone can be found in Ahlers (2002 [161045], pp. 38–39, 49).

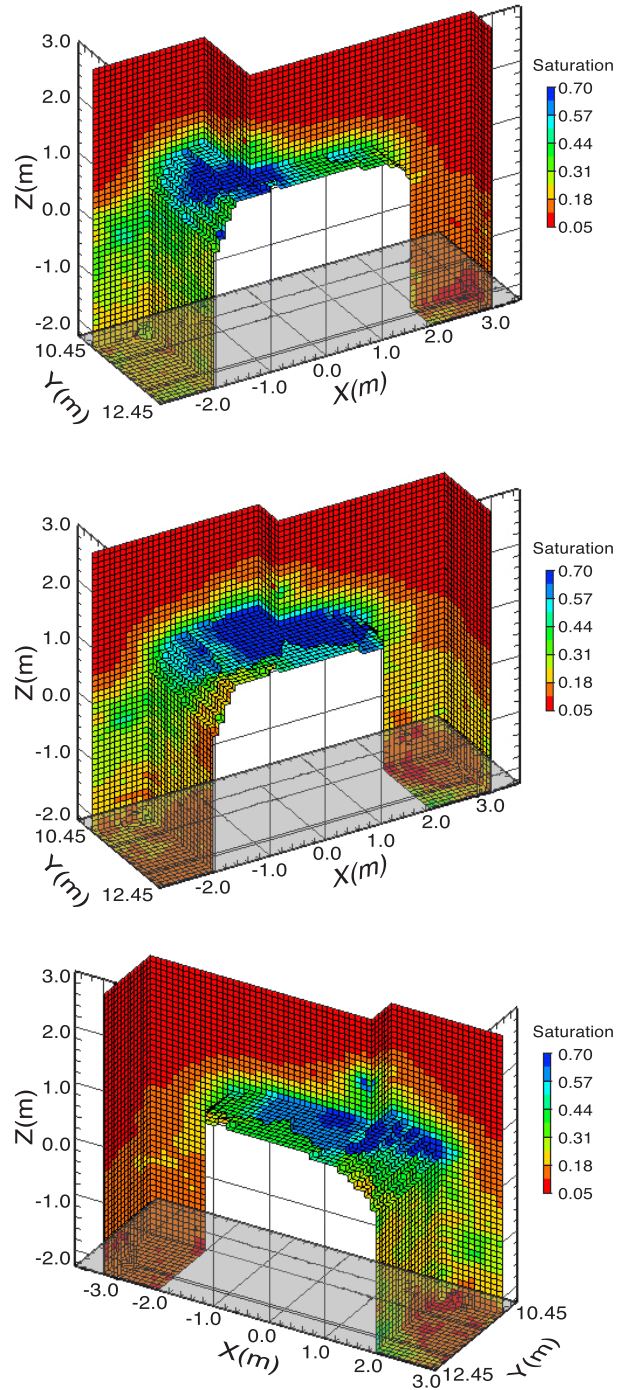


Figure 30. Simulated late-time saturation distribution for liquid-release tests in Niche 4788, intervals (a) UL 6.72–7.93 (11/03/1999), (b) UM 6.10–6.40 (11/16/1999), and (c) UR 5.18–5.48 (12/07/1999). The step in the displayed grid contains the injection interval. Figure based on DTN: LB0010SCMREV01.001 [154292].

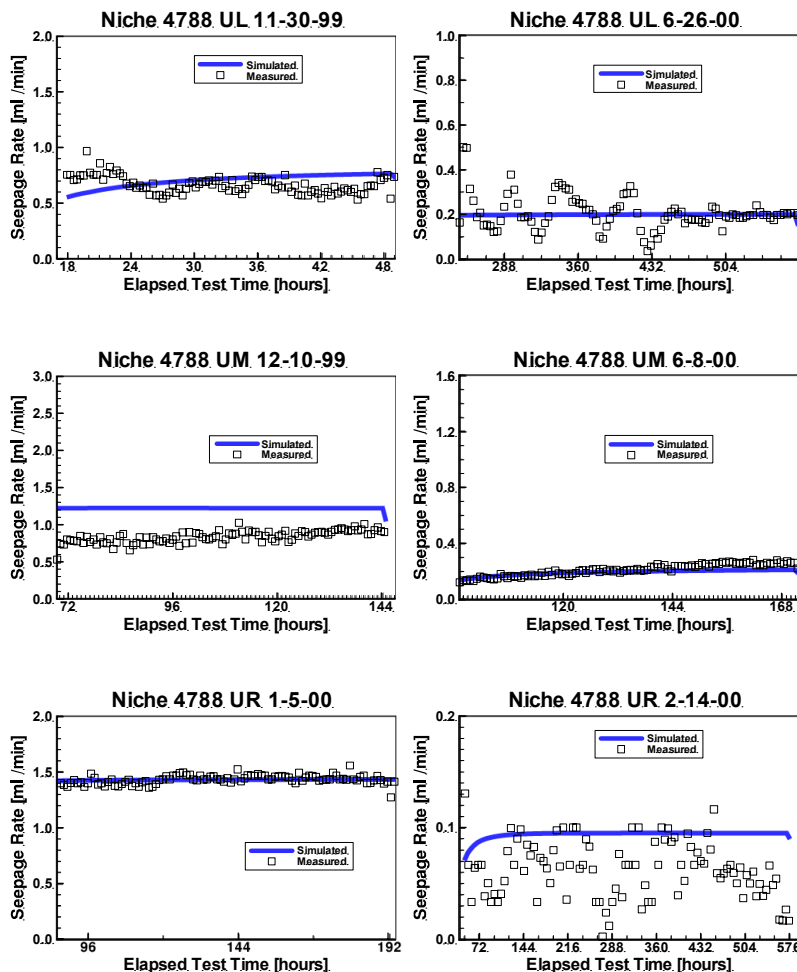


Figure 31. Comparison between simulated and measured seepage rates from six liquid-release tests conducted in three different borehole intervals of Niche 4788. Data from a given interval are inverted simultaneously. Measured data derived from DTN: LB0010NICH4LIQ.001 [153145]; calculated seepage in DTN: LB0010SCMREV01.001 [154292].

6.6.4 Summary and Compilation of Results

Multiple three-dimensional, heterogeneous models representing niche locations and sections of the ECRB Cross Drift were developed. The permeability fields were constructed and conditioned on local air-permeability data (see Section 6.6.2.1). Seepage-rate data from multiple test events, using different liquid-release rates, were inverted simultaneously. Inversions for the lower lithophysal zone were repeated for multiple realizations of the underlying stochastic permeability field to capture the uncertainty induced by local heterogeneity. A total of 22 test events were used for model calibration (13 from tests conducted in the lower lithophysal zone and 9 in the middle nonlithophysal zone). Seepage-relevant capillary-strength values (parameter $1/\alpha$ of the van Genuchten capillary pressure-saturation relationship—see Equation (5)) were estimated for each location.

A summary is provided in Table 14 and visualized in Figure 32 (see also Wang (2003 [161456], SN-LBNL-SCI-223-V1, p. 37) and Wang (2003 [161456], SN-LBNL-SCI-228-V1, p. 31)).

Since multiple inversions with different realizations of the underlying heterogeneous permeability field were performed for test locations in the lower lithophysal zone, the capillary-strength parameter $1/\alpha$ is calculated as the average for all inverse modeling results at that location, and a standard deviation σ representing the related uncertainty is given. The standard error of the mean is calculated as $\bar{\sigma} = \sigma/\sqrt{i}$, where i is the number of inversions performed. The estimates for the middle nonlithophysal zone are based on a single inversion, i.e., no estimation uncertainty as a result of uncertainty in small-scale heterogeneity can be given. The estimation uncertainty stemming from the misfit between the calibrated model and the data and the sensitivity of the calculated seepage rates with respect to $1/\alpha$ (see Equation (15)) is on the order of a few pascals, i.e., significantly less than the uncertainty from small-scale heterogeneity (which is greater than 50 Pa) or spatial variability (which is on the order of 100 Pa); this contribution to the estimation uncertainty is therefore ignored.

An average capillary-strength parameter for each of the two units is calculated from the estimates at the different locations within a given unit. The related standard deviation is considered to be a measure of spatial variability in $1/\alpha$. In summary, the $1/\alpha$ parameter of the lower lithophysal zone is about 580 Pa with a variability of approximately 100 Pa; the middle nonlithophysal zone has slightly a higher $1/\alpha$ value of about 600 Pa and a variability of approximately 130 Pa. These values can be used to derive a probability distribution for the capillary-strength parameter for each unit (see Figure 32); they will be used as a basis for probabilistic predictions during model validation (see Section 7.2). Note that such a distribution reflects spatial variability only. Multiple realizations of the underlying permeability field must be created to capture the uncertainty in predicted seepage rates, on account of uncertainty in stochastic small-scale heterogeneity.

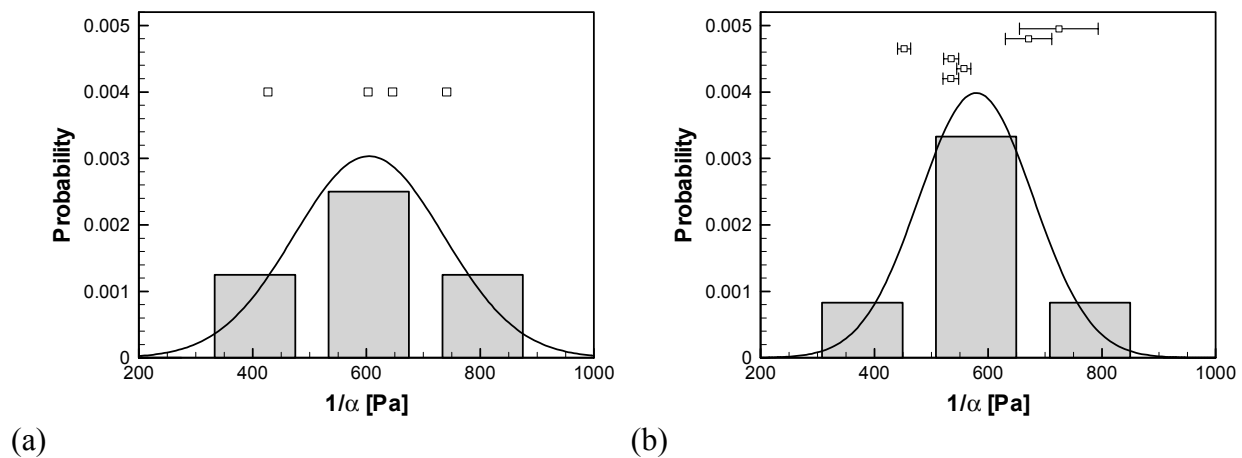


Figure 32. Histograms and related Normal distributions of van Genuchten capillary-strength parameter $1/\alpha$ for (a) the middle nonlithophysal zone, and (b) the lower lithophysal zone. These distributions represent spatial variability. The squares indicate the values obtained at individual locations. For the lower lithophysal zone, the squares represent means from multiple inversions, which are plotted along with the standard error of the mean. (The vertical position of the symbols is of no significance.) Parameters in output DTN: LB0302SCMREV02.002.

Table 14. Summary Statistics of Estimated Capillary-Strength Parameter for Lower Lithophysal Zone and Middle Nonlithophysal Zone (DTN: LB0302SCMREV02.002)

Lower Lithophysal Zone (Ttptll)								
Test Event ⁽¹⁾	Location	Interval	Number of Inversions ⁽²⁾	Estimate $1/\alpha$ [Pa]				
				Mean	Std. Dev. ⁽³⁾	Std. Error ⁽⁴⁾	Min.	Max.
65–69	SYBT-ECRB-LA#1	zone 2	17	534.3	56.8	13.8	447.7	674.1
61, 62	SYBT-ECRB-LA#2	zone 2	21	557.1	56.4	12.3	457.1	676.1
63, 64	SYBT-ECRB-LA#2	zone 3	19	534.8	57.8	13.3	443.1	645.7
70, 71	SYBT-ECRB-LA#3	zone 1	23	452.0	54.7	11.4	382.8	616.6
80	Niche 1620	BH #4	30	671.2	223.2	40.8	356.0	1197.0
83	Niche 1620	BH #5	24	740.5	339.0	69.2	231.1	1840.8
Mean ⁽⁵⁾ =				581.6				
Std. Dev. ⁽⁶⁾ =				105.0				
Middle Nonlithophysal Zone (Ttptmn)								
4, 6, 8	Niche 3107	UM	1	741	—	—	—	—
41, 43	Niche 4788	UL	1	646	—	—	—	—
45, 48	Niche 4788	UM	1	603	—	—	—	—
50, 51	Niche 4788	UR	1	427	—	—	—	—
Mean ⁽⁵⁾ =				604.3				
Std. Dev. ⁽⁶⁾ =				131.5				
<p>(1) See Table 11 on Page 62. Data from all indicated test events were jointly inverted.</p> <p>(2) Each inversion is based on a different realization of the heterogeneous permeability field.</p> <p>(3) Represents estimation uncertainty on account of small-scale heterogeneity (not available for estimates for the middle nonlithophysal zone).</p> <p>(4) Standard error of mean.</p> <p>(5) Represents average for given hydrogeologic unit.</p> <p>(6) Represents spatial variability.</p>								

6.7 IMPACT OF RELATIVE HUMIDITY ON SEEPAGE

As outlined in Section 6.3.3.4, evaporation losses during the seepage experiments conducted in closed-off niches are expected to be insignificant and are thus neglected in the analyses of seepage data from Niches 3107 and 4788. If evaporation were significant during liquid-release tests, measured seepage rates would be lower than those expected in a niche with 100% relative humidity. Analyzing these lower seepage rates with a model that assumes 100% relative humidity in the opening would lead to biased estimates, i.e., the estimated capillary-strength parameter $1/\alpha$ would be increased to match the lower rates, compensating for the systematic modeling error, which is a result of a conceptual difference. Neglecting evaporation effects in an inverse model is thus nonconservative and requires justification. (Note, however, that assuming 100% relative humidity in the drift in a prediction model always yields seepage rates that are higher than those calculated with a model that includes evaporation effects; neglecting evaporation in a prediction model is thus conservative.)

The SCM developed for the analysis of seepage data from liquid-release tests conducted in interval 10–11 ft of borehole #4 in Niche 1620 includes evaporation effects. This model is therefore suitable for examining the impact of evaporation on calculated seepage rates as relative humidity is reduced from near 100% to 85% (the value used in the inversions).

Figure 33 shows the calculated seepage and evaporation rates as a function of the relative-humidity boundary condition in the niche. Evaporation from the entire niche wall surface is relatively high and comparable to the amount of seepage. Evaporation decreases almost linearly as relative humidity increases, as expected. Nevertheless, the impact of evaporation on the calculated seepage rate is small for these high relative humidity values. Neglecting evaporation effects for the analysis of seepage-rate data from Niches 3107 and 4788, where relative humidity was close to 100%, is thus acceptable. Note that evaporation in the open, ventilated ECRB Cross Drift is considered substantial and is thus incorporated into the respective seepage models.

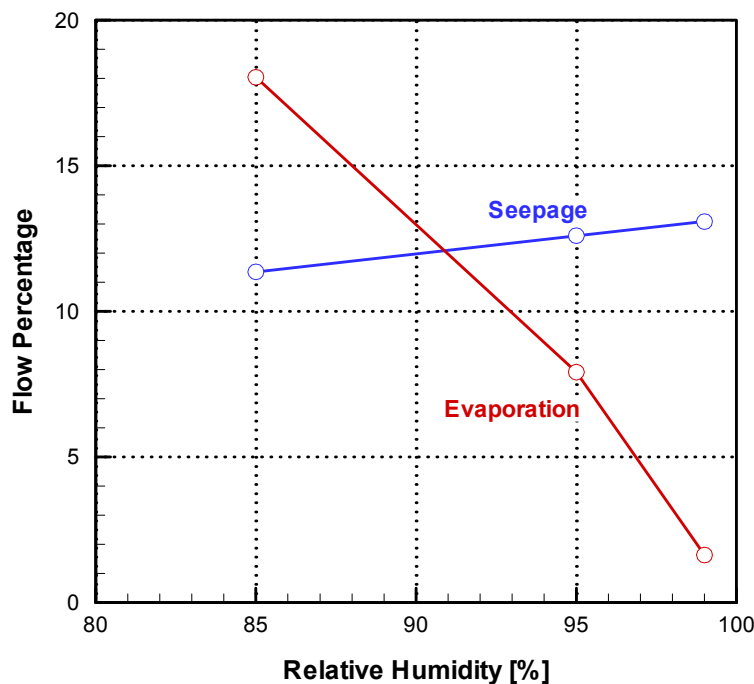


Figure 33. Effect of relative humidity on seepage and evaporation percentages, based on the simulation of a liquid-release test in interval 10–11 ft of borehole #4 in Niche 1620. Flow percentages are plotted 13 days after the start of liquid release. See Figure 34 for the seepage and evaporation rates as a function of time with relative humidity of 85%. Note that flow percentage is calculated relative to liquid-release rate. Simulation results in output DTN: LB0302SCMREV02.001.

6.8 DESCRIPTION OF BARRIER CAPABILITY

In the unsaturated zone, percolation water encountering a waste emplacement drift is partly diverted around the opening on account of the capillary barrier effect. This effect is referred to as the seepage exclusion phenomenon (Philip et al. 1989 [105743]). Seepage exclusion reduces the amount of water entering the waste emplacement drift or prevents dripping altogether, i.e., the seepage flux is always smaller than the percolation flux (see also discussion in Section 6.3.1). This barrier effect is an attribute of the natural system at Yucca Mountain, where unsaturated conditions prevail.

The seepage-exclusion phenomenon has been extensively described in the literature (see Philip et al. 1989 [105743] and references therein). The related water diversion capability is exploited in practical applications for the protection of landfills and hazardous waste sites (the corresponding engineering designs are sometimes referred to as “Richards Barriers”). These standard engineering applications consider porous materials rather than fractured rocks. However, since the key factors affecting a capillary barrier are permeability and capillarity (see Section 6.3.3), which are properties of fractured rock, the same barrier effect can also be expected to apply at Yucca Mountain.

This hypothesis has been extensively tested through the *in situ* seepage experiments described in BSC (2001 [158463], Sections 6.2 and 6.11), Trautz and Wang (2002 [160335]) and Section 6.5 above. All experiments show that the seepage rate is less than the injection rate. Because of storage effects and evaporation, the reduced seepage rate by itself does not conclusively prove that water is diverted around the opening, which would assess the barrier capability of the natural system at Yucca Mountain. Evidence that seepage exclusion and flow diversion occurs is provided by the numerical model, which accounts for storage and evaporation effects, and which is capable of reproducing the observed seepage data. The following mass balance can be formulated:

$$M_{release} = M_{seepage} + M_{storage} + M_{evaporation} + M_{diversion} \quad (18)$$

The cumulative amount of water that was released ($M_{release}$) and that seeped into the capture system ($M_{seepage}$) are known from measurements. Cumulative evaporation ($M_{evaporation}$) is calculated by the model. The rest of the water is either stored in the formation above the opening ($M_{storage}$) or was diverted around the drift and percolated to depth ($M_{diversion}$). Both terms can be inferred from the calibrated model. A similar balance can be written for steady-state rates (where the storage term drops out) instead of cumulative amounts of water. The rate balance for the simulation of a typical liquid-release test in Niche 1620 is shown in Figure 34.

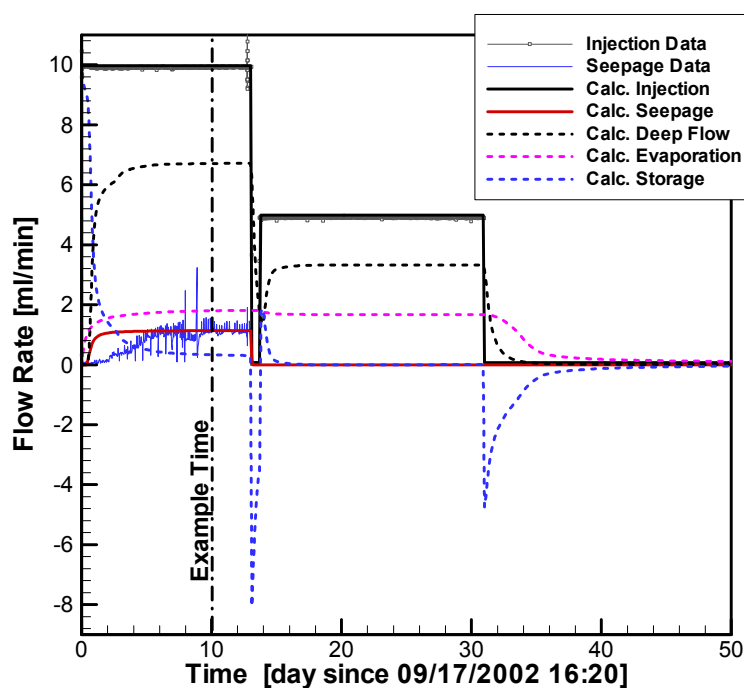


Figure 34. Rates of water released, evaporated, diverted around the niche, stored in the formation above the niche, and captured in the seepage collection system as a function of time. A detailed rate balance on Day 10 (denoted by Example Time) is given in Table 15. Seepage-rate data from DTN: LB0211NICH5LIQ.001 [160792]; simulation results in output DTN: LB0302SCMREV02.001.

Measured and calculated flow rates for typical liquid-release test in borehole #4 of Niche 1620, on Day 10 (since 9/27/2002 16:20) are summarized in Table 15.

Table 15. Mass Balance for Typical Seepage Test in Borehole #4 of Niche 1620, on 9/27/2002 at 16:20 (Day 10). Note that the model release includes an ambient infiltration rate of 2.20 mm/year (0.067 ml/min). Measured data derived from DTN: LB0211NICH5LIQ.001 [160792]; simulation results in output DTN: LB0302SCMREV02.001.

	Measured Flow Rate (ml/min)		Calculated Flow Rate (ml/min)	
Release	9.915	(100.00%)	9.967	(100.00%)
Seepage	1.130	(11.40%)	1.132	(11.36%)
Diversion	—		6.707	(67.30%)
Evaporation	—		1.798	(18.04%)
Storage	—		0.329	(3.30%)

The mass balance indicates that a substantial amount of water is diverted around the opening, confirming the seepage exclusion phenomena and barrier potential of the unsaturated zone at Yucca Mountain.

The mass-balance calculation presented above includes measured values and quantities inferred from the calibrated model. The key quantity of interest demonstrating the barrier capability of the natural system ($M_{diversion}$) was obtained from the model. To obtain direct evidence that flow diversion occurs during liquid-release tests, a horizontal slot (also referred to as “batwing”; see schematic in Figure 4) was excavated from the side of Niche 1620. Water released near the center above the niche and eventually collected in the slot at the spring line (Figure 35) must have been diverted around the opening, corroborating the barrier capability of the seepage-exclusion effect known to exist in unsaturated formations.

In summary, partial or complete diversion of water around underground openings on account of the capillary barrier effect reduces seepage or even prevents water from dripping into a waste emplacement drift. This effective barrier at the interface between the natural and engineered system has the potential to significantly reduce corrosion, waste dissolution, mobilization of radionuclides and their transport from the invert of the waste emplacement drift to the accessible environment. In addition, the extent of the “shadow zone” beneath the drift and its effectiveness in delaying radionuclide transport is strongly related to the seepage-exclusion phenomenon. (For a discussion of the shadow zone, see also Philip et al. (1989 [105743])). The barrier capability of flow diversion around underground openings in unsaturated fractured formations has been established theoretically, through modeling and extensive field testing at Yucca Mountain. The Seepage Model for Performance Assessment (SMPA) examines the effectiveness of the seepage barrier for a multitude of conditions. Uncertainty and spatial variability in the seepage-relevant model parameters have been quantified and will be propagated through the downstream seepage models.

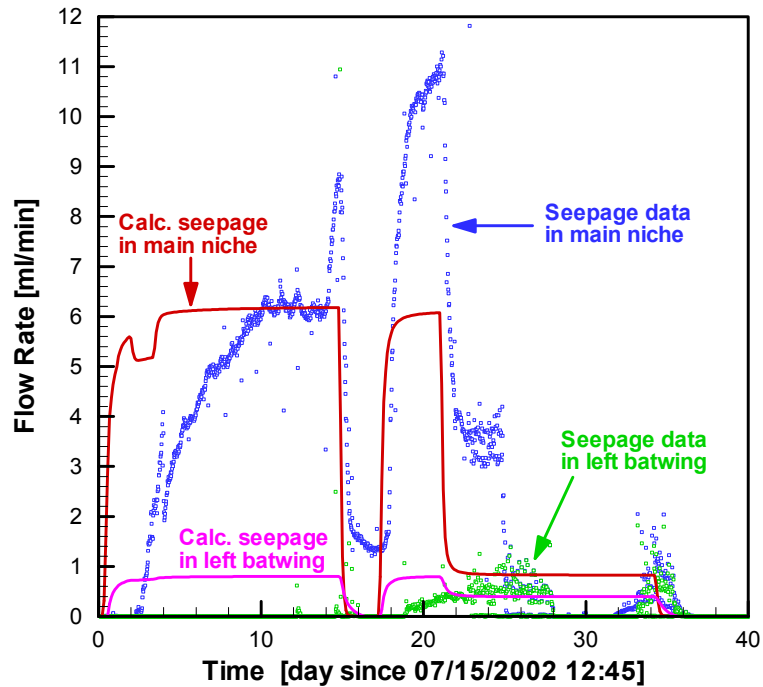


Figure 35. Water collected in the slot on the side of Niche 1620 proving flow diversion around the opening. Liquid was released in interval 28–29 ft of borehole #5. All curves representing measured data are derived from DTN: LB0209NICH5LIQ.001 [160796]; simulation results in output DTN: LB0302SCMREV02.001.

INTENTIONALLY LEFT BLANK

7. VALIDATION

7.1 LEVEL OF RELATIVE MODEL IMPORTANCE

According to AP-SIII.10Q, *Models*, Section 3.16, model validation is a “process used to establish confidence that a mathematical model and its underlying conceptual model adequately represent with sufficient accuracy the system, process, or phenomenon in question.”

While rigorous model testing is fundamentally not possible (Oreskes et al. 1994 [152512]), confidence can be gained that the Seepage Calibration Model (SCM) is adequate for its intended purpose to the level of confidence required by the model’s relative importance to the potential performance of the repository system.

The primary purpose of the SCM is to provide a general modeling framework for the development of the Seepage Model for Performance Assessment (SMPA). The purpose of the SMPA is to provide predicted seepage rates over a large range of conditions. These seepage rates will be further abstracted and used in a probabilistic performance assessment (PA) calculation.

The secondary purpose of the SCM is to provide seepage-relevant $1/\alpha$ estimates. This information will be used in the seepage abstraction process for the development of probabilistic parameter distributions. However, additional data and assumptions enter the development of these distributions: the PA calculations do not rely solely on the $1/\alpha$ values provided by the SCM, but may use broader sampling distributions to reflect additional uncertainties and variabilities.

The relative importance of the SCM to the potential performance of the repository system has been evaluated based on sensitivity analyses as documented in *Risk Information to Support Prioritization of Performance Assessment Models* (BSC 2002 [160780]). These sensitivity analyses indicate that seepage rate does not significantly change the mean annual dose estimate for the nominal scenario (BSC 2002 [160780], Section 3.3.2). For the igneous activity groundwater release scenario, which is dominated by the solubility-limited radionuclides ^{239}Pu and ^{240}Pu , the annual dose is affected by the amount of flow contacting the waste. Nevertheless, it was concluded that the details of the seepage model do not play a significant role in the estimate of mean annual dose. Consequently, the lowest level of validation (Level I) for the TSPA seepage model and the process models supporting it (such as the SCM) was considered appropriate (BSC 2002 [160780], Section 4.3), requiring a demonstration that basic physical principles are appropriately represented.

The guidance of BSC (2002 [160313], p. B-1) refers to the *minimum* level of model validation. However, the SCM is evaluated against the stricter acceptance criteria as defined in the TWP for this Model Report (BSC 2002 [160819], Attachment I, Section I-4-1).

7.2 VALIDATION ACTIVITIES AND CONFIDENCE EVALUATION CRITERIA

The model validation activities and acceptance criteria presented in the remainder of this section follow those of the TWP for this Model Report (BSC 2002 [160819], Attachment I, Section I-4-1); they exceed the Level I validation activities outlined in BSC (2002 [160780], Section 4.3)

and BSC (2002 [160313], p. B-1). Confidence in the adequacy of the SCM for its intended purpose has been gained during the model development process as well as through pre-test predictions of seepage experiments and rigorous post-development model testing as outlined in the TWP for this Model Report (BSC 2002 [160819], Attachment I, Section I-4-1).

7.2.1 Confidence Building during Model Development

During model development, input data and parameters have been carefully selected (1) to best represent the conditions encountered at the liquid-release test sites, (2) to be compatible with the general modeling approach and parameters from upstream models, and (3) to provide a useful conceptual basis and mathematical model for the downstream modeling activities. Seepage-rate data used for calibration have been selected to minimize the potential estimation bias (see Section 6.6.3.2). Moreover, the model is calibrated using a minimum number of adjustable parameters (see Section 6.6.3.1). Being able to match seepage-rate data by adjusting only one or two parameters provides confidence that the model appropriately represents the relevant physical processes and features at the experimental site. Sensitivity analyses have been performed in support of the parameter selection process and to test the appropriateness of certain model simplifications.

The simulations are carried out using a well-established numerical simulator, which ensures mass conservation at each time step. Nevertheless, an explicit mass-balance calculation has been performed (see Section 6.8) to demonstrate that “basic physical principles such as conservation of mass” (BSC 2002 [160780], p. 4-2) are appropriately represented.

The main activity presented in this Model Report is the calibration of the SCM against seepage-rate data from liquid-release tests conducted at Yucca Mountain. Development of the SCM is closely coupled with seepage testing in niches and along boreholes of the systematic hydrologic characterization program. The iteration between testing and modeling lead to improvements in test design and confidence in the modeling approach. As outlined in Section 6.3.4, the approach ensures that the estimated drift-scale parameters are site-specific, seepage-relevant, and model-related, and therefore suitable for the prediction of seepage into waste emplacement drifts using the conceptually compatible Seepage Model for Performance Assessment.

The uncertainty and spatial variability of seepage is evaluated and described by means of a parameter distribution (see Section 6.6.4), which is provided as input to the seepage abstraction process.

Natural analogues as those reported in TDR-NBS-GS-000027 REV 00 ICN 02, *Natural Analogue Synthesis Report* (BSC 2002 [160405], Section 8) provide evidence that the concept of seepage exclusion describes a process that actually occurs in caves, lava tubes, rock shelters and buildings. The qualitative evidence for seepage exclusion and flow diversion was substantiated by quantitative seepage measurements in limestone caves. These studies show that seepage is considerably smaller than the pertinent percolation flux (BSC 2002 [160405], Section 8.2), corroborating the seepage testing and modeling results at Yucca Mountain. Calcite-deposition data in lithophysal cavities (see Section 6.4.3) further corroborate the seepage exclusion concept.

7.2.2 Post-Development Activities

7.2.2.1 Corroboration with Data from Field Experiments

Blind predictions of seepage rates were performed with the calibrated SCM, simulating tests that were not used for model calibration, and that involve a different portion of the fracture system and a different section of the drift or niche. If seepage rates are successfully predicted (according to an acceptance criterion discussed below), confidence is gained that the seepage process is adequately conceptualized in the SCM. The proposed modeling approach is therefore reasonable and can be used as the basis for the development of the predictive SMPA. This addresses the primary purpose of the SCM.

Given the probabilistic nature of the TSPA calculations, a probabilistic acceptance criterion is adopted to ensure that prediction uncertainty is included in the validation process as well as in future model predictions. This addresses the secondary purpose of the SCM. The acceptance criteria were defined in the TWP (BSC 2002 [160819], Attachment I, Section I-4-1). The SCM will be considered validated if one of the following is met:

- (1) 95% of the measured late-time seepage-rate data fall within the 95% confidence region predicted by the model. A poor prediction of early-time seepage data is considered acceptable, because the intended use of the model does not include the accurate simulation of short-term, transient seepage events. Seepage will be calculated in response to steady percolation flux predictions.
- (2) The model overpredicts seepage.
- (3) An explanation can be found for why the observed and predicted seepage rates deviate significantly for a residual that fails to meet criteria (1) and (2) above, and this explanation does not concern and thus invalidate the general approach.

The combination of Criteria (1) and (2) implies that the 95% confidence region should be regarded as one-sided, i.e., 95% of the measured seepage-rate data should be less than the upper bound of the uncertainty band. Figure 36 through Figure 44 show a two-sided error band where 90% of the Monte Carlo simulations fall within that band, and 95% are between zero seepage (the physical minimum) and the upper bound.

Note that these acceptance criteria are more strict than the general acceptance criterion of BSC (2002 [160780], p. 4-2) which only requires a demonstration that “basic physical principles such as conservation of mass” are appropriately represented.

If the acceptance criteria are met, the SCM can be considered validated for its primary and secondary purpose, according to the definition in Section 3.16 of AP-SIII.10Q, *Models*.

Several methods can be employed to assess the uncertainty of model predictions as a result of input parameter uncertainty. When computationally feasible, Monte Carlo simulations (Finsterle 1999 [104367], pp. 76–79) are the method of choice because they automatically account for nonlinearities in the model. A simplified linear uncertainty-propagation analysis can be chosen in cases where running many simulations is prohibitive. The first-order-second-moment (FOSM)

uncertainty propagation analysis (see Equation (16)) is valid for predicting uncertainties that can be approximated by a normal distribution (Finsterle 1999 [104367], pp. 74–76).

Both methods require that probability distributions be determined for each input parameter considered variable or uncertain. Since the seepage experiments used for validation were conducted at locations different from those used for calibration, input parameters other than the ones estimated during calibration can be considered variable or uncertain. Selecting $1/\alpha$ as the only parameter reduces the prediction uncertainty, i.e., it is more difficult for the SCM to pass the validation acceptance criteria. The approach followed here is therefore conservative.

The van Genuchten parameter $1/\alpha$ is both spatially variable and uncertain. A measure of spatial variability was obtained by analyzing data from liquid-release tests performed at multiple locations. The resulting distribution is discussed in Section 6.6.4 and visualized in Figure 32.

Small-scale heterogeneity has been identified as the key source of estimation uncertainty. For the validation of the model and parameters for the lower lithophysal zone, the combined impact of spatial variability and uncertainty was propagated through the prediction models by means of Monte Carlo simulations, in which the van Genuchten parameter $1/\alpha$ was sampled from a Normal distribution (with a mean of 580 Pa, a standard deviation of 100 Pa, and an admissible parameter range from 280 Pa to 880 Pa), and a new realization of the random permeability field was generated for each simulation. For the prediction of seepage rates (and their uncertainty bands) from liquid-release tests conducted in Niches 3107 and 4788 (middle nonlithophysal zone), linear uncertainty-propagation analysis was used. These FOSM analyses only consider spatial variability in the input parameters (standard deviations for $\log(1/\alpha)$ and $\log(k)$ were set to reasonable values of 0.1, and for $\log(\phi)$ to 0.3); uncertainty as a result of small-scale heterogeneity is not included. (Note that while the model itself is heterogeneous, only one realization can be considered in a FOSM analysis.) This approach is conservative because it reduces the range of predicted seepage rates, making it more difficult for the SCM to meet the stringent validation criteria outlined above.

7.2.2.2 Corroboration through Comparison of Data with Pre-Test Model Predictions

A representative seepage test conducted in Niche 1620 as planned in SITP-02-UZ-002 (BSC 2001 [158200]) was predicted based on the proposed conceptual model, but using preliminary parameters, which were derived from testing in a single systematic testing borehole (SYBT-ECRB-LA#2) in the Ttptll unit (see previous revision of *Seepage Calibration Model and Seepage Testing Data*, CRWMS M&O 2001 [153045]). The pre-test predictions were submitted to the TDMS under DTN: LB0207PRESCMN5.001 [160410] and DTN: LB0207PRESCMN5.002 [161192]. These predictions are qualitatively compared with seepage data collected in Niche 1620. It is important to realize that these pre-test predictions were made based on a preliminary understanding of seepage behavior in the Ttptll unit.

The Seepage Calibration Model will be considered corroborated by pre-test predictions if (1) 95% of the measured data fall within the 95% confidence region predicted by the model using linear uncertainty-propagation analysis, (2) if the model overpredicts seepage, or (3) if an explanation can be found for why the observed and predicted seepage rates deviate significantly.

7.2.2.3 Corroboration Through Technical Review by Publication in Refereed Journals

The general modeling approach has been reviewed and published in a number of scientific journals (Birkholzer et al. 1999 [105170]; Finsterle 2000 [151875]; Salve et al. 2002 [161318]; Doughty et al. 2002 [161320]; Finsterle and Trautz 2001 [161148]; Trautz and Wang 2002 [160335]).

7.3 RESULTS OF MODEL VALIDATION ACTIVITIES

In this section, the range of predicted seepage rates is compared to seepage-rate data collected from liquid-release tests that were not used for model calibration. The range was evaluated by means of Monte Carlo simulations (all tests in lower lithophysal zone and short-term tests in Niche 3650) and using first-order-second-moment (FOSM) error propagation analyses (tests in Niches 3107 and 4788, middle nonlithophysal zone). The indicated range contains 90% of the Monte Carlo simulation results, or—if FOSM error propagation analysis is used—represents the 90% confidence band. Note that the linearity and normality assumption inherent in FOSM breaks down for large standard deviations and for experiments near or below the seepage threshold, where nonlinearities prevail. If no seepage is predicted with the mean parameter set, the uncertainty band vanishes. Furthermore, FOSM may assign a certain probability to negative seepage rates. This specific artifact of the normality assumption inherent in FOSM is of no concern because it only affects the lower bound of the predicted seepage rates.

SYBT-ECRB-LA#2, Lower Lithophysal Zone

Three liquid-release tests (Events 52–54 of Table 11) were performed in zone 1 of borehole SYBT-ECRB-LA#2. No data from this zone have been used for model calibration. Starting 5/11/2000, 09:30, approximately 652 liters of water were released at a very high average rate of approximately 464 ml/min. A second test was conducted starting 5/17/2000, 11:39, in which about 20 liters of water were released at an approximate rate of 35 ml/min. The final, long-term seepage test started on 5/23/2000, 14:22, releasing approximately 334 liters of water at an average rate of 26 ml/min (Finsterle 2002 [161043], p. 74). Input files for simulating this test sequence are created analogous to the procedure described in Section 6.6.2 (Finsterle 2002 [161043], pp. 82–83). The software iTOUGH2 V5.0 (LBNL 2002 [160106]) is used to perform 100 Monte Carlo simulations. The resulting predictions of seepage rates into the drift are shown in Figure 36.

The calibrated SCM predicts seepage rates for the first test event that are higher than the observed data (Figure 36a). This result is expected because the high release rate caused an unknown amount of the seepage water to bypass the capture system, i.e., the measured seepage rates are known to be too low. This test event therefore cannot be used for rigorous model validation, but it does serve to qualitatively corroborate the SCM predictions.

As shown in Figure 36b and Figure 36c, the measured seepage-rate data for the lower-rate test events lie within the band containing 90% of the Monte Carlo simulations. Thus, an interpretation of probabilistic seepage predictions made with the calibrated SCM would not lead to erroneous statements about seepage, meeting the validation acceptance criterion.

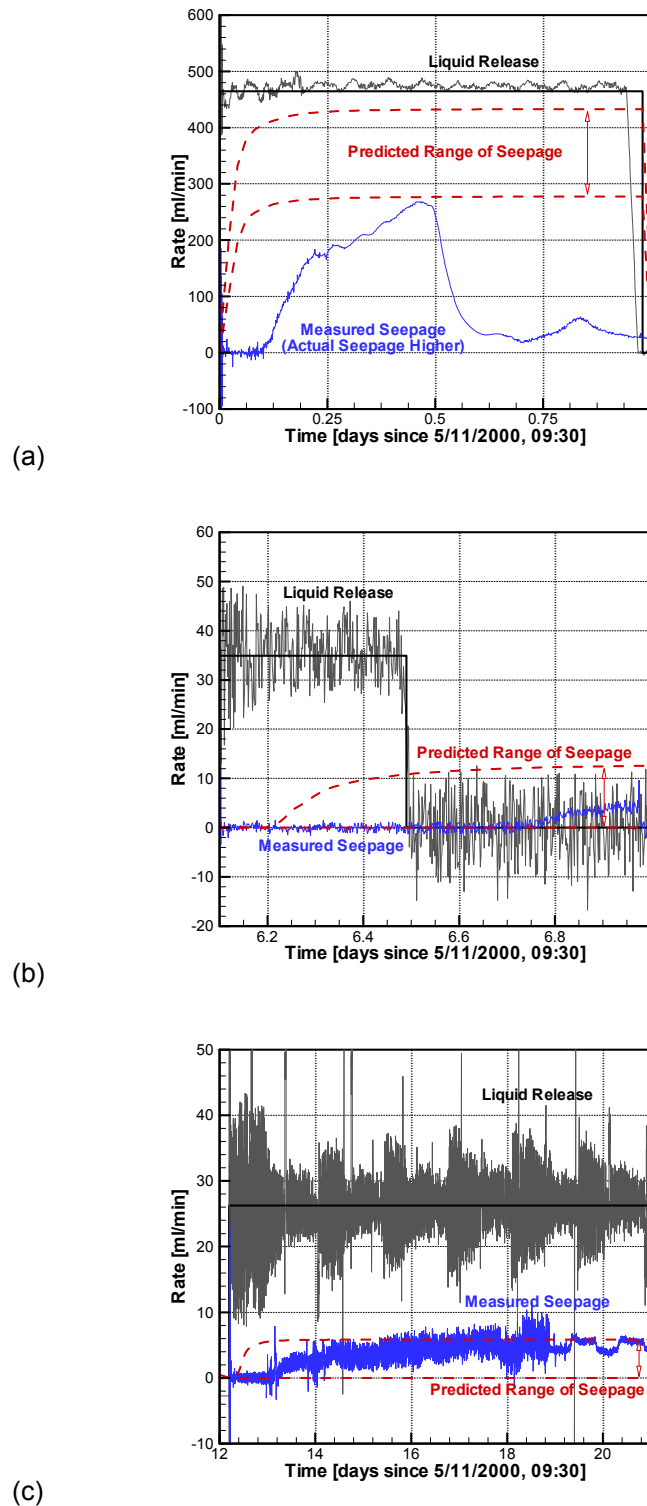


Figure 36. Liquid-release rates, measured seepage rates, and range of predicted seepage rates containing 90% of the 100 Monte Carlo simulations of the experiment conducted in zone 1 of borehole SYBT-ECRB-LA#2; (a) Event 52, (b) Event 53, and (c) Event 54. All curves representing measured data are derived from DTN: LB00090012213U.002 [153154]; simulation results in output DTN: LB0302SCMREV02.001.

A long-term liquid-release test was conducted in zone 2 of borehole SYBT-ECRB-LA#2, starting 5/11/2000, 05:20 (Events 55 and 56 of Table 11). Figure 37 shows the liquid-release rate, the measured seepage rate, and the range of predicted seepage rates containing 95% of 100 Monte Carlo simulations. Water release occurs at a rate of approximately 30 ml/min for more than two weeks. (The noise seen in the release and seepage-rate data changes with time as the water tank is emptied or filled, respectively.) It takes about 10 days for the water to migrate to the drift ceiling and to build up sufficient saturation for seepage to occur. The fluctuations in the observed seepage rates reflect the change in ventilation conditions during daytime (ventilation is on) and nighttime and weekends (ventilation is off), which is approximately implemented in the model by changing the water potential in the drift, accounting for both the reduction in relative humidity and the reduction in the evaporative boundary-layer thickness during active ventilation (for details, see Finsterle (2002 [161043], pp. 134–135)). The data fall within the uncertainty band of the model prediction, meeting the validation acceptance criterion.

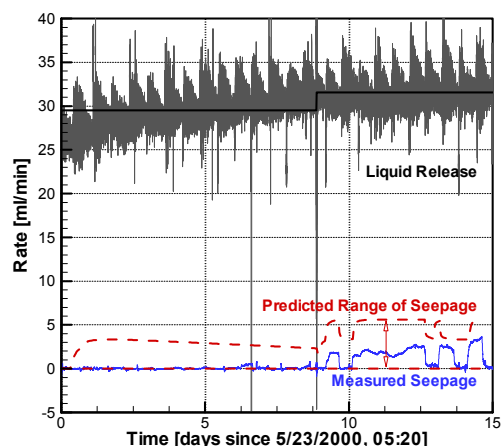


Figure 37. Liquid-release rates, measured seepage rates, and range of predicted seepage rates containing 90% of the 100 Monte Carlo simulations of the experiment conducted in zone 2 of borehole SYBT-ECRB-LA#2. All curves representing measured data are derived from DTN: LB00090012213U.002 [153154]; simulation results in output DTN: LB0302SCMREV02.001.

Four consecutive liquid-release tests (Events 57–60 of Table 11) were performed in zone 3 of borehole SYBT-ECRB-LA#2. Starting 5/17/2000, 11:39, more than 1000 liters of water were released during the 41-day testing period. However, seepage occurred only during the last 1 ½ days of testing (see Figure 38), i.e., shortly before operational constraints terminated the test on 6/27/2000, 09:37. Only about 1 liter seeped into the drift. Furthermore, the early-time seepage rate is highly dependent on the formation storage capacity, which again is of no relevance for the ultimate purpose of the SCM. The calibrated SCM predicts early seepage initiation and a seepage rate that is somewhat higher than the observed values. Nevertheless, the data lie within the simulation uncertainty band, i.e., the acceptance criterion for model validation is met.

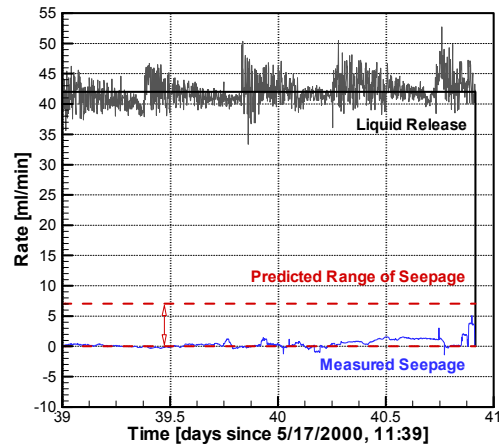


Figure 38. Liquid-release rates, measured seepage rates, and range of predicted seepage rates containing 90% of the 100 Monte Carlo simulations of the experiment conducted in zone 3 of borehole SYBT-ECRB-LA#2. All curves representing measured data are derived from DTN: LB00090012213U.002 [153154]; simulation results in output DTN: LB0302SCMREV02.001.

SYBT-ECRB-LA#3, Lower Lithophysal Zone

Water was released from zone 2 of borehole SYBT-ECRB-LA#3 at various rates over a period of 2 months (Events 72–76 of Table 11) without inducing any observable seepage. No data from this zone have been used for model calibration. While most of the 100 Monte Carlo simulations resulted in zero seepage, the upper bound of the confidence band is determined by the few realizations that promote seepage (see Figure 39). The validation test obviously meets the acceptance criteria.

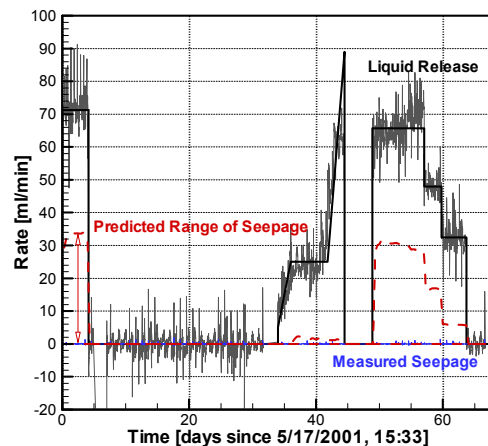


Figure 39. Liquid-release rates, measured seepage rates, and range of predicted seepage rates containing 90% of the 100 Monte Carlo simulations of the experiment conducted in zone 2 of borehole SYBT-ECRB-LA#3. All curves representing measured data are derived from DTN: LB0203ECRBLIQR.001 [158462]; simulation results in output DTN: LB0302SCMREV02.001.

Niche 1620, Borehole #5, Interval 28–29 ft, 05/06/2002, Lower Lithophysal Zone

Water was released from interval 28–29 ft of borehole #5 in Niche 1620 starting on 5/6/2002 at different rates for 4 days (Event 78 of Table 11). Testing resumed again on 5/16/2002 at a rate of approximately 60 ml/min for 5 days, resulting in observable seepage (Event 81) as shown in Figure 40. These test data were not used for calibration. During the first 4 days, the release rate fluctuated significantly, and the test was terminated due to data-logger problems while the seepage rate was still increasing (before it reached near-steady-state conditions). Because the calibrations were performed to match the late-time response (see Section 6.6.3.2), the model prediction during this initial 4 days overestimated the observed seepage rates, meeting the validation acceptance criteria. The release rate during the second period (after 5/16/2002) was relatively constant and allowed enough time for the seepage rate to reach an approximately constant rate. The late-time seepage-rate data in this period fall within the uncertainty band of the model prediction, meeting the validation acceptance criteria.

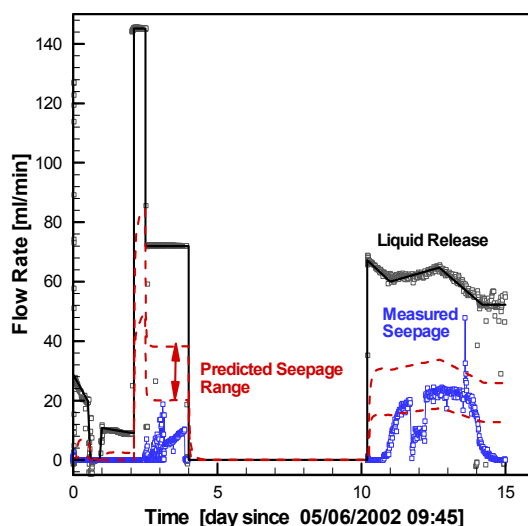


Figure 40. Liquid-release rates, measured seepage rates, and range of predicted seepage rates containing 90% of the 100 Monte Carlo simulations of the experiment conducted in interval 28–29 ft of borehole #5 in Niche 1620, starting on 05/06/2002. All curves representing measured data are derived from DTN: LB0207NICH5LIQ.001 [160408]; simulation results in output DTN: LB0302SCMREV02.001.

Niche 1620, Borehole #5, Interval 28–29 ft, 07/15/2002, Lower Lithophysal Zone

Water was released from interval 28–29 ft of borehole #5 in Niche 1620 starting on 7/15/2002 at different rates for 34 days, resulting in observable seepage (Events 86–88 of Table 11). The seepage data of the first 14 days was used for calibration (see Figure 27). Water released from interval 21–22 ft of borehole #3 between 7/31/2002 (Day 15) and 8/14/2002 (Day 25) was partially collected by the capture system intended for borehole #5 (see Figure 17, Days 210 through 221). Therefore, only data between Day 25 and Day 35 is used for validation. Most of the 100 Monte Carlo simulations resulted in zero seepage during this validation period. The

observed seepage rate falls within the 90% confidence interval and thus meets the acceptance criteria (see Figure 41).

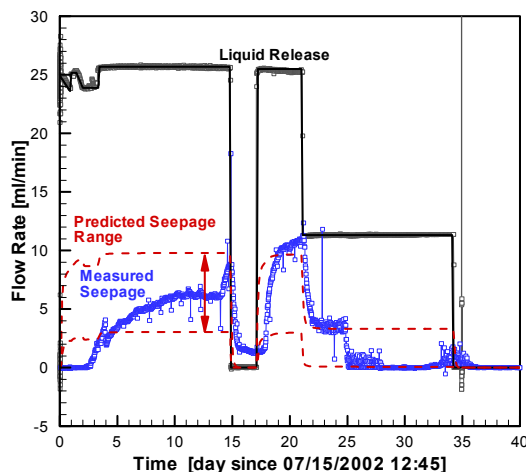


Figure 41. Liquid-release rates, measured seepage rates, and range of predicted seepage rates containing 90% of the 100 Monte Carlo simulations of the experiment conducted in interval 28–29 ft of borehole #5 in Niche 1620, starting 07/15/2002. Effective validation period is between Day 25 and Day 35. All curves representing measured data are derived from DTN: LB0209NICH5LIQ.001 [160796]; simulation results in output DTN: LB0302SCMREV02.001.

Niche 1620, Borehole #4, Interval 10–11 ft, Lower Lithophysal Zone

Water was released from interval 10–11 ft of Borehole #4 in Niche 1620 starting on 9/17/2002 and lasting for approximately one month. Two rates were applied; Event 89 (see Table 11) (Day 0 to Day 13) resulted in observable seepage and was used for calibration (see Figure 25). Event 90 (Day 14 to Day 31) did not result in observable seepage and is used for validation. While most of the 100 Monte Carlo simulations resulted in zero seepage during this validation period, a few simulations yielded seepage and thus a non-zero upper bound of the confidence region. The validation meets the acceptance criteria (see Figure 42).

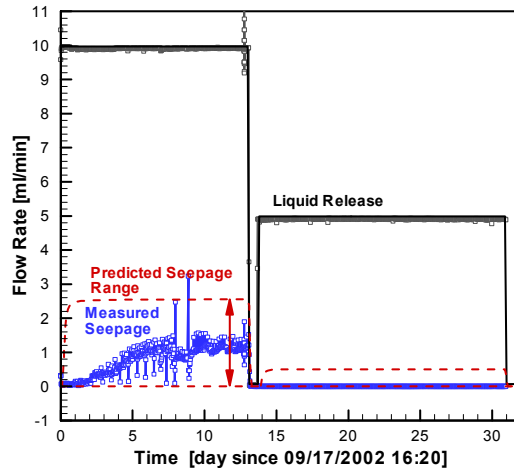


Figure 42. Liquid-release rates, measured seepage rates, and range of predicted seepage rates containing 90% of the 100 Monte Carlo simulations of the experiment conducted in interval 10–11 ft of borehole #4 Niche 1620. Data for Days 1 through 13 were used for calibration; validation period is between Day 14 and Day 31. All curves representing measured data are derived from DTN: LB0211NICH5LIQ.001 [160792]; simulation results in output DTN: LB0302SCMREV02.001.

Niche 3107, Middle Nonlithophysal Zone

Predictions of seepage rates from eight liquid-release tests performed in Niche 3107 were performed. The prediction uncertainty as a result of spatial variability in the input parameters is evaluated using FOSM uncertainty-propagation analysis.

Figure 43 shows the observed seepage-rate data, the predicted seepage rates, and the simulation uncertainty bands for the eight liquid-release tests performed in interval UM 4.88–5.18 and interval UL 5.49–5.80 of Niche 3107. Based on the acceptance criteria outlined in Section 7.2, seven of the eight tests are considered acceptable. In Test UM 4.88–5.18 (Event 12 of Table 11), which started 10/11/1999, the observed late-time seepage rates are slightly larger than the relatively narrow uncertainty band. The tests would be considered acceptable if the chosen uncertainty in the input parameters were marginally increased (e.g., to account for uncertainty as a result of the stochastic nature of the underlying heterogeneous permeability field). Such an increase is likely to occur during seepage abstraction (see upcoming Model Report MDL-NBS-HS-000019 REV 00, which supersedes (CRWMS M&O 2001 [154291])).

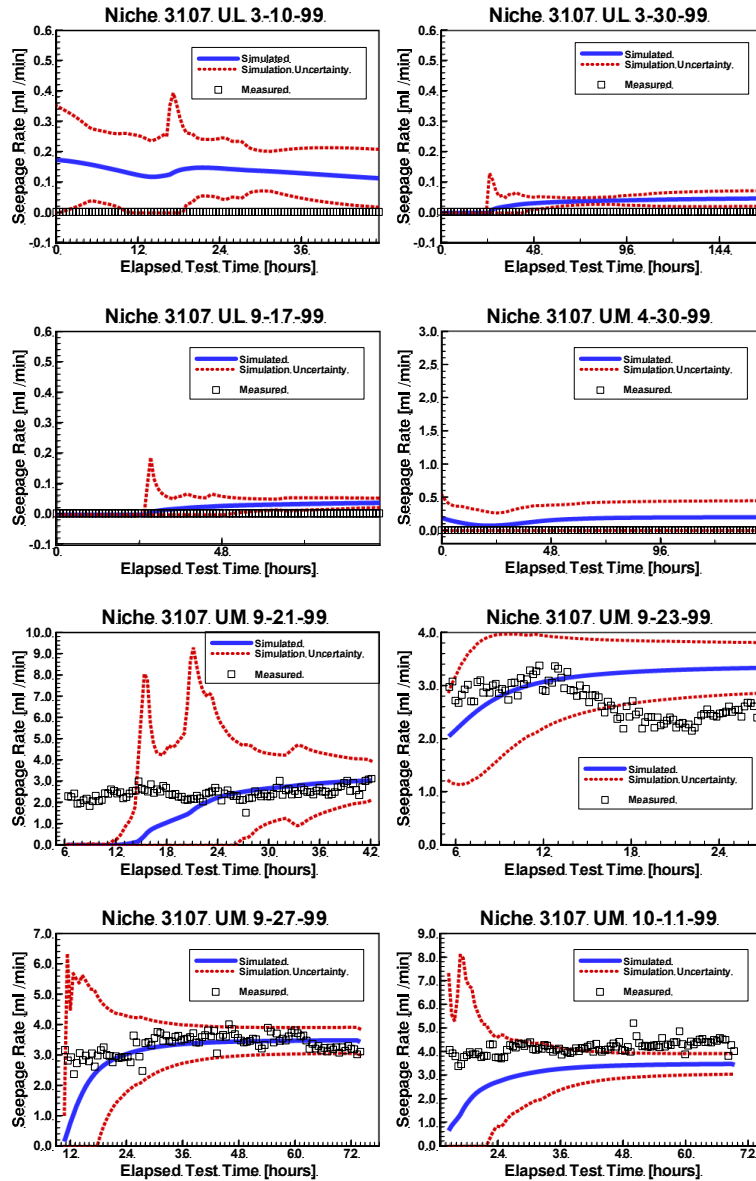


Figure 43. Validation of Seepage Calibration Model and Tptpmn seepage-relevant parameters using data from Niche 3107 (Events 1, 2, 3, 4, 7, 9, 10, 11, 12 of Table 11). Linear uncertainty propagation analysis was used to calculate the uncertainty band of the model predictions. All curves representing measured data derived from DTN: LB0010NICH3LIQ.001 [153144]; simulation results in DTN: LB0010SCMREV01.001 [154292].

Niche 4788, Middle Nonlithophysal Zone

Predictions of seepage rates from five liquid-release tests performed in Niche 4788 were conducted. The prediction uncertainty as a result of uncertainty in the input parameters is evaluated using FOSM error propagation analysis.

Figure 44 shows the observed seepage-rate data, the predicted seepage rates, and the simulation uncertainty bands for the five liquid-release tests performed in interval UL 7.62–7.93, interval UM 6.10–6.40, and interval UR 5.18–5.48 of Niche 4788. Based on the acceptance criteria outlined in Section 7.2, four of the five tests are considered acceptable. In Test UL 7.62–7.93 (Event 40 of Table 11), which started 11/03/1999, the observed late-time seepage rates are slightly larger than the relatively narrow uncertainty band. The tests would be considered acceptable if the chosen uncertainty in the input parameters were somewhat increased, e.g., to account for aleatory uncertainty.

The seepage-rate data from the test in interval UL 7.62–7.93, starting 11/3/1999, show some outliers that appear to be random, possibly caused by a disturbance of the balance measuring cumulative seepage mass. The seepage-rate data from the test in interval UR 5.18–5.48, starting 12/7/1999, shows a spike approximately 60 hours after water release. The cause for this erratic behavior is unknown. Note, however, that despite these outliers, 95% of the observed data is within the predicted range.

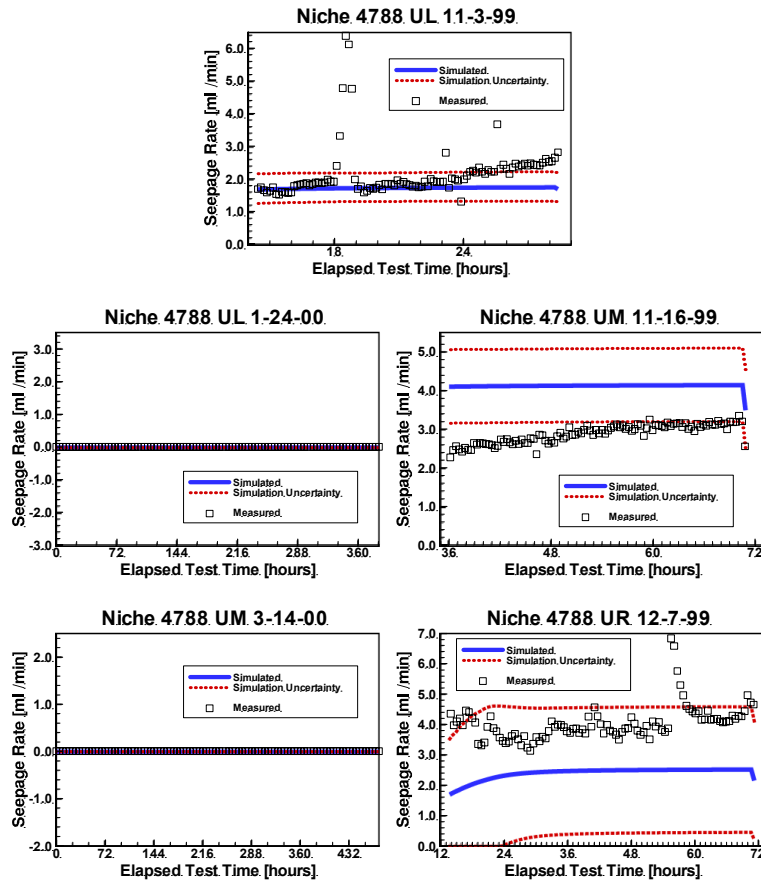


Figure 44. Validation of Seepage Calibration Model and Tptpmn seepage-relevant parameters using data from Niche 4788 (Events 40, 42, 44, 47, and 49 of Table 11). Linear uncertainty propagation analysis was used to calculate the uncertainty band of the model predictions. All curves representing measured data derived from DTN: LB0010NICH4LIQ.001 [153145]; simulation results in DTN: LB0010SCMREV01.001 [154292].

Niche 3650, Middle Nonlithophysal Zone

Twenty-seven liquid-release tests were performed in Niche 3650 (DTN: LB980001233124.004 [136583]), thirteen resulting in seepage (see Table 11, Events 13–39). The short-term tests are very sensitive to storage effects and the properties of a few fractures connecting the injection interval to the niche opening. Therefore, information derived from these tests is considered much less reliable than the long-term tests discussed before. Unlike in all the other tests, only the total seepage amount at the end of the experiment was recorded.

These tests, while providing qualitative seepage information, were not used for calibration purposes to avoid a potential bias in the estimates. A similar bias renders them unsuitable for stringent model validation; the data and model predictions are shown here for completeness only. Their weight in the overall evaluation of the model validation activities should be considered minimal.

Fifty Monte Carlo simulations were performed for the prediction of seepage rates in Niche 3650 (Ahlers 2002 [161045], p. 57). Figure 45 shows the results of the Monte Carlo simulations.

The data fall outside the range defined by the Monte Carlo simulations in only three of the 27 test events. All three cases (Events 19, 20, and 22) concern data from interval UM 4.27–4.57. In a fourth test event conducted in the same interval (Event 21), the observed data point is near the upper bound of the predicted seepage range. Conditions in this interval seem to be specific and significantly different from those encountered elsewhere in Niche 3650 and the other two niches in the middle nonlithophysal zone. In several other intervals, the simulations show (minor) seepage where no seepage was observed.

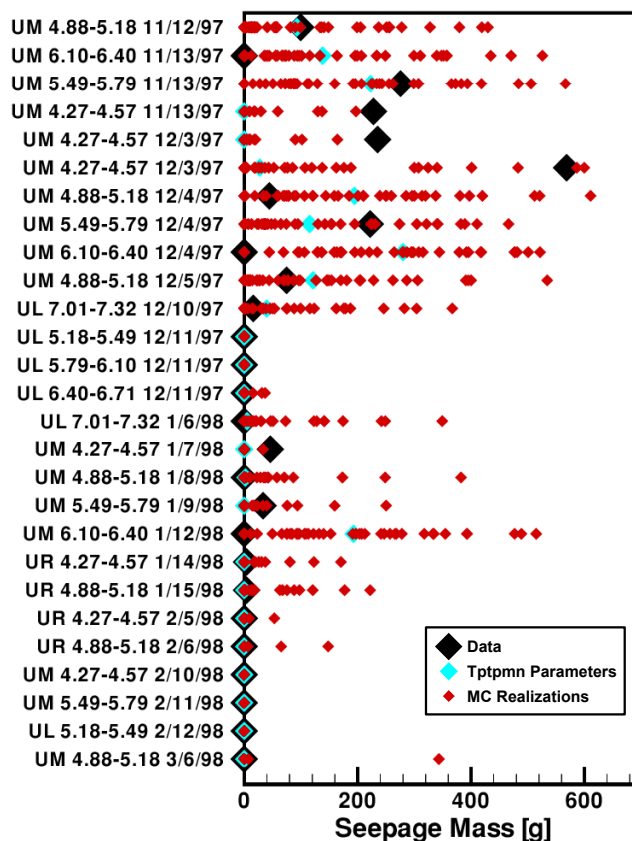


Figure 45. Validation of Seepage Calibration Model and Tptpmn seepage-relevant parameters using data from Niche 3650. Monte Carlo simulations were performed to estimate the prediction range. Measured data are derived from DTN: LB980001233124.004 [136583]; simulation results in DTN: LB0010SCMREV01.001 [154292].

Pre-Test Prediction

A blind pre-test prediction of a representative liquid-release test with a rate of 30 ml/min was performed prior to actual testing in Niche 1620. The predicted range of seepage rates (DTN: LB0207PRESCMN5.002 [161192], Figure 1) is shown in Figure 46, along with the measured seepage-rate data from a liquid-release test in borehole #5 of Niche 1620 (using a rate of approximately 25 ml/min).

The prediction cannot be directly compared to the data because of the different release rates. However, it is evident that the predicted rates are consistent with the seepage amounts actually observed during the test. The model overpredicted the seepage rates by a small amount, which was expected because of conservative assumptions made in that model. (Note that the seepage percentage—the ratio between the seepage and release rates—is not expected to be constant; it increases with the release rate). In summary, the pre-test prediction of seepage rates performed with the preliminary Seepage Calibration Model meet the acceptance criteria outlined in Section 7.2 and thus provides confidence in the appropriateness of the general modeling approach.

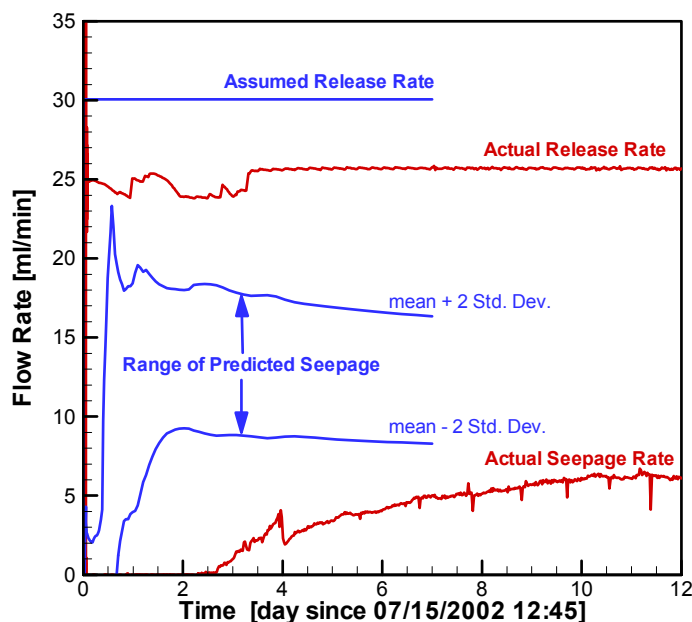


Figure 46. Comparison between pre-test seepage-rate prediction with preliminary Seepage Calibration Model and observed seepage-rate data. The range of predicted seepage covers the uncertainty band approximately on the 95% confidence level. The pre-test prediction results from DTN: LB0207PRESCMN5.002 [161192]; the seepage data from DTN: LB0209NICH5LIQ.001 [160796].

7.4 SUMMARY OF MODEL VALIDATION

Estimates of the seepage-relevant van Genuchten parameter $1/\alpha$ for the lower lithophysal zone and the middle nonlithophysal zone of the Topopah Spring welded unit were obtained by calibration of a process model against seepage-rate data collected in the ECRB Cross Drift and in Niches 1620, 3107 and 4788. As outlined in Section 7.2.1, the development and calibration of the models is fully documented (see specifically Section 6 and the supporting references and scientific notebooks), generating confidence in the conceptual and mathematical model used as a basis for the analysis of seepage data. A preliminary version of the model was used for a pre-test prediction of a representative liquid-release test planned for Niche 1620. The predicted seepage rates were consistent with the associated test observations, corroborating the appropriateness of the conceptual model.

The calibrated parameter values obtained at different locations were compiled and described by means of a statistical distribution to represent spatial variability within a given hydrogeologic unit (see Section 6.6.4). Small-scale heterogeneity was identified as the main source of estimation uncertainty. The combined impact of spatial variability and uncertainty was propagated through the prediction models during model validation by means of Monte Carlo simulations, in which the van Genuchten parameter $1/\alpha$ was sampled from the respective statistical distribution, and a new realization of the random permeability field was generated for each simulation. (Note that this approach is identical to that used in the downstream seepage models—the Seepage Model for Performance Assessment, which uses multiple realizations of the underlying

heterogeneous permeability field to account for uncertainty, and the sampling strategy employed during TSPA calculations, which makes use of an abstracted statistical distribution representing spatial variability.)

The observed late-time seepage-rate data (1) fell within the range of predicted seepage rates in all test cases for the lower lithophysal zone, and in almost all test cases for the middle nonlithophysal zone, or (2) were lower than the predicted seepage rates in a few cases, i.e., the model prediction was conservative. The data were marginally higher in two longer-term tests (Events 12 and 40) and in three short-term tests in Niche 3650 (Events 19, 20, and 22), which are considered of minor relevance.

The conceptual basis and mathematical model of the Seepage Calibration Model has been presented to the technical community through publication in refereed scientific journals, passing the review process.

Based on the evidence presented in Section 7.3, the conceptual and mathematical basis of the Seepage Calibration Model and the parameters derived from calibrating the model against seepage-rate data are considered adequate for the intended purpose and to the level of confidence required by the model's relative importance to the postclosure performance of the proposed repository system. No further activities are needed to complete the validation of the SCM for its intended use.

8. CONCLUSIONS

8.1 SUMMARY AND CONCLUSIONS

Seepage into waste emplacement drifts affects the performance of the proposed high-level nuclear waste repository at Yucca Mountain, Nevada. Theoretical analyses, numerical modeling studies, and field experiments suggest that seepage into underground openings excavated in unsaturated formations is smaller than the percolation flux at the given location. This is mainly a result of capillary pressures holding water in the formation, diverting it around the cavity, and preventing it from entering the underground opening. The effectiveness of this capillary barrier depends on the percolation flux, the hydrogeologic properties of the formation, the geometry of the drift, the properties of the drift surface, and the in-drift conditions determining the evaporation potential.

This Model Report describes the development, calibration, and validation of the Seepage Calibration Model (SCM). The purpose of the SCM is to provide the conceptual basis for the Seepage Model for Performance Assessment (SMPA), which calculates seepage into waste emplacement drifts for a variety of hydrogeologic conditions. The SCM was calibrated against *in situ* seepage-rate data to provide seepage-relevant, model-related parameters appropriate for use in a drift-scale process model with a comparable model structure (such as the SMPA). These parameters will be used as base-case parameters for certain SMPA sensitivity analyses and will contribute to the development of parameter probability distributions for subsequent Performance Assessment calculations.

Three-dimensional process models were developed, representing niche locations in the middle nonlithophysal zone of the Topopah Spring Tuff (Ttpmn) and one niche and three boreholes in the ECRB Cross Drift, which are located in the lower lithophysal zone of the Topopah Spring Tuff (Ttppl). Air-permeability data were geostatistically analyzed to provide the basis for generating heterogeneous, spatially correlated permeability fields.

A total of 90 experiments using different release rates were performed (Table 11). Eighty-one of these test events were simulated with the SCM, a numerical process model that captures transient unsaturated flow through a heterogeneous fracture continuum and seepage into the underground openings. In addition, evaporation effects were accounted for when deemed significant. Measured seepage-rate data from 22 liquid-release tests were used to calibrate the SCM and to estimate the seepage-relevant van Genuchten capillary-strength parameter $1/\alpha$ (see Section 6.6.3). The remainder of the seepage-rate data were used to validate the SCM, that is, to determine whether it is appropriate and adequate for its intended use (see Section 7.3).

The capillary-strength parameter was determined by calibrating the model against multiple tests using different liquid-release rates. Some of these release rates induced a local percolation flux above the seepage threshold, i.e., water dripped into the opening and yielded seepage-rate data valuable for calibration. However, the joint inversion of multiple data sets also included data from tests performed *below* the seepage threshold. Moreover, the model was validated against tests conducted *above and below* the seepage threshold. That is, the system was probed and the model was validated for the critical range of percolation rates about the seepage threshold.

Seepage predictions for natural percolation fluxes that are even lower than the low fluxes (below the seepage threshold) induced during the low-rate tests will yield the correct result, namely zero seepage. As a result of a high-infiltration climate or strong flow focusing, the natural percolation flux may be high and exceed the seepage threshold. These would be the critical scenario for performance. Obviously, the parameters estimated from the liquid-release tests would be most suitable for those critical circumstances, because they were determined under similar high-rate conditions. In summary, the parameters determined from relatively high-rate liquid-release tests are appropriate and provide a solid basis for seepage predictions under low and higher natural percolation fluxes.

The insignificant impact of reduced relative humidity on calculated seepage into closed-off niches in the middle nonlithophysal zone has been confirmed (see Section 6.7 and discussion in Section 6.3.3.4). Significant evaporation effects in the ventilated ECRB Cross Drift have been addressed through moisture control, monitoring of relative humidity, and inclusion of evaporation in the numerical model.

The following general conclusions are drawn:

- The testing and modeling approach documented in this Model Report is adequate for providing the conceptual basis and parameters for the TSPA seepage model. The approach consists of analyzing seepage by means of a numerical process model that is calibrated against seepage-rate data from liquid-release tests conducted within the repository host units.
- The estimation of seepage-relevant, model-related, effective parameters on the appropriate scale is a methodology that reduces the risk of introducing significant systematic errors, provided that the structure of the prediction model (such as the SMPA) is consistent with the model used for calibration (the SCM).
- Seepage properties are spatially variable. The variability has been examined by performing liquid-release tests at various sites along the ESF and the ECRB Cross Drift. Spatial variability in the estimated van Genuchten capillary-strength parameter $1/\alpha$ is relatively strong compared to the estimation uncertainty at a given location. The main contribution to the estimation uncertainty is small-scale heterogeneity that can only be described stochastically. Random fluctuations in seepage-rate data leads to insignificant uncertainty in the parameter estimates.
- The seepage-relevant van Genuchten capillary-strength parameter $1/\alpha$ in the lower lithophysal zone is on the order of 580 Pa, with a standard deviation, representing spatial variability, of approximately 100 Pa. The corresponding values for the middle nonlithophysal zone are 600 Pa and 130 Pa.

The general conclusions listed above must be viewed considering the caveats and limitations discussed throughout this Model Report and summarized in Section 8.2. Further justification for the modeling and analysis approach can be found in Section 8.3 below.

8.2 MODEL OUTPUT, UNCERTAINTIES, AND LIMITATIONS

As outlined in Sections 1 and 6.1.1, this Model Report produces (1) a methodological and conceptual basis for the subsequent development of the Seepage Model for Performance Assessment (SMPA), and (2) seepage-relevant parameters that will be used for drift seepage abstraction. The parameter distribution developed as a result of the abstraction process will then be used—in combination with the results from the SMPA—as input to the seepage TSPA model. The Seepage Calibration Model (SCM) is intended to be used only within this Model Report for parameter estimation purposes.

The two products from this Model Report—conceptual model and model-related parameters—are described below.

Conceptual Basis for Seepage Prediction Models

The conceptual basis to be used for the SMPA or similar modeling efforts to predict seepage has been described in Section 6.3; recommendations for downstream users are summarized in Section 8.4. The SCM must be viewed as an integral element of a consistent approach involving data analysis, parameter estimation, model prediction, and abstraction. The adequacy of the approach is further discussed in Section 8.3. Alternative approaches were described in Section 6.4.

Seepage-Relevant van Genuchten Capillary-Strength Parameter

The second output from this Model Report consists of model-related estimates of the van Genuchten capillary-strength parameter $1/\alpha$. The estimates were obtained through calibration of the SCM against seepage-rate data from liquid-release tests; they are summarized in Table 16. The estimates from the different locations are combined to obtain seepage characteristics for the two hydrogeologic units Tptpl and Tptpmn. The standard deviations reported in Table 16 reflect spatial variability.

The estimates are uncertain because they are derived from limited data, which exhibit random and potentially systematic measurement errors, and because the model is a simplification of the real system, which introduces systematic and random modeling errors. Estimating model-related parameters mitigates the impact of some of the residual systematic errors. The following uncertainties have been evaluated:

- The uncertainty as a result of undetermined details of small-scale heterogeneity was quantified for the $1/\alpha$ estimates in the Tptpl (see Table 14) by performing multiple inversions with different realizations of the underlying heterogeneous permeability field. Note, that the impact of this uncertainty on seepage predictions can be directly evaluated using the Seepage Model for Performance Assessment (SMPA; see upcoming REV 02 of CRWMS M&O 2000 [153314]), i.e., this uncertainty does not need to be incorporated in the parameter distribution used for sampling in TSPA calculations (see upcoming Model Report MDL-NBS-HS-000019 REV 00 (CRWMS M&O 2001 [154291])).

- Estimation uncertainty resulting from unexplained fluctuations in the seepage-rate data is propagated through the model and evaluated using Equation (14); its contribution to the overall parameter uncertainty is negligible (see Section 6.6.3.3).
- A potential bias in the estimated parameters as a result of evaporation effects is minimized by an appropriate test design, moisture monitoring, and inclusion of evaporation effects into the model using site-specific relative humidity and evaporation-rate data. Sensitivity analyses were performed, demonstrating that residual uncertainty resulting from incomplete knowledge about the evaporative boundary-layer thickness in a ventilated drift and uncertainty in the relative humidity data is minor (see Sections 6.6.3.1 and 6.7). The chosen values are cautiously realistic.
- Sensitivity analyses were performed to examine the potential impact of selected, uncertain parameters on the estimation of seepage-relevant parameters (see Section 6.6.3.1). These synthetic inversions also provided the correlation structure, indicating that a potential error in one (relatively insensitive) parameter can be partly compensated for by the estimation of the model-related parameters that are most sensitive.

Table 16. Mean and Standard Deviation of Capillary-Strength Parameter $1/\alpha$ for Lower Lithophysal Zone and Middle Nonlithophysal Zone (DTN: LB0302SCMREV02.002)

Unit	Location	Interval	$1/\alpha$ [Pa]	Mean $1/\alpha$ [Pa]	Std. Dev. [Pa] [#]
Tptpll	SYBT-ECRB-LA#1	zone 1	534	582	105
	SYBT-ECRB-LA#2	zone 2	557		
		zone 3	535		
	SYBT-ECRB-LA#3	zone 1	452		
	Niche 1620	borehole #4	671		
		borehole #5	741		
Tptpmn	Niche 3107	UM	741	604	131
	Niche 4788	UL	646		
		UM	603		
		UR	427		

[#] Characterizes spatial variability; the impact of uncertainty from undetermined details of small-scale heterogeneity on seepage predictions is directly evaluated in the Seepage Model for Performance Assessment. Other epistemic uncertainties are comparatively small.

The primary caveats and limitations for usage of the results from the SCM are as follows:

- The seepage models described in this Model Report provide estimates of the seepage flux averaged over a drift segment of a certain length. The seepage models are not expected to accurately predict individual seepage events or the precise spatial seepage distribution along a waste emplacement drift. By definition, the derived parameters (see Table 16) are related to the specific model structure used, i.e., these parameters are only applicable to a conceptual and numerical model similar to the SCM. (Note that the

SCM and the SMPA are compatible in this sense.) The parameters are also process specific and scale dependent, i.e., while they can be considered optimal for seepage calculations on the drift scale, they are not necessarily applicable to other processes on different scales. If the downstream models cannot be developed to be fully compatible with the SCM, appropriate adjustments to the parameter values should be made.

- The effective parameters derived in this Model Report capture many processes and features leading to dripping of formation water into a large underground opening. However, this does not include water dripping as a result of condensate accumulation on the drift surface or other in-drift moisture redistribution processes.
- Seepage during the thermal period is examined separately in the TH Seepage Model (see BSC 2003 [161530]).

8.3 ADEQUACY OF INPUT DATA AND MODELING APPROACH

The two key elements of the overall approach described in this Model Report are (1) the use of a physically based, numerical process model as the basis for predicting seepage into large underground openings and (2) the calibration of this model against data from *in situ* liquid-release experiments. This approach is considered appropriate for the following reasons:

- Unsaturated flow and seepage into drifts are complex, highly nonlinear phenomena. Hydrological process modeling is the preferred means for predicting seepage, because (1) the key process relevant to seepage (i.e., flow of water under unsaturated conditions) is directly modeled based on established physical laws, (2) only a few presumptions need to be made, because the model directly simulates the seepage process of interest, (3) the approach has the potential to simulate conditions that cannot be observed in the field, (4) numerical models are flexible enough to accommodate the nonideal initial and boundary conditions as they occur during seepage experiments.
- The SCM is based on a process model that is consistent and compatible with the conceptual and numerical models used for calculating flow and transport in the unsaturated zone at Yucca Mountain.
- Seepage experiments provide calibration data that reflect the process of interest. The measured data automatically reflect the factors and features pertinent to seepage. The effective parameters are capable of reproducing observed seepage data and are thus likely to yield reasonable seepage predictions.
- The experiments test the capillary-barrier effect on the scale of interest, i.e., no upscaling is required. The water encountering the niche or drift is partly diverted around the opening, engaging the relevant portion of the fracture network on the appropriate scale.
- Water is released from a localized point or line source, simulating the arrival of focused percolation water. Since the injection point lies outside the region of saturation buildup

caused by the capillary barrier effect, the (relatively short) flow distance from the release point to the opening does not significantly affect the seepage behavior.

- The seepage experiments are conducted in the excavation-disturbed zone. The estimated parameters therefore reflect the seepage-relevant properties and conditions to be expected in the vicinity of a waste emplacement drift.

Confidence into the appropriateness of the proposed approach was obtained by meeting acceptance criteria during the validation exercises (Section 7). While alternative approaches are viable (see Section 6.4), they often require currently unavailable characterization data, additional model assumptions, or extensive computational resources. Moreover, they usually need a calibration step similar to that described in this Model Report—they suffer from the same potential limitations and caveats. The approach outlined in this Model Report is considered adequate for the intended purpose and for the use of the SCM and its results.

8.4 RECOMMENDATIONS

The modeling and data-analysis approach outlined in this Model Report are considered suitable for providing a solid basis and sufficient characterization data for predicting seepage into waste emplacement drifts in the repository host rock. The Seepage Calibration Model has been validated applying acceptance criteria that are stricter than those required based on an evaluation of the model's relative importance to the potential performance of the repository system. The recommendations provided below concern the use of the conceptual model for further seepage-related studies.

- Seepage predictions should make use of a physically based process model capable of simulating unsaturated flow under viscous, capillary pressure, and gravitational forces.
- A heterogeneous continuum model should be developed. The computational grid should capture the overall shape of the drift; small-scale surface roughness should not be explicitly discretized; lithophysal cavities should not be explicitly discretized; the nodal distance between the formation and the drift element should be 0.05 m; and gravity must be acting along those vertical connections.
- Seepage-relevant input parameters should be used that are specifically determined for this conceptual model, based on data that represent the key mechanism affecting drift seepage.
- Multiple prediction runs with different realizations of the underlying heterogeneous permeability field should be performed and appropriately averaged.

8.5 OUTPUT DTNs

All computer files needed to reproduce the model results discussed in this Model Report were submitted to the Technical Data Management System (TDMS). As mentioned in Section 1, the analyses of seepage-rate data from liquid-release tests performed in the middle nonlithophysal zone were fully documented in the previous revision of this report (CRWMS M&O 2001 [153045]), and all related files were previously submitted to the TDMS under output DTN: LB0010SCMREV01.001 [154292]. The files supporting the analyses of data from the lower lithophysal zone are listed in Attachment I and are submitted with this Model Report under DTN: LB0302SCMREV02.001. Reproducibility by an appropriately qualified individual is possible by consulting this Model Report and the pertinent scientific notebook pages as listed in Table 7. Air-permeability data developed in the Model Report (see Table 10) and the $1/\alpha$ estimates (see Table 16) are submitted to the TDMS under output DTN: LB0302SCMREV02.002. All data submittals described in this section and summarized in Table 17 are considered Technical Product Outputs (TPOs).

Table 17. Output DTNs

DTN	Description
LB0302SCMREV02.001	Files supporting analyses of seepage data from lower lithophysal zone
LB0302SCMREV02.002	Summary tables of derived air permeabilities and capillary-strength parameters

INTENTIONALLY LEFT BLANK

9. INPUTS AND REFERENCES

The following is a list of the references cited in this document. Column 1 represents the unique six digit numerical identifier (the Document Input Reference System [DIRS] number), which is placed in the text following the reference callout (e.g., BSC 2002 [160819]). The purpose of these numbers is to assist the reader in locating a specific reference. Within the reference list, multiple sources by the same author (e.g., BSC 2002) are sorted alphabetically by title.

9.1 DOCUMENTS CITED

- 161045 Ahlers, C.F. 2002. The Seepage Calibration Model (YMP-LBNL-DSM-CFA-1). Scientific Notebook SN-LBNL-SCI-180-V1. ACC: MOL.20020925.0108.
- 156269 Bear, J. 1972. *Dynamics of Fluids in Porous Media*. Environmental Science Series. Biswas, A.K., ed. New York, New York: Elsevier. TIC: 217356.
- 119397 Birkholzer, J. and Tsang, C.F. 1997. "Solute Channeling in Unsaturated Heterogeneous Porous Media." *Water Resources Research*, 33, (10), 2221-2238. Washington, D.C.: American Geophysical Union. TIC: 235675.
- 105170 Birkholzer, J.; Li, G.; Tsang, C-F.; and Tsang, Y. 1999. "Modeling Studies and Analysis of Seepage into Drifts at Yucca Mountain." *Journal of Contaminant Hydrology*, 38, (1-3), 349-384. New York, New York: Elsevier. TIC: 244160.
- 158463 BSC (Bechtel SAIC Company) 2001. *In Situ Field Testing of Processes*. ANL-NBS-HS-000005 REV 01. Las Vegas, Nevada: Bechtel SAIC Company. ACC: MOL.20020108.0351.
- 158200 BSC (Bechtel SAIC Company) 2001. *Test Plan for: Niche 5 Seepage Testing*. SITP-02-UZ-002 REV 00. Las Vegas, Nevada: Bechtel SAIC Company. ACC: MOL.20020117.0200.
- 160247 BSC (Bechtel SAIC Company) 2002. *Analysis of Geochemical Data for the Unsaturated Zone*. ANL-NBS-HS-000017 REV 00 ICN 02. Las Vegas, Nevada: Bechtel SAIC Company. ACC: MOL.20020314.0051.
- 158375 BSC (Bechtel SAIC Company) 2002. *Drift-Scale Coupled Processes (DST and THC Seepage) Models*. MDL-NBS-HS-000001 REV 01 ICN 02. Las Vegas, Nevada: Bechtel SAIC Company. ACC: MOL.20020312.0156.
- 160405 BSC (Bechtel SAIC Company) 2002. *Natural Analogue Synthesis Report*. TDR-NBS-GS-000027 REV 00 ICN 02. Las Vegas, Nevada: Bechtel SAIC Company. ACC: MOL.20020520.0288.
- 161067 BSC (Bechtel SAIC Company) 2002. *Requirements Document (RD) for iTOUGH2 V5.0-00*. DI: 10003-RD-5.0-0. Las Vegas, Nevada: Bechtel SAIC Company. ACC: MOL.20020923.0143.

- 160780 BSC (Bechtel SAIC Company) 2002. *Risk Information to Support Prioritization of Performance Assessment Models*. TDR-WIS-PA-000009 REV 01 ICN 01. Las Vegas, Nevada: Bechtel SAIC Company. ACC: MOL.20021017.0045.
- 160313 BSC (Bechtel SAIC Company) 2002. *Scientific Processes Guidelines Manual*. MIS-WIS-MD-000001 REV 01. Las Vegas, Nevada: Bechtel SAIC Company. ACC: MOL.20020923.0176.
- 160819 BSC (Bechtel SAIC Company) 2002. *Technical Work Plan for: Performance Assessment Unsaturated Zone*. TWP-NBS-HS-000003 REV 02. Las Vegas, Nevada: Bechtel SAIC Company. ACC: MOL.20030102.0108.
- 160146 BSC (Bechtel SAIC Company) 2002. *Total System Performance Assessment-License Application Methods and Approach*. TDR-WIS-PA-000006 REV 00. Las Vegas, Nevada: Bechtel SAIC Company. ACC: MOL.20020923.0175.
- 161066 BSC (Bechtel SAIC Company) 2002. *User's Manual (UM) for iTOUGH2 V5.0*. DI: 10003-UM-5.0-00. Las Vegas, Nevada: Bechtel SAIC Company. ACC: MOL.20020923.0147.
- 161530 BSC (Bechtel SAIC Company) 2003. *Drift-Scale Coupled Processes (DST and TH Seepage) Models*. MDL-NBS-HS-000015 REV 00. Las Vegas, Nevada: Bechtel SAIC Company. URN-1087.
- 150929 Campbell, G.S. and Norman, J.M. 1998. *An Introduction to Environmental Biophysics*. 2nd Edition. New York, New York: Springer-Verlag. TIC: 243951.
- 104368 Carrera, J. and Neuman, S.P. 1986. "Estimation of Aquifer Parameters Under Transient and Steady State Conditions: 1. Maximum Likelihood Method Incorporating Prior Information." *Water Resources Research*, 22, (2), 199-210. Washington, D.C.: American Geophysical Union. TIC: 245915.
- 141187 CRWMS M&O (Civilian Radioactive Waste Management System Management and Operating Contractor) 2000. *Conceptual and Numerical Models for UZ Flow and Transport*. MDL-NBS-HS-000005 REV 00. Las Vegas, Nevada: CRWMS M&O. ACC: MOL.19990721.0526.
- 153314 CRWMS M&O 2000. *Seepage Model for PA Including Drift Collapse*. MDL-NBS-HS-000002 REV 01. Las Vegas, Nevada: CRWMS M&O. ACC: MOL.20010221.0147.
- 154291 CRWMS M&O 2001. *Abstraction of Drift Seepage*. ANL-NBS-MD-000005 REV 01. Las Vegas, Nevada: CRWMS M&O. ACC: MOL.20010309.0019.
- 153045 CRWMS M&O 2001. *Seepage Calibration Model and Seepage Testing Data*. MDL-NBS-HS-000004 REV 01. Las Vegas, Nevada: CRWMS M&O. ACC: MOL.20010122.0093.

- 157916 Curry, P.M. and Loros, E.F. 2002. *Project Requirements Document*. TER-MGR-MD-000001 REV 00. Las Vegas, Nevada: Bechtel SAIC Company. ACC: MOL.20020806.0027.
- 100567 Deutsch, C.V. and Journel, A.G. 1992. *GSLIB Geostatistical Software Library and User's Guide*. New York, New York: Oxford University Press. TIC: 224174.
- 161320 Doughty, C.; Salve, R.; and Wang, J.S.Y. 2002. "Liquid-Release Tests in Unsaturated Fractured Welded Tuffs: II. Numerical Modeling." *Journal of Hydrology*, 256, ([1-2]), 80-105. [New York, New York]: Elsevier. TIC: 253773.
- 103783 Finsterle, S. 1998. *ITOUGH2 V3.2 Verification and Validation Report*. LBNL-42002. Berkeley, California: Lawrence Berkeley National Laboratory. ACC: MOL.19981008.0014.
- 104367 Finsterle, S. 1999. *ITOUGH2 User's Guide*. LBNL-40040. Berkeley, California: Lawrence Berkeley National Laboratory. TIC: 243018.
- 153448 Finsterle, S. 1999. UZ Drift Scale Model. Scientific Notebook YMP-LBNL-SAF-1. ACC: MOL.19990723.0301.
- 151875 Finsterle, S. 2000. "Using the Continuum Approach to Model Unsaturated Flow in Fractured Rock." *Water Resources Research*, 36, (8), 2055-2066. [Washington, D.C.]: American Geophysical Union. TIC: 248769.
- 161043 Finsterle, S. 2002. UZ Drift Scale Model (YMP-LBNL-SAF-2). Scientific Notebook SN-LBNL-SCI-171-V1. ACC: MOL.20021203.0495.
- 161148 Finsterle, S. and Trautz, R.C. 2001. "Numerical Modeling of Seepage into Underground Openings." *Mining Engineering*, [53], ([9]), 52-56. [Littleton, Colorado: Society for Mining, Metallurgy and Exploration]. TIC: 253738.
- 154365 Freeze, G.A.; Brodsky, N.S.; and Swift, P.N. 2001. *The Development of Information Catalogued in REV00 of the YMP FEP Database*. TDR-WIS-MD-000003 REV 00 ICN 01. Las Vegas, Nevada: Bechtel SAIC Company. ACC: MOL.20010301.0237.
- 161046 Hedegaard, R. 2002. Niche Excavation; Liquid Flow Testing; Borehole Drilling and Pneumatic Testing; Drift Seepage Testing. Scientific Notebook YMP-LBNL-RCT-RH-1. ACC: MOL.20020725.0450.
- 155955 Hinds, J. 2001. Unsaturated Zone Modeling & Synthesis. Scientific Notebook YMP-LBNL-YSW-JH-2. ACC: MOL.20010725.0216.
- 141521 Ho, C.K. 1997. "Evaporation of Pendant Water Droplets in Fractures." *Water Resources Research*, 33, (12), 2665-2671. Washington, D.C.: American Geophysical Union. TIC: 246969.

- 141523 Jackson, C.P.; Hoch, A.R.; and Todman, S. 2000. "Self-Consistency of a Heterogeneous Continuum Porous Medium Representation of a Fractured Medium." *Water Resources Research*, 36, (1), 189-202. Washington, D.C.: American Geophysical Union. TIC: 247466.
- 101700 LeCain, G.D. 1995. *Pneumatic Testing in 45-Degree-Inclined Boreholes in Ash-Flow Tuff Near Superior, Arizona*. Water-Resources Investigations Report 95-4073. Denver, Colorado: U.S. Geological Survey. ACC: MOL.19960715.0083.
- 160230 Liu, H.H.; Bodvarsson, G.S.; and Finsterle, S. 2002. "A Note on Unsaturated Flow in Two-Dimensional Fracture Networks." *Water Resources Research*, 38, (9), 15-1 to 15-9. [Washington, D.C.]: American Geophysical Union. TIC: 253307.
- 105729 Liu, H.H.; Doughty, C.; and Bodvarsson, G.S. 1998. "An Active Fracture Model for Unsaturated Flow and Transport in Fractured Rocks." *Water Resources Research*, 34, (10), 2633-2646. Washington, D.C.: American Geophysical Union. TIC: 243012.
- 151018 Marshall, B.D.; Neymark, L.A.; Paces, J.B.; Peterman, Z.E.; and Whelan, J.F. 2000. "Seepage Flux Conceptualized from Secondary Calcite in Lithophysal Cavities in the Topopah Spring Tuff, Yucca Mountain, Nevada." *SME Annual Meeting, February 28-March 1, 2000, Salt Lake City, Utah*. Preprint 00-12. [Littleton, Colorado]: Society for Mining, Metallurgy, and Exploration. TIC: 248608.
- 149850 Mongano, G.S.; Singleton, W.L.; Moyer, T.C.; Beason, S.C.; Eatman, G.L.W.; Albin, A.L.; and Lung, R.C. 1999. *Geology of the ECRB Cross Drift - Exploratory Studies Facility, Yucca Mountain Project, Yucca Mountain, Nevada*. [Deliverable SPG42GM3]. Denver, Colorado: U.S. Geological Survey. ACC: MOL.20000324.0614.
- 162418 NRC (U.S. Nuclear Regulatory Commission) 2003. *Yucca Mountain Review Plan, Information Only*. NUREG-1804, Draft Final Revision 2. Washington, D.C.: U.S. Nuclear Regulatory Commission, Office of Nuclear Material Safety and Safeguards. TIC: 254002.
- 144773 Or, D. and Ghezzehei, T.A. 2000. "Dripping into Subterranean Cavities from Unsaturated Fractures under Evaporative Conditions." *Water Resources Research*, 36, (2), 381-393. Washington, D.C.: American Geophysical Union. TIC: 246982.
- 152512 Oreskes, N.; Shrader-Frechette, K.; and Belitz, K. 1994. "Verification, Validation, and Confirmation of Numerical Models in the Earth Sciences." *Science*, 263, (5147), 641-646. Washington, D.C.: American Association for the Advancement of Science. TIC: 248958.
- 105743 Philip, J.R.; Knight, J.H.; and Waechter, R.T. 1989. "Unsaturated Seepage and Subterranean Holes: Conspectus, and Exclusion Problem for Circular Cylindrical Cavities." *Water Resources Research*, 25, (1), 16-28. Washington, D.C.: American Geophysical Union. TIC: 239117.

- 100684 Pruess, K. 1987. *TOUGH User's Guide*. NUREG/CR-4645. Washington, D.C.: U.S. Nuclear Regulatory Commission. TIC: 217275.
- 117112 Pruess, K.; Faybishenko, B.; and Bodvarsson, G.S. 1999. "Alternative Concepts and Approaches for Modeling Flow and Transport in Thick Unsaturated Zones of Fractured Rocks." *Journal of Contaminant Hydrology*, 38, (1-3), 281-322. New York, New York: Elsevier. TIC: 244160.
- 104252 Richards, L.A. 1931. "Capillary Conduction of Liquids Through Porous Mediums." *Physics*, 1, 318-333. [New York, New York: American Physical Society]. TIC: 225383.
- 158324 Rohsenow, W.M. and Choi, H.Y. 1961. *Heat, Mass, and Momentum Transfer*. Englewood Cliffs, New Jersey: Prentice-Hall. TIC: 249864.
- 161318 Salve, R.; Wang, J.S.Y.; and Doughty, C. 2002. "Liquid-Release Tests in Unsaturated Fractured Welded Tuffs: I. Field Investigations." *Journal of Hydrology*, 256, ([1-2]), 60-79. [New York, New York]: Elsevier. TIC: 253774.
- 139195 Tokunaga, T.K. and Wan, J. 1997. "Water Film Flow Along Fracture Surfaces of Porous Rock." *Water Resources Research*, 33, (6), 1287-1295. Washington, D.C.: American Geophysical Union. TIC: 242739.
- 161044 Trautz, R. 2001. UZ Drift Scale Model (YMP-LBNL-RCT-DSM-1). Scientific Notebook SN-LBNL-SCI-157-V1. ACC: MOL.19990723.0302; MOL.20010201.0423; MOL.20010724.0145.
- 156903 Trautz, R.C. 2001. Moisture Monitoring in the ESF (Phase 2)/Drift Seepage Test. Scientific Notebook YMP-LBNL-RCT-2. ACC: MOL.20011030.0706.
- 160335 Trautz, R.C. and Wang, J.S.Y. 2002. "Seepage into an Underground Opening Constructed in Unsaturated Fractured Rock Under Evaporative Conditions." *Water Resources Research*, 38, (10), 6-1 through 6-14. [Washington, D.C.]: American Geophysical Union. TIC: 253348.
- 100610 van Genuchten, M.T. 1980. "A Closed-Form Equation for Predicting the Hydraulic Conductivity of Unsaturated Soils." *Soil Science Society of America Journal*, 44, (5), 892-898. Madison, Wisconsin: Soil Science Society of America. TIC: 217327.
- 153449 Wang, J. 1999. Characterization of Yucca Mountain Percolation in the Unsaturated Zone - ESF Study. Scientific Notebook YMP-LBNL-JSW-6C. ACC: MOL.19991013.0462.
- 161456 Wang, J.S. 2003. "Scientific Notebooks Referenced in Model Report U0080, Seepage Calibration Model and Seepage Testing Data MDL-NBS-HS-000004 REV 02." Memorandum from J.S. Wang (BSC) to File, March 13, 2003, with attachments. ACC: MOL.20030320.0082.

- 104366 Wang, J.S.Y. and Elsworth, D. 1999. "Permeability Changes Induced by Excavation in Fractured Tuff." *Rock Mechanics for Industry, Proceedings of the 37th U.S. Rock Mechanics Symposium, Vail, Colorado, USA, 6-9 June 1999*. Amadei, B.; Kranz, R.L.; Scott, G.A.; and Smeallie, P.H., eds. 2, 751-757. Brookfield, Vermont: A.A. Balkema. TIC: 245246.
- 160442 Whelan, J.F.; Paces, J.B.; and Peterman, Z.E. 2002. "Physical and Stable-Isotope Evidence for Formation of Secondary Calcite and Silica in the Unsaturated Zone, Yucca Mountain, Nevada." *Applied Geochemistry*, 17, ([6]), 735-750. [New York, New York]: Elsevier. TIC: 253462.

Software Cited

- 147402 CRWMS M&O 1999. *Software Routine: ECRB-XYZ*. V.03. PC. 30093-V.03.
- 162369 Dynamic Graphics 2003. *EarthVision*. V4.0. SGI/IRIX 6.2. 10174-4.0-00.
- 139918 LBNL (Lawrence Berkeley National Laboratory) 09/16/1999. *Software Code: iTOUGH2*. V4.0. SUN, DEC. 10003-4.0-00.
- 152823 LBNL (Lawrence Berkeley National Laboratory) 10/17/2000. *Software Routine: AddBound*. V1.0. SUN w/Unix OS. 10357-1.0-00.
- 152814 LBNL (Lawrence Berkeley National Laboratory) 10/17/2000. *Software Routine: AddCoord*. V1.0. SUN w/Unix OS. 10355-1.0-00.
- 152816 LBNL (Lawrence Berkeley National Laboratory) 10/17/2000. *Software Routine: CutDrift*. V1.0. SUN w/Unix OS. 10375-1.0-00.
- 152815 LBNL (Lawrence Berkeley National Laboratory) 10/17/2000. *Software Routine: CutNiche*. V1.2. SUN w/Unix OS. 10356-1.2-00.
- 152824 LBNL (Lawrence Berkeley National Laboratory) 10/17/2000. *Software Routine: MoveMesh*. V1.0. SUN w/Unix OS. 10358-1.0-00.
- 152826 LBNL (Lawrence Berkeley National Laboratory) 10/17/2000. *Software Routine: Perm2Mesh*. V1.0. SUN w/Unix OS. 10359-1.0-00.
- 134141 LBNL (Lawrence Berkeley National Laboratory) 1999. *Software Code: EXT*. V1.0. Sun. 10047-1.0-00.
- 134139 LBNL (Lawrence Berkeley National Laboratory) 1999. *Software Code: GSLIB*. V1.0MGAMV2V1.201. Sun. 10087-1.0MGAMV2V1.201-00.
- 134136 LBNL (Lawrence Berkeley National Laboratory) 1999. *Software Code: GSLIB*. V1.0MSISIMV1.203. Sun, PC. 10001-1.0MSISIMV1.203-00.

- 153099 LBNL (Lawrence Berkeley National Laboratory) 2000. *Software Code: GSLIB*. V1.0GAMV3V1.201. SUN w/Unix OS. 10398-1.0GAMV3V1.201-00.
- 153100 LBNL (Lawrence Berkeley National Laboratory) 2000. *Software Code: GSLIB*. V1.0SISIMV1.204. SUN w/Unix OS. 10397-1.0SISIMV1.204-00.
- 152822 LBNL (Lawrence Berkeley National Laboratory) 2000. *Software Routine: AddBorehole*. V1.0. SUN w/Unix OS. 10373-1.0-00.
- 152828 LBNL (Lawrence Berkeley National Laboratory) 2000. *Software Routine: CutNiche*. V1.3. SUN w/Solaris OS. 10402-1.3-00.
- 160106 LBNL (Lawrence Berkeley National Laboratory) 2002. *Software Code: iTOUGH2*. V5.0. SUN UltraSparc., DEC ALPHA, LINUX. 10003-5.0-00.

9.2 CODES, STANDARDS, REGULATIONS, AND PROCEDURES

- 156605 10 CFR 63. Energy: Disposal of High-Level Radioactive Wastes in a Geologic Repository at Yucca Mountain, Nevada. Readily available.
- AP-2.22Q, Rev. 0, ICN 0. *Classification Criteria and Maintenance of the Monitored Geologic Repository Q-List*. Washington, D.C.: U.S. Department of Energy, Office of Civilian Radioactive Waste Management. ACC: MOL.20020314.0046.
- AP-SI.1Q, Rev. 4, Mod 0. *Software Management*. Washington, D.C.: U.S. Department of Energy, Office of Civilian Radioactive Waste Management. ACC: MOL.20030113.0149.
- AP-SIII.10Q, Rev. 1, ICN 0. *Models*. Washington, D.C.: U.S. Department of Energy, Office of Civilian Radioactive Waste Management. ACC: DOC.20030312.0039.

9.3 SOURCE DATA, LISTED BY DATA TRACKING NUMBER

- 153141 LB00090012213U.001. Air K Testing in Borehole SYBT-ERCB-LA#2 at CS 17+26 in Cross Drift. Submittal date: 11/03/2000.
- 153154 LB00090012213U.002. Liquid Release Tests from Borehole SYBT-ECRB-LA#2 at CS 17+26 in Cross Drift. Submittal date: 11/09/2000.
- 153144 LB0010NICH3LIQ.001. Niche 3107 Seepage Test. Submittal date: 11/02/2000.
- 153145 LB0010NICH4LIQ.001. Niche 4788 Seepage Test. Submittal date: 11/02/2000.

- 154292 LB0010SCMREV01.001. Input/Output for Seepage Calibration Modeling AMR U0080. Submittal date: 11/29/2000.
- 153155 LB0011AIRKTEST.001. Air Permeability Testing in Niches 3566 and 3650. Submittal date: 11/08/2000.
- 156904 LB0110AKN5POST.001. Niche 5 (1620 in ECRB) Post-Excavation Air-K. Submittal date: 11/12/2001.
- 156879 LB0110ECRB LIQR.002. Systematic Testing in ECRB-SYBT-LA#1, 2/28/2001. Submittal date: 11/12/2001.
- 160409 LB0110SYST0015.001. Developed Data for Systematic Testing. Submittal date: 12/06/2001.
- 158462 LB0203ECRB LIQR.001. Systematic Testing in ECRB-SYBT-LA#3 (May-July 2001). Submittal date: 03/20/2002.
- 159525 LB0205REVUZPRP.001. Fracture Properties for UZ Model Layers Developed from Field Data. Submittal date: 05/14/2002.
- 160408 LB0207NICH5LIQ.001. Niche 5 Seepage Tests (CD 1620). Submittal date: 07/09/2002.
- 160410 LB0207PRESCMN5.001. Pre-Test Prediction of Seepage into Niche 5: Modeling Input/Output Files. Submittal date: 07/26/2002.
- 161192 LB0207PRESCMN5.002. Pre-Test Prediction of Seepage into Niche 5: Data Summary. Submittal date: 07/26/2002.
- 160796 LB0209NICH5LIQ.001. Niche 5 Seepage Tests (CD 1620), June-August 2002. Submittal date: 09/11/2002.
- 160792 LB0211NICH5LIQ.001. Niche 5 Seepage Tests (CD 1620), August-October 2002. Submittal date: 11/14/2002.
- 161733 LB0301N5CEILNG.001. Niche 5 Field Measurements of the Niche Ceiling and Slot Geometry. Submittal date: 01/27/2003.
- 136583 LB980001233124.004. Liquid Release Test Data from Niche 3566 and Niche 3650 of the ESF in Milestone Report, "Drift Seepage Test and Niche Moisture Study: Phase 1 Report on Flux Threshold Determination, Air Permeability Distribution, and Water Potential Measurement. Submittal date: 11/23/1999.
- 105888 LB990601233124.001. Seepage Data Feed to UZ Drift-Scale Flow Model for TSPA-SR. Submittal date: 06/18/1999.

- 106785 LB990701233129.001. 3-D UZ Model Grids for Calculation of Flow Fields for PA for AMR U0000, "Development of Numerical Grids for UZ Flow and Transport Modeling". Submittal date: 09/24/1999.
- 122757 LB990801233129.003. TSPA Grid Flow Simulations for AMR U0050, "UZ Flow Models and Submodels" (Flow Field #3). Submittal date: 11/29/1999.
- 104055 LB997141233129.001. Calibrated Basecase Infiltration 1-D Parameter Set for the UZ Flow and Transport Model, FY99. Submittal date: 07/21/1999.
- 152625 MO0002GSC00064.000. Exploratory Studies Facilities (ESF) Niche #3 (Niche 3107) Borehole As-Built Information. Submittal date: 02/09/2000.
- 152623 MO0002GSC00076.000. Exploratory Studies Facility (ESF) Niche #2 (Niche 3650) Borehole As-Built Information. Submittal date: 02/15/2000.
- 152167 MO0003GSC00096.000. Exploratory Studies Facility (ESF) Niche #2 Profile Alignment. Submittal date: 03/01/2000.
- 152176 MO0003GSC00103.000. Exploratory Studies Facility (ESF) Niche 3 Profile Alignment. Submittal date: 03/03/2000.
- 152626 MO0008GSC00273.000. Exploratory Studies Facility (ESF) Niche 4, Profile Alignment. Submittal date: 08/01/2000.
- 152627 MO0008GSC00310.000. ESF Niche #4 (Niche 4788) Borehole As-Built Information. Submittal date: 08/28/2000.
- 155370 MO0009GSC00332.000. Exploratory Studies Facility (ESF) Niche 5, Plan and Profile As-Built. Submittal date: 09/27/2000.
- 155369 MO0107GSC01061.000. As-Built Profile of Bat-Wing Excavation, Niche #5 ECRB. Submittal date: 07/03/2001.
- 156941 MO0107GSC01069.000. ESF Niche #4 (Niche 4788) Borehole As-Built Information. Submittal date: 07/19/2001.
- 160407 MO0209GSC02116.000. Enhanced Characterization of the Repository Block (ECRB) Niche 5 (Niche 1620), Borehole As-Built Information. Submittal date: 09/23/2002.
- 161496 MO0301SEPFEPS1.000. LA FEP List. Submittal date: 01/21/2003.

9.4 OUTPUT DATA, LISTED BY DATA TRACKING NUMBER

LB0302SCMREV02.001. Seepage-Related Model Parameters K and $1/\alpha$: Supporting Files.
Submittal date: 02/28/2003.

LB0302SCMREV02.002. Seepage-Related Model Parameters K and $1/\alpha$: Data Summary.
Submittal date: 02/28/2003.

10. ATTACHMENTS

ATTACHMENT I-LIST OF COMPUTER FILES SUBMITTED WITH THIS MODEL REPORT UNDER DTN: LB0302SCMREV02.001

ATTACHMENT II-VARIOGRAM FITTING

ATTACHMENT III-MESH GENERATION FOR SIMULATION OF SEEPAGE TESTS IN ECRB

ATTACHMENT IV-MESH GENERATION FOR SIMULATION OF SEEPAGE TESTS IN NICHES 3107, 3650, AND 4788

ATTACHMENT V-MESH GENERATION FOR SEEPAGE TEST SIMULATIONS IN NICHE 1620

ATTACHMENT VI-PREPARATION OF SEEPAGE RATE AND RELATIVE-HUMIDITY DATA FOR THE SIMULATION OF LIQUID-RELEASE TESTS IN THE ECRB CROSS DRIFT

ATTACHMENT VII-EXECUTION OF MULTIPLE INVERSIONS OF DATA FROM ECRB

INTENTIONALLY LEFT BLANK

ATTACHMENT I

LIST OF COMPUTER FILES SUBMITTED WITH THIS MODEL REPORT UNDER DTN: LB0302SCMREV02.001

Computer files needed to reproduce the model results discussed in this Model Report are listed below and are submitted to the TDMS under DTN: LB0302SCMREV02.001. Reproducibility is given by referring to the pertinent scientific notebook pages as listed in Table 7 and throughout this Model Report. Each file name is complemented with a short description of its contents and/or purpose.

Table I-1 contains the files pertaining to the modeling of liquid-release tests conducted in Niche 1620; Table I-2 contains those for the modeling of test in the ECRB Cross Drift. The files used to analyze data from seepage experiments in Niches 3107, 3560, and 4788 (located in the middle nonlithophysal zone) have been previously submitted under DTN: LB0010SCMREV01.001 [154292].

Table I-1. File Name and Description for Modeling of Liquid-Release Tests in Niche 1620

File/Folder Name	Description/File Location
Meshgeneration/	
Meshgeneration/Permeability/	
measured_log-k_12_N5.dat	Measured air permeability data, input file mesh generation
N5-airK.dat	Measured air permeability data, input file to GAMV3
N5-airK.par	Parameter file, input to GAMV3
N5-airK.var	Computed variogram by GAMV3
N5-airK.xls	Excel file to compile variogram
Meshgeneration/Roughness/	
ceiling_N5_survey.dat	Compilation of the original survey and roughness measurements of the main niche
ceiling_N5_interpolated.dat	Interpolated data on a regular x-y coordinate (10 cm x 10 cm grid)
ceiling_N5_1.dat	Interpolated main niche ceiling for 15.60<y<17.60
ceiling_N5_2.dat	Interpolated main niche ceiling for 18.60<y<20.60
ceiling_N5_3.dat	Interpolated main niche ceiling for 20.90<y<22.90
leftbatwing_N5_survey.dat	Compilation of the original survey and roughness measurements of the left batwing niche
leftbatwing_N5_interpolated.dat	Interpolated data on a regular x-y coordinate (10 cm x 10 cm grid)
leftbatwing_N5_1.dat	Interpolated left batwing niche ceiling for 15.60<y<17.60
leftbatwing_N5_2.dat	Interpolated left batwing niche ceiling for 18.60<y<20.60
leftbatwing_N5_3.dat	Interpolated left batwing niche ceiling for 20.90<y<22.90
rightbatwing_N5_survey.dat	Compilation of the original survey and roughness measurements of the right batwing niche
rightbatwing_N5_interpolated.dat	Interpolated data on a regular x-y coordinate (10 cm x 10 cm grid)

rightbatwing_N5_1.dat	Interpolated right batwing niche ceiling for 15.60<y<17.60
rightbatwing_N5_2.dat	Interpolated right batwing niche ceiling for 18.60<y<20.60
rightbatwing_N5_3.dat	Interpolated right batwing niche ceiling for 20.90<y<22.90
Niche1620_ceiling.lpk	Tecplot file with the top view of the niche 5 ceiling
Niche1620_ceiling.wmf	Tecplot file with the top view of the niche 5 ceiling
Niche5SurveySummary.xls	Excel file to compile the survey data

Meshgeneration/N5BH4_10-11ft/

N5BH4_10-11ft	TOUGH2 input file with MESHMAKER block
onestep	TOUGH2 input file to perform a single time step
N5BH4_10-11ft_sisim.par	Parameter file for generation of random permeability field
sh.N5BH4_10-11ft_mesh	Sequence of instructions to execute multiple steps of mesh generations
sh.N5BH4_10-11ft_run	Sequence of instructions to run the above Sequence of instructions multiple times by changing the permeability field seed number
sh.onestep	Sequence of instructions to run one time step
N5BH4_10-11ft.mes1	Mesh with permeability realization #1
N5BH4_10-11ft.mes2	Mesh with permeability realization #2
N5BH4_10-11ft.mes3	Mesh with permeability realization #3
N5BH4_10-11ft.mes4	Mesh with permeability realization #4
N5BH4_10-11ft.mes5	Mesh with permeability realization #5
N5BH4_10-11ft.mes6	Mesh with permeability realization #6
N5BH4_10-11ft.mes7	Mesh with permeability realization #7
N5BH4_10-11ft.mes8	Mesh with permeability realization #8
N5BH4_10-11ft.mes9	Mesh with permeability realization #9
N5BH4_10-11ft.mes10	Mesh with permeability realization #10
N5BH4_10-11ft.mes11	Mesh with permeability realization #11
N5BH4_10-11ft.mes12	Mesh with permeability realization #12
N5BH4_10-11ft.mes13	Mesh with permeability realization #13
N5BH4_10-11ft.mes14	Mesh with permeability realization #14
N5BH4_10-11ft.mes15	Mesh with permeability realization #15
N5BH4_10-11ft.mes16	Mesh with permeability realization #16
N5BH4_10-11ft.mes17	Mesh with permeability realization #17
N5BH4_10-11ft.mes18	Mesh with permeability realization #18
N5BH4_10-11ft.mes19	Mesh with permeability realization #19
N5BH4_10-11ft.mes20	Mesh with permeability realization #20
N5BH4_10-11ft.mes21	Mesh with permeability realization #21
N5BH4_10-11ft.mes22	Mesh with permeability realization #22
N5BH4_10-11ft.mes23	Mesh with permeability realization #23
N5BH4_10-11ft.mes24	Mesh with permeability realization #24
N5BH4_10-11ft.mes25	Mesh with permeability realization #25
N5BH4_10-11ft.mes26	Mesh with permeability realization #26

N5BH4_10-11ft.mes27	Mesh with permeability realization #27
N5BH4_10-11ft.mes28	Mesh with permeability realization #28
N5BH4_10-11ft.mes29	Mesh with permeability realization #29
N5BH4_10-11ft.mes30	Mesh with permeability realization #30
ceiling_N5_1.dat	File is in folder: Meshgeneration/Roughness/
measured_log-k_12_N5.dat	File is in folder: Meshgeneration/Permeability/

Meshgeneration/N5BH5_21-22ft/

N5BH5_21-22ft	TOUGH2 input file
sh.N5BH5_21-22ft_mes	Sequence of instructions to execute multiple steps of mesh generations
N5BH5_21-22ft.mes	Mesh with permeability realization #
onestep	File is in folder: Meshgeneration/N5BH4_10-11ft/
sh.onestep	File is in folder: Meshgeneration/N5BH4_10-11ft/
ceiling_N5_2.dat	File is in folder: Meshgeneration/Roughness/
leftbatwing_N5_2.dat	File is in folder: Meshgeneration/Roughness/
rightbatwing_N5_2.dat	File is in folder: Meshgeneration/Roughness/

Meshgeneration/N5BH5_28-29ft/

N5BH5_28-29ft	TOUGH2 input file
N5BH5_28-29ft_sisim.par	Parameter file for generation of random permeability field
sh.N5BH5_28-29ft_mesh	Sequence of instructions to execute multiple steps of mesh generations
sh.N5BH5_28-29ft_run	Sequence of instructions to run the above sequence of instructions multiple times by changing the permeability field seed number
N5BH5_28-29ft.mes1	Mesh with permeability realization #1
N5BH5_28-29ft.mes2	Mesh with permeability realization #2
N5BH5_28-29ft.mes3	Mesh with permeability realization #3
N5BH5_28-29ft.mes4	Mesh with permeability realization #4
N5BH5_28-29ft.mes5	Mesh with permeability realization #5
N5BH5_28-29ft.mes6	Mesh with permeability realization #6
N5BH5_28-29ft.mes7	Mesh with permeability realization #7
N5BH5_28-29ft.mes8	Mesh with permeability realization #8
N5BH5_28-29ft.mes9	Mesh with permeability realization #9
N5BH5_28-29ft.mes10	Mesh with permeability realization #10
N5BH5_28-29ft.mes11	Mesh with permeability realization #11
N5BH5_28-29ft.mes12	Mesh with permeability realization #12
N5BH5_28-29ft.mes13	Mesh with permeability realization #13
N5BH5_28-29ft.mes14	Mesh with permeability realization #14
N5BH5_28-29ft.mes15	Mesh with permeability realization #15
N5BH5_28-29ft.mes16	Mesh with permeability realization #16
N5BH5_28-29ft.mes17	Mesh with permeability realization #17

N5BH5_28-29ft.mes18	Mesh with permeability realization #18
N5BH5_28-29ft.mes19	Mesh with permeability realization #19
N5BH5_28-29ft.mes20	Mesh with permeability realization #20
N5BH5_28-29ft.mes21	Mesh with permeability realization #21
N5BH5_28-29ft.mes22	Mesh with permeability realization #22
N5BH5_28-29ft.mes23	Mesh with permeability realization #23
N5BH5_28-29ft.mes24	Mesh with permeability realization #24
N5BH5_28-29ft.mes25	Mesh with permeability realization #25
N5BH5_28-29ft.mes26	Mesh with permeability realization #26
N5BH5_28-29ft.mes27	Mesh with permeability realization #27
N5BH5_28-29ft.mes28	Mesh with permeability realization #28
N5BH5_28-29ft.mes29	Mesh with permeability realization #29
N5BH5_28-29ft.mes30	Mesh with permeability realization #30
measured_log-k_12_N5.dat	File is in folder: Meshgeneration/Permeability/
ceiling_N5_3.dat	File is in folder: Meshgeneration/Roughness/
leftbatwing_N5_3.dat	File is in folder: Meshgeneration/Roughness/
rightbatwing_N5_3.dat	File is in folder: Meshgeneration/Roughness/
Onestep	File is in folder: Meshgeneration/N5BH4_10-11ft/
sh.onestep	File is in folder: Meshgeneration/N5BH4_10-11ft/

LiquidReleaseTestData/

LB0207NICH5LIQ5-01-RH-T.xls	Compilation of Relative humidity and temperature data from DTN: LB0207NICH5LIQ.001 [160408]
LB0207NICH5LIQ5-01.xls	Compilation of Liquid release test data from DTN: LB0207NICH5LIQ.001 [160408]
LB0207NICH5LIQ5-02.xls	Compilation of Liquid release test data from DTN: LB0207NICH5LIQ.001 [160408]
LB0209NICH5LIQ7-15.xls	Compilation of Liquid release test data from DTN: LB0209NICH5LIQ.001 [160796]
LB0209NICH5LIQ7-16.xls	Compilation of Liquid release test data from DTN: LB0209NICH5LIQ.001 [160796]
LB0211NICH5LIQ9-17#1.xls	Compilation of Liquid release test data from DTN: LB0211NICH5LIQ.001 [160792]
LB0211NICH5LIQ9-17#2.xls	Compilation of Liquid release test data from DTN: LB0211NICH5LIQ.001 [160792]
N5BH4_10-11ft_rate.dat	Seepage rate for Borehole #4 (10–11ft)
N5BH5_21-22ft_rate.dat	Seepage rate for Borehole #5 (21–22ft)
N5BH5_28-29ft_05-06-02_rate.dat	Seepage rate for Borehole #5 (28–29ft), for test started on 5/6/02
N5BH5_28-29ft_rate.dat	Seepage rate for Borehole #5 (28–29ft), for test started on 7/15/02

Calibration/

CalibrationSummary.xls	Excel file with compilation of the calibration results
------------------------	--

Calibration/N5B4_10-11ft/

sh.N5BH4_101-11ft_cal	Sequence of commands to start iTOUGH2 on a numbered
-----------------------	---

	node (Node 1 to Node 10)
sh.N5BH4_101-11ft_calm	Sequence of commands to start iTOUGH2 on the master node
N5BH4_10-11ft_SS	TOUGH2 input file for initial condition without evaporation
N5BH4_10-11ft_cal	TOUGH2 input file
N5BH4_10-11ft_cali	iTOUGH2 input file
N5BH4_10-11ft_call1i.out	iTOUGH2 output file, permeability realization #1
N5BH4_10-11ft_cal2i.out	iTOUGH2 output file, permeability realization #2
N5BH4_10-11ft_cal3i.out	iTOUGH2 output file, permeability realization #3
N5BH4_10-11ft_cal4i.out	iTOUGH2 output file, permeability realization #4
N5BH4_10-11ft_cal5i.out	iTOUGH2 output file, permeability realization #5
N5BH4_10-11ft_cal6i.out	iTOUGH2 output file, permeability realization #6
N5BH4_10-11ft_cal7i.out	iTOUGH2 output file, permeability realization #7
N5BH4_10-11ft_cal8i.out	iTOUGH2 output file, permeability realization #8
N5BH4_10-11ft_cal9i.out	iTOUGH2 output file, permeability realization #9
N5BH4_10-11ft_cal10i.out	iTOUGH2 output file, permeability realization #10
N5BH4_10-11ft_cal11i.out	iTOUGH2 output file, permeability realization #11
N5BH4_10-11ft_cal12i.out	iTOUGH2 output file, permeability realization #12
N5BH4_10-11ft_cal13i.out	iTOUGH2 output file, permeability realization #13
N5BH4_10-11ft_cal14i.out	iTOUGH2 output file, permeability realization #14
N5BH4_10-11ft_cal15i.out	iTOUGH2 output file, permeability realization #15
N5BH4_10-11ft_cal16i.out	iTOUGH2 output file, permeability realization #16
N5BH4_10-11ft_cal17i.out	iTOUGH2 output file, permeability realization #17
N5BH4_10-11ft_cal18i.out	iTOUGH2 output file, permeability realization #18
N5BH4_10-11ft_cal19i.out	iTOUGH2 output file, permeability realization #19
N5BH4_10-11ft_cal20i.out	iTOUGH2 output file, permeability realization #20
N5BH4_10-11ft_cal21i.out	iTOUGH2 output file, permeability realization #21
N5BH4_10-11ft_cal22i.out	iTOUGH2 output file, permeability realization #22
N5BH4_10-11ft_cal23i.out	iTOUGH2 output file, permeability realization #23
N5BH4_10-11ft_cal24i.out	iTOUGH2 output file, permeability realization #24
N5BH4_10-11ft_cal25i.out	iTOUGH2 output file, permeability realization #25
N5BH4_10-11ft_cal26i.out	iTOUGH2 output file, permeability realization #26
N5BH4_10-11ft_cal27i.out	iTOUGH2 output file, permeability realization #27
N5BH4_10-11ft_cal28i.out	iTOUGH2 output file, permeability realization #28
N5BH4_10-11ft_cal29i.out	iTOUGH2 output file, permeability realization #29
N5BH4_10-11ft_cal30i.out	iTOUGH2 output file, permeability realization #30
N5BH4_10-11ft_rate.dat	File is in folder: LiquidReleaseTestData/

Calibration/N5B5_28-29ft/

sh.N5BH5_28-29ft_cal	Sequence of commands start iTOUGH2 on a numbered node (Node 1 to Node 10)
sh.N5BH5_28-29ft_calm	Sequence of commands to start iTOUGH2 on the master node
N5BH5_28-29ft_ininevap	TOUGH2 input file for initial condition without evaporation

N5BH5_28-29ft_inievap	TOUGH2 input file for initial condition with evaporation
N5BH5_28-29ft_cal	TOUGH2 input file
N5BH5_28-29ft_cal_i	iTOUGH2 input file
N5BH5_28-29ft_cal11i.out	iTOUGH2 output file, permeability realization #1
N5BH5_28-29ft_cal13i.out	iTOUGH2 output file, permeability realization #2
N5BH5_28-29ft_cal14i.out	iTOUGH2 output file, permeability realization #3
N5BH5_28-29ft_cal16i.out	iTOUGH2 output file, permeability realization #4
N5BH5_28-29ft_cal17i.out	iTOUGH2 output file, permeability realization #5
N5BH5_28-29ft_cal18i.out	iTOUGH2 output file, permeability realization #6
N5BH5_28-29ft_cal19i.out	iTOUGH2 output file, permeability realization #7
N5BH5_28-29ft_cal111i.out	iTOUGH2 output file, permeability realization #8
N5BH5_28-29ft_cal112i.out	iTOUGH2 output file, permeability realization #9
N5BH5_28-29ft_cal113i.out	iTOUGH2 output file, permeability realization #10
N5BH5_28-29ft_cal114i.out	iTOUGH2 output file, permeability realization #11
N5BH5_28-29ft_cal115i.out	iTOUGH2 output file, permeability realization #12
N5BH5_28-29ft_cal116i.out	iTOUGH2 output file, permeability realization #13
N5BH5_28-29ft_cal118i.out	iTOUGH2 output file, permeability realization #14
N5BH5_28-29ft_cal119i.out	iTOUGH2 output file, permeability realization #15
N5BH5_28-29ft_cal120i.out	iTOUGH2 output file, permeability realization #16
N5BH5_28-29ft_cal121i.out	iTOUGH2 output file, permeability realization #17
N5BH5_28-29ft_cal123i.out	iTOUGH2 output file, permeability realization #18
N5BH5_28-29ft_cal124i.out	iTOUGH2 output file, permeability realization #19
N5BH5_28-29ft_cal125i.out	iTOUGH2 output file, permeability realization #20
N5BH5_28-29ft_cal126i.out	iTOUGH2 output file, permeability realization #21
N5BH5_28-29ft_cal127i.out	iTOUGH2 output file, permeability realization #22
N5BH5_28-29ft_cal128i.out	iTOUGH2 output file, permeability realization #23
N5BH5_28-29ft_cal129i.out	iTOUGH2 output file, permeability realization #24
N5BH5_28-29ft_mesX	Files are in folder: Meshgeneration/N5BH4_10-11ft/ where X is mesh number
N5BH5_28-29ft_rate.dat	File is in folder: LiquidReleaseTestData/

Validation/**Validation/N5BH4_1011ft/**

N5BH4_10-11ft_val	TOUGH2 input file
N5BH4_10-11ft_val_i	iTOUGH2 input file
N5BH4_10-11ft_val_i.out	iTOUGH2 output file
N5BH4_10-11ft_val_i.tec	iTOUGH2 output file for Tecplot
N5BH4_10-11ft_val_i.mc.tec	iTOUGH2 output file for Tecplot (Monte Carlo)
N5BH4_10-11ft_val.dat	Tecplot input file
N5BH4_10-11ft_val.lpk	Tecplot file (packaged data)
N5BH4_10-11ft_val.wmf	Image file
measured_log-k_12_N5.dat	File is in folder: Meshgeneration/Permeability/

N5BH4_10-11ft.mes1	File is in folder: Meshgeneration/N5BH4_10-11ft/
N5BH4_10-11ft_rate.dat	File is in folder: LiquidReleaseTestData/

Validation/N5BH5_21-22ft/

N5BH5_21-22ft_val	TOUGH2 input file
N5BH5_21-22ft_vali	iTOUGH2 input file
N5BH5_21-22ft_vali.out	iTOUGH2 output file
N5BH5_21-22ft_vali.tec	iTOUGH2 output file for Tecplot
N5BH5_21-22ft_vali_mc.tec	iTOUGH2 output file for Tecplot (Monte Carlo)
N5BH5_21-22ft_val.dat	Input file for Tecplot
N5BH5_21-22ft_val.lpk	Tecplot file (packaged data)
N5BH5_21-22ft_val.wmf	Image file
measured_log-k_12_N5.dat	File is in folder: Meshgeneration/Permeability/
N5BH5_21-22ft.mes	File is in folder: Meshgeneration/N5BH5_21-22ft/
N5BH5_21-22ft_rate.dat	File is in folder: LiquidReleaseTestData/

Validation/N5BH5_28-29ft_05-06-02/

N5BH5_28-29ft_05-06-02_val	TOUGH2 input file
N5BH5_28-29ft_05-06-02_vali	iTOUGH2 input file
N5BH5_28-29ft_05-06-02_vali.out	iTOUGH2 output file
N5BH5_28-29ft_05-06-02_vali.tec	iTOUGH2 output file for Tecplot
N5BH5_28-29ft_05-06-02_vali_mc.tec	iTOUGH2 output file for Tecplot (Monte Carlo)
N5BH5_28-29ft_05-06-02_val.dat	Input file for Tecplot
N5BH5_28-29ft_05-06-02_val.lpk	Tecplot file (packaged data)
N5BH5_28-29ft_05-06-02_val.wmf	Image file
measured_log-k_12_N5.dat	File is in folder: Meshgeneration/Permeability/
N5BH5_28-29ft.mes1	File is in folder: Meshgeneration/N5BH5_28-29ft/
N5BH5_28-29ft_05-06-02_rate.dat	File is in folder: LiquidReleaseTestData/

Validation/N5BH5_28-29ft_07-15-02/

N5BH5_28-29ft_07-15-02_val	TOUGH2 input file
N5BH5_28-29ft_07-15-02_vali	iTOUGH2 input file
N5BH5_28-29ft_07-15-02_vali.out	iTOUGH2 output file
N5BH5_28-29ft_07-15-02_vali.tec	iTOUGH2 output file for Tecplot
N5BH5_28-29ft_07-15-02_vali_mc.tec	iTOUGH2 output file for Tecplot (Monte Carlo)
N5BH5_28-29ft_07-15-02_val.dat	Input file for Tecplot
N5BH5_28-29ft_07-15-02_val.lpk	Tecplot file (packaged data)
N5BH5_28-29ft_07-15-02_val.wmf	Image file
measured_log-k_12_N5.dat	File is in folder: Meshgeneration/Permeability/
N5BH5_28-29ft.mes1	File is in folder: Meshgeneration/N5BH5_28-29ft/
N5BH5_28-29ft_rate.dat	File is in folder: LiquidReleaseTestData/

MassBalance/

N5BH4 10-11ft_forwardevap	TOUGH2 input file
N5BH4 10-11ft_forwardevapi	iTOUGH2 input file, with evaporation connections
N5BH4 10-11ft_forwardevapi.out	iTOUGH2 output file, with evaporation connections
N5BH4 10-11ft_forwardevapi.tec	Tecplot input file, with evaporation connections
N5BH4 10-11ft_forwardseep	TOUGH input file
N5BH4 10-11ft_forwardseepi	iTOUGH2 input file, with seepage and deep flow connections
N5BH4 10-11ft_forwardseepi.out	iTOUGH2 output file, with seepage and deep flow connections
N5BH4 10-11ft_forwardseepi.tec	iTOUGH2 output file for Tecplot, with seepage and deep flow connections
N5BH5 28-29ft.mes1	File is in folder: Meshgeneration/N5BH4_10-11ft/

FlowDiversion/

N5BH5 28-29ft_forwarddeep	TOUGH2 input file
N5BH5 28-29ft_forwarddeepi	iTOUGH2 input file, with seepage components connections
N5BH5 28-29ft_forwarddeepi.out	iTOUGH2 output file, with seepage components connections
N5BH5 28-29ft_forwarddeepi.tec	iTOUGH2 output file for Tecplot, with seepage components connections
N5BH5 28-29ft_forwardseep	TOUGH2 input file
N5BH5 28-29ft_forwardseepi	iTOUGH2 input file, with seepage connections
N5BH5 28-29ft_forwardseepi.out	iTOUGH2 output file, with seepage connections
N5BH5 28-29ft_forwardseepi.tec	iTOUGH2 output file for Tecplot, with seepage connections
N5BH5 28-29ft.mes1	File is in folder: Meshgeneration/N5BH5_28-29ft/

Evaporation/

Evaporation_Calibration.xls	Estimation of boundary-layer thickness (δ) for evaporation by vapor diffusion
-----------------------------	--

Table I-2. File Name and Description for Modeling of Liquid-Release Tests in ECRB Cross Drift

File/Folder Name	Description/File Location
ST/	
ST/Figures/ (files used for visualization purposes only)	
122.dat	For plot rate vs. time, LA#1, Zone 2, Set 2
122Sat.dat	For saturation and flux distribution plot, LA#1, Zone 2, Set 2
211.dat	For plot rate vs. time, LA#2, Zone 1, Set 1
221.dat	For plot rate vs. time, LA#2, Zone 2, Set 1
222.dat	For plot rate vs. time, LA#2, Zone 2, Set 2
222_0Sat.dat	For saturation distribution plot after 0 days, LA#2, Zone 2, Set 2
222_10Sat.dat	For saturation distribution plot after 10 days, LA#2, Zone 2, Set 2
222_20Sat.dat	For saturation distribution plot after 20 days, LA#2, Zone 2, Set 2
222_30Sat.dat	For saturation distribution plot after 30 days, LA#2, Zone 2, Set 2
231.dat	For plot rate vs. time, LA#2, Zone 3, Set 1
232.dat	For plot rate vs. time, LA#2, Zone 3, Set 2
311.dat	For plot rate vs. time, LA#3, Zone 1, Set 1
321.dat	For plot rate vs. time, LA#3, Zone 2, Set 1

ST/LA1/ (files used for simulation of liquid-release tests in borehole SYBT-ECRB-LA#1)

ST/LA1/Zone2

LA1_zone2.mes1	Mesh with permeability realization #1
LA1_zone2.mes2	Mesh with permeability realization #2
LA1_zone2.mes3	Mesh with permeability realization #3
LA1_zone2.mes4	Mesh with permeability realization #4
LA1_zone2.mes6	Mesh with permeability realization #6
LA1_zone2.mes10	Mesh with permeability realization #10
LA1_zone2.mes11	Mesh with permeability realization #11
LA1_zone2.mes12	Mesh with permeability realization #12
LA1_zone2.mes13	Mesh with permeability realization #13
LA1_zone2.mes14	Mesh with permeability realization #14
LA1_zone2.mes16	Mesh with permeability realization #16
LA1_zone2.mes17	Mesh with permeability realization #17
LA1_zone2.mes21	Mesh with permeability realization #21
LA1_zone2.mes23	Mesh with permeability realization #23
LA1_zone2.mes24	Mesh with permeability realization #24
LA1_zone2.mes25	Mesh with permeability realization #25
LA1_zone2.mes26	Mesh with permeability realization #26

ST/LA1/Zone2/Set2

Cum.xls	Excel file with processed seepage data from DTN: LB0110ECRBLIQR.002 [156879]
LA1_zone2_inievap	TOUGH2 input file to create initial conditions with dry-out zone
LA1_zone2_inioevap	TOUGH2 input file to create initial conditions without ventilation
LA1_zone2_set2.bc	Relative humidity boundary condition file
LA1_zone2_set2.dat	Seepage-rate data file for calibration
LA1_zone2_set2	TOUGH2 input for simulating liquid-release test
LA1_zone2_set2i	iTOUGH2 input for calibrating against seepage-rate data
LA1_zone2_set2i.out1	iTOUGH2 output file with permeability realization #1
LA1_zone2_set2i.out2	iTOUGH2 output file with permeability realization #2
LA1_zone2_set2i.out3	iTOUGH2 output file with permeability realization #3
LA1_zone2_set2i.out4	iTOUGH2 output file with permeability realization #4
LA1_zone2_set2i.out6	iTOUGH2 output file with permeability realization #6
LA1_zone2_set2i.out10	iTOUGH2 output file with permeability realization #10
LA1_zone2_set2i.out11	iTOUGH2 output file with permeability realization #11
LA1_zone2_set2i.out12	iTOUGH2 output file with permeability realization #12
LA1_zone2_set2i.out13	iTOUGH2 output file with permeability realization #13
LA1_zone2_set2i.out14	iTOUGH2 output file with permeability realization #14
LA1_zone2_set2i.out16	iTOUGH2 output file with permeability realization #16
LA1_zone2_set2i.out17	iTOUGH2 output file with permeability realization #17
LA1_zone2_set2i.out21	iTOUGH2 output file with permeability realization #21
LA1_zone2_set2i.out23	iTOUGH2 output file with permeability realization #23
LA1_zone2_set2i.out24	iTOUGH2 output file with permeability realization #24
LA1_zone2_set2i.out25	iTOUGH2 output file with permeability realization #25
LA1_zone2_set2i.out26	iTOUGH2 output file with permeability realization #26
RH.xls	Excel file with processed relative-humidity data from DTN: LB0110ECRBLIQR.002 [156879]
inievapi	Dummy iTOUGH2 input file for generating initial conditions with evaporation

ST/LA2/ (files used for simulation of liquid-release tests in borehole SYBT-ECRB-LA#2)

ST/LA2/Zone1

ST/LA2/Zone1/Set1

Cum.xls	Excel file with processed seepage data from DTN: LB00090012213U.002 [153154]
LA2_zone1_set1.dat	Seepage-rate data file for validation
LA2_zone1_set1_val	TOUGH2 input file for simulating liquid-release test
LA2_zone1_set1_vali	iTOUGH2 input file for performing Monte Carlo simulations
LA2_zone1_set1_vali.out	iTOUGH2 output file
LA2_zone1_val.mes	Mesh file used for validation runs

ST/LA2/Zone2

LA2_zone2.mes1	Mesh with permeability realization #1
----------------	---------------------------------------

LA2_zone2.mes2	Mesh with permeability realization #2
LA2_zone2.mes3	Mesh with permeability realization #3
LA2_zone2.mes4	Mesh with permeability realization #4
LA2_zone2.mes5	Mesh with permeability realization #5
LA2_zone2.mes6	Mesh with permeability realization #6
LA2_zone2.mes8	Mesh with permeability realization #8
LA2_zone2.mes9	Mesh with permeability realization #9
LA2_zone2.mes10	Mesh with permeability realization #10
LA2_zone2.mes11	Mesh with permeability realization #11
LA2_zone2.mes12	Mesh with permeability realization #12
LA2_zone2.mes13	Mesh with permeability realization #13
LA2_zone2.mes14	Mesh with permeability realization #14
LA2_zone2.mes16	Mesh with permeability realization #16
LA2_zone2.mes17	Mesh with permeability realization #17
LA2_zone2.mes18	Mesh with permeability realization #18
LA2_zone2.mes21	Mesh with permeability realization #21
LA2_zone2.mes22	Mesh with permeability realization #22
LA2_zone2.mes24	Mesh with permeability realization #24
LA2_zone2.mes25	Mesh with permeability realization #25
LA2_zone2.mes26	Mesh with permeability realization #26
LA2_zone2.mes98	Mesh, boundary-layer thickness 0.5 cm
LA2_zone2.mes99	Mesh, boundary-layer thickness 2.0 cm
LA2_zone2.mes200	Mesh, extended mesh

ST/LA2/Zone2/Set1

(seepage data from DTN: LB00090012213U.002 [153154])

LA2_zone2_set1.bc	Relative humidity boundary condition file
LA2_zone2_set1.dat	Seepage-rate data file
LA2_zone2_set1_val	TOUGH2 input file for simulating liquid-release test
LA2_zone2_set1_vali	iTOUGH2 input file for performing Monte Carlo simulations
LA2_zone2_set1_vali.out	iTOUGH2 output file
LA2_zone2_val.mes	Mesh file used for validation runs

ST/LA2/Zone2/Set2

(seepage data from DTN: LB0110SYST0015.001 [160409])

LA2_zone2_inievap	TOUGH2 input file to create initial conditions with dry-out zone
LA2_zone2_ininoevap	TOUGH2 input file to create initial conditions without ventilation
LA2_zone2_set2.bc	Relative humidity boundary condition file
LA2_zone2_set2.dat	Seepage-rate data file for calibration
LA2_zone2_set2	TOUGH2 input for simulating liquid-release test
LA2_zone2_set2_rates_RH.pm	Processed seepage and relative humidity data from DTN: LB0110SYST0015.001 [160409]
LA2_zone2_set2i	iTOUGH2 input for calibrating against seepage-rate data
LA2_zone2_set2i.out1	iTOUGH2 output file with permeability realization #1

LA2_zone2_set2i.out2	iTOUGH2 output file with permeability realization #2
LA2_zone2_set2i.out3	iTOUGH2 output file with permeability realization #3
LA2_zone2_set2i.out4	iTOUGH2 output file with permeability realization #4
LA2_zone2_set2i.out5	iTOUGH2 output file with permeability realization #5
LA2_zone2_set2i.out6	iTOUGH2 output file with permeability realization #6
LA2_zone2_set2i.out8	iTOUGH2 output file with permeability realization #8
LA2_zone2_set2i.out9	iTOUGH2 output file with permeability realization #9
LA2_zone2_set2i.out10	iTOUGH2 output file with permeability realization #10
LA2_zone2_set2i.out11	iTOUGH2 output file with permeability realization #11
LA2_zone2_set2i.out12	iTOUGH2 output file with permeability realization #12
LA2_zone2_set2i.out13	iTOUGH2 output file with permeability realization #13
LA2_zone2_set2i.out14	iTOUGH2 output file with permeability realization #14
LA2_zone2_set2i.out16	iTOUGH2 output file with permeability realization #16
LA2_zone2_set2i.out17	iTOUGH2 output file with permeability realization #17
LA2_zone2_set2i.out18	iTOUGH2 output file with permeability realization #18
LA2_zone2_set2i.out21	iTOUGH2 output file with permeability realization #21
LA2_zone2_set2i.out22	iTOUGH2 output file with permeability realization #22
LA2_zone2_set2i.out24	iTOUGH2 output file with permeability realization #24
LA2_zone2_set2i.out25	iTOUGH2 output file with permeability realization #25
LA2_zone2_set2i.out26	iTOUGH2 output file with permeability realization #26
LA2_zone2_set2i.out98	iTOUGH2 output file, boundary-layer thickness 0.5 cm
LA2_zone2_set2i.out99	iTOUGH2 output file, boundary-layer thickness 2.0 cm

ST/LA2/Zone2/Set2half (sensitivity to reduction in seepage rate)

LA2_zone2_inievp	TOUGH2 input file to create initial conditions with dry-out zone
LA2_zone2_ininoevap	TOUGH2 input file to create initial conditions without ventilation
LA2_zone2_set2.dat	Seepage-rate data file for calibration
LA2_zone2_set2half.bc	Relative humidity boundary condition file
LA2_zone2_set2half	TOUGH2 input for simulating liquid-release test
LA2_zone2_set2halfi	iTOUGH2 input for calibrating against seepage-rate data
LA2_zone2_set2halfi.out17	iTOUGH2 output for calibrating against seepage-rate data

ST/LA2/Zone2/Set2large (sensitivity to extent of model domain)

LA2_zone2_inievp	TOUGH2 input file to create initial conditions with dry-out zone
LA2_zone2_ininoevap	TOUGH2 input file to create initial conditions without ventilation
LA2_zone2_set2.dat	Seepage-rate data file for calibration
LA2_zone2_set2large.bc	Relative humidity boundary condition file
LA2_zone2_set2large_forward	TOUGH2 input for simulating liquid-release test
LA2_zone2_set2large_forwardi	iTOUGH2 input for calibrating against seepage-rate data
LA2_zone2_set2large_forwardi.out	iTOUGH2 output for calibrating against seepage-rate data

ST/LA2/Zone2/Set2lessevap (sensitivity to evaporative surface area)

LA2_zone2_inievap	TOUGH2 input file to create initial conditions with dry-out zone
LA2_zone2_ininoevap	TOUGH2 input file to create initial conditions without ventilation
LA2_zone2_set2.dat	Seepage-rate data file for calibration
LA2_zone2_set2lessevap.bc	Relative humidity boundary condition file
LA2_zone2_set2lessevap	TOUGH2 input for simulating liquid-release test
LA2_zone2_set2lessevapi	iTOUGH2 input for calibrating against seepage-rate data
LA2_zone2_set2lessevapi.out	iTOUGH2 output for calibrating against seepage-rate data

ST/LA2/Zone2/Set2noevap (sensitivity to evaporation)

LA2_zone2_inievap	Dummy TOUGH2 input file to create initial conditions
LA2_zone2_ininoevap	TOUGH2 input file to create initial conditions without ventilation
LA2_zone2_set2.dat	Seepage-rate data file for calibration
LA2_zone2_set2noevap.bc	Relative humidity boundary condition file
LA2_zone2_set2noevap	TOUGH2 input for simulating liquid-release test
LA2_zone2_set2noevapi	iTOUGH2 input for calibrating against seepage-rate data
LA2_zone2_set2noevapi.out	iTOUGH2 output for calibrating against seepage-rate data

ST/LA2/Zone2/Set2sens (sensitivity to input parameters)

LA2_zone2_inievap	TOUGH2 input file to create initial conditions with dry-out zone
LA2_zone2_ininoevap	TOUGH2 input file to create initial conditions without ventilation
LA2_zone2_set2.dat	Seepage-rate data file for calibration
LA2_zone2_set2sens.bc	Relative humidity boundary condition file
LA2_zone2_set2sens_forward	TOUGH2 input for simulating liquid-release test
LA2_zone2_set2sens_forwardi	iTOUGH2 input for performing sensitivity analysis
LA2_zone2_set2sens_forwardi.out	iTOUGH2 output for sensitivity analysis

ST/LA2/Zone3

LA2_zone3.mes1	Mesh with permeability realization #1
LA2_zone3.mes2	Mesh with permeability realization #2
LA2_zone3.mes3	Mesh with permeability realization #3
LA2_zone3.mes4	Mesh with permeability realization #4
LA2_zone3.mes5	Mesh with permeability realization #5
LA2_zone3.mes6	Mesh with permeability realization #6
LA2_zone3.mes9	Mesh with permeability realization #9
LA2_zone3.mes10	Mesh with permeability realization #10
LA2_zone3.mes11	Mesh with permeability realization #11
LA2_zone3.mes12	Mesh with permeability realization #12
LA2_zone3.mes13	Mesh with permeability realization #13
LA2_zone3.mes14	Mesh with permeability realization #14
LA2_zone3.mes15	Mesh with permeability realization #15

LA2_zone3.mes16	Mesh with permeability realization #16
LA2_zone3.mes18	Mesh with permeability realization #18
LA2_zone3.mes19	Mesh with permeability realization #19
LA2_zone3.mes20	Mesh with permeability realization #20
LA2_zone3.mes21	Mesh with permeability realization #21
LA2_zone3.mes22	Mesh with permeability realization #22

ST/LA2/Zone3/Set1

(seepage data from DTN: LB00090012213U.002 [153154])

LA2_zone3_set1.dat	Seepage-rate data file
LA2_zone3_set1_val	TOUGH2 input file for simulating liquid-release test
LA2_zone3_set1_vali	iTOUGH2 input file for performing Monte Carlo simulations
LA2_zone3_set1_vali.out	iTOUGH2 output file
LA2_zone3_val.mes	Mesh file used for validation runs

ST/LA2/Zone3/Set2

(seepage data from DTN: LB0110SYST0015.001 [160409])

LA2_zone3_inievap	TOUGH2 input file to create initial conditions with dry-out zone
LA2_zone3_ininoevap	TOUGH2 input file to create initial conditions without ventilation
LA2_zone3_set2.bc	Relative humidity boundary condition file
LA2_zone3_set2.dat	Seepage-rate data file for calibration
LA2_zone3_set2	TOUGH2 input for simulating liquid-release test
LA2_zone3_set2i	iTOUGH2 input for calibrating against seepage-rate data
LA2_zone3_set2i.out1	iTOUGH2 output file with permeability realization #1
LA2_zone3_set2i.out2	iTOUGH2 output file with permeability realization #2
LA2_zone3_set2i.out3	iTOUGH2 output file with permeability realization #3
LA2_zone3_set2i.out4	iTOUGH2 output file with permeability realization #4
LA2_zone3_set2i.out5	iTOUGH2 output file with permeability realization #5
LA2_zone3_set2i.out6	iTOUGH2 output file with permeability realization #6
LA2_zone3_set2i.out9	iTOUGH2 output file with permeability realization #9
LA2_zone3_set2i.out10	iTOUGH2 output file with permeability realization #10
LA2_zone3_set2i.out11	iTOUGH2 output file with permeability realization #11
LA2_zone3_set2i.out12	iTOUGH2 output file with permeability realization #12
LA2_zone3_set2i.out13	iTOUGH2 output file with permeability realization #13
LA2_zone3_set2i.out14	iTOUGH2 output file with permeability realization #14
LA2_zone3_set2i.out15	iTOUGH2 output file with permeability realization #15
LA2_zone3_set2i.out16	iTOUGH2 output file with permeability realization #16
LA2_zone3_set2i.out18	iTOUGH2 output file with permeability realization #18
LA2_zone3_set2i.out19	iTOUGH2 output file with permeability realization #19
LA2_zone3_set2i.out20	iTOUGH2 output file with permeability realization #20
LA2_zone3_set2i.out21	iTOUGH2 output file with permeability realization #21
LA2_zone3_set2i.out22	iTOUGH2 output file with permeability realization #22

ST/LA3/

(files used for simulation of liquid-release tests in borehole SYBT-ECRB-LA#3)

ST/LA3/Zone1

LA3_zone1.mes1	Mesh with permeability realization #1
LA3_zone1.mes2	Mesh with permeability realization #2
LA3_zone1.mes3	Mesh with permeability realization #3
LA3_zone1.mes4	Mesh with permeability realization #4
LA3_zone1.mes5	Mesh with permeability realization #5
LA3_zone1.mes6	Mesh with permeability realization #6
LA3_zone1.mes7	Mesh with permeability realization #7
LA3_zone1.mes8	Mesh with permeability realization #8
LA3_zone1.mes9	Mesh with permeability realization #9
LA3_zone1.mes10	Mesh with permeability realization #10
LA3_zone1.mes11	Mesh with permeability realization #11
LA3_zone1.mes12	Mesh with permeability realization #12
LA3_zone1.mes13	Mesh with permeability realization #13
LA3_zone1.mes14	Mesh with permeability realization #14
LA3_zone1.mes15	Mesh with permeability realization #15
LA3_zone1.mes16	Mesh with permeability realization #16
LA3_zone1.mes17	Mesh with permeability realization #17
LA3_zone1.mes18	Mesh with permeability realization #18
LA3_zone1.mes19	Mesh with permeability realization #19
LA3_zone1.mes20	Mesh with permeability realization #20
LA3_zone1.mes21	Mesh with permeability realization #21
LA3_zone1.mes22	Mesh with permeability realization #22
LA3_zone1.mes23	Mesh with permeability realization #23
LA3_zone1.mes24	Mesh with permeability realization #24
LA3_zone1.mes25	Mesh with permeability realization #25

ST/LA3/Zone1/Set1

Cum.xls	Excel file with processed seepage data from DTN: LB0203ECRBLIQR.001 [158462]
LA3_zone1_inievap	TOUGH2 input file to create initial conditions with dry-out zone
LA3_zone1_ininoevap	TOUGH2 input file to create initial conditions without ventilation
LA3_zone1_set1.bc	Relative humidity boundary condition file
LA3_zone1_set1.dat	Seepage-rate data file for calibration
LA3_zone1_set1	TOUGH2 input for simulating liquid-release test
LA3_zone1_set1i	iTOUGH2 input for calibrating against seepage-rate data
LA3_zone1_set1i.out1	iTOUGH2 output file with permeability realization #1
LA3_zone1_set1i.out2	iTOUGH2 output file with permeability realization #2
LA3_zone1_set1i.out3	iTOUGH2 output file with permeability realization #3
LA3_zone1_set1i.out4	iTOUGH2 output file with permeability realization #4
LA3_zone1_set1i.out5	iTOUGH2 output file with permeability realization #5

LA3_zone1_set1i.out6	iTOUGH2 output file with permeability realization #6
LA3_zone1_set1i.out7	iTOUGH2 output file with permeability realization #7
LA3_zone1_set1i.out8	iTOUGH2 output file with permeability realization #8
LA3_zone1_set1i.out9	iTOUGH2 output file with permeability realization #9
LA3_zone1_set1i.out10	iTOUGH2 output file with permeability realization #10
LA3_zone1_set1i.out11	iTOUGH2 output file with permeability realization #11
LA3_zone1_set1i.out12	iTOUGH2 output file with permeability realization #12
LA3_zone1_set1i.out13	iTOUGH2 output file with permeability realization #13
LA3_zone1_set1i.out14	iTOUGH2 output file with permeability realization #14
LA3_zone1_set1i.out15	iTOUGH2 output file with permeability realization #15
LA3_zone1_set1i.out16	iTOUGH2 output file with permeability realization #16
LA3_zone1_set1i.out17	iTOUGH2 output file with permeability realization #17
LA3_zone1_set1i.out18	iTOUGH2 output file with permeability realization #19
LA3_zone1_set1i.out20	iTOUGH2 output file with permeability realization #20
LA3_zone1_set1i.out22	iTOUGH2 output file with permeability realization #22
LA3_zone1_set1i.out23	iTOUGH2 output file with permeability realization #23
LA3_zone1_set1i.out24	iTOUGH2 output file with permeability realization #24
LA3_zone1_set1i.out25	iTOUGH2 output file with permeability realization #25

ST/LA3/Zone2**ST/LA3/Zone2/Set1**

Cum.xls	Excel file with processed seepage data from DTN: LB0203ECRBLIQR.001 [158462]
LA3_zone2_set1.dat	Seepage-rate data file
LA3_zone2_set1_val	TOUGH2 input file for simulating liquid-release test
LA3_zone2_set1_vali	iTOUGH2 input file for performing Monte Carlo simulations
LA3_zone2_set1_vali.out	iTOUGH2 output file
LA3_zone2_val.mes	Mesh file used for validation runs

ST/Meshgeneration/

(files used for mesh generation)

mesh3dblock	TOUGH2 input file with MESHMAKER block
mesh3dlargeblock	TOUGH2 input file with MESHMAKER block, extended model
onestep	TOUGH2 input file to perform single time step
perm.par	SISIM input file for generating heterogeneous log-permeability modifier field
primary.mes	Primary mesh file
primarylarge.mes	Primary mesh file, extended model domain
sh.LA1_zone2_mesh	Sequence of commands used to generate meshes for tests in zone 2 of borehole SYBT-ECRB-LA#1
sh.LA2_zone1_mesh	Sequence of commands used to generate meshes for tests in zone 1 of borehole SYBT-ECRB-LA#2
sh.LA2_zone2_largemesh	Sequence of commands used to generate extended mesh for tests in zone 2 of borehole SYBT-ECRB-LA#2
sh.LA2_zone2_mesh	Sequence of commands used to generate meshes for tests in

	zone 2 of borehole SYBT-ECRB-LA#2
sh.LA2_zone3_mesh	Sequence of commands used to generate meshes for tests in zone 3 of borehole SYBT-ECRB-LA#2
sh.LA3_zone1_mesh	Sequence of commands used to generate meshes for tests in zone 1 of borehole SYBT-ECRB-LA#3
sh.LA3_zone2_mesh	Sequence of commands used to generate meshes for tests in zone 2 of borehole SYBT-ECRB-LA#3
sh.onestep	Sequence of commands used to run iTOUGH2 simulation with a single time step

results.xls	Excel file with compilation of inverse modeling results
sh.run	Sequence of commands used to perform multiple inversions with multiple realizations of underlying permeability field
sh.run_forward	Sequence of commands used to perform a single forward run
sh.run_val	Sequence of commands used to perform validation runs

INTENTIONALLY LEFT BLANK

ATTACHMENT II

VARIOGRAM FITTING

Section 6.6.2.1 discusses the fitting of a spherical variogram model to the empirical variogram data obtained from the geostatistical analysis of air-permeability data. The purpose of the fitting is to determine the nugget effect, sill value, and correlation length of the log-permeability field. Weighted least-squares fitting was performed using standard functions of the exempt software EXCEL (97 SR-2). The following narrative explains the fitting process for clarification, using worksheet *N3107_airk_SD* of file *Vario.xls* as an example.

1. The result of the variogram calculation using GAMV3 V1.201 (LBNL 2000 [153099]) (see file *N3107_airk.var*, submitted with this Model Report under Output-DTN: LB0302SCMREV02.001) was loaded into the worksheet. Each data line in file *N3107_airk.var* is labeled. Lines 3 through 31 contain the empirical variogram information; Lines 1, 2, and 32 through 52 contain unrelated information and are removed. The relevant information is now contained in Rows 7 through 35 of the worksheet *N3107_airk_SD* of spreadsheet *Vario.xls* (in the remainder of this attachment, all references to a column are restricted to Rows 7 through 35).
2. Performing a weighted least-square fit consists of minimizing the following objective function S :

$$S = \sum_{i=1}^m \frac{(\gamma_i - \gamma^*_i)^2}{w_i^2}, \quad (\text{II-1})$$

where γ_i is the value calculated with the spherical variogram model at lag distance h_i , γ^*_i is the corresponding empirical variogram value, and w_i is a coefficient for weighting the data. The spherical variogram with a nugget effect is given by (after Deutsch and Journel 1992 [100567], p. 23, Eq. II-2):

$$\begin{aligned} \gamma(h; n, a, c) &= n + c \left[1.5 \frac{h}{a} - 0.5 \left(\frac{h}{a} \right)^3 \right] && \text{if } h < a \\ &= n + c && \text{if } h \geq a \end{aligned} \quad (\text{II-2})$$

Here, h is the lag distance (stored in Column C), n is the nugget effect (stored in Cell J2), a is the correlation length (stored in Cell J3), and c is the sill value (stored in Cell J4). The coefficient w in Equation (II-1) is taken to be the inverse of the number of data pairs supporting the empirical variogram value (stored in Column E; the inverse is stored in a newly inserted Column F).

3. Column J contains Equation (II-2), Column K holds the squared weighted differences (see Equation (II-1)), and Cell K6 holds the objective function S .
4. The objective function of Cell K6 is minimized by updating the three parameters stored in Cells J2, J3, and J4 using the EXCEL Solver Add-in (to be loaded by clicking on “Tools |

Add-ins... | Solver Add-in”). Click on “Tools | Solver...,” set “Set Target Cell” to \$K\$6, “Equal to” to “Min”, “By Changing Cells” to \$J\$2:\$J\$4, and “Subject to the Constraints” to \$J\$2>=0, \$J\$3>=0, and \$J\$4>=0. Looking at the empirical variogram, provide reasonable initial guesses for the three parameters (e.g., $n=0.1$, $a=1.0$, $c=0.5$) and click on “Solve” to get the best-fit parameters, which are displayed in Cells J2 through J4.

The appropriateness of the fitting procedure was checked as follows:

1. The spreadsheet was developed by Rick Ahlers. Stefan Finsterle has verified that Equations (II-1) and (II-2) were correctly coded into the appropriate cells.
2. The calculated variogram value (shown in Column H) was spot-checked.
3. Figure 12 shows that the variogram model fits the data in a least-square sense.

The EXCEL spreadsheet *Vario.xls* has been submitted as part of the previous revision (CRWMS M&O 2001 [153045]) under DTN: LB0010SCMREV01.001 [154292]; therefore, the input, equations used (click on the appropriate cells), and output is available, traceable, and reproducible by an appropriately qualified individual. The spreadsheet is reproduced in Table II-1.

Table II-1. EXCEL Spreadsheet *Vario.xls* for Fitting Spherical Variogram to Empirical Log-Permeability Variogram

A	B	C	D	E	F	G	H	I	J	K
2								nugget	0.005957	
3							correlation length		0.608829	
4								sill	0.487922	
5										K6=objective func.
6		Lag [m]	Gamma	# of pairs	1/(# of pairs)	log(k_head)	Log(k_tail)		Spherical	3173.542618
7	3	0.305	0.34193	138	0.00725	-12.21159	-12.21159		0.34193	6.78058E-12
8	4	0.609	0.51454	132	0.00758	-12.23576	-12.23576		0.493878	7.430211773
9	5	0.928	0.48461	282	0.00355	-12.24096	-12.24096		0.493878	6.815955381
10	6	1.226	0.43619	454	0.0022	-12.19152	-12.19152		0.493878	687.5866471
11	7	1.512	0.48658	332	0.00301	-12.20027	-12.20027		0.493878	5.878806928
12	8	1.817	0.4684	320	0.00313	-12.201	-12.201		0.493878	66.25919213
13	9	2.145	0.48656	564	0.00177	-12.23769	-12.23769		0.493878	17.09435459
14	10	2.45	0.50127	386	0.00259	-12.23959	-12.23959		0.493878	8.145356588
15	11	2.733	0.55705	318	0.00314	-12.2467	-12.2467		0.493878	404.751331
16	12	3.033	0.47056	318	0.00314	-12.22242	-12.22242		0.493878	55.14775388
17	13	3.342	0.46302	298	0.00336	-12.23587	-12.23587		0.493878	84.34520866
18	14	3.653	0.49027	266	0.00376	-12.20598	-12.20598		0.493878	0.920845218
19	15	3.963	0.5031	244	0.0041	-12.22635	-12.22635		0.493878	5.059074452
20	16	4.265	0.54863	214	0.00467	-12.24701	-12.24701		0.493878	137.4561849
21	17	4.576	0.53108	216	0.00463	-12.22051	-12.22051		0.493878	64.56062946
22	18	4.89	0.62485	178	0.00562	-12.18056	-12.18056		0.493878	543.1046002
23	19	5.198	0.59026	168	0.00595	-12.14107	-12.14107		0.493878	262.3957768
24	20	5.507	0.55459	136	0.00735	-12.15426	-12.15426		0.493878	68.22957436
25	21	5.806	0.6776	124	0.00806	-12.16726	-12.16726		0.493878	519.5790967
26	22	6.114	0.56408	116	0.00862	-12.20509	-12.20509		0.493878	66.32586675
27	23	6.433	0.39963	94	0.01064	-12.21426	-12.21426		0.493878	78.46250161
28	24	6.745	0.49685	74	0.01351	-12.30514	-12.30514		0.493878	0.048389527
29	25	7.041	0.42472	58	0.01724	-12.29034	-12.29034		0.493878	16.09206783
30	26	7.34	0.55424	44	0.02273	-12.30341	-12.30341		0.493878	7.052232487
31	27	7.638	0.66126	32	0.03125	-12.33875	-12.33875		0.493878	28.68909386
32	28	7.938	0.48026	20	0.05	-12.1745	-12.1745		0.493878	0.074181294
33	29	8.233	0.86247	14	0.07143	-12.03286	-12.03286		0.493878	26.62748957
34	30	8.522	0.75716	8	0.125	-12.06625	-12.06625		0.493878	4.43631024
35	31	8.753	0.00045	2	0.5	-11.625	-11.625		0.493878	0.973885245
										K7-K35 =weighted residuals

INTENTIONALLY LEFT BLANK

ATTACHMENT III

MESH GENERATION FOR SIMULATION OF SEEPAGE TESTS IN ECRB

Multiple numerical meshes of a 12 ft (3.6576 m) long section of the ECRB Cross Drift are developed, each with a different statistical realization of the underlying heterogeneous permeability field. The following steps are performed:

1. A mesh is generated with X-Y-Z dimensions of 4.0 m × 3.6576 m × 11.0 m, respectively, discretized into regular gridblocks with side lengths of 0.1 m × 0.3 m × 0.1 m. The Y-axis is aligned with the drift axis. Figure III-1 shows the input file *mesh3dblock* and the command used to generate the mesh.
2. The Z-coordinate of the mesh is shifted by 8 m using software MoveMesh V1.0 (LBNL 2000 [152824]) to translate the origin of the mesh to the center of the drift. The resulting grid is referred to as the primary mesh (file *primary.mes*).
3. For each realization, a new seed number is inserted into the SISIM V1.204 input file *perm.par* (see Figure III-2). SISIM V1.204 (LBNL 2000 [153100]) is then executed to generate a random, spatially correlated field of log-permeability modifiers (file *perm.dat*).
4. The heterogeneous field of permeability modifiers is mapped onto the mesh using software Perm2Mesh V1.0 (LBNL 2000 [152826]).
5. A cylindrical drift of radius 2.5 m is cut from the mesh using software CutDrift V1.0 (LBNL 2000 [152816]). The drift is centered at X = 0 and Z = 0 with its axis parallel to the Y-axis.
6. Software AddBound V1.0 (LBNL 2000 [152823]) is used to attach boundary elements at the top and bottom of the model domain. The bottom-boundary gridblock is assigned to a special material domain (DRAIN) to allow specifying a free-drainage boundary condition.
7. Software AddBorehole V1.0 (LBNL 2000 [152822]) is used to insert gridblocks representing a 6 ft (1.8288 m) long injection interval with a diameter of 3 inches (0.076 m). The injection interval lies within the Y-Z plane at a 15° angle from the horizontal, centered at X = 0.0 m, Y = 1.8288 m, and a Z coordinate that depends on the packed-off zone being tested (see Table III-1). The elevations Z [m] of the beginning and end of the borehole interval are calculated from their respective distances from the borehole collar *d* [ft] as follows:

$$Z = d \cdot 0.3048 \cdot \sin(15^\circ) + 2.5 \quad (\text{III-1})$$

8. Drift elements (DRI98 and DRI99) are assigned a large volume so that Dirichlet boundary conditions can be specified. Flux into the drift elements represents seepage.
9. Two new evaporation elements (EVA98 and EVA99) are added and connected to the same formation elements as the drift elements. The nodal distance from the formation elements to the evaporation elements is set to the diffusive boundary-layer thickness. Flux into these elements represents evaporation.

10. A single time step is performed using a generic TOUGH2 input file *onestep* (as input to iTOUGH2 V5.0; see Figure III-3) to test the mesh and to obtain cross-referencing information. The execution of the simulation is performed using file *sh.onestep* (Figure III-4)
11. The final mesh is stored on file *LAx_zoneY.mesZ*, where *x* refers to the borehole number, *Y* designates the test interval, and *Z* labels the realization of the underlying random permeability field.

File *sh.LAx_zoneY_mes* (see Figure III-5) was used to execute Mesh Generation Steps 3–11. The file documents all the Unix commands used as well as input variables to the individual software codes. An excerpt from a final sample mesh file *LAx_zoneY.mesZ* is shown in Figure III-6.

Table III-1. Input Z-Coordinates to Software AddBorehole V1.0 (Borehole Interval Elevations)

Borehole	Zone	Beginning of Interval		End of interval	
		Distance from Collar <i>d</i> [ft]	Elevation <i>Z</i> [m]	Distance from Collar <i>d</i> [ft]	Elevation <i>Z</i> [m]
SYBT-ECRB-LA#1	2	~10 (3.0 m)	3.29	~16 (4.9 m)	3.76
SYBT-ECRB-LA#2	1	17	3.84	23	4.31
	2	33	5.10	39	5.58
	3	49	6.37	55	6.84
SYBT-ECRB-LA#3	1	18	3.92	24	4.39
	2	34	5.18	40	5.66

```

TOUGH2 input file for generating 3D block
Command: tough2 -mesh mesh3dblock 9
MESHMAKER ----*----2----*----3----*----4----*----5----*----6----*----7----*----8
XYZ

NX      1 0.0500000
NX     40 0.1000000
NY     12 0.3048000
NZ      1 0.600E-10
NZ    110 0.1000000
NZ      1 0.600E-10

ENDFI ---1---*---2---*---3---*---4---*---5---*---6---*---7---*---8

```

Figure III-1. Input file *mesh3dblock* to generate primary mesh

```

SISIM V1.204 INPUT FILE perm.par
*****

Generates weakly correlated random field of log-permeability modifiers
for the seepage model of the systematic testing area in the ECRB Cross Drift.

START OF PARAMETERS:
dummy.dat          \data file
1  2  3  4        \column: x,y,z,vr
-1.0e21  1.0e21   \data trimming limits
-2.0  2.0        \minimum and maximum data value
1      2.5       \lower tail option and parameter
1      1.0       \middle option and parameter
4      2.5       \upper tail option and parameter
dummy.dat         \tabulated values for classes
3  0             \column for variable, weight
direct.ik        \direct input of indicators
perm.dat         \output file for simulation
1               \debugging level: 0,1,2,3
perm.dbg         \output File for Debugging
0               \0=standard order relation corr
59067           \seed number
1               \number of simulations
41  0.00 0.10   \nx,xmn,xsiz
12  0.1524 0.3048 \ny,ymn,ysiz
110 -3.00 0.10  \nz,zmn,zsiz
1               \0=two part search, 1=data-nodes
0               \ max per octant(0 -> not used)
2.0            \ maximum search radius
0.0 0.0 0.0 1.0 1.0 \ sang1,sang2,sang3,sanis1,2
0 20           \ min, max data for simulation
12            \number simulated nodes to use
0 2.5         \0=full IK, 1=med approx(cutoff)
0            \0=SK, 1=OK
8            \number cutoffs
-1.75 0.025 1 0.0 \cutoff, global cdf, nst, nugget
1 0.2 1.00 \ it, aa, cc
0.0 0.0 0.0 1.0 1.0 \ ang1,ang2,ang3,anis1,2
-1.25 0.10 1 0.0 \cutoff, global cdf, nst, nugget
1 0.2 1.00 \ it, aa, cc
0.0 0.0 0.0 1.0 1.0 \ ang1,ang2,ang3,anis1,2
-0.75 0.225 1 0.0 \cutoff, global cdf, nst, nugget
1 0.2 1.00 \ it, aa, cc
0.0 0.0 0.0 1.0 1.0 \ ang1,ang2,ang3,anis1,2
-0.25 0.40 1 0.0 \cutoff, global cdf, nst, nugget
1 0.2 1.00 \ it, aa, cc
0.0 0.0 0.0 1.0 1.0 \ ang1,ang2,ang3,anis1,2
0.25 0.60 1 0.0 \cutoff, global cdf, nst, nugget
1 0.2 1.00 \ it, aa, cc
0.0 0.0 0.0 1.0 1.0 \ ang1,ang2,ang3,anis1,2
0.75 0.775 1 0.0 \cutoff, global cdf, nst, nugget
1 0.2 1.00 \ it, aa, cc
0.0 0.0 0.0 1.0 1.0 \ ang1,ang2,ang3,anis1,2
1.25 0.90 1 0.0 \cutoff, global cdf, nst, nugget
1 0.2 1.00 \ it, aa, cc
0.0 0.0 0.0 1.0 1.0 \ ang1,ang2,ang3,anis1,2
1.75 0.975 1 0.0 \cutoff, global cdf, nst, nugget
1 0.2 1.00 \ it, aa, cc
0.0 0.0 0.0 1.0 1.0 \ ang1,ang2,ang3,anis1,2

```

Figure III-2. Input file *perm.par* to generate random field of log-permeability modifiers.

```

Generic TOUGH2 input file; performs a single small time step
ROCKS-----1-----*-----2-----*-----3-----*-----4-----*-----5-----*-----6-----*-----7-----*-----8
FRACT      0      2650.      .1000 1.000E-12                                1000.
LITHO      0      2650.      .9900 1.000E-06                                100000.
DRIFT      0      2650.      .9900 1.000E-08                                100000.
EVAPO      0      2650.      .9900 1.000E-08                                100000.
BOREH      0      2650.      .9900 1.000E-08                                100000.
BOUND      0      2650.      .9900 1.000E-08                                100000.
DRAIN      0      2650.      .9900 1.000E-08                                100000.
SKINZ      0      2650.      .2000 1.000E-12                                1000.
MATRI      0      2650.      .1000 1.000E-17                                1000.
PACKE      0      2650.      .1000 1.000E-20                                1000.
NICHE      0      2650.      .9900 1.000E-08                                100000.
CAVIT      0      2650.      .9900 1.000E-06                                100000.

PARAM-----1-----*-----2-----*-----3-----*-----4-----*-----5-----*-----6-----*-----7-----*-----8
  2  1      11000000000000000400003000
                        1.000E-10

                        0.5
TIMES-----1-----*-----2-----*-----3-----*-----4-----*-----5-----*-----6-----*-----7-----*-----8
  1
  1.000E-11
START-----1-----*-----2-----*-----3-----*-----4-----*-----5-----*-----6-----*-----7-----*-----8
INCON-----1-----*-----2-----*-----3-----*-----4-----*-----5-----*-----6-----*-----7-----*-----8

ENDCY-----1-----*-----2-----*-----3-----*-----4-----*-----5-----*-----6-----*-----7-----*-----8

```

Figure III-3. Input file *onestep* used to perform a single time step.

```

#!/bin/sh
#
# Unix shell script file sh.onestep
# usage: sh.onestep MeshFileName
#
# Performs a single time step to create TOUGH2 mesh file
#
# S. Finsterle, August 2002
#
echo
echo Start shell script sh.onestep $1
echo =====
#
echo
echo Run one time step
echo -----
tough2 -v 5.0 -mesh -m $1 onestep 9
mv onestep.mes $1

```

Figure III-4. File *sh.onestep* used to execute a forward run with a single time step.

```

#!/bin/sh
#
# Unix shell script file to generate TOUGH2 mesh
#
# sh.LAx_zoneY_mesh
#
# S. Finsterle, 8/27/2002, V1.0
#
echo
echo Start shell script sh.LAx_zoneY_mesh
echo =====
echo Date      : `date`
echo Directory : `pwd`
echo
#
i=0
j=0
runs=50
# Start loop
while test $j -lt $runs
do
# generate new seed number
  j=`expr $j + 1`
  i=`expr $j + $j`
  i=`expr $i + 59067`
  echo " "
  echo "=====
  echo "Run $j of $runs"
  echo "=====
  echo "Create permeability modifier field, seed number: $i"
  cat perm.par | sed "s/^.*/seed/$i" >>perm.par$j
  xSisim << eof
perm.par$j
eof
#
#
echo Map permeability field
echo -----
xPerm2Mesh << eof
perm.dat          # input permeability field
primary.mes      # input mesh file
temp2.mes        # output mesh file
2                # number of header lines
3                # dimension of permeability field
3                # TOUGH2 mesh is xyz
1                # replace/add/multiply
histdrift.tec    # histogram file name
0.1              # class size
eof
#
echo
echo Cut out drift
echo -----
xCutDrift << eof
temp2.mes        # input mesh file
temp3.mes        # output mesh file
35.91           # 1/2 drift volume
1.0e-10         # nodal distance niche - wall
1.0              # cosine multiplication factor
0.0              # XCenter
0.0              # ZCenter

```

```

    2.5                                # Radius
eof
#
echo
echo Add top boundary
echo -----
xAddBound << eof
temp3.mes                             # input mesh file
temp4.mes                             # output mesh file
TOP99                                 # boundary element name
BOUND                                 # boundary material type
1.5e-1                                # boundary element volume
1.0e-5                                # nodal distance to boundary element
-100.0                                # xmin
 100.0                                # xmax
-100.0                                # ymin
 100.0                                # ymax
 7.99                                 # zmin
 8.01                                 # zmax
eof
#
echo
echo Add bottom boundary
echo -----
xAddBound << eof
temp4.mes                             # input mesh file
temp5.mes                             # output mesh file
BOT99                                 # boundary element name
DRAIN                                 # boundary material type
 1.0e+20                              # boundary element volume
1.0e-5                                # nodal distance to boundary element
-100.0                                # xmin
 100.0                                # xmax
-100.0                                # ymin
 100.0                                # ymax
-3.01                                 # zmin
-2.99                                 # zmax
eof
#
echo
echo Add Borehole
echo -----
xAddBorehole << eof
temp5.mes                             # input mesh file
temp6.mes                             # output mesh file
0.05                                  # dx
0.3048                                # dy
0.10                                  # dz
0.0                                    # XStart
0.9145                                # YStart=3*0.3048+0.0001
5.1033                                # ZStart=33*0.3048*sin(15)+2.5
0.0                                    # XEnd
2.681                                 # YEnd=YStart+6*0.3048*cos(15)
5.57663                              # ZEnd=39*0.3048*sin(15)+2.5
0.01905                              # Radius/2 (symmetry plane; d=3")
eof
#
echo
echo Edit elements and connections
echo -----
#
# increase drift element volume
sed 's/DRIFT...../DRIFT0.5000E+52/g' temp6.mes > LAX_zoneY_noevap.mes

```

```

#
# separate blocks ELEME and CONNE
cat LAX_zoneY_noevap.mes | sed -n '1,/BOR 0/p' > eleme
cat LAX_zoneY_noevap.mes | sed -n '/TOP99A21 1/, $p' > conne
#
# extract all drift elements and duplicate them for evaporation b.c.
grep DRI LAX_zoneY_noevap.mes | sed 's/DRI/EVA/' | sed 's/DRIFT/EVAPO/' > elemeconne
rm LAX_zoneY_noevap.mes
#
# append the two evaporation elements at the end of block ELEME
grep EVAPO elemeconne >> eleme
#
# add empty line and keyword CONNE
cat << eof >> eleme

CONNE
eof
#
# change ISOT and nodal distances of connections to evaporation elements
grep -v EVAP elemeconne | \
  sed 's/EVA\(\.....\) .*0.1000E-090.5000E-01\(\.....\) .*$/EVA\1
-180.1000E-090.7500E-02\2/' >> eleme
#
# concatenate blocks ELEME and CONNE
cat eleme conne | sed 's/+++/' > LAX_zoneY.mes$j
#
# run one time step to get "+++ " block in mesh file
sh.onestep LAX_zoneY.mes$j
#
echo
echo Mesh generated: LAX_zoneY.mes$j
echo =====
done
echo Script sh.LAX_zoneY_mesh completed: `date`
echo =====

```

Figure III-5. File *sh.LAX_zoneY_mes* used to execute mesh generation steps 3–11.

ELEME5	NX=	41	NY=	12	NZ=	112	dx/dy/dz	0.0000E+000	0.0000E+000	0.8000E+01		
A21	1							-.4604E+020	.2500E-010	.1524E+000	.7950E+01	
A31	1							-.1644E-010	.2500E-010	.1524E+000	.7850E+01	
A41	1							-.1477E+010	.2500E-010	.1524E+000	.7750E+01	
A51	1							-.1477E+010	.2500E-010	.1524E+000	.7650E+01	
.....											
D3C41								-.1320E+010	.4000E+010	.3505E+01-	.2650E+01	
D4C41								-.1236E+010	.4000E+010	.3505E+01-	.2750E+01	
D5C41								-.1236E+010	.4000E+010	.3505E+01-	.2850E+01	
D6C41								-.6929E+000	.4000E+010	.3505E+01-	.2950E+01	
DRI98			DRIFT0	.5000E+52				0.0000E+000	.0000E+000	.0000E+000	.0000E+00	
DRI99			DRIFT0	.5000E+52				0.0000E+000	.0000E+000	.0000E+000	.0000E+00	
TOP99			BOUND0	.1500E+00				0.0000E+00-	.1000E+04-	.1000E+04-	.1000E+04	
BOT99			DRAIN0	.1000E+21				0.0000E+00-	.1000E+04-	.1000E+04-	.1000E+04	
B	1		BOREH0	.3598E-03				0.08633-	.1000E+010	.0000E+000	.1067E+010	.5144E+01
B	2		BOREH0	.6585E-04				0.18851-	.1000E+010	.0000E+000	.1247E+010	.5193E+01
B	3		BOREH0	.2939E-03				0.27478-	.1000E+010	.0000E+000	.1400E+010	.5233E+01
B	4		BOREH0	.1475E-03				0.38019-	.1000E+010	.0000E+000	.1586E+010	.5283E+01
B	5		BOREH0	.2122E-03				0.46646-	.1000E+010	.0000E+000	.1738E+010	.5324E+01
B	6		BOREH0	.2280E-03				0.57215-	.1000E+010	.0000E+000	.1925E+010	.5374E+01
B	7		BOREH0	.1317E-03				0.65842-	.1000E+010	.0000E+000	.2078E+010	.5415E+01
B	8		BOREH0	.3085E-03				0.76411-	.1000E+010	.0000E+000	.2264E+010	.5465E+01
B	9		BOREH0	.5121E-04				0.85039-	.1000E+010	.0000E+000	.2417E+010	.5506E+01
B	10		BOREH0	.2861E-03				0.93139-	.1000E+010	.0000E+000	.2560E+010	.5544E+01
BOR	0		BOREH0	.2085E-02				-.1000E+010	.0000E+000	.1798E+010	.5340E+01	
EVA98			EVAP00	.5000E+52				0.0000E+000	.0000E+000	.0000E+000	.0000E+00	
EVA99			EVAP00	.5000E+52				0.0000E+000	.0000E+000	.0000E+000	.0000E+00	
CONNE												
EVA99BL1	1							-180.1000E-090	.7500E-020	.1524E-01		
EVA99D21	1							-180.1000E-090	.7500E-020	.1524E-01		
EVA99BL2	1							-180.1000E-090	.7500E-020	.1524E-01		
.....											
EVA98CHC26								-180.1000E-090	.7500E-020	.3048E-01		
EVA98CIC26								-180.1000E-090	.7500E-020	.3048E-01		
EVA99CJC25								-180.1000E-090	.7500E-020	.3048E-01		
TOP99A21	1							30.1000E-040	.5000E-010	.1524E-010	.1000E+01	
A21	1A21	2						10.2500E-010	.5000E-010	.3048E-010	.0000E+00	
A21	1A22	1						20.1524E+000	.1524E+000	.5000E-020	.0000E+00	
A21	1A31	1						30.5000E-010	.5000E-010	.1524E-010	.1000E+01	
.....											
BK1	1BL1	1						30.5000E-010	.5000E-010	.1524E-010	.1000E+01	
BL1	1BL1	2						10.2500E-010	.5000E-010	.3048E-010	.0000E+00	
BL1	1BL2	1						20.1524E+000	.1524E+000	.5000E-020	.0000E+00	
DRI99BL1	1							30.1000E-090	.5000E-010	.1524E-01-	.1000E+01	
DRI99D21	1							30.1000E-090	.5000E-010	.1524E-010	.1000E+01	
D21	1D21	2						10.2500E-010	.5000E-010	.3048E-010	.0000E+00	
D21	1D22	1						20.1524E+000	.1524E+000	.5000E-020	.0000E+00	
D21	1D31	1						30.5000E-010	.5000E-010	.1524E-010	.1000E+01	
.....											
D61	1D61	2						10.2500E-010	.5000E-010	.3048E-010	.0000E+00	
D61	1D62	1						20.1524E+000	.1524E+000	.5000E-020	.0000E+00	
D61	1BOT99							30.5000E-010	.1000E-040	.1524E-010	.1000E+01	
TOP99A22	1							30.1000E-040	.5000E-010	.1524E-010	.1000E+01	
A22	1A22	2						10.2500E-010	.5000E-010	.3048E-010	.0000E+00	
A22	1A23	1						20.1524E+000	.1524E+000	.5000E-020	.0000E+00	
A22	1A32	1						30.5000E-010	.5000E-010	.1524E-010	.1000E+01	
.....											
D4C41D5C41								30.5000E-010	.5000E-010	.3048E-010	.1000E+01	
D5C41D6C41								30.5000E-010	.5000E-010	.3048E-010	.1000E+01	
D6C41BOT99								30.5000E-010	.1000E-040	.3048E-010	.1000E+01	
B	1AU4	1						10.1000E-090	.5000E-010	.3777E-010	.9659E+00	
B	2AU5	1						10.1000E-090	.5000E-010	.6913E-020	.9659E+00	

B	3AT5	1				10.1000E-090.5000E-010.3086E-010.9659E+00				
B	4AT6	1				10.1000E-090.5000E-010.1549E-010.9659E+00				
B	5AS6	1				10.1000E-090.5000E-010.2228E-010.9659E+00				
B	6AS7	1				10.1000E-090.5000E-010.2394E-010.9659E+00				
B	7AR7	1				10.1000E-090.5000E-010.1383E-010.9659E+00				
B	8AR8	1				10.1000E-090.5000E-010.3239E-010.9659E+00				
B	9AQ8	1				10.1000E-090.5000E-010.5377E-020.9659E+00				
B	10AQ9	1				10.1000E-090.5000E-010.3004E-010.9659E+00				
B	1B	2				20.1578E+000.2888E-010.1140E-02-.2588E+00				
B	2B	3				20.2888E-010.1289E+000.1140E-02-.2588E+00				
B	3B	4				20.1289E+000.6470E-010.1140E-02-.2588E+00				
B	4B	5				20.6470E-010.9307E-010.1140E-02-.2588E+00				
B	5B	6				20.9307E-010.1000E+000.1140E-02-.2588E+00				
B	6B	7				20.1000E+000.5777E-010.1140E-02-.2588E+00				
B	7B	8				20.5777E-010.1353E+000.1140E-02-.2588E+00				
B	8B	9				20.1353E+000.2246E-010.1140E-02-.2588E+00				
B	9B	10				20.2246E-010.1255E+000.1140E-02-.2588E+00				
BOR	0B	1				30.1000E-090.1905E-010.3777E-010.1000E+01				
BOR	0B	2				30.1000E-090.1905E-010.6913E-020.1000E+01				
BOR	0B	3				30.1000E-090.1905E-010.3086E-010.1000E+01				
BOR	0B	4				30.1000E-090.1905E-010.1549E-010.1000E+01				
BOR	0B	5				30.1000E-090.1905E-010.2228E-010.1000E+01				
BOR	0B	6				30.1000E-090.1905E-010.2394E-010.1000E+01				
BOR	0B	7				30.1000E-090.1905E-010.1383E-010.1000E+01				
BOR	0B	8				30.1000E-090.1905E-010.3239E-010.1000E+01				
BOR	0B	9				30.1000E-090.1905E-010.5377E-020.1000E+01				
BOR	0B	10				30.1000E-090.1905E-010.3004E-010.1000E+01				
+++										
	42113	55	42113	56	42113	115	42113	116	42113	175
	42113	176	42113	235	42113	236	42113	295	42113	296
	42113	355	42113	356	42113	415	42113	416	42113	475

	42109	42110	42111	42101	42111	42102	42111	42103	42111	42104
	42111	42105	42111	42106	42111	42107	42111	42108	42111	42109
	42111	42110								

Figure III-6. Excerpt from sample mesh file *LAX_zoneY.mesZ*.

INTENTIONALLY LEFT BLANK

ATTACHMENT IV
MESH GENERATION FOR SIMULATION OF SEEPAGE TESTS IN
NICHES 3107, 3650, AND 4788

Four 3D meshes for the simulation of liquid-release tests in niches located in the middle nonlithophysal zone are generated: two 1.5 m long sections of Niche 3650 centered (a) 4.42 m and (b) 5.64 m from the collar of borehole UM, (c) a 1.5 m long section of Niche 3107 centered at Niche 3107 station 00+10.25 m, and (d) a 2.0 m long section of Niche 4788 centered at Niche 4788 station 00+11.45 m. The meshes are created in several steps as follows (where steps differ, information for each mesh is preceded by the letter referring to a specific panel of Figure 16):

1. Primary meshes are generated with X-Y-Z dimensions of (a & b) $6.0 \text{ m} \times 1.5 \text{ m} \times 5.0 \text{ m}$, (c) $6.5 \text{ m} \times 1.5 \text{ m} \times 5.0 \text{ m}$, and (d) $6.0 \text{ m} \times 2.0 \text{ m} \times 5.0 \text{ m}$, respectively, that are discretized into regular gridblocks with side lengths of $0.1 \text{ m} \times 0.1 \text{ m} \times 0.1 \text{ m}$. The Y-axis is parallel to the niche axis.
2. The X-, Y-, and Z-coordinates of each primary mesh are translated using software MoveMesh V1.0 (LBNL 2000 [152824]) so that $X = 0$ is at the center of the Niche, $Y = 0$ coincides with Niche station 00 + 0.0 m for Meshes (c) and (d), and $Z = 0$ is (a & b) at the bottom of the mesh and (c & d) coincides with the local survey Z datum.
3. The heterogeneous permeability fields are mapped onto their respective meshes using routine Perm2Mesh V1.0 (LBNL 2000 [152826]).
4. (a & b) A niche with vertical walls at $X = -2 \text{ m}$ and $X = 2 \text{ m}$ and a ceiling of radius 3.04 m with the crown at (a) $Z = 3.13 \text{ m}$ and (b) $Z = 3.33 \text{ m}$ is cut from the mesh using software CutNiche V1.3 (LBNL 2000 [152828]). (c & d) Niches with vertical walls at (c) $X = -2.15 \text{ m}$ and $X = 2.35 \text{ m}$ and (d) $X = -2.00 \text{ m}$ and $X = 1.90 \text{ m}$ and ceilings defined by survey data are cut from their respective meshes using software CutNiche V1.2 (LBNL 2000 [152815]). A very small nodal distance is defined between the interfaces representing the drift surface and the gridblocks denoting the drift, which sets boundary conditions directly at the drift wall. The length of the last vertical connection from the gridblocks representing the formation and the interface denoting the drift surface is thus $\Delta Z/2 = 0.05 \text{ m}$.
5. Software AddBound V1.0 (LBNL 2000 [152823]) is used to attach boundary elements at the top and bottom of the model domain. The bottom boundary gridblock is assigned to a special material domain to allow specifying a free-drainage boundary condition.
6. Gridblocks along the alignment of the injection boreholes are modified to represent 1 ft (0.3048 m) long injection intervals with a diameter of 3 inches (0.076 m).

The final meshes (see Figure 16) contain approximately (a) 28,000 gridblocks and 79,000 connections between them, (b) 26,000 gridblocks and 76,000 connections between them, (c) 34,000 gridblocks and 99,000 connections between them, (d) 36,000 gridblocks and 108,000 connections between them. Mesh generation is further documented in various SNs (Finsterle 1999 [153448], pp. 100–102; Ahlers 2002 [161045], pp. 27–29, 42–44, 54; Hedegaard 2002 [161046], pp. 27–29; Wang 1999 [153449], pp. 108–123; and Trautz 2001 [156903], pp. 35–45).

INTENTIONALLY LEFT BLANK

ATTACHMENT V

MESH GENERATION FOR SEEPAGE TEST SIMULATIONS IN NICHE 1620

Preparation of the computational meshes for simulating liquid-release tests performed in Niche 1620 involved three major steps: (1) preparation of niche ceiling coordinates, (2) preparation of geostatistical parameters of the permeability field, and (3) preparation of numerical grids.

V-1. Preparation of Niche Ceiling Coordinates

The niche surface roughness was reproduced by interpolation from niche survey data (data sources are listed in Table V-1).

Table V-1. Survey Data Sources for the Ceiling of Niche 1620

DTN	DIRS #	Description	Coordinate System
MO0009GSC00332.000	[155370]	ECRB Niche 1620 profile survey data	Nevada State Plane
MO0107GSC01061.000	[155369]	ECRB Niche 1620 slot survey data	
LB0301N5CEILNG.001	[161733]	ECRB Niche 1620 survey data for collars, projected bottoms, and intervals	
LB0301N5CEILNG.001	[161733]	ECRB Niche 1620 detailed profile survey data	Distance from reference frame

The steps followed in preparing the interpolated Niche 1620 ceiling profiles are described below. The datum point for the meshes was selected to be the intersection of the ECRB centerline and Niche 1620 centerline (DTN: MO0009GSC00332.000 [155370]). The location of the datum in the Nevada coordinate system is given in Table V-2.

Table V-2. Datum of Niche 1620 in the Nevada Coordinate System
(DTN: MO0009GSC00332.000 [155370])

Northing N_D [m]	Easting ES_D [m]	Elevation EL_D [m]	Azimuth A [degrees]
233276.41	170662.51	1105.91	181

The coordinates of the ECRB Niche 1620 profile survey data (DTN: MO0009GSC00332.000 [155370]), slot survey data (DTN: MO0107GSC01061.000 [155369]), and survey data for collars, projected bottoms, and intervals (DTN: MO0209GSC02116.000 [160407]) were transformed to a regular $X - Y - Z$ coordinate system using the following elementary analytical geometry formulae:

$$X = (ES - ES_D) \cdot \cos(\theta) + (N - N_D) \cdot \sin(\theta) \quad (V-1)$$

$$Y = (N - N_D) \cdot \cos(\theta) + (ES - ES_D) \cdot \sin(\theta) \quad (V-2)$$

$$Z = (EL - EL_D) \quad (V-3)$$

where ES [m] is easting, N [m] is northing, EL [m] is elevation, and the subscript D denotes the values of the datum (see Table V-2). The angle θ [degrees] is related to the azimuth angle A [m] by,

$$\theta = 360^\circ - A \quad (V-4)$$

The original ECRB Niche 1620 profile survey data (DTN: MO0009GSC00332.000 [155370]), slot survey data (DTN: MO0107GSC01061.000 [155369]) and their corresponding values in $X - Y - Z$ are given in Table V-3.

Table V-3. Niche 1620 Profile Survey Data (DTN: MO0009GSC00332.000 [155370]) and Slot Survey Data (DTN: MO0107GSC01061.000 [155369]) and Their Corresponding Values in the $X - Y - Z$ Coordinate System

Niche 1620 Profile						
Station	Easting [m]	Northing [m]	Elevation [m]	X [m]	Y [m]	Z [m]
0+00.97	170667.36	233277.30	1108.24	-4.83	-0.81	2.33
0+00.83	170665.36	233275.54	1108.23	-2.86	0.92	2.32
0+01.48	170662.48	233274.93	1106.39	0.00	1.48	0.48
0+01.49	170662.48	233274.92	1110.70	0.00	1.49	4.79
0+02.11	170662.47	233274.31	1110.63	0.00	2.10	4.72
0+02.12	170662.47	233274.30	1106.42	0.00	2.11	0.51
0+02.37	170662.47	233274.04	1111.72	0.00	2.37	5.81
0+02.38	170662.47	233274.04	1106.42	0.00	2.37	0.51
0+05.12	170662.42	233271.29	1112.09	0.00	5.12	6.18
0+05.12	170662.42	233271.29	1106.51	0.00	5.12	0.60
0+06.18	170659.37	233270.29	1108.42	3.03	6.06	2.51
0+06.88	170658.44	233269.60	1107.96	3.95	6.74	2.05
0+07.45	170665.05	233268.92	1108.40	-2.67	7.53	2.49
0+07.86	170659.65	233268.60	1108.46	2.72	7.76	2.55
0+09.57	170662.34	233266.84	1112.87	0.00	9.57	6.96
0+09.57	170662.34	233266.84	1106.59	0.00	9.57	0.68
0+09.88	170659.75	233266.58	1108.52	2.59	9.78	2.61
0+11.57	170665.07	233264.80	1108.38	-2.76	11.65	2.47
0+12.50	170659.63	233263.96	1108.48	2.66	12.40	2.57
0+13.04	170662.28	233263.37	1112.82	0.00	13.03	6.91
0+13.24	170662.28	233263.18	1106.60	0.00	13.22	0.69
0+13.26	170662.28	233263.16	1111.52	0.00	13.24	5.61
0+13.69	170659.76	233262.77	1108.62	2.51	13.59	2.71
0+14.00	170662.27	233262.42	1110.09	0.00	13.98	4.18
0+14.02	170662.27	233262.39	1106.57	0.00	14.01	0.66
0+14.17	170664.52	233262.21	1108.48	-2.26	14.23	2.57
0+14.18	170660.22	233262.28	1108.57	2.04	14.09	2.66
0+14.96	170662.25	233261.45	1110.08	0.00	14.95	4.17
0+14.98	170662.25	233261.44	1106.64	0.00	14.96	0.73
0+14.98	170660.22	233261.47	1108.21	2.03	14.90	2.30
0+15.10	170664.42	233261.27	1108.41	-2.17	15.17	2.50

0+17.47	170662.21	233258.94	1106.58	0.00	17.46	0.67
0+17.47	170662.21	233258.94	1110.10	0.00	17.46	4.19
0+18.63	170660.11	233257.82	1108.55	2.08	18.55	2.64
0+18.75	170664.04	233257.64	1108.55	-1.86	18.79	2.64
0+20.39	170662.16	233256.02	1106.65	-0.01	20.38	0.74
0+20.41	170662.16	233256.01	1110.17	-0.01	20.39	4.26
0+21.52	170660.00	233254.94	1108.68	2.13	21.42	2.77
0+21.94	170664.00	233254.44	1108.57	-1.87	21.99	2.66
0+24.77	170660.11	233251.68	1108.50	1.97	24.68	2.59
0+24.89	170664.26	233251.49	1108.56	-2.18	24.95	2.65
0+25.94	170662.06	233250.47	1106.70	0.00	25.93	0.79
0+25.95	170662.06	233250.47	1110.29	0.00	25.93	4.38
0+26.79	170664.49	233249.58	1108.61	-2.45	26.86	2.70
0+27.33	170664.12	233249.05	1108.55	-2.09	27.38	2.64
0+28.45	170662.02	233247.97	1110.16	-0.01	28.43	4.25
0+28.46	170662.02	233247.96	1106.71	-0.01	28.44	0.80
0+28.46	170659.96	233247.99	1108.78	2.05	28.37	2.87
0+28.57	170664.02	233247.81	1108.66	-2.01	28.62	2.75
0+28.97	170662.01	233247.45	1110.10	-0.01	28.95	4.19
0+28.97	170662.01	233247.45	1106.88	-0.01	28.95	0.97
0+29.21	170662.00	233247.21	1108.73	0.00	29.19	2.82
Niche 1620 Slots						
Point No.	Easting [m]	Northing [m]	Elevation [m]	X [m]	Y [m]	Z [m]
100	170664.23	233256.66	1108.93	-2.06	19.78	3.02
101	170664.58	233256.63	1108.94	-2.41	19.81	3.03
102	170665.03	233256.61	1109.09	-2.87	19.84	3.18
103	170665.35	233256.60	1108.96	-3.19	19.86	3.05
104	170665.55	233256.65	1108.91	-3.38	19.81	3.00
105	170665.75	233256.68	1108.86	-3.58	19.78	2.95
106	170665.72	233256.66	1108.51	-3.55	19.80	2.60
107	170665.62	233256.66	1108.27	-3.45	19.80	2.36
108	170665.23	233256.58	1108.06	-3.07	19.87	2.15
109	170664.89	233256.60	1107.96	-2.73	19.85	2.05
110	170664.48	233256.57	1107.84	-2.32	19.87	1.93
111	170664.24	233256.50	1107.55	-2.08	19.94	1.64
112	170664.10	233256.79	1109.08	-1.93	19.64	3.17
113	170664.06	233255.67	1109.15	-1.91	20.76	3.24
114	170664.20	233255.72	1108.97	-2.05	20.72	3.06
115	170664.69	233255.79	1108.97	-2.54	20.65	3.06
116	170664.89	233255.91	1109.02	-2.74	20.54	3.11
117	170665.16	233255.79	1109.28	-3.01	20.66	3.37
118	170665.55	233255.76	1109.32	-3.40	20.70	3.41
119	170665.85	233255.79	1109.18	-3.70	20.68	3.27
120	170666.00	233255.84	1108.87	-3.85	20.63	2.96
121	170665.97	233255.78	1108.54	-3.82	20.69	2.63
122	170665.60	233255.71	1108.19	-3.45	20.75	2.28
123	170665.35	233255.76	1107.95	-3.20	20.70	2.04
124	170665.16	233255.71	1107.90	-3.01	20.74	1.99

125	170664.57	233255.62	1107.72	-2.42	20.82	1.81
126	170664.40	233255.49	1107.38	-2.25	20.95	1.47
127	170664.08	233254.52	1109.29	-1.95	21.91	3.38
128	170664.34	233254.59	1109.11	-2.21	21.85	3.20
129	170664.78	233254.58	1109.35	-2.65	21.87	3.44
130	170665.34	233254.54	1109.33	-3.21	21.92	3.42
131	170665.61	233254.52	1109.27	-3.48	21.94	3.36
132	170665.84	233254.42	1109.01	-3.71	22.04	3.10
133	170665.73	233254.43	1108.61	-3.60	22.03	2.70
134	170665.63	233254.29	1108.40	-3.51	22.17	2.49
135	170665.50	233254.31	1108.10	-3.38	22.15	2.19
136	170665.15	233254.39	1108.01	-3.02	22.06	2.10
137	170664.59	233254.48	1107.94	-2.46	21.96	2.03
138	170664.18	233254.48	1107.45	-2.05	21.96	1.54
139	170664.16	233253.96	1109.11	-2.04	22.48	3.20
140	170664.34	233253.91	1109.06	-2.22	22.53	3.15
141	170664.68	233253.90	1109.17	-2.56	22.54	3.26
142	170665.07	233253.99	1109.26	-2.95	22.46	3.35
143	170665.30	233254.03	1109.24	-3.18	22.43	3.33
144	170665.75	233253.98	1109.41	-3.63	22.48	3.50
145	170666.06	233253.77	1109.25	-3.94	22.70	3.34
146	170666.12	233253.75	1109.01	-4.00	22.72	3.10
147	170665.73	233253.78	1108.73	-3.61	22.68	2.82
148	170665.74	233253.82	1108.37	-3.62	22.64	2.46
149	170665.40	233253.91	1108.15	-3.28	22.55	2.24
150	170665.07	233253.88	1108.12	-2.95	22.57	2.21
151	170664.71	233253.81	1108.04	-2.59	22.63	2.13
152	170664.44	233253.66	1107.96	-2.33	22.78	2.05
153	170664.35	233253.75	1107.83	-2.24	22.69	1.92
154	170664.22	233254.08	1108.87	-2.10	22.36	2.96
155	170664.28	233257.61	1108.66	-2.10	18.83	2.75
156	170664.35	233257.44	1108.66	-2.17	19.00	2.75
157	170664.44	233257.30	1107.87	-2.26	19.14	1.96
158	170664.34	233257.33	1108.65	-2.16	19.11	2.74
159	170664.47	233257.22	1107.86	-2.29	19.22	1.95
160	170664.22	233256.09	1108.76	-2.06	20.35	2.85
161	170664.25	233256.04	1106.73	-2.10	20.40	0.82
162	170664.18	233254.74	1107.45	-2.05	21.70	1.54
163	170664.20	233254.76	1108.87	-2.07	21.68	2.96
164	170664.24	233254.20	1108.93	-2.12	22.24	3.02
165	170664.25	233254.13	1107.53	-2.13	22.31	1.62
166	170664.40	233252.89	1108.74	-2.30	23.55	2.83
167	170664.36	233253.57	1108.67	-2.25	22.87	2.76
168	170664.65	233253.77	1108.73	-2.53	22.67	2.82
169	170665.15	233253.86	1108.67	-3.03	22.59	2.76
170	170665.64	233253.87	1108.71	-3.52	22.59	2.80
171	170664.20	233257.98	1108.63	-2.01	18.46	2.72
172	170664.36	233257.73	1108.75	-2.18	18.71	2.84

173	170664.73	233257.23	1108.81	-2.55	19.22	2.90
174	170665.26	233257.03	1109.12	-3.09	19.43	3.21
175	170665.46	233256.97	1109.14	-3.29	19.49	3.23
176	170665.31	233257.07	1108.04	-3.14	19.39	2.13
177	170664.88	233257.14	1108.02	-2.71	19.31	2.11
178	170664.31	233257.45	1107.90	-2.13	18.99	1.99
179	170664.24	233257.79	1107.88	-2.05	18.65	1.97
180	170664.25	233257.80	1108.32	-2.06	18.64	2.41
181	170664.34	233257.46	1108.32	-2.16	18.98	2.41
182	170664.73	233257.32	1108.38	-2.55	19.13	2.47
183	170664.86	233257.16	1108.42	-2.69	19.29	2.51
184	170665.36	233257.08	1108.50	-3.19	19.38	2.59
185	170660.10	233255.84	1109.44	2.05	20.52	3.53
186	170659.81	233255.88	1109.15	2.34	20.48	3.24
187	170659.58	233255.87	1108.88	2.57	20.49	2.97
188	170659.29	233255.88	1108.73	2.86	20.47	2.82
189	170659.34	233255.88	1108.55	2.81	20.47	2.64
190	170659.66	233255.83	1108.42	2.49	20.53	2.51
191	170659.91	233255.74	1108.19	2.24	20.62	2.28
192	170660.01	233255.80	1107.87	2.14	20.56	1.96
193	170659.92	233256.93	1108.65	2.25	19.43	2.74
194	170659.82	233256.57	1108.62	2.34	19.79	2.71
195	170659.52	233256.31	1108.61	2.64	20.04	2.70
196	170659.39	233256.02	1108.68	2.76	20.33	2.77
197	170659.26	233255.84	1108.62	2.89	20.51	2.71
198	170659.42	233255.68	1108.61	2.73	20.67	2.70
199	170659.70	233255.42	1108.58	2.44	20.94	2.67
200	170659.68	233255.04	1108.62	2.46	21.32	2.71
201	170659.82	233254.56	1108.66	2.31	21.80	2.75

Detailed measurement of the niche ceiling roughness was carried out with reference to a horizontal frame located 2.98 m above the datum as shown in Table V-4 (DTN: LB0301N5CEILNG.001 [161733]).

Table V-4. Niche 1620 Ceiling Roughness Data

X [m]	Y [m]	Z [m]
-1.40	27.86	4.02
-1.09	27.86	4.29
-0.78	27.86	4.38
-0.48	27.86	4.54
-0.17	27.86	4.30
0.14	27.86	4.27
0.45	27.86	4.25
0.76	27.86	4.26
1.06	27.86	4.30
1.37	27.86	4.17
1.68	27.86	3.96
-1.40	26.56	4.21
-1.09	26.56	4.30
-0.78	26.56	4.36
-0.48	26.56	4.40
-0.17	26.56	4.54
0.14	26.56	4.46
0.45	26.56	4.39
0.76	26.56	4.37
1.06	26.56	4.35
1.37	26.56	4.20
1.68	26.56	3.98
-1.40	25.26	4.06
-1.09	25.26	4.26
-0.78	25.26	4.27
-0.48	25.26	4.57
-0.17	25.26	4.36
0.14	25.26	4.35
0.45	25.26	4.38
0.76	25.26	4.38
1.06	25.26	4.28
1.37	25.26	4.15
1.68	25.26	4.09
-1.40	23.96	4.18
-1.09	23.96	4.29
-0.78	23.96	4.33
-0.48	23.96	4.36
-0.17	23.96	4.49
0.14	23.96	4.42
0.45	23.96	4.42
0.76	23.96	4.47
1.06	23.96	4.38
1.37	23.96	4.28
1.68	23.96	4.05
-1.40	22.66	3.98
-1.09	22.66	4.18
-0.78	22.66	4.32

-0.48	22.66	4.42
-0.17	22.66	4.58
0.14	22.66	4.42
0.45	22.66	4.71
0.76	22.66	4.38
1.06	22.66	4.36
1.37	22.66	4.26
1.68	22.66	4.36
-1.40	21.36	3.97
-1.09	21.36	4.13
-0.78	21.36	4.18
-0.48	21.36	4.25
-0.17	21.36	4.35
0.14	21.36	4.33
0.45	21.36	4.63
0.76	21.36	4.28
1.06	21.36	4.19
1.37	21.36	4.18
1.68	21.36	3.99
-1.40	20.06	3.90
-1.09	20.06	4.11
-0.78	20.06	4.17
-0.48	20.06	4.25
-0.17	20.06	4.27
0.14	20.06	4.21
0.45	20.06	4.22
0.76	20.06	4.32
1.06	20.06	4.31
1.37	20.06	4.16
1.68	20.06	4.00
-1.40	18.76	3.96
-1.09	18.76	3.89
-0.78	18.76	4.03
-0.48	18.76	4.10
-0.17	18.76	4.09
0.14	18.76	4.07
0.45	18.76	4.08
0.76	18.76	4.08
1.06	18.76	4.13
1.37	18.76	4.20
1.68	18.76	3.79
-1.40	17.46	4.00
-1.09	17.46	3.91
-0.78	17.46	3.93
-0.48	17.46	3.99
-0.17	17.46	4.17
0.14	17.46	4.19
0.45	17.46	4.06
0.76	17.46	4.10
1.06	17.46	4.05

1.37	17.46	3.92
1.68	17.46	3.62
-1.40	16.16	3.83
-1.09	16.16	3.86
-0.78	16.16	4.06
-0.48	16.16	4.14
-0.17	16.16	4.12
0.14	16.16	4.09
0.45	16.16	4.18
0.76	16.16	4.09
1.06	16.16	4.07
1.37	16.16	3.92
1.68	16.16	3.77
-1.40	14.87	3.65
-1.09	14.87	3.79
-0.78	14.87	3.92
-0.48	14.87	4.15
-0.17	14.87	4.20
0.14	14.87	4.05
0.45	14.87	4.18
0.76	14.87	4.24
1.06	14.87	4.34
1.37	14.87	3.90
1.68	14.87	3.98
-1.40	15.19	3.66
-1.40	15.51	3.62
-1.40	15.84	3.63
-1.40	16.49	3.77
-1.40	16.81	3.91
-1.40	17.14	3.78
-1.40	17.79	4.08
-1.40	18.11	3.70
-1.40	18.44	3.73
-1.40	19.09	3.88
-1.40	19.41	3.93
-1.40	19.74	3.97
-1.40	20.39	4.16
-1.40	20.71	4.09
-1.40	21.04	4.10
-1.40	21.69	4.00
-1.40	22.01	3.96
-1.40	22.34	3.96
-1.40	22.99	4.09
-1.40	23.31	4.19
-1.40	23.64	4.17
-1.40	24.29	4.12
-1.40	24.61	4.18
-1.40	24.94	4.28
-1.40	25.59	4.20
-1.40	25.91	4.27

-1.40	26.24	4.34
-1.40	26.89	4.40
-1.40	27.21	4.11
-1.40	27.54	4.07
1.68	15.19	3.87
1.68	15.51	3.74
1.68	15.84	3.79
1.68	16.49	3.84
1.68	16.81	3.82
1.68	17.14	3.81
-2.19	14.87	2.98
-2.49	16.16	2.98
-2.21	17.46	2.98
-2.15	18.76	2.98
-1.87	20.06	2.98
-1.98	21.36	2.98
-1.85	22.66	2.98
-1.77	23.96	2.98
-1.85	25.26	2.98
-1.91	26.56	2.98
-2.11	27.86	2.98
2.13	14.87	2.98
2.14	16.16	2.98
2.19	17.46	2.98
2.22	18.76	2.98
2.33	20.06	2.98
2.34	21.36	2.98
2.21	22.66	2.98
2.38	23.96	2.98
2.18	25.26	2.98
2.22	26.56	2.98
2.09	27.86	2.98
-1.40	27.86	2.98
0.14	27.86	2.98
1.68	27.86	2.98

The survey data shown in Table V-3 and Table V-4 were interpolated onto a regular $X - Y$ plane of $0.1 \text{ m} \times 0.1 \text{ m}$ resolution using a linear interpolation tool of the software Tecplot V9.0. Excerpts of the resulting Niche 1620 ceiling and slot profiles are shown in Figure V-1, and Figure V-4 shows the plan view of the ceiling roughness.

```

Niche 1620 ceiling
x y z
-3.050000E+000 1.455000E+001 0.000000E+000
-2.950000E+000 1.455000E+001 0.000000E+000
-2.850000E+000 1.455000E+001 0.000000E+000
...
6.500000E-001 1.505000E+001 4.222630E+000
7.500000E-001 1.505000E+001 4.225305E+000
8.500000E-001 1.505000E+001 4.252642E+000
...
2.750000E+000 2.355000E+001 0.000000E+000
2.850000E+000 2.355000E+001 0.000000E+000
2.950000E+000 2.355000E+001 0.000000E+000

```

Figure V-1. Excerpts from interpolated ceiling profile of Niche 1620.

```

Niche 1620 left batwing
x y z
-4.450000E+000 1.455000E+001 0.000000E+000
-4.350000E+000 1.455000E+001 0.000000E+000
-4.250000E+000 1.455000E+001 0.000000E+000
....
-2.850000E+000 1.965000E+001 3.026709E+000
-2.650000E+000 1.965000E+001 2.910188E+000
-2.550000E+000 1.965000E+001 2.883803E+000
....
-1.650000E+000 2.355000E+001 0.000000E+000
-1.550000E+000 2.355000E+001 0.000000E+000
-1.450000E+000 2.355000E+001 0.000000E+000

```

Figure V-2. Excerpts from interpolated left slot profile of Niche 1620.

```

Niche 1620 right batwing data
x y z
2.050000E+000 1.455000E+001 0.000000E+000
2.150000E+000 1.455000E+001 0.000000E+000
2.250000E+000 1.455000E+001 0.000000E+000

2.250000E+000 2.005000E+001 2.991148E+000
2.350000E+000 2.005000E+001 2.904599E+000
2.450000E+000 2.005000E+001 2.835122E+000

2.750000E+000 2.355000E+001 0.000000E+000
2.850000E+000 2.355000E+001 0.000000E+000
2.950000E+000 2.355000E+001 0.000000E+000

```

Figure V-3. Excerpts from interpolated right slot profile of Niche 1620.

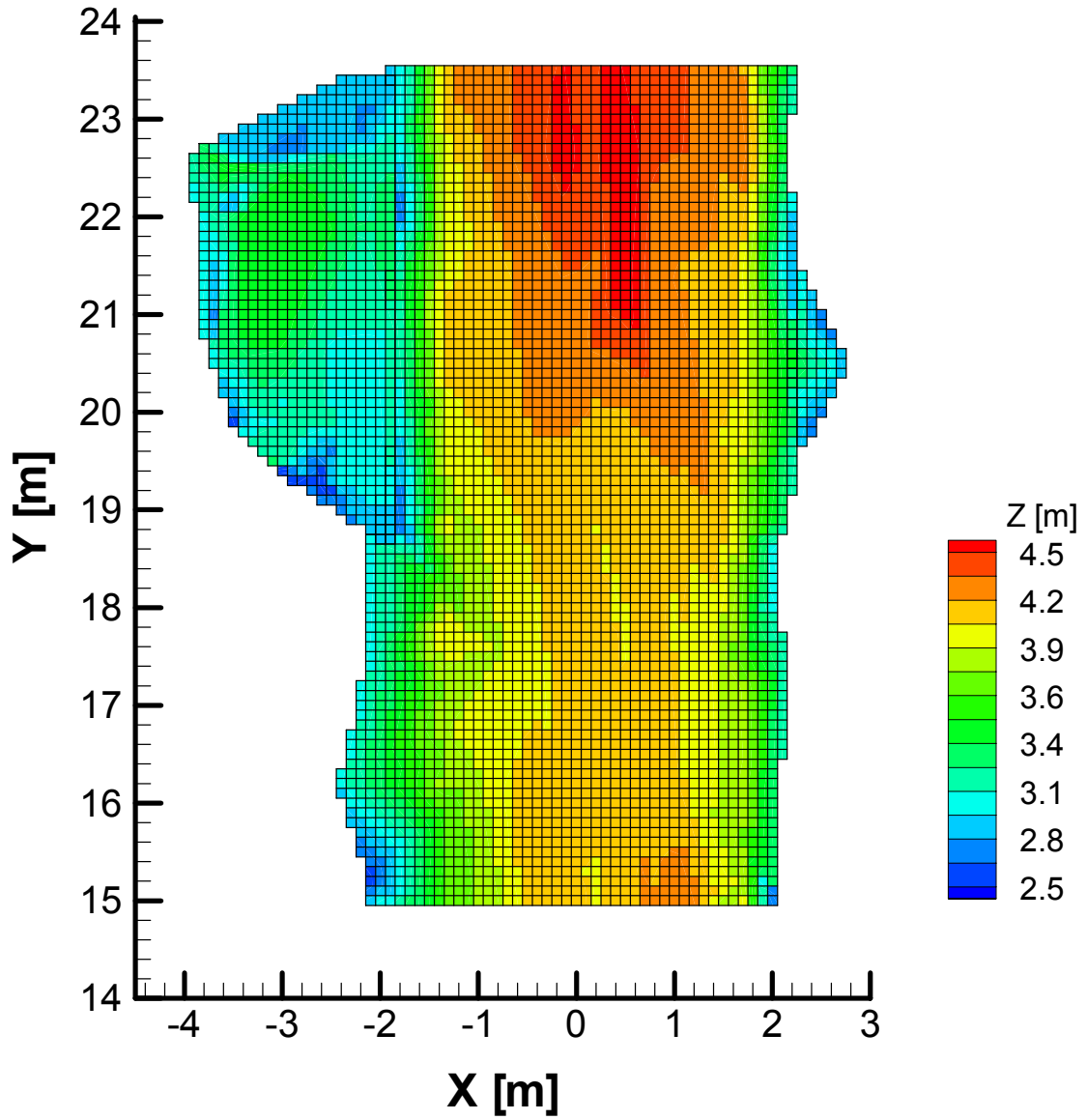


Figure V-4. Plan view of Niche 1620 ceiling and slot surface roughness (output DTN: LB0302SCMREV02.002)

V-2. Location of Boreholes and Preparation of Geostatistical Parameters of Air-Permeability

The locations of the borehole collars and projected endpoints (DTN: MO0209GSC02116.000 [160407]) were transformed from the Nevada coordinate system to the regular $X-Y-Z$ coordinate system using Equations (V-1) to (V-4). The original borehole surveys and their transformed equivalents are listed in Table V-5.

Table V-5. Original and Transformed Coordinates of Borehole Collars and Projected Bottoms

Borehole Collar/Bottom	Easting (m)	Northing (m)	Elevation (m)	Depth (m)	X (m)	Y (m)	Z (m)
ECRB-NICHE1620 #1							
Collar #1	170662.22	233262.19	1108.99	15.39	0.04	14.21	3.08
Projected Bottom	170661.91	233246.82	1109.14		0.08	29.58	3.23
ECRB-NICHE1620 #2							
Collar #2	170663.25	233262.93	1110.99	16.02	-0.98	13.49	5.08
Projected Bottom	170662.83	233246.93	1111.61		-0.83	29.48	5.70
ECRB-NICHE1620 #3							
Collar #3	170662.25	233262.72	1111.00	15.50	0.02	13.68	5.09
Projected Bottom	170661.98	233247.23	1111.29		0.02	29.17	5.38
ECRB-NICHE1620 #4							
Collar #4	170661.26	233262.76	1111.04	15.02	1.01	13.63	5.13
Projected Bottom	170661.16	233247.76	1111.57		0.85	28.62	5.66
ECRB-NICHE1620 #5							
Collar #5	170663.27	233262.84	1111.42	15.88	-1.00	13.58	5.51
Projected Bottom	170662.87	233247.08	1113.25		-0.87	29.33	7.34
ECRB-NICHE1620 #6							
Collar #6	170662.26	233262.78	1111.44	16.00	0.01	13.62	5.53
Projected Bottom	170662.21	233246.93	1113.58		-0.21	29.47	7.67
ECRB-NICHE1620 #7							
Collar #7	170661.28	233262.71	1111.47	14.81	0.99	13.68	5.56
Projected Bottom	170661.17	233248.01	1113.27		0.84	28.37	7.36

Permeability was measured by air-injection tests conducted in boreholes #2, #3, and #5 (see Section 6.5.2). The tests were performed by isolating a 1 ft section of the boreholes using an inflatable packer system (DTN: LB0110AKN5POST.001 [156904]), and then injecting compressed air at a constant rate into the isolated injection interval. The pressure buildup in the injection interval and in nearby observation intervals was monitored with time until steady-state conditions were reached, which typically occurred within a few minutes. Air-permeability values were derived from the steady-state pressure data. For the purpose of air-injection tests, the

boreholes were named differently (borehole ECRB-NICHE1620 #5 was renamed as #0, ECRB-NICHE1620 #2 was renamed as #3, and ECRB-NICHE1620 #3 was renamed as #4). The locations of the air-injection test intervals were reported as distances in feet from the borehole collars. These distances were first converted to meters and then transformed to their corresponding $X - Y - Z$ coordinates by the following elementary analytical geometry formulae:

$$X = x' + \frac{d(x'' - x')}{\sqrt{(x' - x'')^2 + (y' - y'')^2 + (z' - z'')^2}} \quad (\text{V-5})$$

$$Y = y' + \frac{d(y'' - y')}{\sqrt{(x' - x'')^2 + (y' - y'')^2 + (z' - z'')^2}} \quad (\text{V-6})$$

$$Z = z' + \frac{d(z'' - z')}{\sqrt{(x' - x'')^2 + (y' - y'')^2 + (z' - z'')^2}} \quad (\text{V-7})$$

where d is the midpoint of the test interval. The collar and projected endpoints of the borehole are denoted by (x', y', z') and (x'', y'', z'') , respectively (see Table V-5 for coordinates of endpoints). The transformation of coordinates is shown in Table V-6.

Table V-6. Locations of Air-Injection Test Intervals and Measured Air-Permeabilities

DTN: LB0110AKN5POST.001				Calculated					
BH	Start [ft]	End [ft]	k [m ²]	Midpoint [ft]	Midpoint [m]	X [m]	Y [m]	Z [m]	Log(k [m ²])
0	3	4	2.70E-12	3.5	1.07	-0.99	14.26	5.63	-11.5686
0	4	5	5.62E-12	4.5	1.37	-0.99	14.56	5.66	-11.2503
0	5	6	5.48E-09	5.5	1.68	-0.98	14.86	5.70	-8.2612
0	6	7	4.27E-09	6.5	1.98	-0.98	15.16	5.73	-8.3696
0	7	8	4.08E-12	7.5	2.29	-0.98	15.47	5.77	-11.3893
0	8	9	1.21E-11	8.5	2.59	-0.98	15.77	5.80	-10.9172
0	9	10	7.77E-12	9.5	2.90	-0.97	16.07	5.84	-11.1096
0	10	11	3.30E-12	10.5	3.20	-0.97	16.38	5.87	-11.4815
0	11	12	2.79E-11	11.5	3.51	-0.97	16.68	5.90	-10.5544
0	12	13	3.83E-11	12.5	3.81	-0.97	16.98	5.94	-10.4168
0	13	14	1.65E-10	13.5	4.11	-0.97	17.28	5.97	-9.7825
0	14	15	1.82E-10	14.5	4.42	-0.96	17.59	6.01	-9.7399
0	15	16	2.35E-11	15.5	4.72	-0.96	17.89	6.04	-10.6289
3	4	5	1.61E-11	4.5	1.37	-0.96	14.57	5.13	-10.7932
3	5	6	3.18E-12	5.5	1.68	-0.96	14.87	5.14	-11.4976
3	6	7	1.56E-11	6.5	1.98	-0.96	15.18	5.16	-10.8069

3	7	8	1.47E-12	7.5	2.29	-0.96	15.48	5.17	-11.8327
3	8	9	4.08E-10	8.5	2.59	-0.95	15.79	5.18	-9.3893
3	9	10	6.23E-10	9.5	2.90	-0.95	16.09	5.19	-9.2055
3	10	11	6.24E-10	10.5	3.20	-0.95	16.40	5.20	-9.2048
3	11	12	5.52E-10	11.5	3.51	-0.94	16.70	5.21	-9.2581
3	12	13	1.19E-12	12.5	3.81	-0.94	17.01	5.22	-11.9245
3	13	14	3.20E-11	13.5	4.11	-0.94	17.31	5.24	-10.4949
3	14	15	3.23E-11	14.5	4.42	-0.94	17.61	5.25	-10.4908
3	15	16	2.23E-12	15.5	4.72	-0.93	17.92	5.26	-11.6517
3	16	17	4.03E-09	16.5	5.03	-0.93	18.22	5.27	-8.3947
3	17	18	1.92E-09	17.5	5.33	-0.93	18.53	5.28	-8.7167
4	3	4	5.85E-09	3.5	1.07	0.02	14.39	5.11	-8.2328
4	4	5	9.51E-09	4.5	1.37	0.02	14.70	5.12	-8.0218
4	5	6	9.32E-12	5.5	1.68	0.02	15.00	5.12	-11.0306
4	6	7	8.85E-12	6.5	1.98	0.02	15.31	5.13	-11.0531
4	7	8	9.68E-12	7.5	2.29	0.02	15.61	5.13	-11.0141
4	8	9	4.16E-13	8.5	2.59	0.02	15.92	5.14	-12.3809
4	9	10	1.87E-12	9.5	2.90	0.02	16.22	5.14	-11.7282
4	10	11	1.16E-13	10.5	3.20	0.02	16.53	5.15	-12.9355
4	11	12	4.87E-14	11.5	3.51	0.02	16.83	5.15	-13.3125
4	12	13	5.25E-13	12.5	3.81	0.02	17.14	5.16	-12.2798
4	13	14	2.20E-11	13.5	4.11	0.02	17.44	5.17	-10.6576
4	14	15	3.66E-11	14.5	4.42	0.02	17.75	5.17	-10.4365
4	15	16	4.82E-14	15.5	4.72	0.02	18.05	5.18	-13.3170
4	16	17	5.91E-13	16.5	5.03	0.02	18.36	5.18	-12.2284
4	17	18	1.34E-11	17.5	5.33	0.02	18.66	5.19	-10.8729
4	18	19	3.71E-11	18.5	5.64	0.02	18.97	5.19	-10.4306
4	19	20	8.39E-13	19.5	5.94	0.02	19.27	5.20	-12.0762
4	20	21	2.48E-12	20.5	6.25	0.02	19.58	5.20	-11.6055
4	21	22	1.82E-12	21.5	6.55	0.02	19.88	5.21	-11.7399
4	22	23	1.86E-13	22.5	6.86	0.02	20.18	5.22	-12.7305
4	23	24	2.33E-13	23.5	7.16	0.02	20.49	5.22	-12.6326
4	24	25	2.65E-12	24.5	7.47	0.02	20.79	5.23	-11.5768
4	25	26	2.14E-12	25.5	7.77	0.02	21.10	5.23	-11.6696
4	26	27	2.11E-13	26.5	8.08	0.02	21.40	5.24	-12.6757
4	27	28	2.95E-13	27.5	8.38	0.02	21.71	5.24	-12.5302
4	28	29	6.71E-11	28.5	8.69	0.02	22.01	5.25	-10.1733
4	29	30	6.87E-11	29.5	8.99	0.02	22.32	5.25	-10.1630

4	30	31	1.64E-11	30.5	9.30	0.02	22.62	5.26	-10.7852
4	31	32	7.19E-12	31.5	9.60	0.02	22.93	5.27	-11.1433
4	32	33	2.43E-12	32.5	9.91	0.02	23.23	5.27	-11.6144
4	33	34	4.88E-13	33.5	10.21	0.02	23.54	5.28	-12.3116
4	34	35	1.06E-12	34.5	10.52	0.02	23.84	5.28	-11.9747
4	35	36	1.57E-12	35.5	10.82	0.02	24.15	5.29	-11.8041
4	36	37	1.48E-10	36.5	11.13	0.02	24.45	5.29	-9.8297

V-3. Preparation of Meshes

Multiple numerical meshes of a 2 m long section of the Niche 1620 were developed, each with a different statistical realization of the underlying heterogeneous permeability field. There were three test zones labeled as Niche1620a, Niche1620b, and Niche1620c. The locations and primary dimensions of these meshes are listed below in Table V-7.

Table V-7. Primary Dimensions of Niche 1620 Meshes

Location of Test Zone Along Y-axis from ECRB Centerline	Dimensions [m]		
	X	X	Y
0.0 + 15.60	6.0	6.0	2.0
0.0 + 19.60	8.0	8.0	2.0
0.0 + 21.90	8.0	8.0	2.0

The following mesh generation steps are performed. File names in the following steps refer to mesh of borehole #5 (28-29 ft).

1. A mesh is generated with X-Y-Z dimensions as listed in Table V-7, discretized into regular gridblocks with side lengths of 0.1 m × 0.1 m × 0.1 m. The Y-axis is aligned with the Niche centerline. Figure V-5 shows the input file *N5BH5_28-29ft* and the command used to generate the mesh.
2. The mesh is shifted using software MoveMesh V1.0 (LBNL 2000 [152824]) to translate the origin of the mesh to the datum of Niche 1620.
3. The GSLIB module SISIM V1.204 (LBNL 2000 [153100]) is executed to generate a random, spatially correlated field of log-permeability modifiers. For each realization, a new seed number is inserted into the SISIM V1.204 input file *N5BH5_28-29ft_sisim.par* (see Figure V-6). The generated permeability field is conditioned on measured air-permeability data provided in the file *measured_log-k_12_N5.dat* (see Figure V-7). Excerpt of the generated permeability field is shown in Figure V-8.
4. The heterogeneous field of permeability modifiers is mapped onto the mesh using software Perm2Mesh V1.0 (LBNL 2000 [152826]).

5. A niche is cut from the mesh with software CutDrift V1.0 (LBNL 2000 [152816]), using interpolated ceiling surface data given in Figure V-1.
6. Left and right slots are cut from the mesh with software CutDrift V1.0 (LBNL 2000 [152816]), using interpolated ceiling surface data given in Figure V-2 and Figure V-3.
7. Software AddBound V1.0 (LBNL 2000 [152823]) is used to attach boundary elements at the top and bottom of the model domain. The bottom boundary gridblock is assigned to a special material domain (DRAIN) to allow specifying a free-drainage boundary condition.
8. Gridblocks along the alignment of the injection boreholes are modified to represent 1 ft (0.3 m) long injection intervals and 3 ft (0.9 m) long packers on both sides of the injection interval.
9. Drift elements (DRI78, DRI79, DRI88, DRI89, DRI98, and DRI99) are assigned a large volume so Dirichlet boundary conditions can be specified. Flux into the drift elements represents seepage.
10. Six new evaporation elements (EVP78, EVP79, EVP88, EVP89, EVP98 and EVP99) are added and connected to the same formation elements as the drift elements. The nodal distance from the formation elements to the evaporation elements is set to the diffusive boundary-layer thickness. Flux into these elements represents evaporation.
11. A single time step is performed using a generic TOUGH2 input *onestep* file (as input to iTOUGH2 V5.0; see Figure III-3) to test the mesh and to obtain cross-referencing information. The execution of the simulation is performed using file *sh.onestep* (Figure III-4)

The steps 1-11 listed above were executed using file *sh.N5BH5_28-29ft_mesh* shown in Figure V-9. The script file *sh.N5BH5_28-29ft_run* (see Figure V-10) assigns new seed numbers for the generation of permeability field and generates multiple meshes by calling the script file *sh.N5BH5_28-29ft_mesh*.

The final mesh is stored on file *N5BH5_28-29ft.mesZ* where *Z*, labels the realization of the underlying random permeability field.

```

TOUGH2 input file for generating 3D grid for Niche 5
MESMAKER ----*----2----*----3----*----4----*----5----*----6----*----7----*----8
XYZ
NX      80 0.1000000
NY      20 0.1000000
NZ       1 0.600E-10
NZ      50 0.1000000
NZ       1 0.600E-10

ENDFI ---1---*---2---*---3---*---4---*---5---*---6---*---7---*---8

```

Figure V-5. Input file *N5BH5_28-29ft* used to generate primary mesh.

```

Parameters for SISIM
*****
Niche 5 Borehole #5 (28-29 ft)
TAG July 22, 2002
START OF PARAMETERS:
measured_log-k_12_N5.dat
1 2 3 4 \column: x,y,z,vr
-1.0e21 1.0e21 \data trimming limits
-2.0 5.0 \minimum and maximum data value
1 2.5 \lower tail option and parameter
1 1.0 \middle option and parameter
4 2.5 \upper tail option and parameter
dummy.dat \tabulated values for classes
3 0 \column for variable, weight
direct.ik \direct input of indicators
N5BH5_28-29ft_airK.dat \output file for simulation
2 \debugging level: 0,1,2,3
N5BH5_28-29ft_airK.dbg \output File for Debugging
0 \0=standard order relation corr
59069 \random number seed
1 \number of simulations
80 -4.45 0.10
20 20.95 0.10
50 2.05 0.10
1 \0=two part search, 1=data-nodes
0 \ max per octant(0 -> not used)
2.0 \ maximum search radius
0.0 0.0 0.0 1.0 1.0 \ sang1,sang2,sang3,sanis1,2
0 20 \ min, max data for simulation
12 \number simulated nodes to use
0 2.5 \0=full IK, 1=med approx(cutoff)
0 \0=SK, 1=OK
8 \number cutoffs
-0.725 0.066 1 0.02 \cutoff, global cdf, nst, nugget
1 0.96 1.82 \ it, aa, cc
0.0 0.0 0.0 1.0 1.0 \ ang1,ang2,ang3,anis1,2
-0.050 0.197 1 0.02 \cutoff, global cdf, nst, nugget
1 0.96 1.82 \ it, aa, cc
0.0 0.0 0.0 1.0 1.0 \ ang1,ang2,ang3,anis1,2
0.625 0.443 1 0.02 \cutoff, global cdf, nst, nugget
1 0.96 1.82 \ it, aa, cc
0.0 0.0 0.0 1.0 1.0 \ ang1,ang2,ang3,anis1,2
1.300 0.623 1 0.02 \cutoff, global cdf, nst, nugget
1 0.96 1.82 \ it, aa, cc
0.0 0.0 0.0 1.0 1.0 \ ang1,ang2,ang3,anis1,2
1.975 0.787 1 0.02 \cutoff, global cdf, nst, nugget
1 0.96 1.82 \ it, aa, cc
0.0 0.0 0.0 1.0 1.0 \ ang1,ang2,ang3,anis1,2
2.650 0.852 1 0.02 \cutoff, global cdf, nst, nugget
1 0.96 1.82 \ it, aa, cc
0.0 0.0 0.0 1.0 1.0 \ ang1,ang2,ang3,anis1,2
3.325 0.918 1 0.02 \cutoff, global cdf, nst, nugget
1 0.96 1.82 \ it, aa, cc
0.0 0.0 0.0 1.0 1.0 \ ang1,ang2,ang3,anis1,2
4.000 0.999 1 0.02 \cutoff, global cdf, nst, nugget
1 0.96 1.82 \ it, aa, cc
0.0 0.0 0.0 1.0 1.0 \ ang1,ang2,ang3,anis1,2

```

Figure V-6. Input file parameter file *N5BH5_28-29ft_sisim.par* for random permeability field generating software SISIM

```

N5-air K data
4
x
Y
z
log-k+12
-0.98851 14.25626 5.63022 0.43136
-0.98617 14.55911 5.66456 0.74974
-0.98382 14.86196 5.69891 3.73878
-0.98148 15.16481 5.73326 3.63043
-0.97913 15.46766 5.76761 0.61066
-0.97679 15.77051 5.80195 1.08279
-0.97444 16.07336 5.83630 0.89042
-0.97210 16.37621 5.87065 0.51851
-0.96976 16.67906 5.90500 1.44560
-0.96741 16.98191 5.93934 1.58320
-0.96507 17.28476 5.97369 2.21748
-0.96272 17.58761 6.00804 2.26007
-0.96038 17.89046 6.04239 1.37107
-0.96330 14.56905 5.13219 1.20683
-0.96067 14.87362 5.14378 0.50243
-0.95804 15.17818 5.15538 1.19312
-0.95541 15.48275 5.16698 0.16732
-0.95278 15.78732 5.17858 2.61066
-0.95014 16.09189 5.19017 2.79449
-0.94751 16.39645 5.20177 2.79518
-0.94488 16.70102 5.21337 2.74194
-0.94225 17.00559 5.22496 0.07555
-0.93962 17.31016 5.23656 1.50515
-0.93699 17.61473 5.24816 1.50920
-0.93435 17.91929 5.25976 0.34830
-0.93172 18.22386 5.27135 3.60531
-0.92909 18.52843 5.28295 3.28330
0.02101 14.39458 5.10953 3.76716
0.02100 14.69933 5.11511 3.97818
0.02100 15.00408 5.12069 0.96942
0.02099 15.30883 5.12627 0.94694
0.02098 15.61358 5.13185 0.98588
0.02097 15.91833 5.13743 -0.38091
0.02097 16.22307 5.14301 0.27184
0.02096 16.52782 5.14859 -0.93554
0.02095 16.83257 5.15417 -1.31247
0.02095 17.13732 5.15975 -0.27984
0.02094 17.44207 5.16533 1.34242
0.02093 17.74682 5.17091 1.56348
0.02092 18.05157 5.17649 -1.31695
0.02092 18.35632 5.18207 -0.22841
0.02091 18.66107 5.18765 1.12710
0.02090 18.96581 5.19323 1.56937
0.02089 19.27056 5.19881 -0.07624
0.02089 19.57531 5.20439 0.39445
0.02088 19.88006 5.20997 0.26007
0.02087 20.18481 5.21555 -0.73049
0.02087 20.48956 5.22113 -0.63264
0.02086 20.79431 5.22671 0.42325
0.02085 21.09906 5.23229 0.33041
0.02084 21.40381 5.23787 -0.67572
0.02084 21.70855 5.24345 -0.53018
0.02083 22.01330 5.24903 1.82672
0.02082 22.31805 5.25461 1.83696
0.02081 22.62280 5.26019 1.21484
0.02081 22.92755 5.26577 0.85673
0.02080 23.23230 5.27135 0.38561
0.02079 23.53705 5.27693 -0.31158
0.02079 23.84180 5.28251 0.02531
0.02078 24.14655 5.28809 0.19590
0.02077 24.45129 5.29367 2.17026

```

Figure V-7. Measured air-permeability data provided in file *measured_log-k_12_N5.dat* for conditioning the generated permeability field

```

variables = x y z var
zone i= 80 j= 20 k= 50
-0.4450000E+01 0.2095000E+02 0.2050000E+01 0.6853335E+00
-0.4350000E+01 0.2095000E+02 0.2050000E+01 0.1218344E+01
-0.4250000E+01 0.2095000E+02 0.2050000E+01 0.7149986E+00
...
0.3250000E+01 0.2285000E+02 0.6950000E+01 0.2682163E+01
0.3350000E+01 0.2285000E+02 0.6950000E+01 0.3089783E+01
0.3450000E+01 0.2285000E+02 0.6950000E+01 0.2990684E+01

```

Figure V-8. Excerpt from the generated permeability field

```

#!/bin/sh
#
# Unix shell script file sh.N5BH5_28-29ft_mesh
#
# Usage: sh.N5BH5_28-29ft_mesh
#
# Generates TOUGH2 mesh N5BH5_28-29ft.mes
# uses
# airK_N5_3.dat
# ceiling_N5_3.dat
# leftbatwing_N5_3.dat
# rightbatwing_N5_3.dat
#
# TA Ghezzehei (Sept 10, 2002), Version 1.2
#
# modified from S. Finsterle, August 6, 1999, Version 1.1
#
echo
echo ' Start shell script sh.N5BH5_28-29ft_mesh'
echo ' mesh generator for Niche 5, BH5 (28-29ft)'
echo '===== '
echo
#
echo
echo 1. Generate 3d mesh
echo -----
tough2 -mesh N5BH5_28-29ft 9          # general mesh
#
echo
echo 2. Center mesh
echo -----
xMoveMesh << eof
N5BH5_28-29ft.mes                    # input mesh file
temp01.mes                            # output mesh file
-4.50                                # dx
20.90                                # dy    N5_3
7.00                                  # dz
eof
#
echo
echo 3. Map correlated permeability field
echo -----
echo
xPerm2Mesh << eof                    # call program
N5BH5_28-29ft_airK.dat
temp01.mes
temp02.mes
2                                     # number of header lines in permeability field
data

```

```

3          # dimension of permeability field
3          # TOUGH2 mesh is xyz
1          # replace/add/multiply ?? 0 in past, doesn't
fill now ??
hist_N5_3.tec
0.1          # class size
eof
#
echo
echo 4. Cut out main niche
echo -----
xCutNiche1.2 << eof
temp02.mes
temp04.mes
ceiling_N5_3.dat
2          # number of header lines
100.0       # niche volume
1.0e-10     # nodal distance niche - wall
1.0         # cosine multiplication factor
-2.00      # Xmin
2.10       # Xmax
20.80      # Ymin      N5_3
23.00      # Ymax      N5_3
0.0        # Zmin
4.7        # Zmax
eof
#
# Replace all NIC98 and NIC99 elements to NIC88 and NIC89
# main niche is now NIC78 and NIC79, while the left batwing
# will be NIC98 and NIC99 (TA Ghezzehei June 19, 2002)
#
echo
echo 5. Replace NIC9* by NIC7*
echo -----
sed 's/NIC98/NIC78/g' temp04.mes | \
sed 's/NIC99/NIC79/g' > temp05.mes
#
echo
echo 6. Cut out left batwing
echo -----
xCutNiche1.2 << eof
temp05.mes
temp06.mes
leftbatwing_N5_3.dat
2          # number of header lines
100.0       # niche volume
1.0e-10     # nodal distance niche - wall
1.0         # cosine multiplication factor
-4.10      # Xmin
-1.90      # Xmax
20.80      # Ymin      N5_3
23.00      # Ymax      N5_3
0.0        # Zmin
3.6        # Zmax
eof
#
# Replace all NIC98 and NIC99 elements to NIC88 and NIC89
# left batwing is now NIC88 and NIC89, while the right batwing
# will be NIC98 and NIC99 (TA Ghezzehei, June 19, 2002)
#
echo
echo 7. Replace NIC9* by NIC8*
echo -----

```

```

sed 's/NIC98/NIC88/g' temp06.mes | \
sed 's/NIC99/NIC89/g' > temp07.mes
#
echo
echo 8. Cut out right batwing
echo -----
xCutNiche1.2 << eof
temp07.mes
temp08.mes
rightbatwing_N5_3b.dat
2                # number of header lines
100.0            # niche volume
1.0e-10         # nodal distance niche - wall
1.0             # cosine multiplication factor
2.20           # Xmin
3.00           # Xmax
20.80          # Ymin      N5_3
23.00          # Ymax      N5_3
0.0            # Zmin
3.6            # Zmax
eof
#
echo
echo 9. Add top boundary
echo -----
xAddBound << eof
temp08.mes      # input mesh file
temp09.mes      # output mesh file
TOP99           # boundary element name
BOUND          # boundary material type
1.5e-1         # boundary element volume
1.0e-5         # nodal distance to boundary element
-100.0         # xmin
 100.0         # xmax
-100.0         # ymin
 100.0         # ymax
7.00          # zmin
7.05          # zmax
eof
#
echo
echo 10. Add bottom boundary
echo -----
xAddBound << eof
temp09.mes      # input mesh file
temp10.mes      # output mesh file
BOT99           # boundary element name
DRAIN          # boundary material type
-1.0           # boundary element volume
1.0e-5         # nodal distance to boundary element
-100.0         # xmin
 100.0         # xmax
-100.0         # ymin
 100.0         # ymax
1.95          # zmin
2.00          # zmax
eof
#
# Delete Niche to Niche connections
# that result from multiple cuttings
# TAG June 18, 2002
#
#

```

```

echo
echo 11. Remove unnecessary connections
echo -----
grep -v NIC98NIC temp10.mes | \
grep -v NIC99NIC | \
grep -v NIC88NIC | \
grep -v NIC89NIC | \
grep -v NIC78NIC | \
grep -v NIC79NIC | \
grep -v NIC98BOT | \
grep -v NIC99BOT | \
grep -v NIC88BOT | \
grep -v NIC89BOT | \
grep -v NIC78BOT | \
grep -v NIC79BOT > temp11.mes
#
echo
echo 12. Add Packers/Boreholes and Change Connections
echo -----
echo
sed 's/A8136      . . . . .0.1000E-02/A8136      PACKE0.1000E-02/g' temp11.mes | \
sed 's/A8236      . . . . .0.1000E-02/A8236      PACKE0.1000E-02/g' | \
sed 's/A8336      . . . . .0.1000E-02/A8336      PACKE0.1000E-02/g' | \
sed 's/A8436      . . . . .0.1000E-02/A8436      PACKE0.1000E-02/g' | \
sed 's/A8536      . . . . .0.1000E-02/A8536      PACKE0.1000E-02/g' | \
sed 's/A8636      . . . . .0.1000E-02/A8636      PACKE0.1000E-02/g' | \
sed 's/A8736      . . . . .0.1000E-02/A8736      PACKE0.1000E-02/g' | \
sed 's/A7836      . . . . .0.1000E-02/A7836      PACKE0.1000E-02/g' | \
sed 's/A7936      . . . . .0.1000E-02/A7936      BOREHO.1000E-02/g' | \
sed 's/A7A36      . . . . .0.1000E-02/A7A36      BOREHO.1000E-02/g' | \
sed 's/A7B36      . . . . .0.1000E-02/A7B36      BOREHO.1000E-02/g' | \
sed 's/A7C36      . . . . .0.1000E-02/A7C36      PACKE0.1000E-02/g' | \
sed 's/A7D36      . . . . .0.1000E-02/A7D36      PACKE0.1000E-02/g' | \
sed 's/A7E36      . . . . .0.1000E-02/A7E36      PACKE0.1000E-02/g' | \
sed 's/A7F36      . . . . .0.1000E-02/A7F36      PACKE0.1000E-02/g' | \
sed 's/A6G36      . . . . .0.1000E-02/A6G36      PACKE0.1000E-02/g' | \
sed 's/A6H36      . . . . .0.1000E-02/A6H36      PACKE0.1000E-02/g' | \
sed 's/A6I36      . . . . .0.1000E-02/A6I36      PACKE0.1000E-02/g' | \
sed 's/A6J36      . . . . .0.1000E-02/A6J36      PACKE0.1000E-02/g' | \
sed 's/A6K36      . . . . .0.1000E-02/A6K36      PACKE0.1000E-02/g' | \
sed 's/A7935A7936.* /A7935A7936      10.5000E-010.0000E-010.1000E-010.0000E+00 /g' | \
sed 's/A7A35A7A36.* /A7A35A7A36      10.5000E-010.0000E-010.1000E-010.0000E+00 /g' | \
sed 's/A7B35A7B36.* /A7B35A7B36      10.5000E-010.0000E-010.1000E-010.0000E+00 /g' | \
sed 's/A7936A7937.* /A7936A7937      10.0000E-010.1000E-090.1000E-010.0000E+00 /g' | \
sed 's/A7A36A7A37.* /A7A36A7A37      10.0000E-010.5000E-010.1000E-010.0000E+00 /g' | \
sed 's/A7B36A7B37.* /A7B36A7B37      10.0000E-010.5000E-010.1000E-010.0000E+00 /g' | \
sed 's/A7836A7936.* /A7836A7936      20.5000E-010.0000E-010.1000E-010.0000E+00 /g' | \
sed 's/A7B36A7C36.* /A7B36A7C36      20.0000E-010.5000E-010.1000E-010.0000E+00 /g' | \
sed 's/A7936A8936.* /A7936A8936      30.0000E-010.5000E-010.1000E-010.1000E+01 /g' | \
sed 's/A7A36A8A36.* /A7A36A8A36      30.0000E-010.5000E-010.1000E-010.1000E+01 /g' | \
sed 's/A7B36A8B36.* /A7B36A8B36      30.0000E-010.5000E-010.1000E-010.1000E+01 /g' | \
sed 's/A6936A7936.* /A6936A7936      30.5000E-010.0000E-010.1000E-110.1000E+01 /g' | \
sed 's/A6A36A7A36.* /A6A36A7A36      30.5000E-010.0000E-010.1000E-110.1000E+01 /g' | \
sed 's/A6B36A7B36.* /A6B36A7B36      30.5000E-010.0000E-010.1000E-110.1000E+01 /g' | \
sed 's/A7144      . . . . .0.1000E-02/A7144      PACKE0.1000E-02/g' | \
sed 's/A7244      . . . . .0.1000E-02/A7244      PACKE0.1000E-02/g' | \
sed 's/A6344      . . . . .0.1000E-02/A6344      PACKE0.1000E-02/g' | \
sed 's/A6444      . . . . .0.1000E-02/A6444      PACKE0.1000E-02/g' | \
sed 's/A6544      . . . . .0.1000E-02/A6544      PACKE0.1000E-02/g' | \
sed 's/A6644      . . . . .0.1000E-02/A6644      PACKE0.1000E-02/g' | \
sed 's/A6744      . . . . .0.1000E-02/A6744      PACKE0.1000E-02/g' | \
sed 's/A6844      . . . . .0.1000E-02/A6844      PACKE0.1000E-02/g' | \
sed 's/A6944      . . . . .0.1000E-02/A6944      PACKE0.1000E-02/g' | \
sed 's/A5A44      . . . . .0.1000E-02/A5A44      BOREHO.1000E-02/g' | \
sed 's/A5B44      . . . . .0.1000E-02/A5B44      BOREHO.1000E-02/g' | \
sed 's/A5C44      . . . . .0.1000E-02/A5C44      BOREHO.1000E-02/g' | \
sed 's/A5D44      . . . . .0.1000E-02/A5D44      PACKE0.1000E-02/g' | \
sed 's/A5E44      . . . . .0.1000E-02/A5E44      PACKE0.1000E-02/g' | \
sed 's/A5F44      . . . . .0.1000E-02/A5F44      PACKE0.1000E-02/g' | \

```

```

sed 's/A5G44      ....0.1000E-02/A5G44      PACKE0.1000E-02/g' | \
sed 's/A5H44      ....0.1000E-02/A5H44      PACKE0.1000E-02/g' | \
sed 's/A4I44      ....0.1000E-02/A4I44      PACKE0.1000E-02/g' | \
sed 's/A4J44      ....0.1000E-02/A4J44      PACKE0.1000E-02/g' | \
sed 's/A4K44      ....0.1000E-02/A4K44      PACKE0.1000E-02/g' | \
sed 's/A5A43A5A44.* /A5A43A5A44      10.1000E-090.0000E-010.1000E-010.0000E+00 /g' | \
sed 's/A5B43A5B44.* /A5B43A5B44      10.5000E-010.0000E-010.1000E-010.0000E+00 /g' | \
sed 's/A5C43A5C44.* /A5C43A5C44      10.5000E-010.0000E-010.1000E-010.0000E+00 /g' | \
sed 's/A5A44A5A45.* /A5A44A5A45      10.0000E-010.5000E-010.1000E-010.0000E+00 /g' | \
sed 's/A5B44A5B45.* /A5B44A5B45      10.0000E-010.5000E-010.1000E-010.0000E+00 /g' | \
sed 's/A5C44A5C45.* /A5C44A5C45      10.0000E-010.5000E-010.1000E-010.0000E+00 /g' | \
sed 's/A5944A5A44.* /A5944A5A44      20.5000E-010.0000E-010.1000E-010.0000E+00 /g' | \
sed 's/A5C44A5D44.* /A5C44A5D44      20.0000E-010.5000E-010.1000E-010.0000E+00 /g' | \
sed 's/A5A44A6A44.* /A5A44A6A44      30.0000E-010.5000E-010.1000E-010.1000E+01 /g' | \
sed 's/A5B44A6B44.* /A5B44A6B44      30.0000E-010.5000E-010.1000E-010.1000E+01 /g' | \
sed 's/A5C44A6C44.* /A5C44A6C44      30.0000E-010.5000E-010.1000E-010.1000E+01 /g' | \
sed 's/A4A44A5A44.* /A4A44A5A44      30.5000E-010.0000E-010.1000E-110.1000E+01 /g' | \
sed 's/A4B44A5B44.* /A4B44A5B44      30.5000E-010.0000E-010.1000E-110.1000E+01 /g' | \
sed 's/A4C44A5C44.* /A4C44A5C44      30.5000E-010.0000E-010.1000E-110.1000E+01 /g' \
> temp12.mes
#
echo
echo 13. Edit volume of niche elements
echo -----
sed 's/NICHE...../NICHE0.5000E+52/g' temp12.mes > temp13.mes
#
#
echo
echo 14. Add evaporation elements
echo -----
cat temp13.mes | sed -n '1,/BOT99/p' > eleme
cat temp13.mes | sed -n '/TOP99A21 1/, $p' > conne
grep NIC temp13.mes | sed 's/NIC/EVP/' | sed 's/NICHE/EVAPP/' > elemeconne
grep EVAPP elemeconne >> eleme
cat << eof >> eleme

CONNE
eof
grep -v EVAPP elemeconne | \
  sed 's/EVP\(\.....\) .*0.1000E-090.5000E-01\(\.....\) .*$/EVP\1 \
-170.1000E-170.2000E-01\2/' >> eleme
cat eleme conne | sed 's/+++/ /' > temp14.mes
#sh.onestep temp14.mes
#
echo
echo 15. Remove unnecessary files
echo -----
echo
mv temp14.mes N5BH5_28-29ft.mes
rm temp*.*
rm hist*
rm t2.msg
rm fort*
rm *airK.dbg
echo
echo sh.N5BH5_28-29ft_mesh terminated
echo =====

```

Figure V-9. File *sh.N5BH5_28-29ft_mesh* used to execute Mesh Generation Steps 1–11

```

#
# sh.N5BH5_28-29ft_run
#
#
# Unix script to perform multiple inversions of seepage data
# using multiple realizations of permeability field.
# Niche5, Borehole 5 (28-29ft)
#
# uses
# airK_N5_3.par
# ceiling_N5_3.dat
# leftbatwing_N5_3.dat
# rightbatwing_N5_3b.dat
#
# TA Ghezzehei 09/09/2002
# Adapated from S. Finsterle, V1.0, 8/20/02
#
runs=10
clear
#
echo Copy air-K and Niche ceiling survey data
echo
#
echo 'Generate meshes for multiple calibrations of seepage test in Niche 5 (Borehole
5, 28-29ft)'
echo " "
i=0
j=0
while test $j -lt $runs
do
# calculate new seed number
j=`expr $j + 1`
i=`expr $j + $j`
i=`expr $i + 59067`
echo " "
echo "=====
echo "Run $j of $runs"
echo "=====
echo "Create permeability modifier field, seed number: $i"
cat N5BH5_28-29ft_sisim.par | sed "s/^.*seed/$i
\\seed/" \
    > N5BH5_28-29ft_sisim.par$j
xSisim << eof
N5BH5_28-29ft_sisim.par$j
eof
cp N5BH5_28-29ft_airK.dat N5BH5_28-29ft_airK.dat$j
#
echo `date`: Mesh generation
sh.N5BH5_28-29ft_mesh
cp N5BH5_28-29ft.mes N5BH5_28-29ft.mes$j
#
done
#
echo remove unnecessary files
echo
rm N5BH5_28-29ft_sisim.par
#
echo sh.N5BH5_28-29ft_run terminated
echo =====

```

Figure V-10. Script file *sh.N5BH5_28-29ft_run* used to multiple meshes with different permeability field realizations

ATTACHMENT VI

PREPARATION OF SEEPAGE RATE AND RELATIVE-HUMIDITY DATA FOR THE SIMULATION OF LIQUID-RELEASE TESTS IN THE ECRB CROSS DRIFT

Measured data from the liquid-release tests performed in the ECRB were submitted to the TDMS under various DTNs. The SCM is calibrated against seepage-rate data, taking into account evaporation effects, which are driven by relative humidity changes. Time series of seepage rates and relative-humidity data were extracted from the respective DTNs using the steps described in this Attachment. The procedure is outlined in detail for the liquid-release tests conducted in zone 2 of borehole SYBT-ECRB-LA#1 (DTN: LB0110ECRB LIQR.002 [156879]); similar procedures were applied for other liquid-release tests (see Wang 2003 [161456], SN-LBNL-SCI-228-V1, pp. 9, 18–21, 26).

1. DTN: LB0110ECRB LIQR.002 [156879] was obtained from the TDMS.
2. Data are stored in four archive files (*s01221_001.zip*, *s01221_002.zip*, *s01221_003.zip*, and *s01221_004.zip*). Four text files (*zz_sep_193257.txt*, *zz_sep_193258.txt*, *zz_sep_193259.txt*, and *zz_sep_193261.txt*) were extracted from the archive files using WinZip 8.0. The four text files contain four data reports labeled *s01221_001*, *s01221_002*, *s01221_003*, and *s01221_004*, respectively.

For the preparation of a calibration file with seepage-rate data, the following steps are performed:

1. Concatenate *zz_sep_193261.txt* and *zz_sep_193259.txt*; new file name: *Cum.txt*.
2. Open *Cum.txt* using the text editor vim 6.0.12.
3. Delete header lines.
4. Replace all slashes (except those in dates) with spaces to separate the data columns.
5. Save file *Cum.txt* and exit vim.
6. Open file *Cum.txt* in Excel 2000 (9.0.3821 SR-1) such that Column 1 holds the date and time, Column 2 holds the cumulative injection, Column 3 holds cumulative return flow, and Column 4 holds cumulative seepage.
7. Translate date to seconds after 2/28/2001, 13:59:


```
Col. 5 = (RC[-4] - "2/28/2001 13:59") * 86400
```
8. Calculate release rate [ml/min] from cumulative injection [ml] and cumulative return [ml]:


```
Col. 6 = ((RC[-4] - R[-1] C[-4]) - (RC[-3] - R[-1] C[-3])) / (RC[-1] - R[-1] C[-1]) * 60
```
9. Calculate seepage rate [ml/min] from cumulative seepage [ml]:


```
Col. 7 = (RC[-3] - R[-1] C[-3]) / (RC[-2] - R[-1] C[-2]) * 60
```

10. Save as Microsoft Excel Workbook *Cum.xls* (for traceability only) and as space delimited text file *Cum.prn*.
11. Open *Cum.prn* using text editor vim.
12. Delete all columns except time [sec] and seepage rate [ml/min].
13. Add header:

Time [sec] since	Seepage rate
02/28/01 13:59:00	[ml/min]
14. Save as *LAI_zone2_set2.dat* (see excerpt in Figure VI-1). This file will be read as a calibration data file by iTOUGH2 V5.0 (LBNL 2002 [160106]).

Time [sec] since	Seepage rate
02/28/01 13:59:00	[ml/min]
0.0	0.00
1200.0	11.26
2400.0	0.00
3600.0	-0.07
4800.0	-0.07
6000.0	0.00
.....
5241780.0	5.44
5242980.0	0.00
5244180.0	-0.86
5245380.0	-0.73
5246580.0	-0.62

Figure VI-1. Excerpt from calibration data file *LA2_zone1_set2.dat*

For the preparation of a boundary condition file with relative-humidity data, the following steps are performed:

15. Concatenate *zz_sep_193258.txt* and *zz_sep_193257.txt*; new file name: *RH.txt*.
16. Open *RH.txt* using the text editor vim.
17. Delete header lines.
18. Delete all columns except date, time and inside RH.
19. Append "E-02" to RH column to convert from [%] to dimensionless fraction.
20. Save *RH.txt* and exit vim.
21. Open *RH.txt* in Excel.
22. Add new Column 2.
23. Translate date and time to seconds after 2/28/01 13:46:

```
Col. 2 = (RC[-1] - "2/28/2001 13:46") * 86400
```

24. Save as space delimited text file *RH.txt*.
25. Open *RH.txt* using text editor vim.
26. Delete columns with date and time.
27. Add first dummy data point ($-1E20, 0.190$) to provide historic relative humidity.
28. Add last dummy data point ($1E20, 0.252$) to cover potential prediction time frame.
29. Duplicate all 4141 lines twice.
30. Add "4141 2" to top of file.
31. Remove second column from Line 2 to Line 4142.
32. Remove first column from Line 4143 to end of file.
33. Add "EVA98", Line 4143.
34. Add "EVA99", Line 8285.
35. Save as *LAI_zone2_set2.bc*. This file is supplied as time dependent boundary condition file to iTOUGH2 V5.0 (LBNL 2002 [160106]). An excerpt is shown in Figure VI-2.

```

4141 2
  -1.0E20
    0.0
  1200.0
  2400.0
  .....
5245380.0
5246580.0
5247780.0
  1.0E20
EVA98
0.190
0.190
0.190
0.188
.....
0.275
0.260
0.252
0.252
EVA99
0.190
0.190
0.190
0.188
.....
0.275
0.260
0.252
0.252

```

Figure VI-2. Excerpt from boundary condition data file *LA2_zone1_set2.bc*

INTENTIONALLY LEFT BLANK

ATTACHMENT VII

EXECUTION OF MULTIPLE INVERSIONS OF DATA FROM ECRB

Multiple inversions of seepage-rate data from the systematic testing area in the ECRB Cross Drift were performed, based on multiple realizations of the underlying permeability field. The following steps are performed (see also file *sh.run*, Figure VII-1):

1. Go to the appropriate subdirectory *.../L_A/Zone_Y/Set_Z*, where *x* indicates the borehole number, *Y* represents the injection zone, and *Z* designates the data set number (if multiple test sequences were performed in the same interval).
2. Select the appropriate mesh corresponding to the permeability field realization *j*.
3. Perform a steady-state simulation with background percolation, neglecting evaporation effects (vapor diffusion coefficient is set to zero). A representative TOUGH2 input file (as input to iTOUGH2 V5.0) *L_A_zone_Y_ininoevap* is reproduced in Figure VII-2.
4. Take saturation distribution from previous simulation as initial conditions for a simulation with evaporation effects added (vapor diffusion coefficient at standard conditions is set to 2.13×10^{-5} m²/s). A dry-out zone develops around the drift.
5. Take saturation distribution from previous simulation as initial conditions for the inversion. A representative TOUGH2 input file *L_A_zone_Y_set_Z* (as input to iTOUGH2 V5.0) is shown in Figure VII-3; an excerpt from a representative iTOUGH2 V5.0 input file *L_A_zone_Y_set_Zi* is shown in Figure VII-4.
6. Figure VII-5 contains an excerpt from a representative iTOUGH2 V5.0 output file *L_A_zone_Y_set_Zi.out*, showing the best estimate parameter value obtained from a single inversion.

```

#!/bin/sh
#
# sh.run LA ZONE SET [RUNS] [START] [NODE]
#
# LA    = Borehole number
# ZONE  = Zone number
# SET   = Test set number
# RUNS  = Number of inversions
# START = Starting number of inversion
# NODE  = Node number
#
# Perform multiple inversions of seepage data
# using multiple realizations of permeability field.
#
# S. Finsterle, 9/09/02
#
cd $HOME/ym/Seepage/ST/LA$1/Zone$2/Set$3
#
if test "$4" = ""
then
  noruns=1
else
  noruns=$4

```

```

fi
if test "$5" = ""
then
  j=1
else
  j=$5
fi
if test "$6" = ""
then
  node=" "
else
  node="-node node$6"
fi
echo "Date          :" `date`
echo "Directory     :" `pwd`
echo "Borehole       :" SYBT-ECRB-LA#$1
echo "Zone           :" $2
echo "Test set        :" $3
echo "Number of runs  :" $noruns
echo "First run       :" $j
echo "Master node     :" $node
#
runs=`expr $noruns + $j - 1`
#
while test $j -le $runs
do
  echo " "
  echo "=====
  echo "Run $j of $runs"
  echo "=====
#
  echo `date`: Create initial conditions without evaporation
  tough2 -v 5.0 $node -m ../LA$1_zone$2.mes$j LA$1_zone$2_ininoevap 9
#
  echo `date`: Take steady-state conditions as initial conditions for subsequent run
  cat LA$1_zone$2_ininoevap.sav | sed 's/EVA\(\.\.\).*$/EVA\1/' \
    | sed 's/+++/ /' > LA$1_zone$2_inieevap_$$inc
#
  echo `date`: Create initial conditions with dry-out zone
  itough2 -v 5.0 $node -m ../LA$1_zone$2.mes$j -i LA$1_zone$2_inieevap_$$inc \
    inieevapi LA$1_zone$2_inieevap 9
#
  echo `date`: Take steady-state conditions as initial conditions for subsequent run
  cat LA$1_zone$2_inieevap.sav | sed 's/+++/ /' > LA$1_zone$2_$$inc
#
  echo `date`: Invert seepage-rate data
  itough2 -v 5.0 $node -m ../LA$1_zone$2.mes$j -i LA$1_zone$2_$$inc \
    -tvsp LA$1_zone$2_set$3.bc -ito LA$1_zone$2_set$3i.out$j \
    LA$1_zone$2_set$3i LA$1_zone$2_set$3 9
#
  j=`expr $j + 1`
#
done
echo
echo Run completed: `date`
echo =====

```

Figure VII-1. File *sh.run* to execute multiple inversions

```

LAX_zoneY_ininoevap: Create initial conditions (no evaporation)
ROCKS-----1-----*-----2-----*-----3-----*-----4-----*-----5-----*-----6-----*-----7-----*-----8
FRACT      2      2650.      .0096 2.640E-11 2.640E-11 2.640E-11      1000.

      11      0.01
      11      2.57      500.0
DRIFT      0      2650.      0.9999 1.000E-08 1.000E-08 1.000E-08      -1000.
EVAPO      2      2650.      0.9999 1.000E-08 1.000E-08 1.000E-08      -1000.
              1.0
      3      0.900E+00
      19
BOREH      0      2650.      .5000 1.000E-08 1.000E-08 1.000E-08      1000.
BOUND      0      2650.      .9900 1.000E-08 1.000E-08 1.000E-08      -1000.
DRAIN      0      2650.      .9900 1.000E-08 1.000E-08 1.000E-08      -1000.

RPCAP-----1-----*-----2-----*-----3-----*-----4-----*-----5-----*-----6-----*-----7-----*-----8
      3      0.095
      1      0.00      0.00      1.00
PARAM-----1-----*-----2-----*-----3-----*-----4-----*-----5-----*-----6-----*-----7-----*-----8
8-2 150      100100000100021000400004000 0.00E-05      1.80
-1.000E+12      1.000E+03      9.81
1.000E-04
      0.01
SOLVR-----1-----*-----2-----*-----3-----*-----4-----*-----5-----*-----6-----*-----7-----*-----8
5 Z0 00 2.500E-03 1.000E-06
GENER-----1-----*-----2-----*-----3-----*-----4-----*-----5-----*-----6-----*-----7-----*-----8
TOP99INF 0      0      COM1 6.3700E-06

START-----1-----*-----2-----*-----3-----*-----4-----*-----5-----*-----6-----*-----7-----*-----8
INDOM-----1-----*-----2-----*-----3-----*-----4-----*-----5-----*-----6-----*-----7-----*-----8
EVAPO
      0.300
FRACT
      0.015
DRIFT
      0.001
ENDCY-----1-----*-----2-----*-----3-----*-----4-----*-----5-----*-----6-----*-----7-----*-----8
    
```

Figure VII-2. Representative TOUGH2 input file *LAX_zoneY_ininoevap* (as input to iTOUGH2 V5.0) to execute initial steady-state simulation without evaporation effects

```

LAX_zoneY_setZ: simulates liquid-release test in borehole x, zone Y, set Z
TIMBC---1---*---2---*---3---*---4---*---5---*---6---*---7---*---8
ROCKS---1---*---2---*---3---*---4---*---5---*---6---*---7---*---8
FRACT   2   2650.   .0096 2.640E-11 2.640E-11 2.640E-11                -1000.

    11      0.01    0.00
    11      2.57    500.0
DRIFT   0   2650.   0.9999 1.000E-08 1.000E-08 1.000E-08                1000.
EVAPO   2   2650.   1.0000 1.000E-08 1.000E-08 1.000E-08                -1000.
        1.0
    3      0.900E+00 0.000E+00
    19
BOREH   0   2650.   .5000 1.000E-08 1.000E-08 1.000E-08                -1000.
BOUND   0   2650.   .9900 1.000E-08 1.000E-08 1.000E-08                -1000.
DRAIN   0   2650.   .9900 1.000E-08 1.000E-08 1.000E-08                -1000.
rEFCO   0   1.0E5   20.0000 1.000E+03 1.000E-03 4.400E-10                -1000.

RPCAP---1---*---2---*---3---*---4---*---5---*---6---*---7---*---8
    3      0.01
    1      0.00    0.00    1.00
PARAM---1---*---2---*---3---*---4---*---5---*---6---*---7---*---8
6-29000 9000100000100020000400005000 2.13E-05 1.80
-1.7200E+5 1.000E+04 9.81
1.000E-04
        0.01
MOMOP---1---*---2---*---3---*---4---*---5---*---6---*---7---*---8
2
SOLVR---1---*---2---*---3---*---4---*---5---*---6---*---7---*---8
5 Z0 00 2.500E-03 1.000E-06
GENER---1---*---2---*---3---*--- 13.6 mm/year ---*---6---*---7---*---8
TOP99INF 0 0 COM1 6.3700E-06
BOR 0INJ 2 10 COM1
    -1.0E+50 0.0 10.00 2958968.0
    2984607.0 2993032.0 3018835.0 3361935.0
    3387587.0 1.0E50
    0.0 0.0 2.625000E-04 2.873900E-04
    0.0 0.0 2.909100E-04 2.967000E-04
    0.0 0.0
ENDCY---1---*---2---*---3---*---4---*---5---*---6---*---7---*---8

```

Figure VII-3. Representative TOUGH2 input file *LAX_zoneY_setZ* (as input to iTOUGH2 V5.0) used to simulate liquid release test, solving the forward problem

```

Generic command:
itough2 -v 5.0 -m LAx_zoneY.mesj -i LAx_zoneY.inc -tvsp LAx_zoneY_setZ.bc \
LAX_zoneY_setZi LAX_zoneY_setZ 9

> parameters
  >> capillary pressure
    >>> material: FRACT
      >>>> annotation: log(1/alpha)
      >>>> index: 2
      >>>> step: 0.2
      >>>> logarithm
      >>>> variation: 1.0
      <<<<<
    <<<<
  <<<<

> observation
  >> time: 275 equally spaced
    1.44E4 3.96E6

  >> liquid flow rate
    >>> connections: DRI99 BL1_1 DRI99 D21_1 DRI99 BL2_1 DRI99 D22_1 &
                    DRI99 D23_1 DRI99 BL4_1 DRI99 D24_1 DRI99 BL5_1 &
                    ..... ..... ..... ..... ..... ..... &
                    DRI98 CAC26 DRI98 CBC26 DRI98 CCC26 DRI98 CDC26 &
                    DRI98 CFC26 DRI98 CGC26 DRI98 CHC26 DRI98 CIC26
    >>>> factor: 8.3333E-6 (ml/min -- kg/sec; divide by 2 for symmetry)
    >>>> header: 2
    >>>> data file: LAX_zoneY_setZ.dat
    >>>> deviation: 0.1
    <<<<<
  <<<<

> computation
  >> stop
    >>> ignore WARNINGS
    >>> uphill: 6
    >>> iterations: 6
    <<<<
  >> jacobian
    >>> perturb: 0.2 %
    <<<<
  <<<<
<

```

Figure VII-4. Excerpt from representative iTOUGH2 input file *LAX_zoneY_set2i* used to solve the inverse problem

```

!!!!!!!!!!!!!!!!!!!!!!!!!!!!!!!!!!!!!!!!!!!!!!!!!!!!!!!!!!!!!!!!!!!!!!!!!!!!!!!!!!!!!!!!!!!!!!!!!!!!!!!!!!!!!!!!!!!!!!!!
ESTIMATED PARAMETER V/L/F ROCKS PAR INITIAL GUESS BEST ESTIMATE STANDARD DEVIATION
log(1/alpha) LOG10 FRACT 2 0.26990E+01 0.26758E+01 0.164E-02
!!!!!!!!!!!!!!!!!!!!!!!!!!!!!!!!!!!!!!!!!!!!!!!!!!!!!!!!!!!!!!!!!!!!!!!!!!!!!!!!!!!!!!!!!!!!!!!!!!!!!!!!!!!!!!!!!!!!!!!!

```

Figure VII-5. Reformatted excerpt from representative iTOUGH2 output file *LAX_zoneY_set2i.out* showing estimated parameter